5-2003

Dipole-Bound Anions

Nathanael Isaac Hammer
University of Tennessee - Knoxville

To the Graduate Council:

I am submitting herewith a dissertation written by Nathanael Isaac Hammer entitled "Dipole-Bound Anions." I have examined the final electronic copy of this dissertation for form and content and recommend that it be accepted in partial fulfillment of the requirements for the degree of Doctor of Philosophy, with a major in Chemistry.

Dr. Robert N. Compton, Major Professor

We have read this dissertation and recommend its acceptance:

Dr. Ward Plummer, Dr. Alexander Van Hook, Dr. Robert J. Hinde, Dr. George K. Schweitzer, Dr. Kelsey Cook

Accepted for the Council:

Carolyn R. Hodges

Vice Provost and Dean of the Graduate School

(Original signatures are on file with official student records.)

To the Graduate Council:

I am submitting herewith a dissertation written by Nathanael Isaac Hammer entitled "Dipole-Bound Anions." I have examined the final electronic copy of this dissertation for form and content and recommend that it be accepted in partial fulfillment of the requirements for the degree of Doctor of Philosophy, with a major in Chemistry.

Dr. Robert N. Compton

Major Professor

We have read this dissertation
and recommend its acceptance:

Dr. Ward Plummer

Dr. Alexander Van Hook

Dr. Robert J. Hinde

Dr. George K. Schweitzer

Dr. Kelsey Cook

Accepted for the Council:

Dr. Anne Mayhew

Vice Provost and Dean of
Graduate Studies

(Original signatures are on file with official student records.)

Dipole-Bound Anions

A Dissertation

Presented for the

Doctor of Philosophy

Degree

The University of Tennessee, Knoxville

Nathanael Isaac Hammer

May 2003

DEDICATION

To Larissa, Mom & Dad, Kristin, and the rest of my family

for their love and support through the course of this endeavor.

ACKNOWLEDGMENTS

I would like to thank my advisor, Dr. Robert Compton, for his guidance over the past six years. Dr. Compton always puts his students first, and I want to thank him for that commitment. From Dr. Compton I have learned that the unexpected result is sometimes the most important. He has taught me that that there is an explanation for every outcome and that the only way to perform an experiment is the right way. From him I have gained a love of exploration and a dedication to excellence.

I would like to thank Dr. Robert Hinde for teaching me quantum chemistry and for making me discover the answers to the questions I ask rather than simply telling me them.

I would like to thank the other members of my committee, Dr. Kelsey Cook, Dr. Ward Plummer, Dr. George Schweitzer, and Dr. Alex Van Hook for their willingness to serve and their questions and comments. They were chosen because of their high standards and excellence.

I would like to thank the members of the Compton research group and others in the Chemistry Department for their support and friendship.

ABSTRACT

Any molecule with a dipole moment above approximately 2.5 Debye can form a stable negative ion (dipole-bound anion). These anions are best produced by "resonance" charge exchange from atoms in high Rydberg states (Rydberg electron transfer, RET). RET to form dipole-bound anions occurs over a narrow range of effective principle quantum number, n*. Dipole-bound anions for 32 molecules with dipole moments between 2.5 and 6.0 Debye have been studied. The excess electron in such an anion is very diffuse and weakly bound. Binding energies (electron affinities, EAs) are estimated from the narrow range of n* at which charge exchange occurs and also from measurements of the electric field required to detach the electron. Electron affinities range from less than ~1 milli electron volt (meV) to 100 meV. Factors other than dipole moment affect these electron affinities. These include polarizability, molecular shape, and dispersion interactions of the excess electron with the molecule. One of the molecules studied has for one of its conformations a possible quadrupole-bound negative ion state.

TABLE OF CONTENTS

LIST OF TABLES

LIST OF FIGURES

CHAPTER I

INTRODUCTION

Introduction

Negative ions (anions) are atoms, molecules, or clusters that possess a net negative charge. Anions can be created through many possible mechanisms, usually by the addition of one or more electrons into an empty or partially empty low-lying atomic or molecular orbital. Species which form a stable anion are said to possess a positive electron affinity (EA), also known as binding energy. The electron affinity is defined as the energy difference between the ground state of the neutral species and the ground state of the anion.

Experimentally, it is now known that most elements in the periodic table have stable ground state negative ion configurations, i.e. positive electron affinities. Notable exceptions are nitrogen, beryllium, magnesium, mercury, zinc, and the noble gases. The excess electron is added to the lowest unoccupied atomic orbital and for this reason electron affinities for the halogens (ns^2np^5 electron configuration) are quite large, on the order of 3.5 electron volts (eV). Figure 1.1 shows a comparison of the potential energy diagram for the hydrogen atom and for its negative ion. The Coulomb potential for the hydrogen atom supports an infinite number of bound states (Rydberg states). There is no Rydberg series for H^- due to the lack of a long range Coulomb potential. The electron affinity of H has been determined experimentally to be 0.75419 eV.[1,2] However, the hydrogen atom is the only atom whose electron affinity is better known from ab initio calculations than from experiment. Pekeris calculated its electron affinity to be

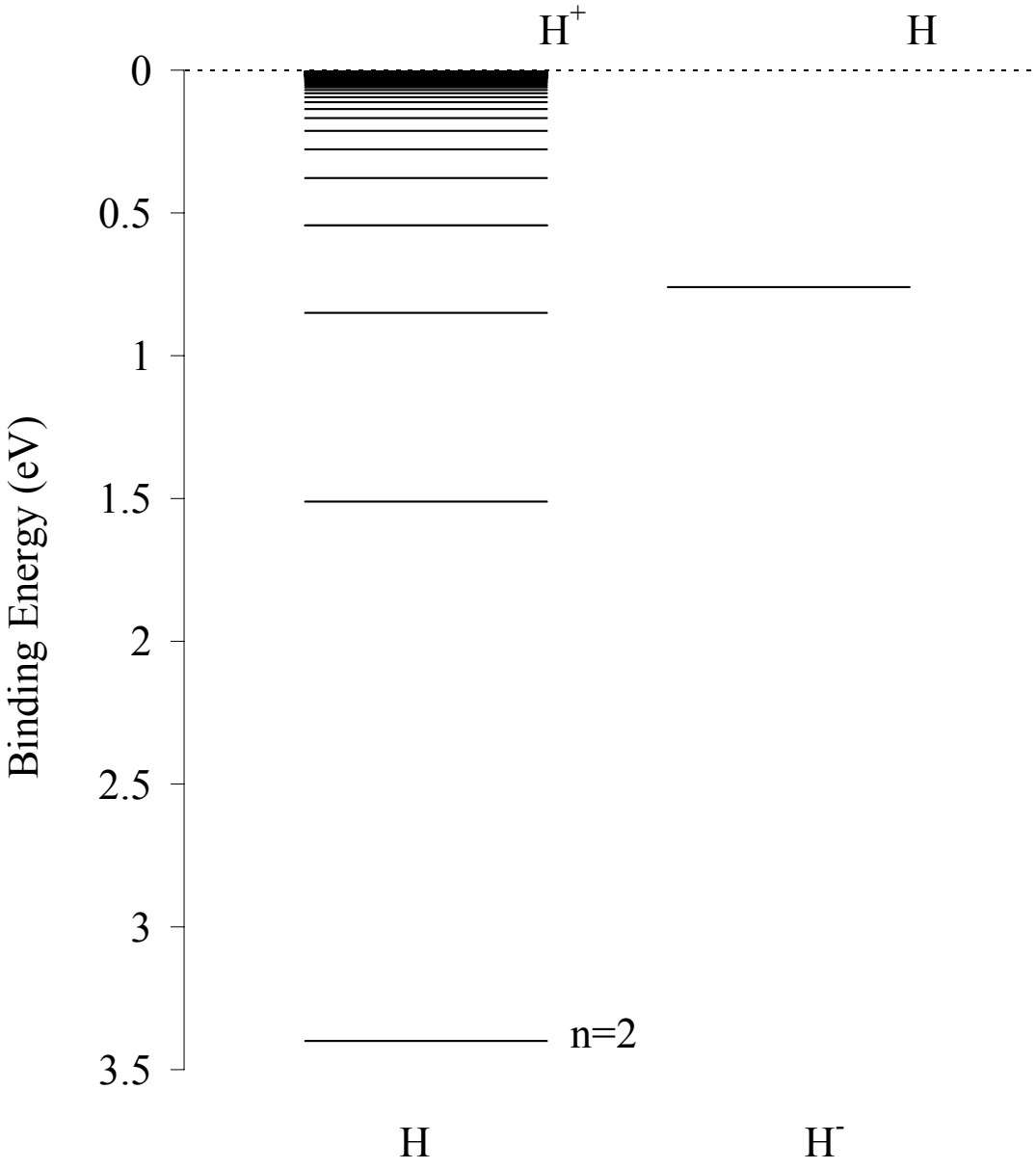

Figure 1.1 Potential energy states of atomic H and H^-. If plotted on the same energy range (vertically) H^- would appear 13.5984 eV lower.

0.7541753 eV.[3] There are many mechanisms for the creation of atomic negative ions and some of these are summarized in Table 1.1.[4-7]

Many molecules form what are termed valence-bound negative ion states with typical electron affinities between 0.01 and 4 eV. The excess electron is usually added to the lowest unoccupied molecular orbital (LUMO). Formation of valence-bound anions generally leads to increased distances between the nuclei (relaxation) and closer spacing in the vibrational energy levels. Even for the case of weak binding (e.g. NO has an electron affinity of ~0.02 eV) the electron exists in an orbital which is localized on the molecule. Shown in Figure 1.2 is a typical potential energy curve for a valence-bound molecular anion. As with atomic negative ions there are many possible mechanisms for the production of molecular anions. A number of these are also shown in Table 1.1.[4-8] Molecular anions that have energies higher than the ground state of the neutral can still be formed through excitation of the neutral. Such a case is shown in Figure 1.3 in which electron capture from AB to AB^- creates a short-lived state which can be stabilized by emitting a photon or by collisions with other molecules. If the anion is not stabilized within a short period of time the electron rapidly autodetaches.

Historical Perspective

In 1947, Fermi and Teller[9] were studying the problem of negative mesons (μ^-) in matter but ended up laying the groundwork for the theoretical treatment of dipole-bound anions. They predicted that an excess electron could be bound to a point dipole if the charge separation had a critical radius of $0.639a_o$, where a_o is the Bohr radius (5.29×10^{-11} m). This means that molecules that do not form valence-bound anions can possibly still form negative ions. Shortly thereafter Wightman[10] came to the same conclusion.

Table 1.1 Mechanisms for negative ion formation.

	Chemical Equation	Name
(a)	$e^- + A \rightarrow A^- + h\nu$	Radiative Attachment (atomic)
(b)	$e^- + AB \rightarrow AB^- + h\nu$	Radiative Attachment (molecular)
(c)	$e^- + AB \rightarrow A^+ + B^- + e^-$	Ion Pair Production
(d)	$e^- + AB \rightarrow A^- + B$	Dissociative Attachment
(e)	$e^- + AB \rightleftharpoons (AB^-)^*$	Temporary Nondissociative Attachment
(f)	$e^- + AB \rightleftharpoons (AB^-)^{**} \rightarrow AB^- + h\nu$	Dielectric Attachment
(g)	$e^- + A + B \rightarrow A^- + B$	Ternary Attachment
(h)	$A + B \rightarrow A^+ + B^-$	Charge Transfer
(i)	$A + B^- \rightarrow A^- + B$	Charge Transfer
(j)	$A + BC \rightarrow A^+ + B + C^-$	Dissociative Charge Transfer
(k)	$A + BC \rightarrow AB^+ + C^-$	Associative Charge Transfer
(l)	$AB + h\nu \rightarrow A^- + B^+$	Polar Dissociation

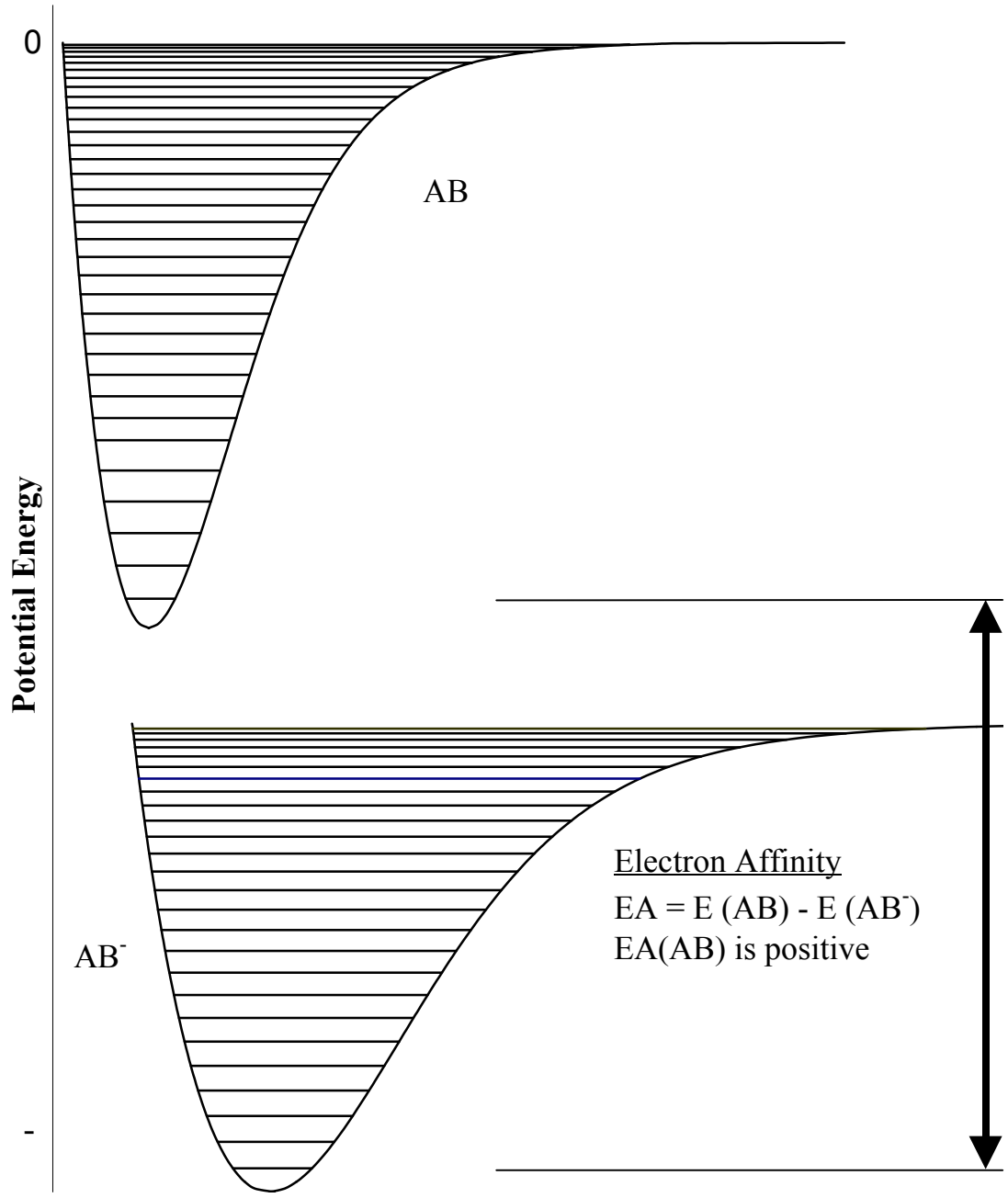

Figure 1.2 Potential energy curves for a neutral diatomic molecule and its valence-bound anion. The electron affinity is taken as the difference in energy of the two ground vibrational states.

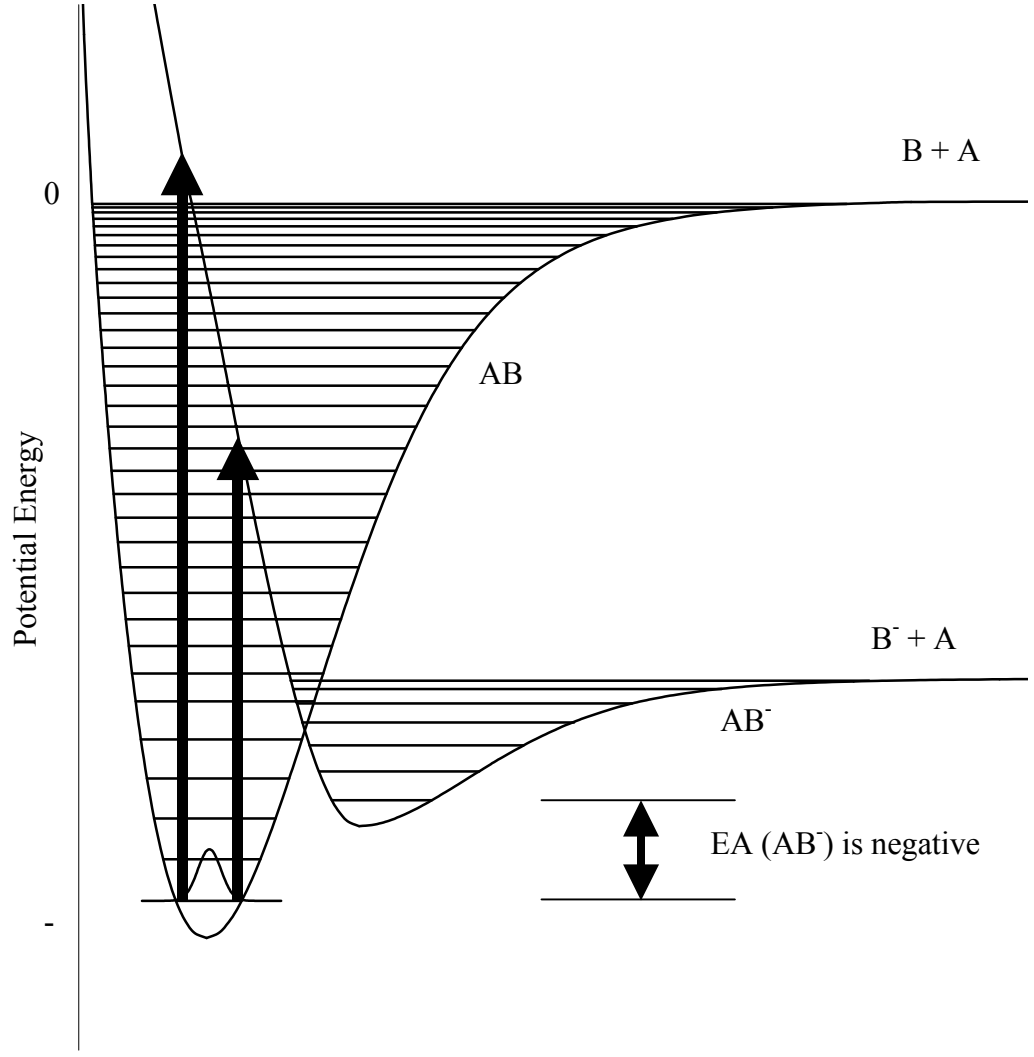

Figure 1.3 Potential energy curves for a neutral diatomic molecule and its valence-bound anion. In this case the anion lies higher in energy than the neutral.

Unaware of these calculations, a flurry of theoretical studies[11-14] in 1966-1967 converged on the minimum dipole moment ($D_{min} = 0.639a_o$ or 1.625 Debye) for electron binding to a stationary point dipole. An interesting account of the history of dipole-bound anions can be found in a paper by Turner.[15] Some authors attempted to calculate the electron affinity as a function of the dipole moment.[16,17] However, it was pointed out by Crawford and Garrett[18-27] that for a freely rotating dipole, the minimum dipole moment required to bind an excess electron depends upon the moment of inertia and the length of the dipole. Garrett further pointed out that the minimum dipole moment required for permanent binding increases with rotational quantum number. This last fact turns out to be very important in the creation and observation of dipole-bound anions. For a dipole-bound anion to be observed experimentally it must exist in a low-lying rotational state and this increases the critical dipole moment for a real, rotating molecule to be ~2.5 D.

The first experimental observation of a negative ion attributed to electron binding to a molecular dipole moment was in the early 1970's by Compton and Klots (ORNL).[28] The acetonitrile, CH_3CN, anion was produced by charge transfer from an excited Rydberg rare gas atom. The Rydberg excited rare gas atoms were produced by electron impact excitation. It was observed that CH_3CN did not attach slow free electrons and theoretical considerations indicated that CH_3CN should not exhibit a valence-bound anion state. From these observations, it was suggested that CH_3CN^- existed in a very diffuse state, much like that of a Rydberg state and that Rydberg charge exchange in this case was different from free-electron attachment in that the Rydberg electron gently changes centers-of-force from the ion to the dipole during the collision. It was suggested

that the acetonitrile anion and later the nitromethane, CH_3NO_2, anion were created as a result of their rather large dipole moments (3.92 and 3.46 Debye, respectively). Soon after, low-energy electron scattering experiments by Schulz[29] (Yale) and Linder[30] (Kaiserslautern) on polar molecules revealed resonances near zero energy. The molecules in these experiments had valence anionic states that had been excited to dipole-bound states which then soon removed the excess electron due to rotational and vibrational autodetachment. The contributions of the groups of Brauman[31-37] (Stanford) and Lineberger[38-44] (Colorado) were also very important in the late 1970's and 1980's in the development of the field of dipole-bound anions. A number of free radicals are known to exhibit both dipole-bound and more tightly bound valence anions. Very narrow resonance features were reported in the photodetachment spectrum corresponding to rotationally excited shape and Feshbach resonances for many of these dipole-bound radical anions.[5,38-44]

Starting in the late 1970's serious attempts at calculating energies of dipole-bound states began.[45-54] Of particular importance are Jordan and Wendoloski's[48] first nonempirical calculations on CH_3CN^- and Clary's study on photodetachment of electrons from dipole-bound anions.[54] Jordan and Wendoloski made use of the following expression for estimating the EA of the CH_3CN neutral molecule:

$$EA \approx \Delta E = E(neutral) - E(anion) \tag{1.1}$$

where E is the total quantum mechanical molecular energy. They calculated an EA of 0.1 meV (experiment gives 19 meV) and this laid the groundwork for most future calculations of EA for dipole-bound anions. Clary[54] developed a rotationally adiabatic theory which provides a theoretical framework for the description of weakly bound

anions with simple electrostatic pseudopotentials that is still the basis for describing dipole-bound anions today.

The early 1990's saw a number of key experiments performed in this field. The first unambiguous observation of dipole-bound states comes from the Bowen[55-58] group (Johns Hopkins) in 1990, who studied the important water dimer dipole-bound anion. The water monomer has a 1.854 D dipole moment which is insufficient to form a dipole-bound anion. The large dipole moment (~2.7 D) of the dimer will support a dipole-bound anion. The Bowen group has also used photodetachment photoelectron spectroscopy to determine electron affinities for a number of the molecules and clusters. In 1991 dipole-bound anions were produced by Hashemi and Ellenberger[59] through dissociative electron attachment to clusters such as $(CH_3CN)_n$. This confirmed the observations of CH_3CN^- in the early 1970's. In 1994 the group of Schermann[60] (Paris-Nord) provided direct evidence for dipole-bound anions in a series of elegant experiments showing a narrow *n* (principal quantum number) dependence in the Rydberg charge transfer rate with molecules having dipole moments above the critical dipole moment of ~2.5 D. Furthermore, this group used electric field detachment to demonstrate that these anions were weakly bound and that the wave function describing the extra electron is indeed very diffuse. The field detachment thresholds were used to determine electron affinities for many of the polar molecules studied. Soon after, the Johnson[61] group (Yale) produced dipole-bound anions from photodissociation of the iodine atom/acetone and iodine atom/acetonitrile neutral clusters. Since the mid 1990's there has been a steady increase in the experimental study of dipole-bound anions.[61-77]

In the mid 1990's, Adamowicz[78] (Arizona) performed an important theoretical study on CH_3CN calculating its EA to be approximately 6 meV. The model they used was based on the earlier work of Jordan and Wendoloski[48] but the result they obtained was a great improvement. Soon after, they used this model to calculate EA's for a number of additional molecules[79] and varying geometries of molecules[80] and compared them to experimental values with good success. Bartlett[81] (Florida) applied this same method for calculating EA to CH_3NO_2 in 1996 and found that the dipole-bound anion and valence-bound anion for this molecule are similar in energy at certain configurations and that the dipole-bound state can be converted into the valence-bound ground state. This was supported in the same year with experimental results[66] and re-examined recently.[82] In these studies the dipole-bound state is referred to as a "door-way" state to the more strongly bound valence-bound state. Electron affinities for many other dipole-bound systems have been studied in the same fashion over the past few years. [68,83-97] More recently, Wang and Jordan[98,99] have developed a Drude-model approach to calculating electron affinities. This method includes special treatment of polarization and dispersion effects and yields very good results with less computational requirements. Jordan and Wang[100] have recently written a review article on the theory of dipole-bound anions that summarizes recent approaches to electron affinity calculations.

Theoretical Background

The minimum dipole moment required to bind an electron is the E=0 solution to the Schrödinger Equation:

$$\hat{H}\Psi(r)=\left[-\frac{\hbar^2}{2m}\nabla^2+eq\left(\frac{1}{r_q}-\frac{1}{r_{-q}}\right)\right]\Psi(r)=E\Psi(r) \tag{1.2}$$

where ±q are fixed point charges separated by a distance R.[45,83] The quantities r_q and r_{-q} define the position of the electron with respect to the two point charges. The dipole moment of the system, μ, is qR. This leads to a minimum dipole moment of 1.625 D. Garrett[17,18] included the influence of rotations and obtained solutions to:

$$\left(\hat{H}_{rot}-\frac{\hbar^2}{2m}\nabla^2+V(r,s)\right)\Psi(r,s)=E\Psi(r,s) \tag{1.3}$$

where

$$\hat{H}_{rot}=\frac{\hbar^2}{2I}\hat{J}^2 \tag{1.4}$$

is the rotational operator, I is the moment of inertia, $\hat{J}^2$ is the operator of the square total angular momentum, and V(r,s) is the interaction potential of the electron charges. In this case r measures the position of the electron with respect to the center of the dipole and the distance between the charges is R=2s. Based on Garrett's results Crawford[19] concluded that the minimum dipole moment for any real, rotating molecule, required to bind an excess electron is approximately 2.5 D.

It has been shown by Garrett,[24,26] Clary,[54] and later Desfrançois[67] that weakly bound anions can be modeled theoretically with simple electrostatic pseudopotentials. The pseudopotential between an excess electron and a molecule can be expressed as:

$$V(r,\theta)=V_{\mu}(r,\theta)+V_{Q}(r,\theta)+V_{\alpha}(r,\theta) \tag{1.5}$$

where r and θ are the electron cylindrical coordinates with respect to the molecular symmetry axis. The respective dipolar, quadrupolar, and polarization potential terms can be taken as (in atomic units):

$$V_{\mu}(r,\theta) = \frac{-\mu\cos(\theta)}{r^2}\left[1-\exp\left(-\left(2r/\mu\right)^3\right)\right] \tag{1.6}$$

$$V_{Q}(r,\theta) = \frac{-Q\left(3\cos^2(\theta)-1\right)}{4r^3}\left[1-\exp\left(-\left(2r/\sqrt{|Q|}\right)^5\right)\right] \tag{1.7}$$

$$V_{\alpha}(r,\theta) = \frac{\alpha_{//}\cos^2(\theta)}{2r_{//}{}^4}\left[\left(\frac{r_{//}}{r}\right)^8-\left(\frac{r_{//}}{r}\right)^4\right]+\frac{\alpha_{\perp}\left(1-\cos^2(\theta)\right)}{2r_{\perp}{}^4}\left[\left(\frac{r_{\perp}}{r}\right)^8-\left(\frac{r_{\perp}}{r}\right)^4\right] \tag{1.8}$$

where μ is the dipole moment and Q is the electric quadrupole moment of the molecule. If the molecules studied are restricted to symmetric top molecules for which the dipole moment and the quadrupole moment are both held by the symmetry axis, the molecular polarizability can be separated into a component parallel to the symmetry axis $\alpha_{//}$ and two equal perpendicular components $\alpha_{\perp}$. The exponential term arises from close range interactions. Starting with these simple interaction potentials, energy levels, wave functions, and approximate values for dipole-bound electron affinities have been obtained.[67]

Most calculations of dipole-bound electron affinities, however, have been performed through the use of Equation 1.1, rather than finding the wave functions and energy levels of the anions. Since the excess electron is thought to exist in a diffuse state far from the molecule, additional basis sets can be included in a quantum mechanical ab initio calculation. The energy of the anion can be subtracted from the neutral and the result is the electron affinity. This works very well for methods that have a higher degree

of electron correlation and when using large basis sets augmented with diffuse molecular orbitals.

Dipole-bound anions are best created in resonance charge transfer reactions from excited Rydberg atoms. Since this is a resonance process the Rydberg states that yield negative ions of a particular molecule can be used to calculate its electron affinity. The ground and excited states of an atom are termed Rydberg states if the energy levels can be described as a quasi-hydrogenic one-electron atom and the energy levels relative to the ground state follow the familiar Rydberg formula:

$$E_{n,\ell} = IP_A - \frac{R_A}{n^{*2}} \tag{1.9}$$

where IP_A represents the ionization potential of the atom, R_A is the Rydberg constant for the atom and n^* is the effective principal quantum number where:

$$n^* = n - \delta_\ell \tag{1.10}$$

with δ_ℓ being the ℓ-dependent quantum defect. The various n and ℓ states can be obtained either by single or multi-photon laser excitation. Some important physical properties of Rydberg atoms are shown in Table 1.2. The interaction of a Rydberg atom and a polar molecule leading to dipole-bound anions has been described by avoided curve crossings between adiabatic neutral and ionic states.[63] Covalent potential curves, corresponding to neutral atoms in $n\ell$ Rydberg states plus neutral polar molecules, cross an ionic Coulombic diabatic curve corresponding to the ionized Rydberg atom plus the newly formed dipole-bound anion. Such a model is shown in Figure 1.4. It is assumed that the newly created anion is in the same molecular rovibrational internal state as its

Table 1.2 Selected properties of Rydberg atoms as a function of the effective principal quantum number, n^*. The ionization potential of the atom is designated as IP_A, a_o denotes the radius of the first Bohr radius, r_n is the mean radius, v_n is the rms velocity of the Rydberg electron, τ_n is the period for electronic motion, and E_{n^*} is the binding energy of the electron in the state n^*. Note that E_{n^*} is equal to $IP_A - E_{n,\ell}$.

Property	n-dependence	n^*=1	n^*=10	n^*=100
$\langle r_n \rangle$ (m)	$n^{*2}a_0$	5.3×10^{-11}	5.3×10^{-9}	5.3×10^{-7}
v_n (m/s)	v_0/n^*	2.2×10^{6}	2.2×10^{5}	2.2×10^{4}
τ_n (s)	$n^{*3}\tau_1$	1.5×10^{-16}	1.5×10^{-13}	1.5×10^{-10}
E_{n^*} (eV)	R_A/n^{*2}	$R_A = 13.6$	$R_A \times 10^{-2}$	$R_A \times 10^{-4}$

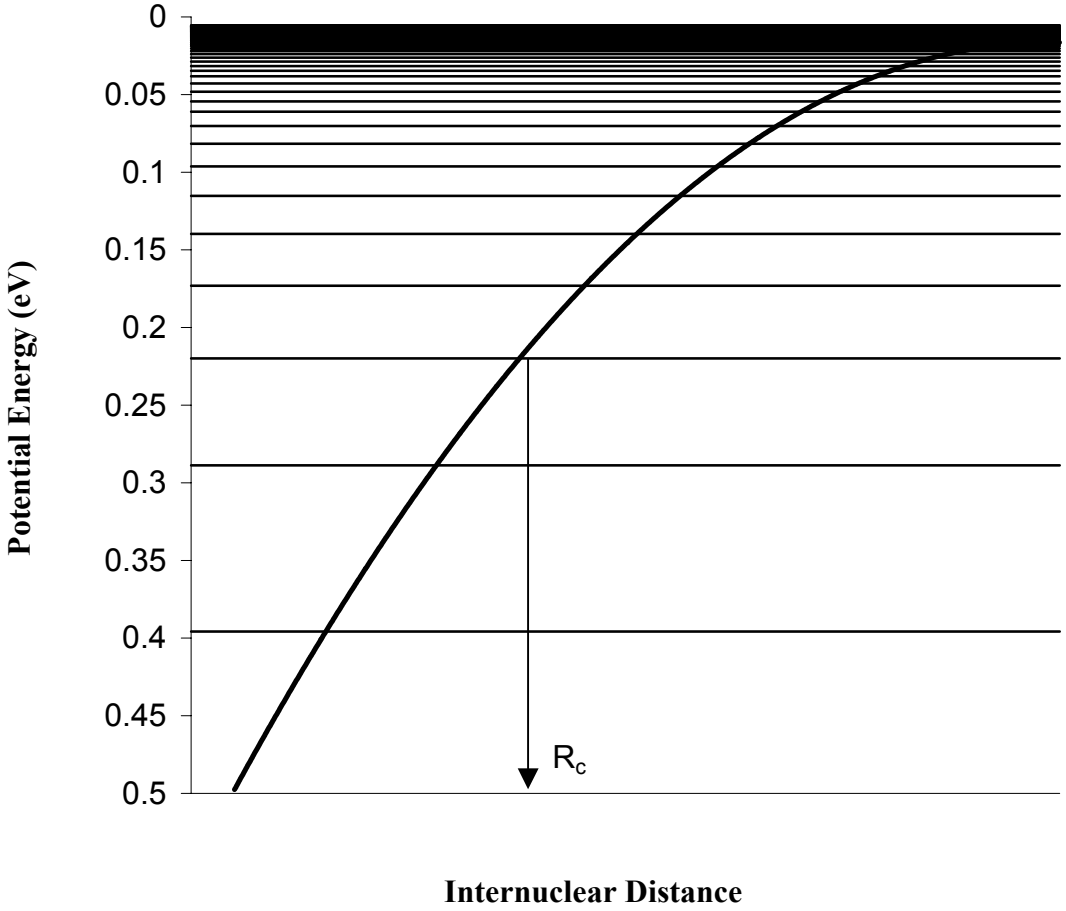

Figure 1.4 Curve-crossing model for the charge exchange process seen in the production of dipole-bound anions and other negative ions. Covalent potential curves corresponding to the neutrals cross an ionic potential curve corresponding to the ions as a function of distance, R. R_c is the crossing radius for a charge exchange energy.[55]

neutral parent since the excess electron is added to a very diffuse orbital on the positive side of the molecular dipole. At each avoided crossing the system can pass from one potential curve to the other with an adiabatic probability. It is possible to compute the total probability for ion- pair formation and the anion formation rate constant for various experimental conditions. Electron affinities can be obtained from this model and an empirical construct has been presented[63] that relates n^*_{max} and electron affinity:

$$EA = \frac{23\ eV}{n^{*2.8}_{\max}}. \tag{1.11}$$

The characteristic frequency of the electronic motion in the dipole-bound anion must be similar to the electron frequency in the Rydberg atom in order to favor the charge exchange process. Since there is most often only one dipole-bound anion state, the first frequency is approximately given by the electron affinity. On the other hand, in the Rydberg atom the electron frequency is approximately given by the difference between two successive Rydberg states, i.e. $2\ R_A/n^{*3}$. Equating these two frequencies leads to the relation EA ~ 27 eV/$n^*_{max}{}^3$, which is rather close to the above empirical law. However, this relation does not take into account the conditions under which the dipole-bound anion is created. It turns out that n^*_{max} depends slightly upon these conditions (i.e., ro-vibrational temperature and laboratory velocity). Nevertheless, this relationship represents a useful empirical relationship of the electron binding energy for dipole-bound anions.

Field detachment of dipole-bound anions is another more accurate method which has been employed to derive the electron affinity of polar molecules.[60,63] The process is

similar to that found in atomic field ionization. For atoms, the presence of an electric field modifies the atomic potential such that the electron experiences a potential:

$$V(r) = -\frac{e}{r} - Fr \tag{1.12}$$

where e is the charge on an electron, r is the distance of the electron from the core, and F is the magnitude of the external electric field. As the field is increased the effective ionization potential of the atom is lowered by:

$$V_{lowering} = -2(eF)^{1/2}. \tag{1.13}$$

The width of the barrier leading to ionization is sufficiently wide that electron tunneling ionization is long compared to normal ionization collection times in most mass spectrometers. Thus, the binding energy of the Rydberg state can be accurately determined from direct measurements of the field required to detach the electron. This is shown in Figure 1.5 for atomic rubidium. The case for field ionization of a dipole-bound or quadrupole-bound anion is very similar to that of the Rydberg atom case except that the potentials are now represented by, respectively:

$$V(r) = -\frac{\mu}{r^2} - Fr \tag{1.14}$$

$$V(r) = -\frac{Q}{r^3} - Fr \tag{1.15}$$

.

Similarly, the critical potentials for field detachment of dipole-bound and quadrupole-bound anions are:

$$V_{lowering,\ dipole} = -3\left(\frac{\mu E^2}{4}\right)^{1/3} \tag{1.16}$$

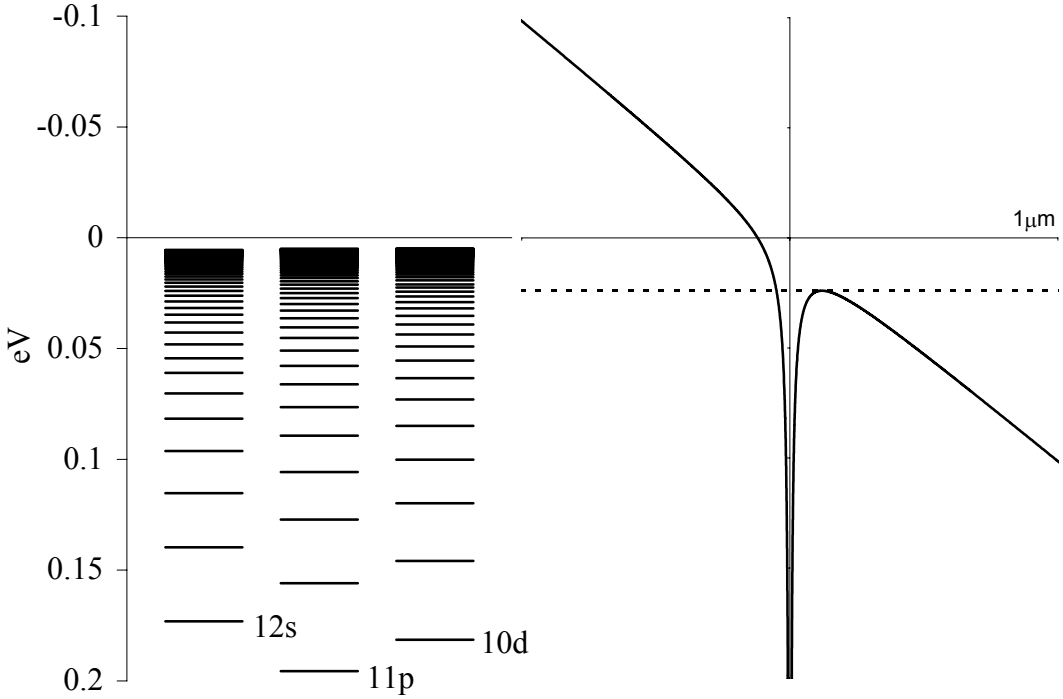

Figure 1.5 Electric field modified potential energy diagram for rubidium. The field in this example is 100000 V/m. Rydberg states with energy above this new effective potential escape over the barrier and those below can only tunnel through the potential barrier.

$$V_{lowering,\ quad} = -4\left(\frac{QE^3}{27}\right)^{1/4} . \tag{1.17}$$

This is shown for a dipole-bound anion in Figure 1.6. However, unlike the case for field ionization of atomic Rydberg states, tunneling through the narrow barrier now becomes important on the time scale of 10^{-6} seconds.[60,63] The fraction of anions left undetached at a particular electric field is given by:

$$f = e^{-\omega T} \tag{1.18}$$

where T is the time (all variables here are in atomic units) spent by the anion in the electric field and ω is given by:

$$\omega = \frac{N^2 F}{4\gamma^2} e^{-\left(\frac{2\gamma^3}{3F}\right)} \tag{1.19}$$

where N is the normalization constant for the dipole-bound anion radial wavefunction, F is the electric field, and γ is given by:

$$\gamma = \sqrt{2EA} \tag{1.20}$$

where EA is the electron affinity of the dipole-bound anion. If the electric field detachment occurs in the source region of a time of flight mass spectrometer it is straightforward to calculate the time elapsed as the anions are accelerated from rest to some final velocity. The time spent in the electric field F is given by:

$$T = \sqrt{\frac{2md}{F}} \tag{1.21}$$

where d is the acceleration distance. The time spent in the electric field is on the order of 300 to 1200 ns for most small molecules. Since f can be experimentally measured as a

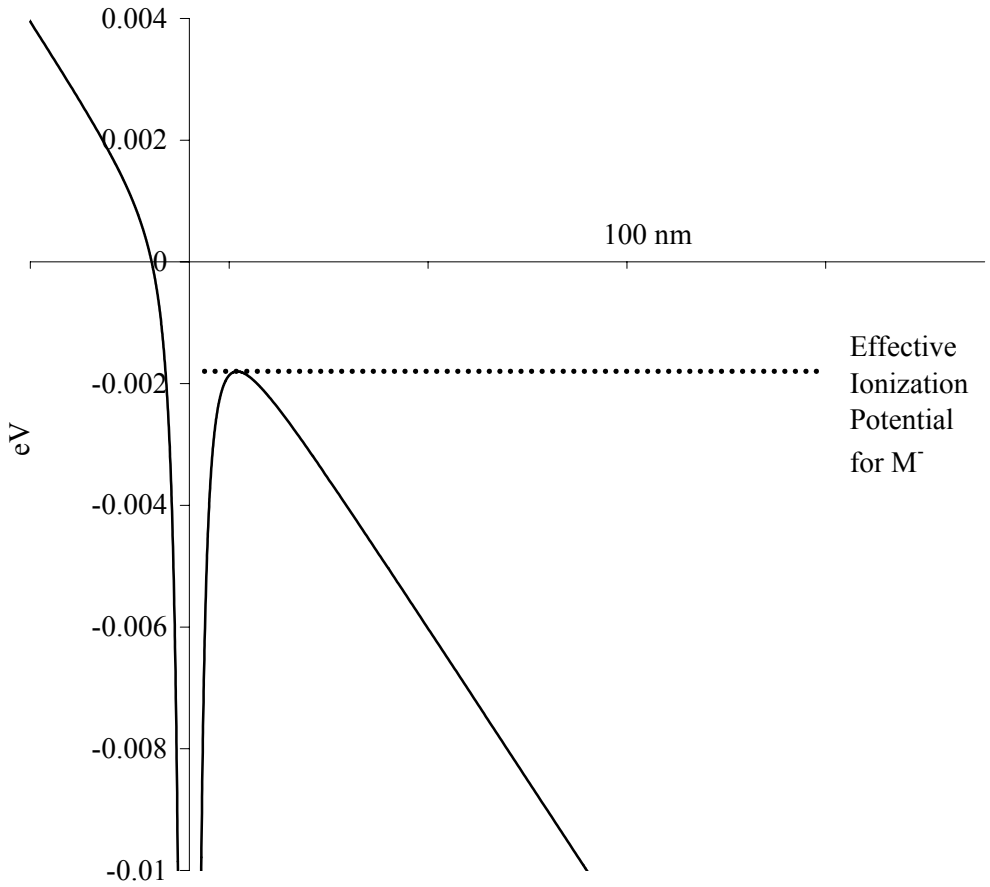

Figure 1.6 Electric field modified potential energy diagram for a dipole-bound anion. The field in this example is 100000 V/m. Tunneling becomes more of an issue when compared to the atomic case.

function of F, it is a straightforward matter to fit the curves to match γ, and therefore determine EA. It is important to point out that this method can only be applied to low electron affinity dipole-bound anions. The electric field required for electron detachment increases rapidly with increasing electron affinity and at some point becomes experimentally challenging.

CHAPTER II

EXPERIMENTAL SETUP

Introduction

The systematic study of dipole-bound anions has become experimentally possible in recent years due to advances in scientific equipment. High resolution tunable lasers that also have high power allow for the controlled creation of a large number of high Rydberg states. Supersonic pulsed valves are able to vibrationally and rotationally cool molecules to approximately 10 degrees Kelvin, which is vital to creating the weakest dipole-bound (and quadrupole-bound) anions. High resolution time-of-flight mass spectrometers allow for easy detection using microchannel plate electron multipliers and varied experimental conditions are possible with simple adjustments. In addition, the use of fast digital oscilloscopes and computer data acquisition programs have greatly increased the speed of data visualization and manipulation, allowing for real-time experimental adjustments. The experimental results presented here were obtained using the apparatus shown in Figure 2.1. The various components and experimental conditions are described below.

Rydberg Atom Source: Rubidium

Atomic rubidium (Rb, 72% mass 85, 28% mass 87) was used as the source of Rydberg atoms in the experiments performed here. Previous studies have primarily used rare gas atoms such as Xe as the Rydberg atom source. Rubidium has a low melting point (38.89 °C) and a high vapor pressure and when heated to ~150-175°C a fairly dense atom beam is created that can easily be excited using a laser. Another attractive feature about using rubidium for these experiments is that its ionization limit (593.65 nm) and

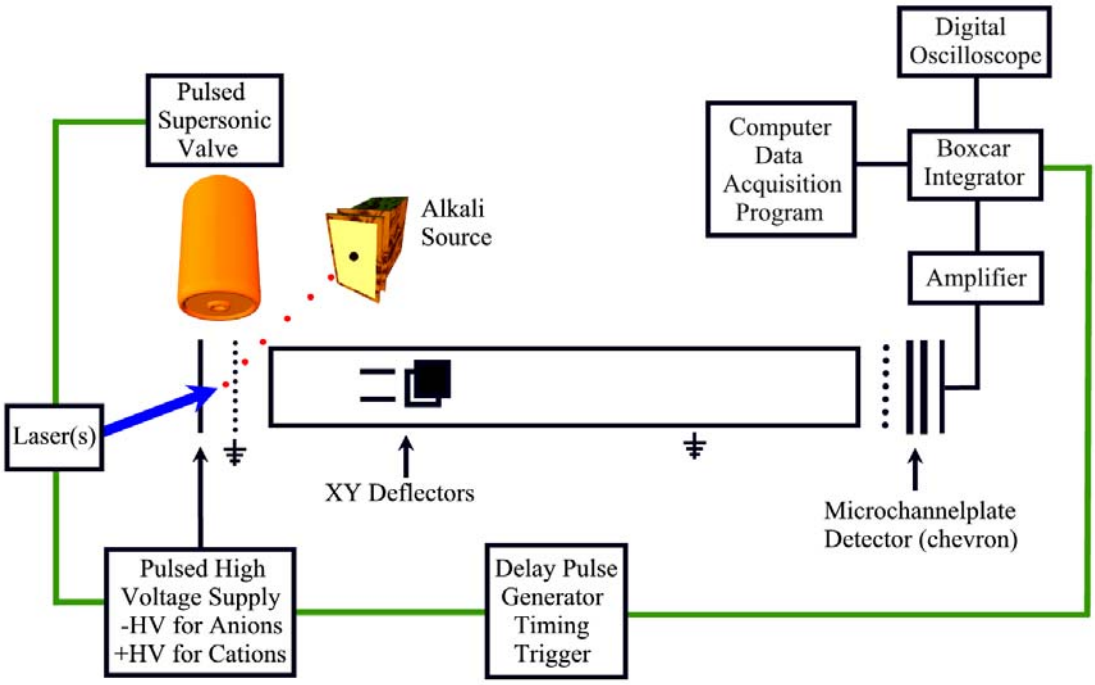

Figure 2.1 Experiment setup for the creation of dipole-bound anions.

high Rydberg states are in the yellow/orange region of the visible spectrum using one-color, two-photon laser excitation. This allows for easier experimental alignment of the beams and a more eye-safe research environment. Two-color, two-photon laser excitation is also easily achieved with rubidium. Since the excitation involves two photons the $ns\ ^2S_{1/2}$ and $nd\ ^2D_{5/2,3/2}$ Rydberg levels are produced. An atomic energy level diagram for rubidium with one- and two-color excitation schemes is showed in Figure 2.2 (also see Figure 1.5). Shown in Table 2.1 are the one-color two-photon transition wavelengths to high $ns\ ^2S_{1/2}$ and $nd\ ^2D_{5/2,3/2}$ Rydberg states. Similarly, shown in Table 2.2 are the two-color two-photon transition wavelengths for the second photon to high $ns\ ^2S_{1/2}$ and $nd\ ^2D_{5/2,3/2}$ Rydberg states using the $5p\ ^2P_{3/2}$ state as an intermediate. The transition energies were taken from *Atomic Energy Levels*.[101] States not listed were calculated using Equation 1.9. An alkali oven was utilized that accommodated a small glass ampoule (1 gram) of rubidium. The rubidium was obtained from Strem Chemicals. It was determined through the course of the experiments that the samples were contaminated with a small amount of cesium. The alkali oven had a small hole that faced the interaction region, which was 0.3 meters away. The oven was heated by resistive heating of two tungsten wires, which were wound throughout the oven and contained in quartz tubing. For heating up the rubidium to 150^{o}C, 10 Volts was applied for 20 minutes on one wire (1.1 Ohms resistance) using a Kepco KS Regulated DC Supply and then 5 Volts was applied to maintain the temperature. The second wire (9.5 Ohms resistance) required 20 Volts for heating using a Power/Mate Corp. Regulated Power Supply and 8 Volts was used to maintain a stable temperature. When heated, a beam of

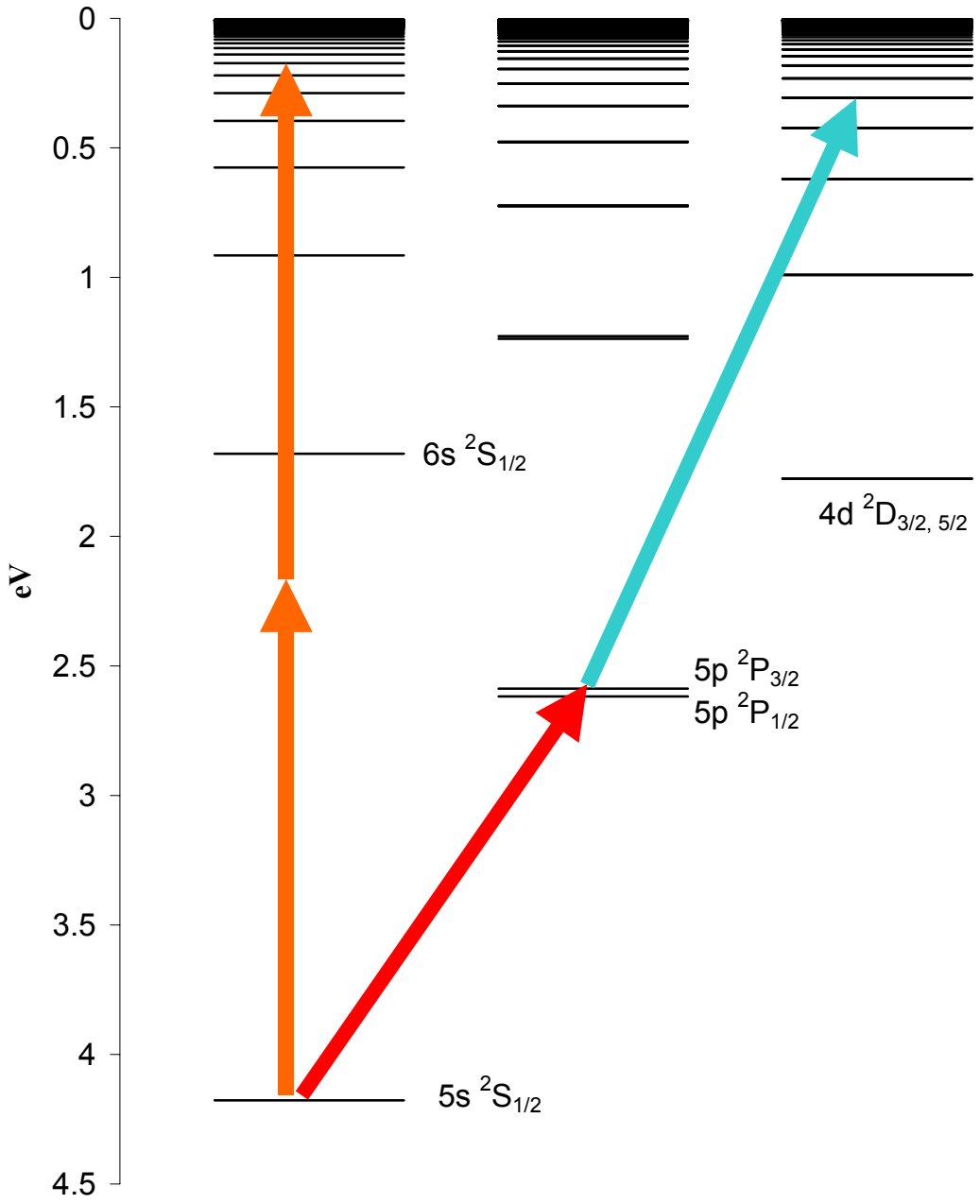

Figure 2.2 Schemes for one- and two-color laser excitation of atomic rubidium.

Table 2.1 One-color two-photon vacuum transition wavelengths to high *ns* $^2S_{1/2}$ and *nd* $^2D_{5/2,3/2}$ Rydberg states of rubidium. Above *nd* = 13 the $^2D_{5/2}$ and $^2D_{3/2}$ states were not resolved.

#s	2 photon λ	#d	2 photon λ	#s	2 photon λ	#d	2 photon λ
50	594.5135	48	594.5222	23	598.5707	21	598.6794
49	594.5515	47	594.5627	22	599.0769	20	599.2438
48	594.5952	46	594.6040	21	599.7394	19	599.9016
47	594.6376	45	594.6500	20	600.5182	18	600.6857
46	594.6871	44	594.6981	19	601.4319	17	601.6082
45	594.7384	43	594.7504	18	602.3872	16	602.7722
44	594.7941	42	594.8060	17	603.7512	15	604.1860
43	594.8553	41	594.8663	16	605.4262	14	605.9534
42	594.9148	40	594.9311	15	607.5934	13 3/2	608.2131
41	594.9861	39	595.0012			13 5/2	608.2094
40	595.0594	38	595.0773	14	610.4402	12 3/2	611.1595
39	595.1449	37	595.1596			12 5/2	611.1549
38	595.2280	36	595.2484	13	614.1363	11 3/2	615.1077
37	595.3263	35	595.3474			11 5/2	615.1020
36	595.4314	34	595.4531	12	619.2901	10 3/2	620.5845
35	595.5447	33	595.5712			10 5/2	620.5753
34	595.6529	32	595.6980	11	626.6204	9 3/2	628.4984
33	595.8109	31	595.8419			9 5/2	628.4846
32	595.9618	30	596.0005	10	637.7071	8 3/2	640.5848
31	596.0953	29	596.1732			8 5/2	640.5641
30	596.2827	28	596.3758	9	655.7579	7 3/2	660.4981
29	596.4970	27	596.6407			7 5/2	660.4651
28	596.7408	26	596.8350	8	688.5430	6 3/2	697.1763
27	597.0191	25	597.1076			6 5/2	697.1213
26	597.3382	24	597.4251	7	760.1250	5 3/2	778.1932
25	597.7057	23	597.7812			5 5/2	778.1035
24	598.1312	22	598.1956	6	993.3643	4 5/2	1033.3242
						4 3/2	1033.3007

Table 2.2 Two-color two-photon vacuum transition wavelengths for the second photon to high *ns* $^2S_{1/2}$ and *nd* $^2D_{5/2,3/2}$ Rydberg states using the *5p* $^2P_{3/2}$ state as an intermediate. Above *nd* = 13 the $^2D_{5/2}$ and $^2D_{3/2}$ states were not resolved.

#s	1 photon λ	#d	1 photon λ	#s	1 photon λ	#d	1 photon λ
50	480.1492	48	480.2174	23	485.5109	21	485.6656
49	480.1988	47	480.2703	22	486.1773	20	486.4088
48	480.2557	46	480.3242	21	487.0506	19	487.2762
47	480.3111	45	480.3842	20	488.0786	18	488.3118
46	480.3757	44	480.4470	19	489.2870	17	489.5321
45	480.4426	43	480.5153	18	490.5527	16	491.0754
44	480.5154	42	480.5879	17	492.3644	15	492.9549
43	480.5953	41	480.6666	16	494.5963	14	495.3124
42	480.6729	40	480.7512	15	497.4956	13 3/2	498.3393
41	480.7660	39	480.8427			13 5/2	498.3343
40	480.8617	38	480.9422	14	501.3241	12 3/2	502.3076
39	480.9735	37	481.0498			12 5/2	502.3013
38	481.0820	36	481.1657	13	506.3293	11 3/2	507.6639
37	481.2105	35	481.2952			11 5/2	507.6562
36	481.3478	34	481.4333	12	513.3241	10 3/2	515.1686
35	481.4960	33	481.5877			10 5/2	515.1559
34	481.6374	32	481.7536	11	523.4764	9 3/2	526.1685
33	481.8440	31	481.9419			9 5/2	526.1491
32	482.0414	30	482.1494	10	539.1377	8 3/2	543.3333
31	482.2620	29	482.3754			8 5/2	543.3035
30	482.5075	28	482.6409	9	565.4578	7 3/2	572.6190
29	482.7882	27	482.9880			7 5/2	572.5695
28	483.1076	26	483.2426	8	616.0488	6 3/2	630.0963
27	483.4725	25	483.6002			6 5/2	630.0066
26	483.8912	24	484.0168	7	740.9087	5 3/2	776.1565
25	484.3738	23	484.4844			5 5/2	775.9782
24	484.9328	22	485.0291	6	1366.3599	4 5/2	1529.4145
						4 3/2	1529.3115

atomic rubidium passed through the exit hole of the oven and directly into the interaction region (see Figure 2.1).

Laser System

The use of lasers was integral to the studies presented here. Various pulsed lasers were used to excite the rubidium atoms to various high Rydberg states. In early experiments, an Optical Parametric Oscillator (OPO) laser was used to excite rubidium atoms via one-color, two-photon excitation. The properties of the dipole-bound anions studied were deduced (n^* range) using this excitation scheme. In later experiments, two dye lasers (two-color, two-photon excitation) gave a much larger yield of anions for other experiments such as field detachment studies and reactions of dipole-bound anions. In all experiments the laser beam(s) intersected the rubidium collinearly (head on) in the reaction chamber (see Figure 2.1).

Over the past decade OPO lasers have become very popular tunable lasers. Two Continuum OPO lasers, the *Mirage* and *Sunlite*, were used in this study. A Nd:YAG (Neodymium-doped yttrium-aluminum-garnet) laser, in both cases a Continuum *Powerlite* model, pumped each OPO. The lasers were pulsed at 10 Hz with ~10ns pulsewidths. The *Mirage* required both the second (532 nm) and third (355 nm) harmonic of the Nd:YAG (fundamental 1064 nm) as pump lasers, whereas the *Sunlite* only required the third harmonic. OPO lasers utilize the optical parametric process, which is a three-photon process. A pump photon interacts with a nonlinear medium which splits the beam into two less energetic photons, known as the signal and idler. The sum of the frequencies of the signal and the idler must equal the original pump frequency. Mathematically, this is expressed as:

$$\omega(pump) = \omega(signal) + \omega(idler). \tag{2.1}$$

A nonlinear birefringent crystal, potassium titanyl phosphate (KTP), is used to split the frequencies because a particular angle can be found with this material in which refractive indices of the crystal allow conservation of momentum. For a given pump frequency numerous frequency pairs can meet the energy conservation condition. It is the momentum conservation, or phase matching, that governs the process to yield a specific frequency pair:

$$k_p = k_s + k_i . \tag{2.2}$$

The magnitude of the *k* vector depends on refractive index and by simply adjusting the angle of the crystal with respect to the polarization of the pump laser, a wide range of output frequencies can be obtained that satisfy this phase-matching condition. Both lasers use Optical Parametric Amplification (OPA) crystals as well to amplify the resulting signal or idler. The *Mirage* has a tuning range of 425 nm to 2120 nm, whereas the *Sunlite* has a range of 225 nm to 1680 nm. The yellow/orange region (590 – 620 nm) of both lasers was used for one-color, two-photon excitation of the rubidium atomic beam to high $ns\ ^2S_{1/2}$ and $nd\ ^2D_{5/2,3/2}$ Rydberg states for dipole-bound anion creation and also for one-color, three-photon ionization of rubidium. The *Sunlite* was easier to scan over large wavelength regions in a short period of time, whereas the *Mirage* has a higher resolution (0.02 cm^{-1} compared to 0.1 cm^{-1} for the *Sunlite*) and higher peak power over narrow (~2 nm) wavelength regions. For two-color, two-photon excitation, the blue region (480 – 500 nm) of both lasers was used for the second photon, although dye lasers were used for both photons in later experiments which required higher peak power.

In order to produce two-color, two-photon excitation of rubidium, one or two Quanta Ray PDL-2 dye lasers were employed. A dye laser employs an organic dye molecule dissolved in a solvent that is excited by a pump laser, in this case either the second or third harmonic of the *Powerlite* Nd:YAG. The dye lases and a new frequency emerges from the dye cell. Due to the high pump power the dye is circulated by a mechanical pump. Dye lasers produce a broad range of colors over a defined wavelength range, but different dyes are needed for different parts of the spectrum. Most dyes fluoresce in the visible part of the electromagnetic spectrum and these lasers were the tunable lasers of choice for a number of years. Whereas easy tuning over a specific wavelength range with high power are readily achieved with dye lasers, the necessity for replacing the dye to change to another part of the spectrum and degradation of the dye (sometimes within a single day of experiments) makes the OPO more attractive to many modern-day experimentalists. In the studies presented here one dye laser was used to pump the $5p\ ^2P_{3/2}$ state of rubidium and either an OPO or in later experiments another dye laser was used to excite the rubidium to high $ns\ ^2S_{1/2}$ and $nd\ ^2D_{5/2,3/2}$ Rydberg levels. For the dye laser pumping the $5p\ ^2P_{3/2}$ state the LDS 765 laser dye was employed and the LD 490 laser dye was used to pump high Rydberg states. Both dyes were acquired from Exciton, Inc. and were dissolved in methanol.

Pulse Generator and Timing

Timing of the sequence of events, especially when the laser fired, was critical to the creation of dipole-bound anions. A Stanford Research Systems (SRS) DG535 delay pulse generator was used to trigger in sequence the supersonic pulsed valve opening and

the laser(s) firing (Q-Switch firing). The pulse generator triggered the pulsed high voltage power supply at the same time as the laser but an internal delay was set in the power supply such that the high voltage pulse was applied 2 μs after the laser fired. Using helium as the expansion (seed) gas, the supersonic pulsed valve opening was triggered 140 μs prior to the laser Q-Switch firing in order to maximize dipole-bound anion creation. This delay was varied with expansion gas due to the fact that different gases travel at different velocities. The velocity of the gas was approximately the speed of sound for each gas. A representation of the timing sequence is shown in Figure 2.3.

Supersonic Pulsed Valve

Pulsed valves are able to create supersonic molecular beams that are vibrationally ($\theta_v \approx 30$ K), rotationally ($\theta_v \approx 3$ K), and translationally ($\theta_T \approx 1$ K) very cold.[102,103] Fite[102] has shown that for an adiabatic expansion at constant entropy the following relation holds true:

$$\frac{1}{2}mv^2 + c_P T = CONSTANT \tag{2.3}$$

where m is the molecular mass, v is the velocity of the molecule, c_P is the specific heat capacity of the gas at constant pressure, and T is the temperature. The pressure in the reaction chamber is essentially a vacuum (10^{-8}– 10^{-7} torr), whereas the pressure in the pulsed valve can vary from a few hundred torr to a couple of atmospheres. When the valve is set to open a large current (up to 5000 Amps) is passed along parallel conductors. This creates a large magnetic force that lifts a plug that had been sealing a small hole in the valve that leads to the vacuum chamber. Whatever gas mixture is in the valve is then expelled at supersonic speeds (relative to velocity of the pure compound) through the

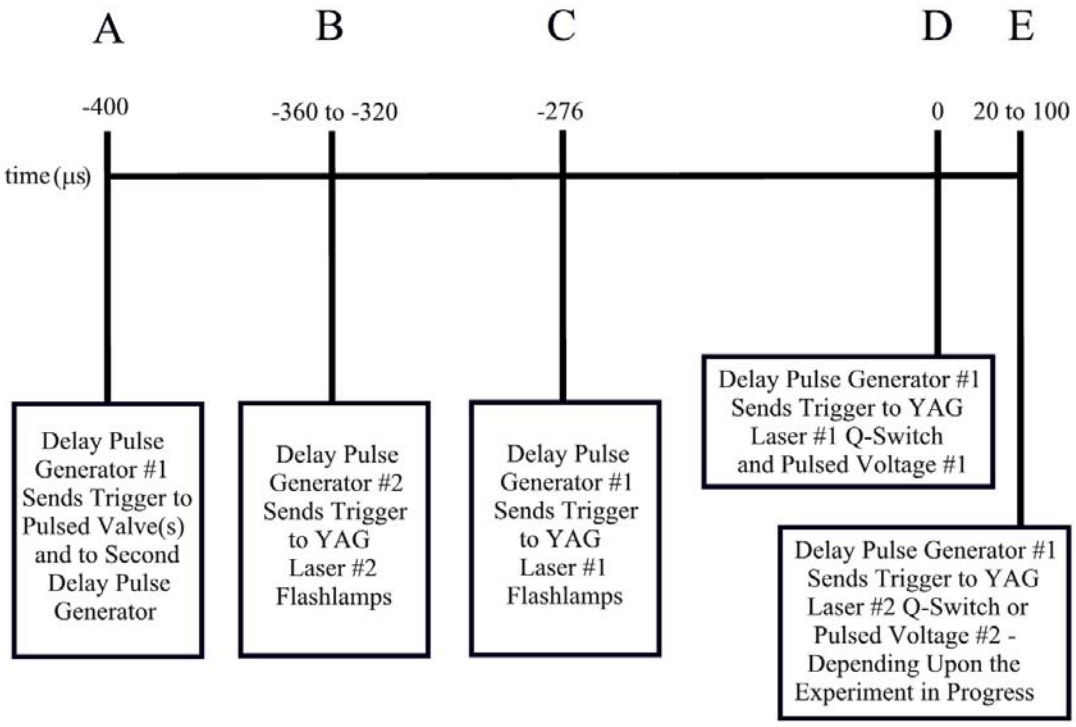

Figure 2.3 Timing sequence for the production of dipole-bound anions.

small opening into a vacuum chamber. The valve is open for approximately 60 μs. The amount of gas that is expelled is very low, usually on the order of 10^{-4} torr along the beam and only 10^{-6} torr in the chamber. Fite has noted that if T_s is the temperature of the gas prior to the valve opening, Equation 2.3 now is equal to $c_p T_s$. Using Relation 2.3 and standard thermodynamic relations for an adiabatic expansion, the temperature, T, of the expelled gas is:

$$T = \frac{T_s}{1 + \frac{\gamma - 1}{2} M^2} \tag{2.4}$$

where γ is the ratio of molar specific heat capacities, $c_p/c_v = 5/3$ for an ideal monatomic gas, and M is the Mach number of the expanded gas. The Mach number for a gas expanding into a vacuum through a small opening can be approximated by:

$$M \approx \left(\frac{\gamma + 1}{\gamma - 1}\right)^{\frac{\gamma+1}{4}} \left(\frac{z}{D}\right)^{\gamma - 1} \tag{2.5}$$

where z is the distance from the opening and D is the opening diameter. When molecules under study are entrained in a carrier gas (usually an inert gas) the velocity of the molecules can be approximated by the velocity of the carrier gas. There is some degree of slippage (i.e. the molecules cannot maintain the velocity of the carrier gas), but for the most part the velocity (and thus the amount of cooling) of the molecules under study can be taken as the velocity of the carrier gas.

For the results reported herein, an RM Jordan PSV Pulsed Supersonic Valve (model C-211) was used to introduce the polar molecules under study to the reaction chamber. The molecules were entrained (seeded) in various carrier gases (H_2, He, Ne,

Ar, Kr, Xe). The apparatus (Figure 2.1) employed a supersonic pulsed valve positioned directly above the interaction region. The molecular beam intersected both the laser and rubidium atomic beam perpendicularly. This allowed for the dependence of reaction velocity and cooling of the molecular beam to be studied.

Time of Flight Mass Spectrometer

A time of flight mass spectrometer was employed in these studies for the mass analysis of negative ions. The kinetic energy of a moving particle is given by:

$$E = \frac{1}{2}mv^2 \tag{2.6}$$

where m is the particle mass and v is its velocity. Assuming instantaneous acceleration, for two particles of different mass it can be shown using Equation 2.6 that:

$$m_1 \cdot t_2^2 = m_2 \cdot t_1^2 \tag{2.7}$$

where m_1 and m_2 are the masses and t_1 and t_2 are the times of flight for the two particles. However, the time of acceleration also depends upon the mass of the particles. If $2x$ is the distance between the backing (acceleration) plate and a grounded grid and anions are created halfway in between the following relation holds true that relates the acceleration to the electric field E:

$$m\ddot{x} = eE \tag{2.8}$$

where e is the unit charge of an electron and the second derivative of x with respect to time, t, is the acceleration. Upon integration (twice) and solving for time one gets:

$$t = \sqrt{\frac{2mx}{eE}} \tag{2.9}$$

which is equivalent to Equation 1.21 when using atomic units. This is a small correction for most molecules.

A high voltage pulsed power supply (Avtech model AVRH-3-B) was employed in these studies (see Figure 2.1) to extract the dipole-bound anions into the time of flight mass spectrometer. The maximum output of the power supply was ±3000 V. Both the pulsed power supply and a dc power supply were used in early experiments probing the high Rydberg states of rubidium. The high voltage pulsed power supply also served to field detach atomic rubidium and dipole-bound anions. The spacing between the stainless steel backing plate and a grounded grid was varied from 0.6 cm to 1.5 cm. This allowed for a maximum electric field of 5000 V/cm. It was empirically found that larger distances yielded more anions. The flight tube was grounded and the anions passed through a grounded grid and into the detector assembly (see below). Horizontal and vertical deflectors (xy deflectors) were used to maximize negative ion detection. Since the molecules have an initial downward velocity greater voltages were needed on the y deflectors. The voltage needed varied with both seed gas and pulsed high voltage.

Detector Assembly

The detector assembly was designed upon the use of microchannel plate electron multipliers. A microchannel plate is an array of miniature electron multipliers (channels) oriented parallel to one another on a lead oxide glass plate. When light or particles hit the microchannel plates secondary electrons are created that create more secondary electrons and these electrons travel through the channels creating even more secondary electrons. Eventually these electrons hit a metal plate. The current that is created is turned into a voltage that is recorded. The microchannels are set at an angle so that there is a reduction

in backward reflection of ions. The microchannel plates were chevron mounted, which means that there were two microchannel plates mounted back to back. In later experiments the microchannel plates used were z-stack mounted, which means that there were three microchannel plates mounted back to back to back. This stacking of microchannel plates gives a much greater enhancement of signal. The gain in signal per microchannel plate is approximately 10^4. Shown in Figure 2.4 is a schematic for the detector assembly used in later experiments (z-stack). The earlier detector assembly was identical except that it employed only two microchannel plates instead of three and the detector plate was split into two outputs, one in the center and a larger ring surrounding it. Approximately 1000 volts are applied across each microchannel plate and each plate has an impedance of approximately 95 MΩ. Other resistors are employed to bias the detecting plate and the input grid for maximum efficiency. A capacitor is used so that only pulsed current is allowed to pass to the data recording instruments.

Data Acquisition

Due to the low signal intensity of many of the species studied, prior to recording positive or negative ion data from the detector assembly the raw signal was amplified and integrated. An Ortec 474 Timing Filter Amplifier was used to both increase the signal intensity and also integrate the signal for a period of time (usually 20 ns). An SRS Gated Integrator and Boxcar Averager SR 250 was employed to gate the signal (so that only the voltage corresponding to the negative or positive ion of interest was recorded) and average a certain number of voltage pulses (shots). For typical wavelength scans 10 shots were averaged, but for high resolution scans and field detachment measurements 30 shots were averaged. The raw data was visualized on an Agilent Technologies Infinium

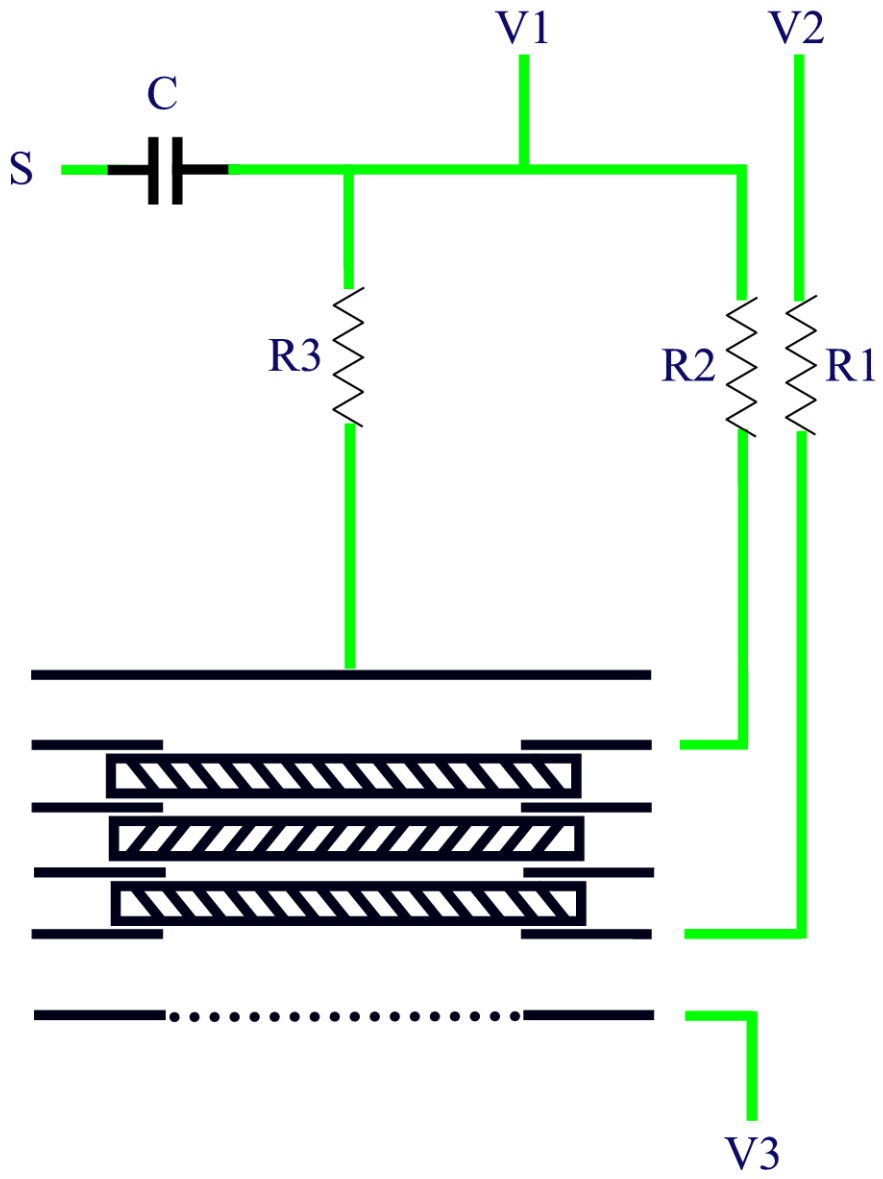

Figure 2.4 Time-of-flight mass spectrometer channel plate multiplier detector assembly (z-stack configuration). The ions enter through the grid at the bottom of the drawing. A voltage (V3) can be applied to this grid. Other voltages are applied at V1 and V2. The ions impact the channel plate multipliers and secondary electrons are created that are amplified further. These eventually impact the detecting plate. Resistors (R1, R2, and R3) and are placed throughout. A capacitor (C) is used so that only pulsed voltages are detected at S.

Digital Oscilloscope model 54810A. A typical time of flight screenshot from the oscilloscope and corresponding mass spectrum are shown in Figure 2.5. Gated voltage readings were sent to a computer acquisition card and then read by a data acquisition computer program on a PC written in *Labview*. The computer program was written as an improvement to earlier code written in *Visual Basic* which did not allow for easy real time visualization of data. An important feature of the *Labview* program is that it could start the *Sunlite* OPO laser wavelength scanning and start taking data at the same time. For the *Mirage* OPO and dye lasers is was easy to start scanning and taking data both at the same time since the computer was right next to the laser scan controls. The most important feature of the *Labview* data acquisition program was its ability to display real time data visually as it was being taken. If there were something wrong with the data run it could be stopped and restarted without wasting time. This was very important since some wavelength scans took up to two hours such as studies of high Rydberg states requiring high resolution or scans over large wavelength ranges. A screenshot of the data acquisition program is shown in Figure 2.6.

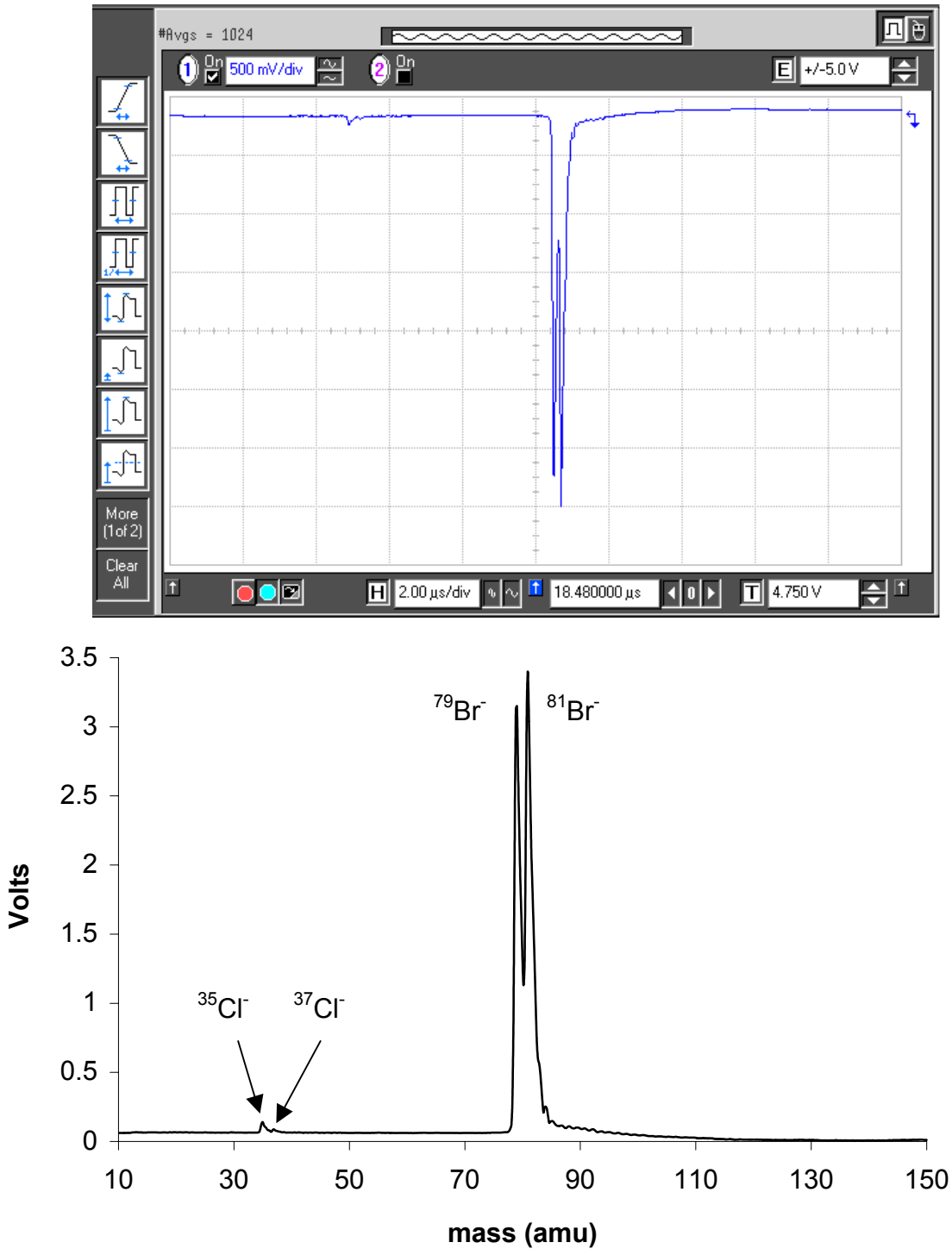

Figure 2.5 Oscilloscope screenshot (top) and resulting mass spectrum (bottom) for the dissociative electron attachment of CHBrClF. The anions created are Cl^- and Br^-.

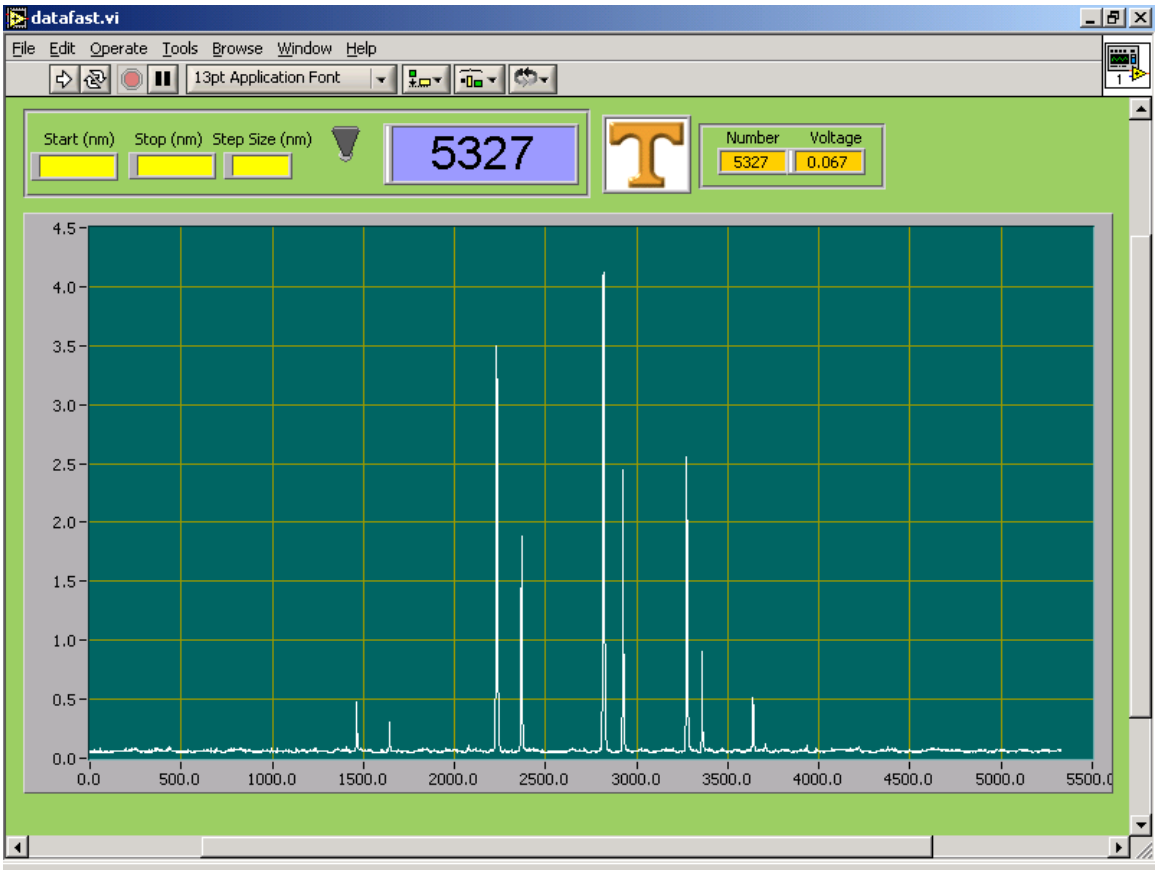

Figure 2.6 Screenshot of the data acquisition program employed in the studies presented here. The program was created using *Labview*. Voltages from the boxcar integrator were acquired approximately three times per second. The data was later plotted as a function of wavelength. Shown here is data for acetonitrile. See Appendix B for a plot of anion intensity as a function of wavelength for this molecule.

CHAPTER III

RYDBERG ELECTRON TRANSFER REACTIONS

Introduction

Rydberg electron transfer (RET) has proven to be a reliable method for creating dipole-bound anions.[57,60,65,73-77] In this method an atom is excited with a laser to various Rydberg states. If the conditions are right, an electron will transfer to the molecule of interest, which is already in the interaction region. In the experiments described here rubidium was chosen as the electron source for creating dipole-bound negative ions. This is because with two photons rubidium can be easily excited to high *ns* $^2S_{1/2}$ and *nd* $^2D_{5/2,3/2}$ Rydberg levels. Many factors influence RET reactions and the resulting negative ion spectra.[75,104] The collision of a Rydberg atom and a molecule can have a range of possible outcomes.[105] These are summarized in Table 3.1. Photoionization of the Rydberg atom prior to electron transfer and collisional detachment of the electron from either the Rydberg atom or the resulting negative ion are perhaps the two most important considerations. Reaction conditions (velocity of the Rydberg atom and molecular beam) and the degree of vibrational cooling of the neutral molecule also play an important role in low electron affinity dipole-bound anions.

Two-Photon Excitation and Three-Photon Ionization

In order to describe two-photon (1+1) excitation and three-photon (2+1) ionization time-dependent pertubation theory can be used.[106-109] A brief description taken from *Multiphoton Spectroscopy of Molecules*[106] is given below. The time dependent Schrödinger equation is given by:

$$\hat{H}\Psi = i\hbar\left(\partial\Psi/\partial t\right) \tag{3.1}$$

Table 3.1 Possible products from the excitation of an atom to a Rydberg state and collision of a Rydberg atom with a molecule.

	Chemical Equation	Name
(a)	$h\nu + A \rightarrow A^{**}$	One-Photon Excitation
(b)	$2h\nu + A \rightarrow A^{**}$	One-Color, Two-Photon Excitation
(c)	$h\nu_1 + A \rightarrow A^{*} + h\nu_2 \rightarrow A^{**}$	Two-Color, Two-Photon Excitation
(d)	$A^{**}(n, \ell) + M(J) \rightarrow A^{**}(n', \ell') + M(J')$	Change in Quantum Numbers
(e)	$A^{**} + M \rightarrow AM^{+} + e^{-}$	Associative Ionization
(f)	$A^{**} + M \rightarrow A^{+} + M + e^{-}$	Collisional Ionization
(g)	$A^{**} + M \rightarrow A + M^{+} + e^{-}$	Penning Ionization
(h)	$A^{**} + M(J) \rightarrow A^{+} + M^{-}(J)$	Charge Transfer
(i)	$A^{**} + BC \rightarrow AB^{+} + C + e^{-}$	Dissociative Associative Ionization
(j)	$A^{**} + BC \rightarrow A + B^{+} + C + e^{-}$	Dissociative Collisional Ionization
(k)	$A^{**} + BC \rightarrow A^{+} + B + C^{-}$	Dissociative Charge Transfer
(l)	$A^{**} + BC \rightarrow AB^{+} + C^{-}$	Associative Charge Transfer

with the Hamiltonian operator given by:

$$\hat{H} = \hat{H}_o + \lambda V \tag{3.2}$$

where V is a perturbation and λ is a perturbative parameter. The unperturbed wavefunction is of the form:

$$\Psi_n^0 = \Psi_n \exp\left(-itE_n/\hbar\right). \tag{3.3}$$

The wavefunction Ψ is expanded in terms of the unperturbed basis such that:

$$\Psi = \sum_n C_n(t)\Psi_n^0. \tag{3.4}$$

Substituting Equation 3.4 into Equation 3.1 yields:

$$i\hbar\left(\partial\Psi/\partial t\right) = \lambda\sum_m C_m\left\langle \Psi_n^0 \mid V \mid \Psi_m^0 \right\rangle \tag{3.5}$$

where

$$C_n = C_n^{(0)} + \lambda C_n^{(1)} + \lambda^2 C_n^{(2)} + \ldots. \tag{3.5}$$

If the system is initially in state *k*, then we can assume:

$$C_k^{(0)} = 1 \text{ and } C_m^{(0)} = 0. \tag{3.6}$$

By substituting these into Equation 3.5 one can obtain:

$$C_n^{(2)} = \sum_m \frac{V_{nm}V_{mk}}{\hbar\varpi_{mk}}\left(\frac{1-e^{it\varpi_{nm}}}{\hbar\varpi_{nm}} - \frac{1-e^{it\varpi_{nk}}}{\hbar\varpi_{nk}}\right). \tag{3.7}$$

In the second-order approximation for the transition k→n only the second term in 3.7 (with ω_{nk}) makes a dominant contribution. Therefore,

$$\left|C_n^{(2)}\right|^2 = \frac{2\left(1-\cos\varpi_{nk}t\right)}{\left(\hbar\varpi_{nk}\right)^2}\left|\sum_m \frac{V_{nm}V_{mk}}{\hbar\varpi_{mk}}\right|^2. \tag{3.8}$$

The transition probability per unit time can be written:

$$W_{k\to n}^{(2)} = \frac{2\pi}{\hbar}\left|\sum_m \frac{V_{nm}V_{mk}}{\hbar\varpi_{mk}}\right|^2 \delta(E_n - E_k) \tag{3.9}$$

where the delta function implies energy conservation between the initial and final state. For two-photon excitation the initial and final states are given by:

$$|I\rangle \equiv |\varepsilon_i, n_1\hbar\varpi_1, n_{1'}\hbar\varpi_{1'}\rangle \tag{3.10}$$

$$|F\rangle \equiv |\varepsilon_f, (n_1 - 1)\hbar\varpi_1, (n_{1'} - 1)\hbar\varpi_{1'}\rangle \tag{3.11}$$

and there are two possible intermediate states:

$$|M\rangle \equiv |\varepsilon_m, (n_1 - 1)\hbar\varpi_1, n_{1'}\hbar\varpi_{1'}\rangle \tag{3.12}$$

$$|M\rangle \equiv |\varepsilon_m, n_1\hbar\varpi_1, (n_{1'} - 1)\hbar\varpi_{1'}\rangle. \tag{3.13}$$

It can be shown that V can be expressed as:

$$V = -\sum_k (\hat{e}_k \cdot P)\frac{e}{m}\left(\frac{2\pi\hbar}{\varpi_k L^3}\right)^{1/2}\left(\hat{a}_k^{\mp} + \hat{a}_k\right). \tag{3.14}$$

where P is the total linear momentum operator of the electrons, e is the charge of an electron, m is the mass of an electron, L is the length of a theoretical cubic box, and the last two operators $\hat{a}_k^{\mp}$ and $\hat{a}_k$ are the photon annihilation and creation operators. Substituting these last three expressions into Equation 3.9 gives:

$$W_{i\to f}^{(2)} = \frac{2\pi}{\hbar^2}\left(\frac{2\pi e^2}{m^2 L^3}\right)^2 \sum_1 \sum_{1'} \frac{n_1 n_{1'}}{\varpi_1 \varpi_{1'}}\left|M_{fi}^{(2)}(\varpi_1, \varpi_{1'})\right|^2 \delta(\varpi_{fi} - \varpi_1 - \varpi_{1'}) \tag{3.15}$$

where:

$$M_{fi}^{(2)}(\varpi_1, \varpi_{1'}) = \sum_m \left(\frac{(\hat{e}_{1'} \cdot P_{fm})(\hat{e}_1 \cdot P_{mi})}{\varpi_{mi} - \varpi_1} + \frac{(\hat{e}_1 \cdot P_{fm})(\hat{e}_{1'} \cdot P_{mi})}{\varpi_{mi} - \varpi_{1'}}\right). \tag{3.16}$$

It can be shown that Equation 3.15 can be simplified to:

$$W_{i\to f}^{(2)} = \frac{2\pi}{\hbar^2}\left(\frac{2\pi e^2}{c}\right)^2 \int_0^\infty d\varpi_1 \varpi_1 \varpi_{1'} I_1(\varpi_1) I_2(\varpi_{1'}) \left|S_{if}(\varpi_1, \varpi_{1'})\right|^2 \qquad (3.17)$$

where S is a simplified form of P and $I_1(\omega_1)$ and $I_1(\omega_{1'})$ are the incident light intensities. Photoionization in the experiments reported here is a three-photon process (2+1) and the three-photon transition probability must be used. It can be expressed as:

$$W_{i\to f}^{(3)} = \frac{2\pi}{\hbar^3}\left(\frac{2\pi e^2}{m^2 c}\right)^3 \times \int_0^\infty \int_0^\infty \int_0^\infty d\varpi_1 d\varpi_{1'} d\varpi_{1''} \frac{I_1(\varpi_1) I_2(\varpi_{1'}) I_3(\varpi_{1''})^2}{\varpi_1 \varpi_{1'} \varpi_{1''}} \times \left|M_{fi}^{(3)}(\varpi_1, \varpi_{1'}, \varpi_{1''})\right|^2 \delta(\varpi_{fi} - \varpi_1 - \varpi_{1'} - \varpi_{1''}) \qquad (3.18)$$

To get the (2+1) photoionization probability from Equation 3-18 the final state is taken as the continuum.

Probing of High Rydberg States: Ionization

Shown in Figure 3.1 is a typical one-color 2+1 multi-photon ionization positive ion spectrum of rubidium showing predominantly *nd* states from *n*=12 up to the ionization potential (593.65 nm). This spectrum was acquired using a pulsed electric field of 35,000 V/m. In this particular case, states created above *nd*=32 were field ionized, giving rise to a sharp increase in Rb^+ intensity below ~595.7 nm. This is explained in Chapter I and shown in Figure 1.5. Such spectra give an indication as to the fraction of states that are actually photo-ionized after being excited to the high Rydberg states. The photo-excitation and photo-ionization cross sections for the *ns* $^2S_{1/2}$ states are much smaller than the *nd* $^2D_{5/2,3/2}$ states and therefore they are not evident except through field ionization. Field ionization of *ns* $^2S_{1/2}$ states can be seen in Figure 3.2. In Figure 3.2 the top spectrum was taken with a pulsed electric field of 37,500 V/m and the bottom

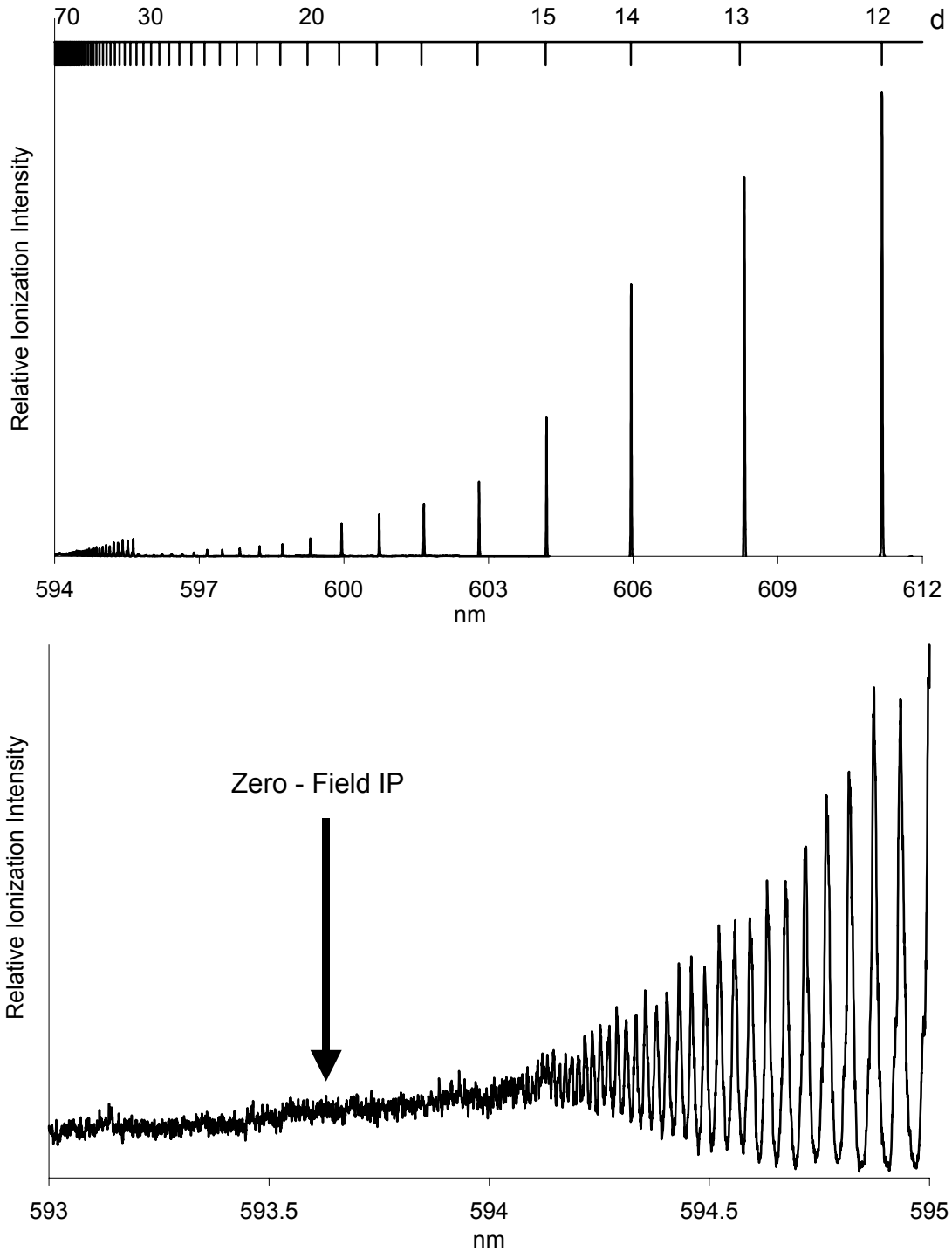

Figure 3.1 Multiphoton ionization (2+1) and field ionization of Rb with a pulsed electric field of 35,000 V/m. The lower spectrum is an enlargement of the high Rydberg states above n~40.

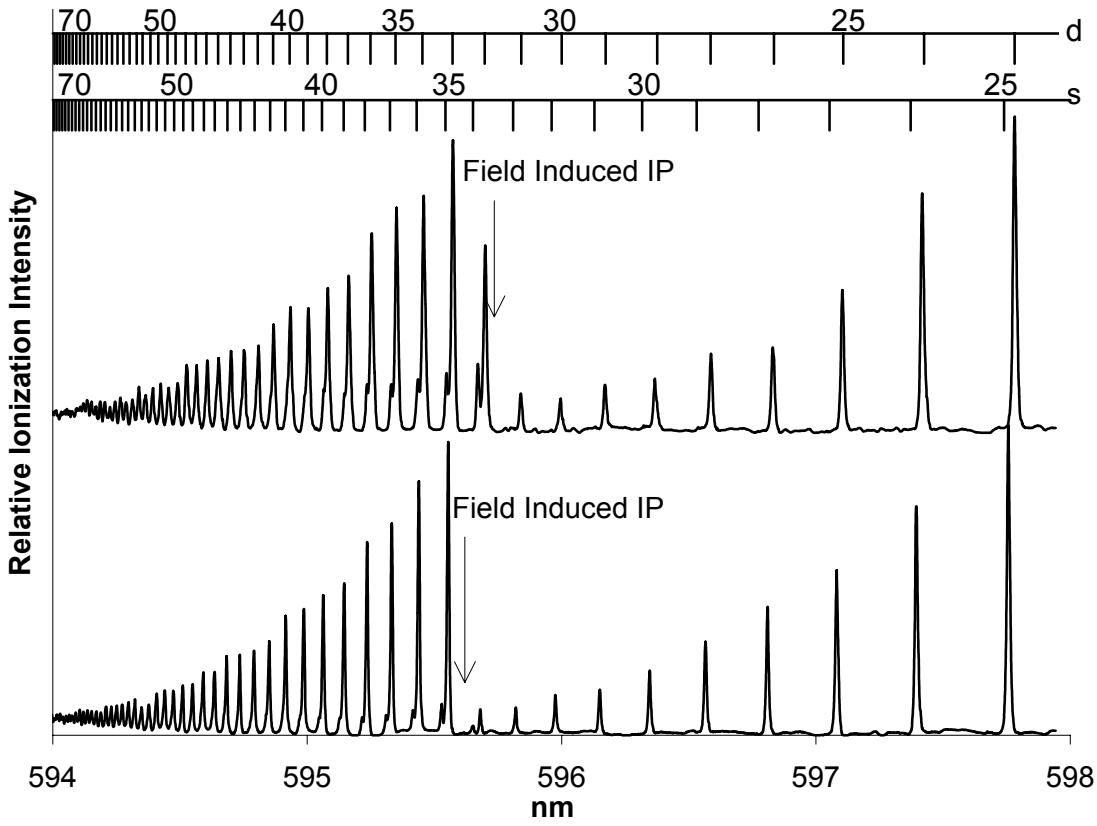

Figure 3.2 Multiphoton ionization (2+1) and field ionization of Rb with a pulsed electric field of 37,500 V/m (top) and 35,000 V/m (bottom).

with 35,000 V/m. Tunneling is evident in the top spectrum with the unresolved *32d* $^2D_{5/2,3/2}$ states where one notices that the field ionization of the *32d* state is surpressed due to incomplete tunneling. This is important when the analogy is made with field ionization of dipole-bound states. Multi-photon ionization of rubidium was also carried out with a constant dc electric field.[104,110] Shown in Figure 3.3 is such a spectrum recorded with a field of 35,000 V/m. This is to be compared with the spectrum in Figure 3.1, which also was recorded with 35,000 V/m but under pulsed field conditions. Unusual features can be seen in Figure 3.3 when compared to Figure 3.1, such as forbidden two-photon transitions to *np* $^2P_{3/2,1/2}$ states, larger *ns* $^2S_{1/2}$ intensity, and resonances above the ionization potential.

Multi-photon ionization spectra were also recorded in the wavelength region of the *5p* $^2P_{3/2}$ state of rubidium, which was used as the first step in the two-color two-photon excitation of high Rydberg states. Shown in Figure 3.4 is a spectrum of this region. A large number of unidentified transitions creating Rb^+ can be seen in this spectrum. These transitions do not correspond to atomic transitions in rubidium, even when ^2F and ^2G states are taken into account. Potential energy curves for rubidium dimmer (Rb_2) were constructed from constants found in Herzberg's *Constants of Diatomic Molecules*[111] and can be found in Figures 3.5 and 3.6. Rb_2 transitions to form Rb^+ did not account for the unknown transitions either. A possible explanation might involve hybrid transitions via dissociative states of Rb_2.[112]

Probing of High Rydberg States: Excitation

Figures 3.1 – 3.3 provide an estimate of the relative ionization rates of the high Rydberg states of rubidium. Charge transfer reactions were carried out with SF_6 and

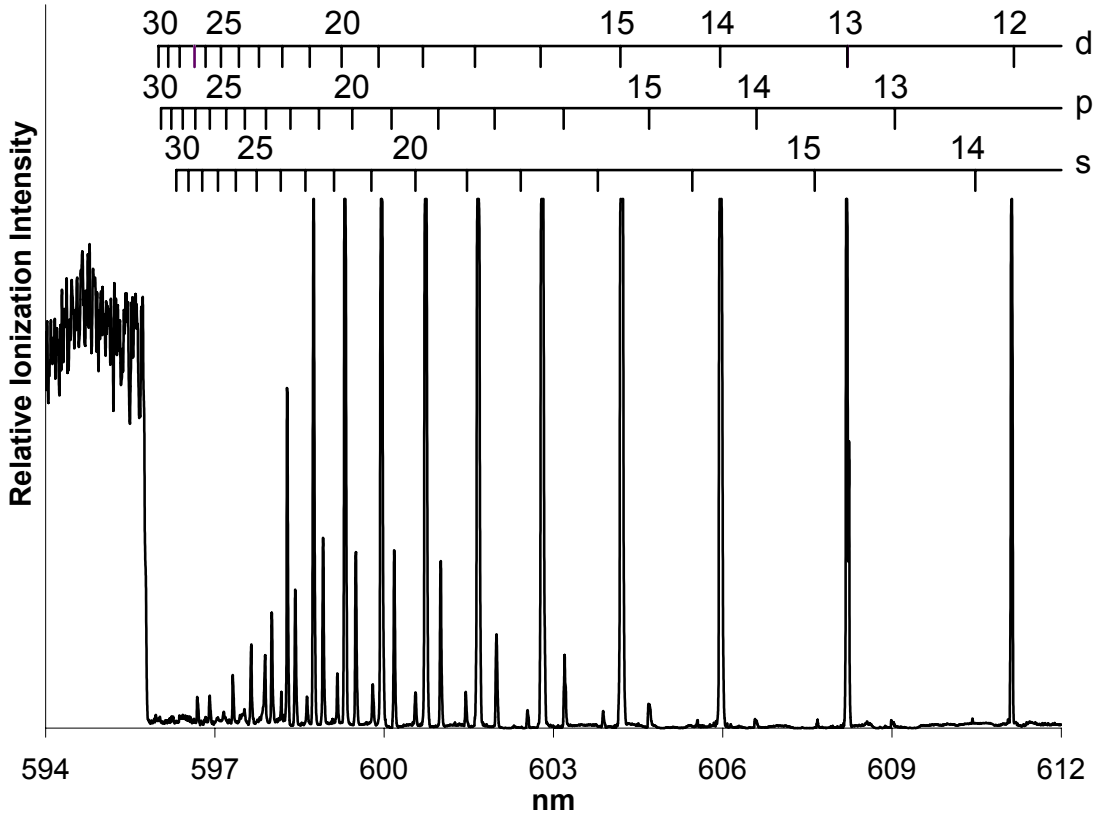

Figure 3.3 Multiphoton ionization (2+1) and field ionization of Rb with a dc electric field of 35,000 V/m.

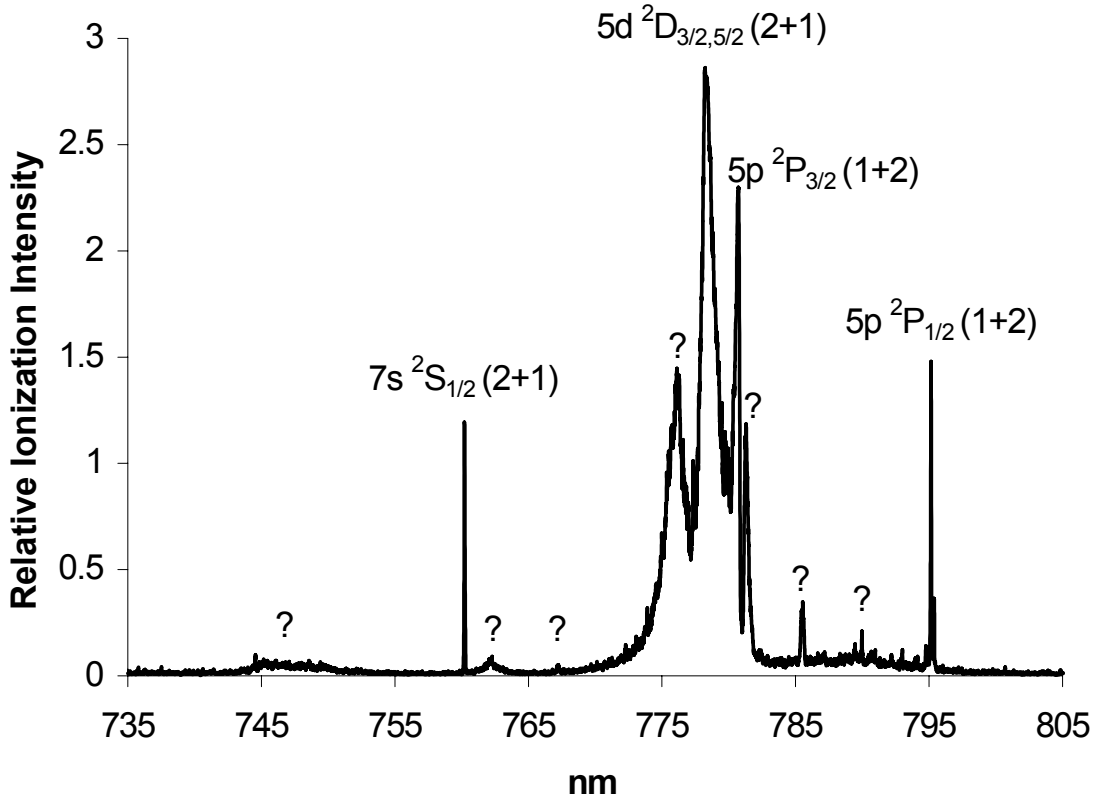

Figure 3.4 Multiphoton ionization signal of Rb with peaks of unknown origins.

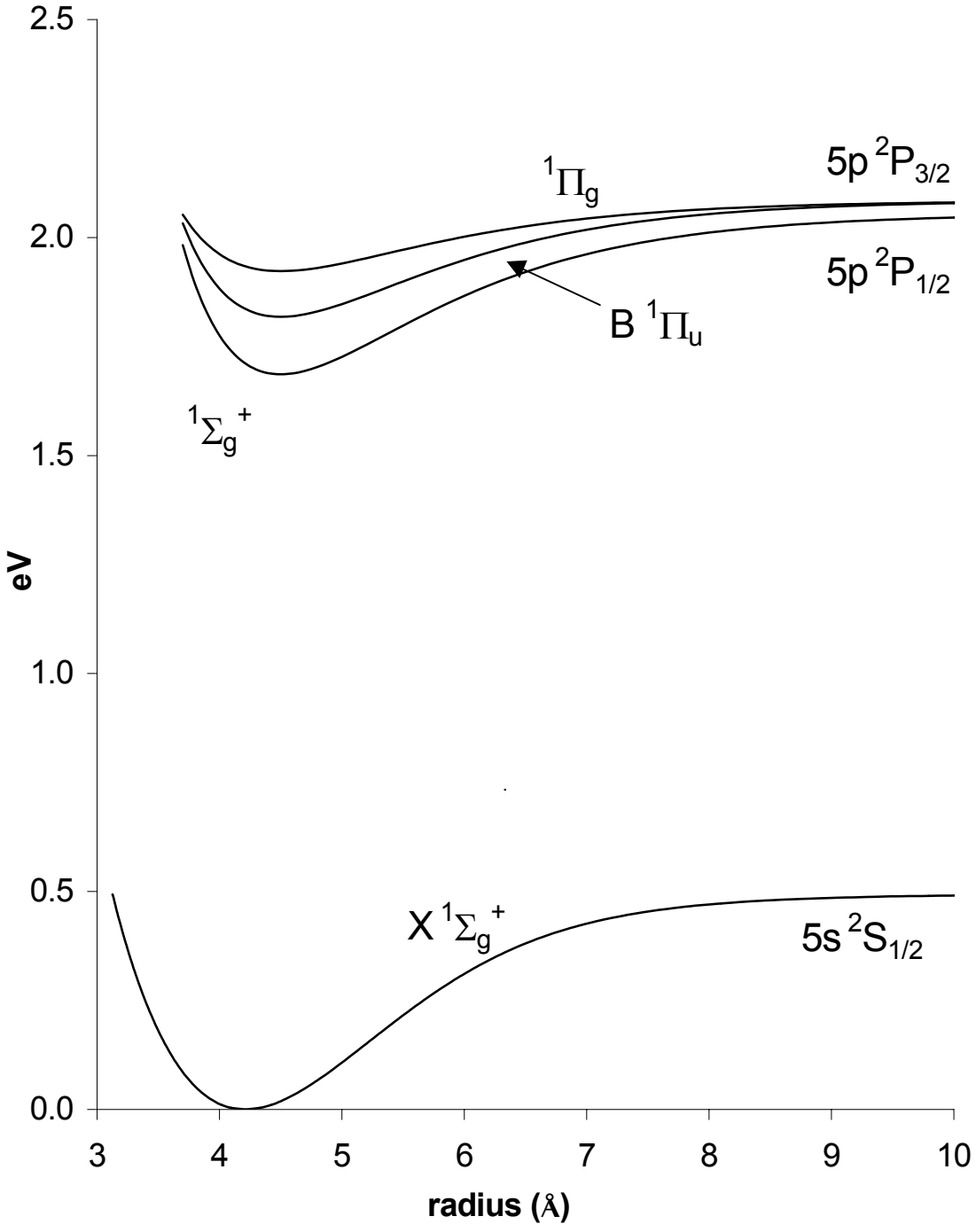

Figure 3.5 Potential Energy curves for the electronic states of Rb_2.

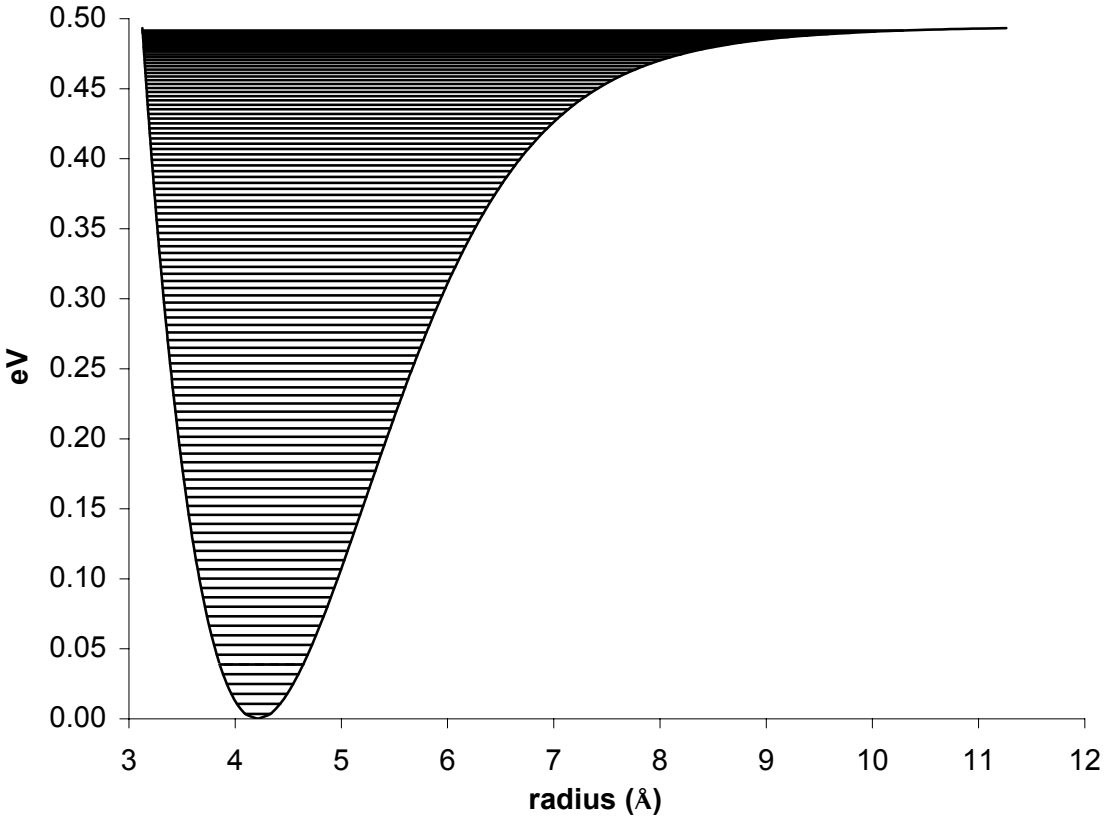

Figure 3.6 Potential energy curve for the ground state ($^1\Sigma_g^+$) of Rb_2.

CCl_4 to study the relative number of states that were excited and not ionized. SF_6 efficiently attaches low energy electrons and has a large charge exchange cross-section at high values of n^*. SF_6 was used through the course of study for alignment of the laser beam(s) and to calibrate the negative ion yield and mass spectra, when necessary. Figure 3.7 shows a charger transfer spectrum of SF_6 over a wide range of n^*. The relative production of SF_6^- roughly mirrors that of Rb^+ at high n^* but drops off at low n^* due to complications in separation of the ion-pair collisional complex. The gradual drop-off of SF_6^- signal above the ionization limit of Rb is due to free electron attachment. Forbidden two-photon transitions from the $5p\ ^2P_{3/2}$ state to high Rydberg states is observed in these SF_6^- spectra. This was seen previously in Cs^+ spectra[112] and can be seen for the one-color two-photon case in an electric field in Figure 3.3. Rydberg electron transfer reactions with CHBrClF, C_6F_6 and $C_8H_{17}I$ (2-iodooctane) also proved useful for calibration purposes.

Competition with Collisional Detachment

Collisional detachment of high Rydberg atoms by polar molecules has been well studied both experimentally and theoretically. A review of the many aspects of Rydberg atoms and collisions of Rydberg atoms with molecules can be found in numerous chapters of the book edited by Stebbings and Dunning[113] and also in the more recent review article by Beigman and Lebedev.[114] Competition between collisional detachment and charge exchange is expected to play a role in the RET process involving dipole-bound anions.[104] It is important to understand the influence of collisional detachment of high Rydberg atoms as it relates to dipole-bound anion formation. Figure 3.8a shows the

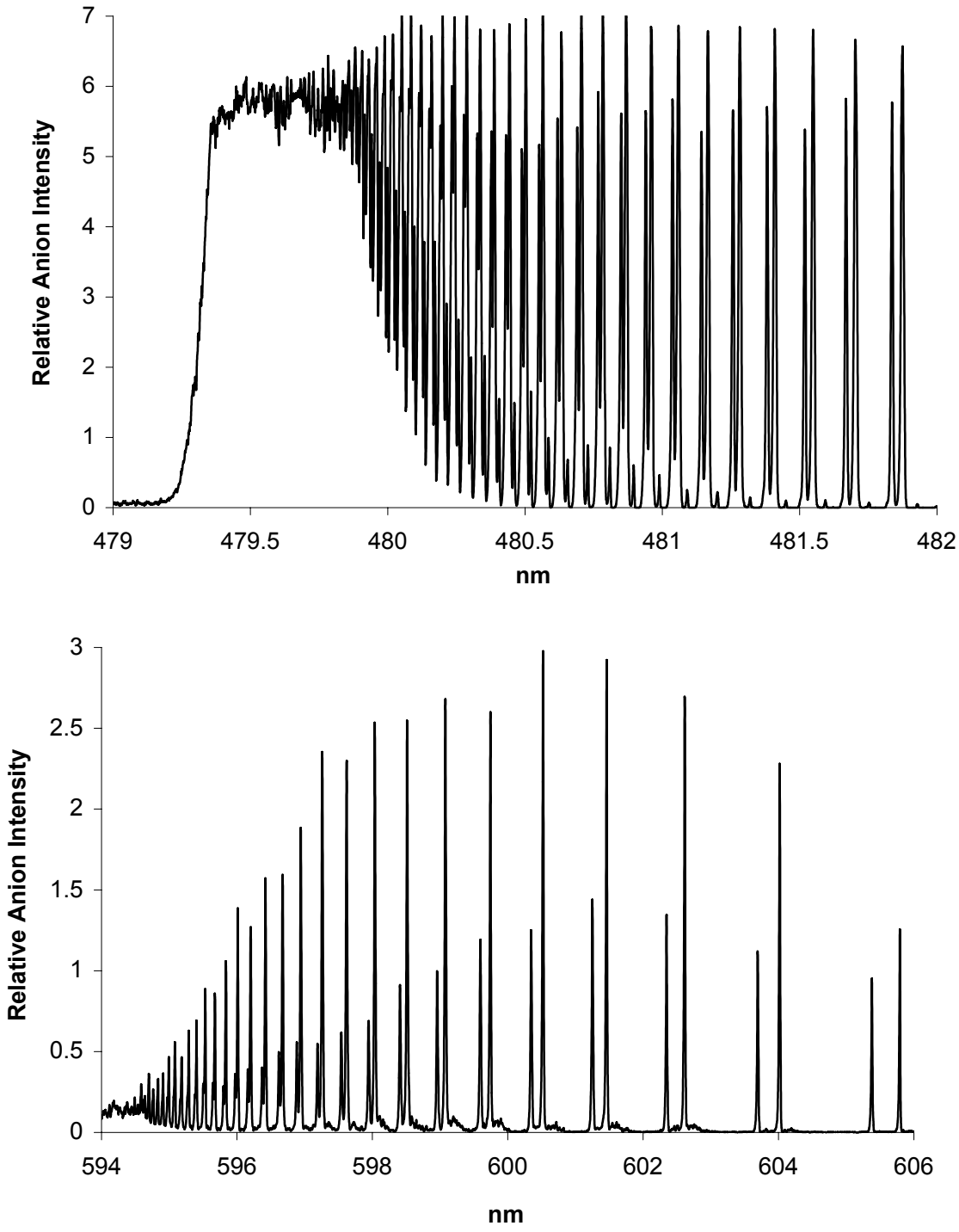

Figure 3.7 SF_6^- signal due to charge exchange reactions from Rb Rydberg states via two-color excitation to high (n* > 30) Rydberg states (top) and one-color excitation to median (n*>11) Rydberg states (bottom).

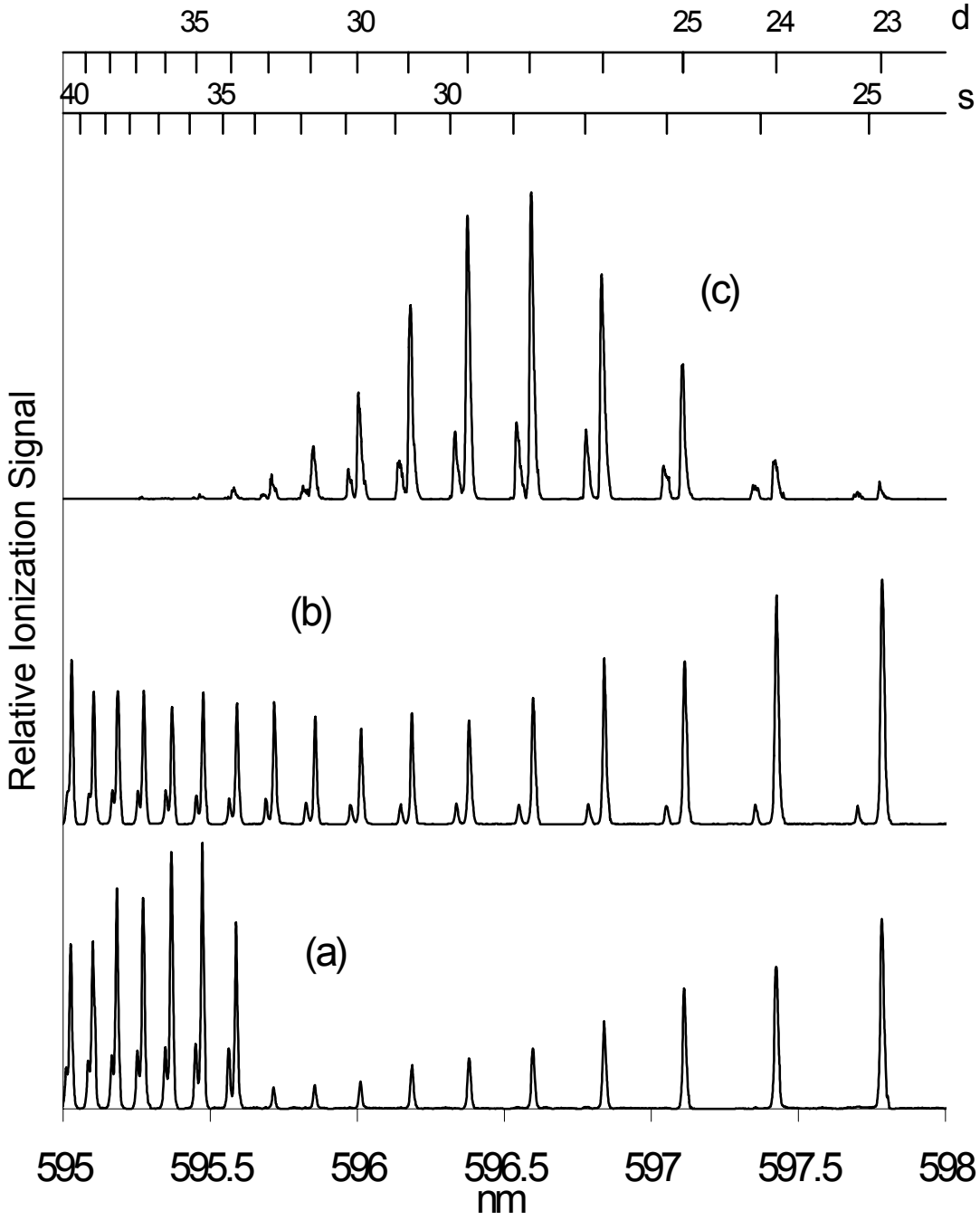

Figure 3.8 Rb^+ ionization signal with no gas jet (a), Rb^+ ionization signal with acetone gas jet (b), and acetone ($CH_3COCH_3^-$) dipole-bound anion signal (c).

Rb^+ ion signal without the presence of a collision gas. Only signal due to (2+1) MPI of *nd* Rb Rydberg states showing the abrupt onset at the field ionization threshold is indicated. Figure 3.8b shows the Rb^+ ion signal resulting from collisions with acetone seeded in a jet of He. Most of the ionizing collisions are believed to be due to the presence of acetone in the nozzle jet. The continuity of signal through the field ionization threshold and the appearance of *ns* states below this limit is apparent. Figure 3.8c shows the dipole-bound negative ion signal for acetone. It is clear that the cross sections for collisional detachment processes are much larger than that for RET in this region of *n*. A similar set of data is shown in Figure 3.9 for the case of acetonitrile. Again, examination of the Rb^+ signal and CH_3CN^- signal clearly shows that collisional ionization is larger for high *ns* and *nd* states, however, RET is seen to clearly dominate the result of the collisions in the region of low *ns* and *nd*. Figure 3.9d (showing only the *ns* Rb^+ signal) clearly exhibits a peak primarily due to RET. These experiments emphasize the importance of a better theoretical understanding of the interaction of Rydberg atoms and polar molecules, with regards to the competition between collisional ionization and dipole-bound anion formation.

Effect of Reaction Conditions

The range of n^* values as well as n^*_{max} observed for RET to dipole-bound anions is dependent upon the carrier gas used to entrain the polar molecules. This observation has implications on the application of Equation 1.9 since it was created from Rydberg charge exchange rates using helium as the carrier gas. A discussion of the expansion of the molecules in a nozzle jet can be found in Chapter II. Figure 3.10 shows the relative anion formation vs n^* for acetone using He, Ar, and Xe as carrier gases. As the velocity

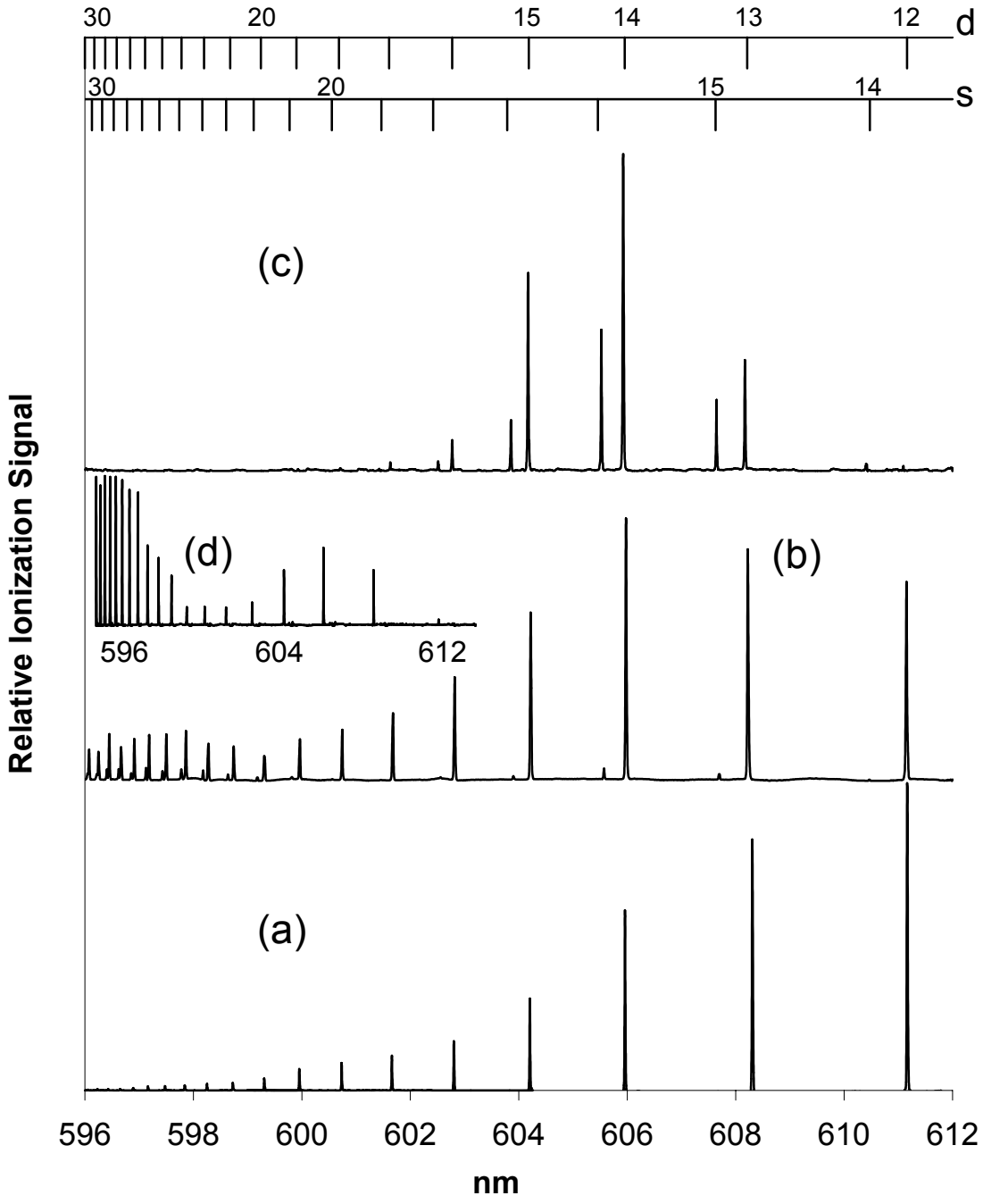

Figure 3.9 Rb^+ ionization signal with no gas jet (a), Rb^+ ionization signal with acetonitrile gas jet (b), acetonitrile (CH_3CN^-) dipole-bound anion signal (c), and Rb^+ *ns* ionization signal with acetonitrile gas jet (d).

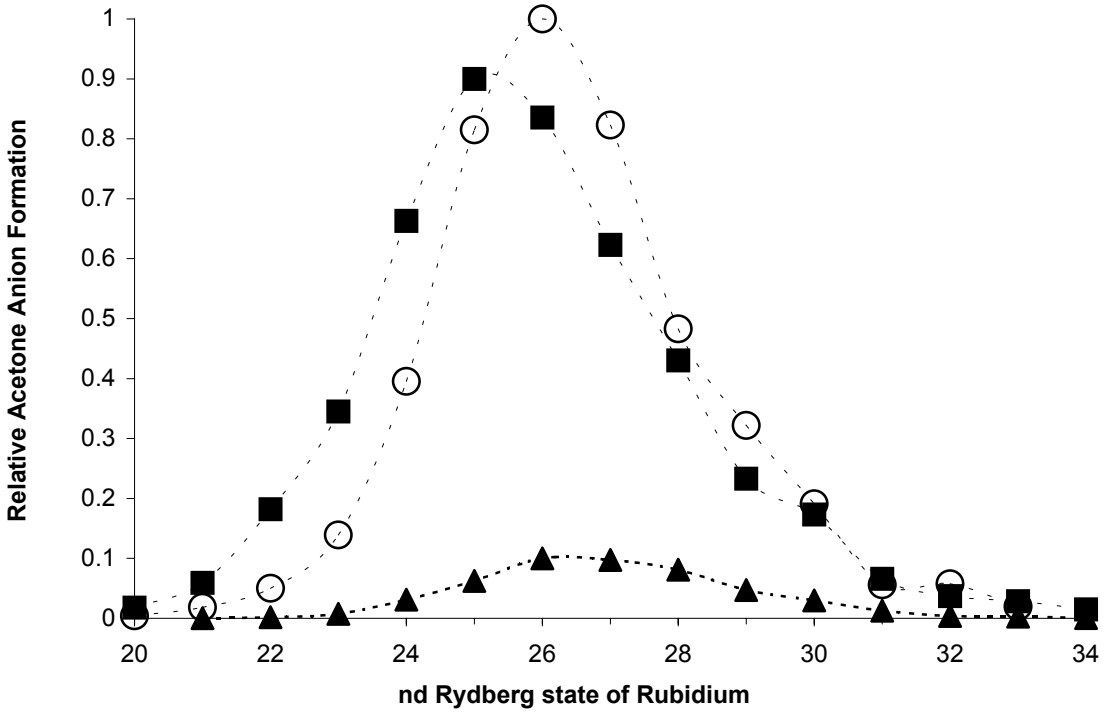

Figure 3.10 Comparison of the relative anion signal for acetone as a function of the carrier gases He (squares), Ar (circles), and Xe (triangles).

of the entrained molecules decreases n^*_{max} is observed to shift slightly to higher values along the series H_2, He, Ne, Ar, Kr, and Xe. When the velocity of the molecule is taken into account in the curve-crossing model the charge exchange profile does indeed shift as experimentally observed. If the relative collision velocity is increased the system tends to diabatically cross more easily the avoided crossing between the initial covalent curve and ionic curve. In order to reset the initial optimal crossing probability, one must go to higher ionic-covalent coupling terms, which quickly increase for decreasing n^* values. In addition, the rate constant for anion creation is also predicted to decrease as the velocity decreases, because the cross-section at n^*_{max} is essentially unchanged while the velocity is lower. This would imply that H_2 and He would yield the largest anion signal. It is observed experimentally, however, that Ar yields the largest anion signal. This implies that rotational cooling via the nozzle jet expansion also plays a significant role in anion production since Ar is known to be a better expansion gas for ro-vibrational cooling. Shown in Figure 3.11 are the RET spectra of 3-methylcyclohexanone using different carrier gases. The relative abundance of the two dipole-bound states changes depending upon the carrier gas employed and n^*_{max} is seen to increase in the order H_2, He, Ne, Ar, Kr, Xe.

Charge Transfer Reactions between Chiral Rydberg Atoms and Chiral Molecules

The stereochemical interactions between chiral reactants is a topic of great fundamental and practical interest in modern science. The simplest of these reactions is circular dichroism, the differential absorption of left- and right-circularly polarized light by a chiral molecule. It is well known that the photochemistry of racemic mixtures of molecules irradiated by circularly polarized light can lead to an excess of one enantiomer

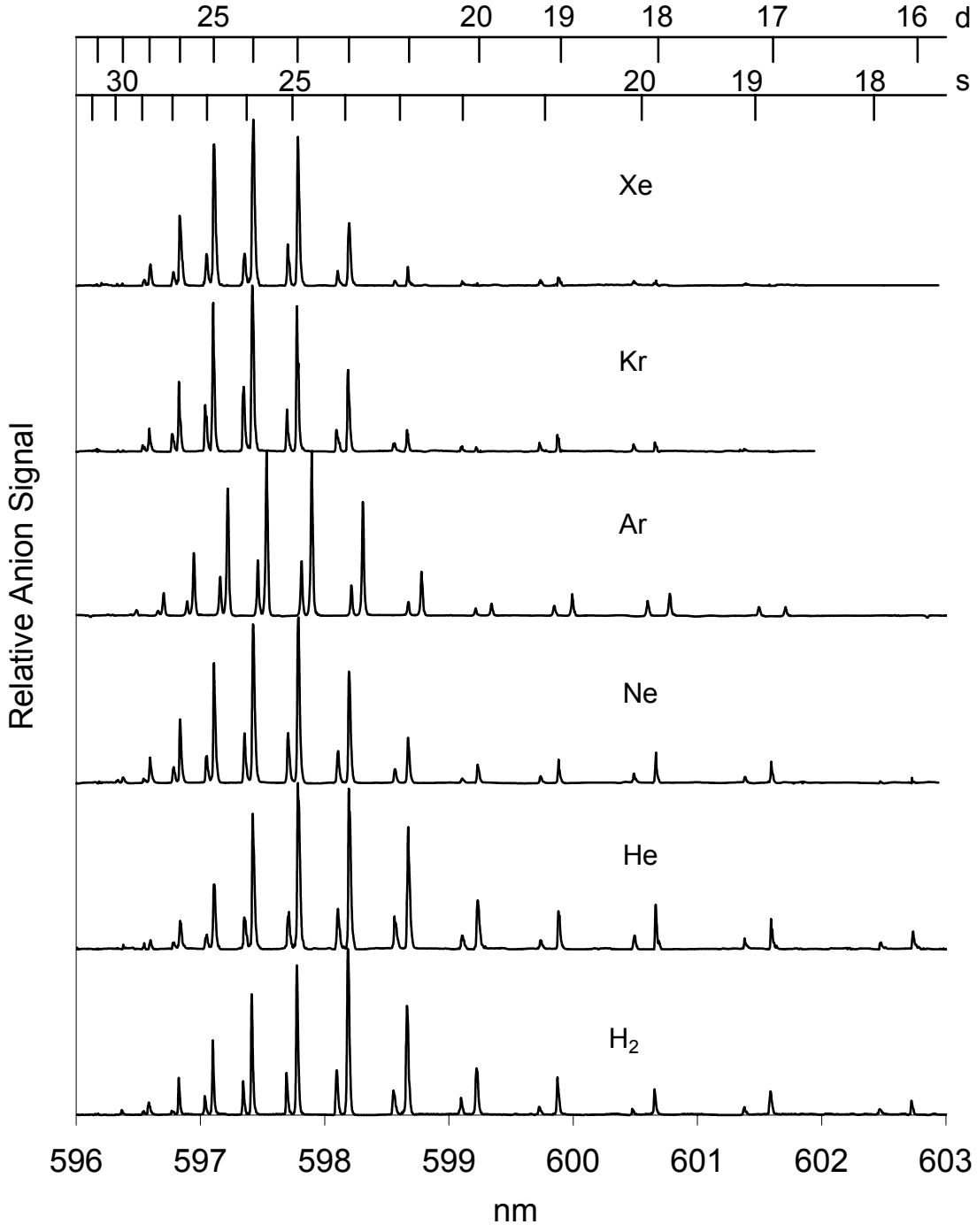

Figure 3.11 Dipole-bound anion spectra of 3-methylcyclohexanone in six different carrier gases.

over the other (i.e., enantiomeric excess, ee = (*R* enantiomer percentage less *S* enantiomer percentage)), either in the product or recovered reactants.[115-118] The interactions of spin polarized electrons, particularly (left-handed) beta particles, with chiral molecules have also received considerable attention in recent years. Unfortunately, the results for spin polarized electron irradiation are far less certain than in the case of circularly polarized photons (see the recent reviews by Frank, Bonner and Zare[119] and Compton and Pagni[120] and others cited therein). Both photon and electron studies are often cited to be relevant to questions surrounding the origins of *specific* homochirality of biomolecules on the earth. Enantiomerically selective reactions of optically active molecules with racemic mixtures are well documented.[121] This dissertation reports the first experiments involving reactions of chiral Rydberg atoms and chiral molecules.

Chiral Rydberg atoms (oriented atoms with selected M_J) can be produced using right- and left-circularly polarized light. A chiral Rydberg atom is defined using the criteria of "true and false" chirality introduced by Barron.[122-124] "True" chirality is shown by systems existing in two distinct enantiomeric states that are interconverted by space inversion, but not by time reversal combined with any proper spatial rotation. Rydberg atoms of rubidium were excited by two right- or two left-circularly polarized (RCPL or LCPL) photons to high $nd\ ^2D_{5/2}$ states. The Rydberg atoms were thus oriented through preferential excitation of $M_J = +5/2$ (RCPL) or $M_J = -5/2$ (LCPL). Classically, the Rydberg atom and its mirror image can be envisioned as shown in Figure 3.12a. A stationary Rydberg atom is achiral; however, motion of the Rydberg atom along the axis of orientation will produce a non-superimposable mirror image and the system will exhibit true chirality, i.e., the system exists in two enantiomeric states that are

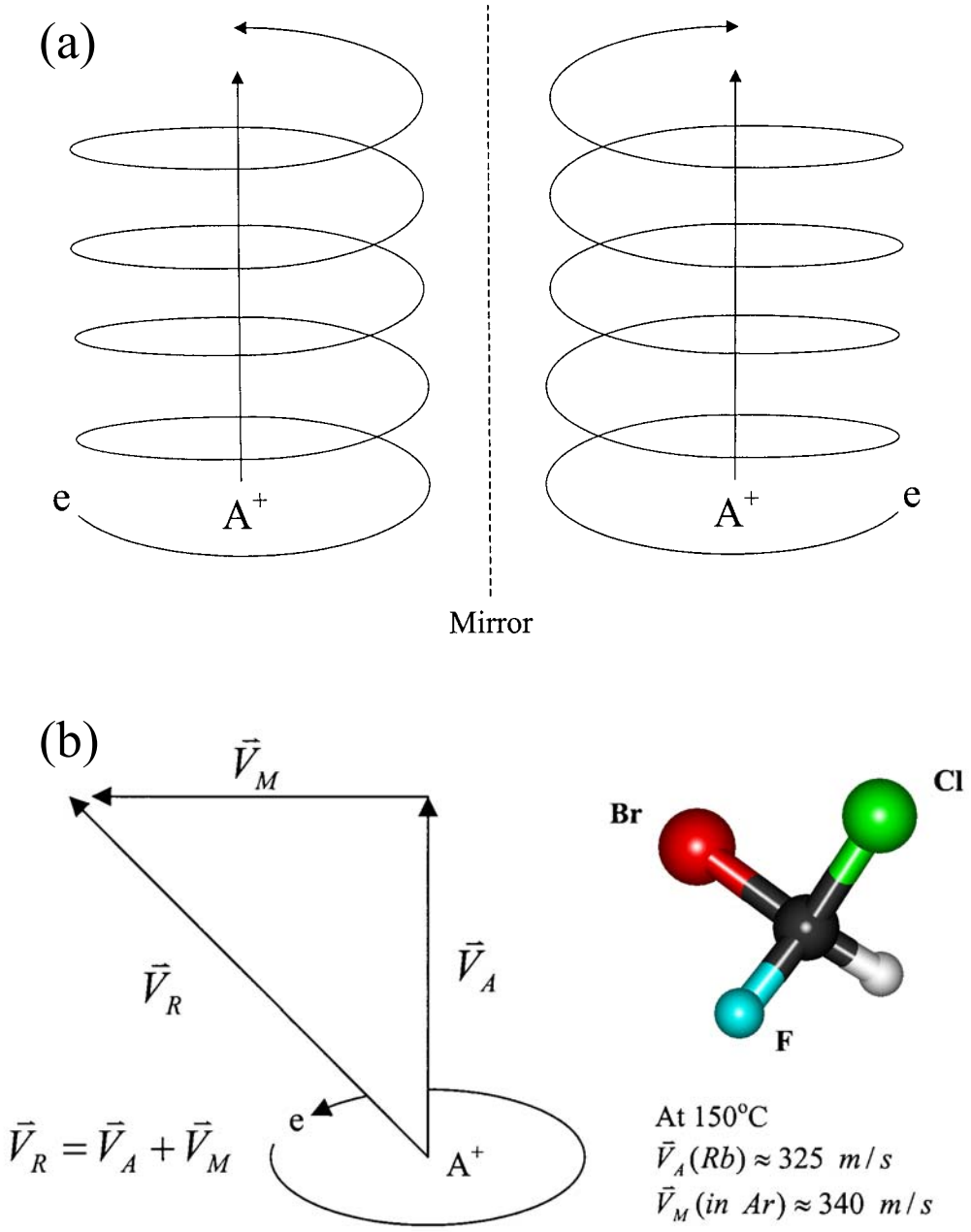

Figure 3.12 Illustration of chiral (helical) Rydberg atoms (classical analogy) (a), and relative velocities of the colliding Rydberg atom and randomly oriented chiral molecules (b).

interconverted by space inversion but not by time reversal combined with any proper spatial rotation. If the spin angular momentum of the electron is along (or against) the axis of orientation, the system could be described as doubly chiral as seen by an observer in relative motion. The relative motion of colliding pairs is illustrated in Figure 12b using chiral CHBrClF as a model.

In order to produce CPL, the angle of the incident linearly polarized laser beam was adjusted to +/- 45^{o} with respect to the optical axis of the double Fresnel Rhomb. The light was judged to be very close to circular polarization as observed by constant transmission intensity through a rotating linear polarization analyzer. Final adjustment was made by attempting to completely extinguish any signal due to one color two-photon excitation of *ns* $^{2}S_{1/2}$ states which are forbidden with excitation by circularly polarized light. The ratio of *ns* ^{2}S signal to (*n*-2)*d* ^{2}D signal was always less than 0.01 using one laser, indicating a high degree of circular polarization.

The *ns* $^{2}S_{1/2}$ signal almost totally disappears under circularly polarized light using non-resonant one-color two-photon excitation. However, *ns* $^{2}S_{1/2}$ signal for the stepwise two-photon excitation through the real *5p* $^{2}P_{3/2}$ state using circularly polarized light in both lasers remains large. Shown in Figure 3.13 is the Br^{-} signal resulting from charge exchange from both the *16s* ^{2}S and *14d* ^{2}D atomic states to CHBrClF. Figure 3.13a and 3.13c show the Br^{-} signal using linearly polarized light (LPL) that is perpendicular to the electric field and Figure 3.13b and 3.13d shown the Br^{-} signal from Rydberg atoms created with left circularly polarized light (LCPL). Whereas the Br^{-} signal from charge exchange from the *16s* ^{2}S state almost entirely disappears (<1%) in the one color experiment, it is relatively unchanged in the two color experiment. Hyperfine coupling

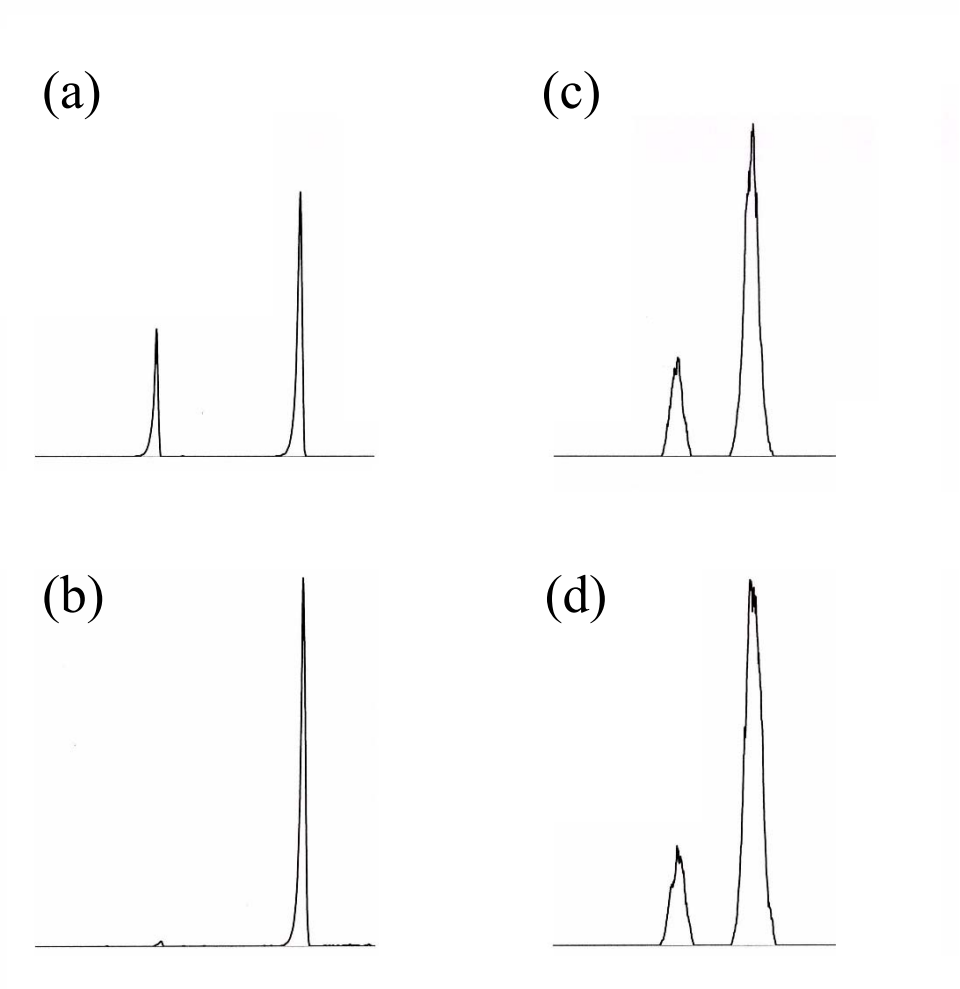

Figure 3.13 Br^- signal from RET to bromochlorofluoromethane from rubidium Rydberg atoms. The Rydberg levels are excited via:

(a) 1-color two-photon excitation using linearly polarized light
(b) 1-color two-photon excitation using left circularly polarized light
(c) 2-color resonantly enhanced two-photon excitation using linearly polarized light
(d) 2-color resonantly enhanced two-photon excitation using left circularly polarized light

of the intermediate level occurs resulting in M_J mixing,[125,126] which in turn allows for the excitation of *ns* states. Under these conditions it is expected that the *ns* ^2S states are spin oriented i.e. preferentially *ns* $^2S_{1/2}$ or *ns* $^2S_{-1/2}$ depending on the sense of circular polarization. One will also note that the two-color signals are considerably broader in wavelength than the one-color experiments. This is likely a result of ac-stark shifting (broadening for pulsed lasers) of the transitions.

Representative data comparing negative ion signal created from either right- or left-circularly polarized light is shown in Figure 3.14. In this particular experiment Br^- anions were created from CHBrClF at *nd* = 25. The average for the anion signal created using RCPL is 5.24 +/- 0.08, whereas the signal from LCPL is 5.21 +/- 0.06. This result is representative of all of the molecules studied in that no difference in the rate of anion creation was discovered for the reaction of opposite enantiomers of the Rydberg atom with resolved enantiomers.

The chiral molecules studied involved excited atoms crossing at right angles with nozzle-jet expanded chiral molecules seeded into a rare gas. This is not the optimum collision geometry to search for stereo-chemical effects between chiral reactants. A collinear collision between reactants would be best for observing a difference in the reaction between an oriented Rydberg atom and a chiral molecule. This was not possible in the present apparatus and is a difficult task in general, but not impossible. Future experiments might also include orientation of the polar molecule using inhomogeneous electric fields.[127] Under these conditions there would exist four distinct collision geometries for collinear beams of chiral Rydberg atoms and *R*, *S*, enantiomers.

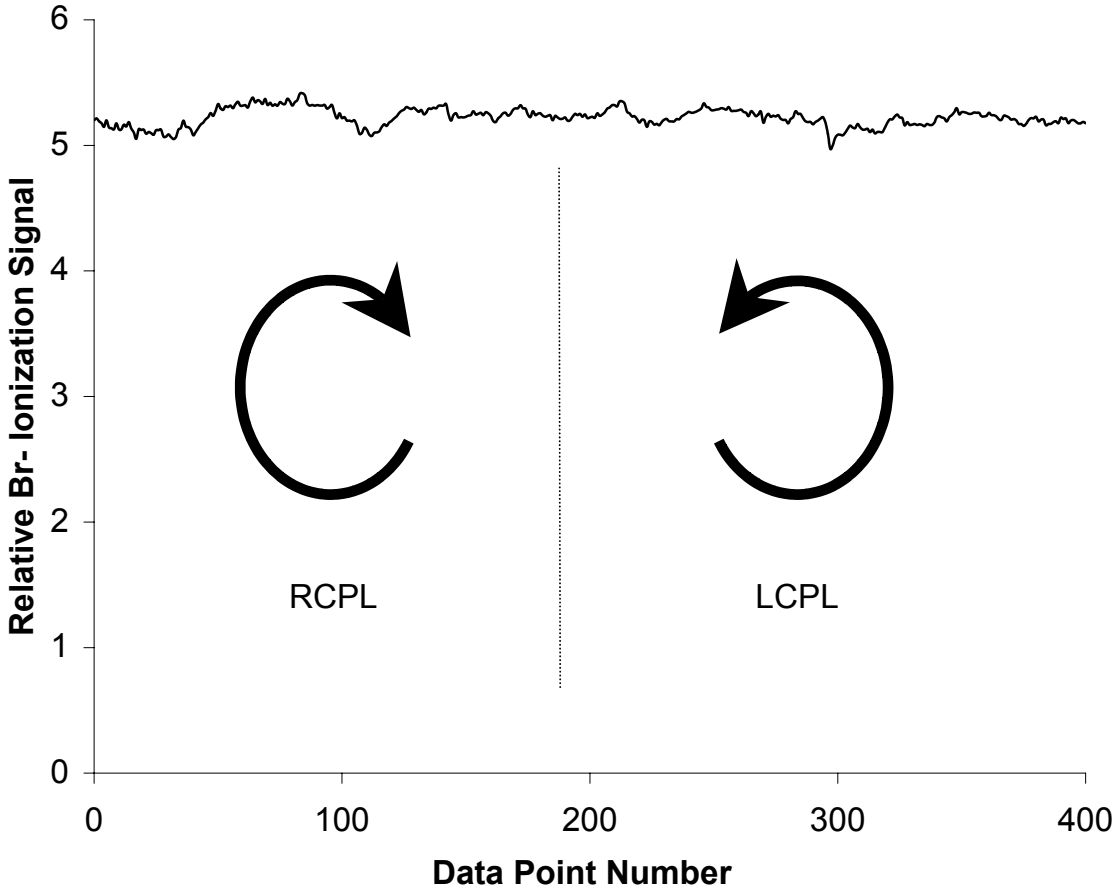

Figure 3.14 Br^- anion creation rate for the reaction of opposite enantiomers of the Rydberg atom with *(R)*-bromochlorofluoromethane at *nd = 25* of rubidium. The average for the anion signal created using RCPL is 5.24 +/- 0.08, whereas the signal from LCPL is 5.21 +/- 0.06.

CHAPTER IV

CALCULATIONS OF MOLECULAR PROPERTIES OF MOLECULES

Introduction

The electron affinities of dipole-bound anions depend primarily on the magnitude of their molecular dipole moments and to a lesser extent on their molecular polarizabilities. For this reason it is necessary to have trustworthy values of these two properties. Most accepted values for dipole moment were determined using microwave spectroscopy and can be found in the CRC Handbook of Chemistry and Physics,[128] with the exception of propanal[129] (gauche conformation), 2-methylpropanal,[130] deuterated acetone,[131] 3-methylcyclopentanone,[132] 4-methylcyclohexanone,[133] vinylene carbonate,[134-136] and ethylene carbonate,[137] which were obtained from other sources. However, for many molecules experimental values have not been reported. Also, many of the experimental values are believed to be suspect. Shown in Figures 4.1-4.8 are the molecular structures as determined from theory (details below) of the molecules studied here. It was necessary to calculate these structures so that other molecular properties could then be calculated. In these figures carbon atoms are blue, oxygen atoms are red, nitrogen atoms are dark blue, hydrogen atoms are gray, sulfur atoms are yellow, and deuterium atoms are purple.

The *Gaussian 98* software package[138] was employed to perform calculations for all of the molecules studied herein. *Gaussian 98* is an integrated software package of programs for performing semi-empirical and ab initio calculations on molecules and systems of molecules. One of *Gaussian 98*'s primary uses is to calculate optimized structures and use these geometries to calculate molecular properties (energies, dipole

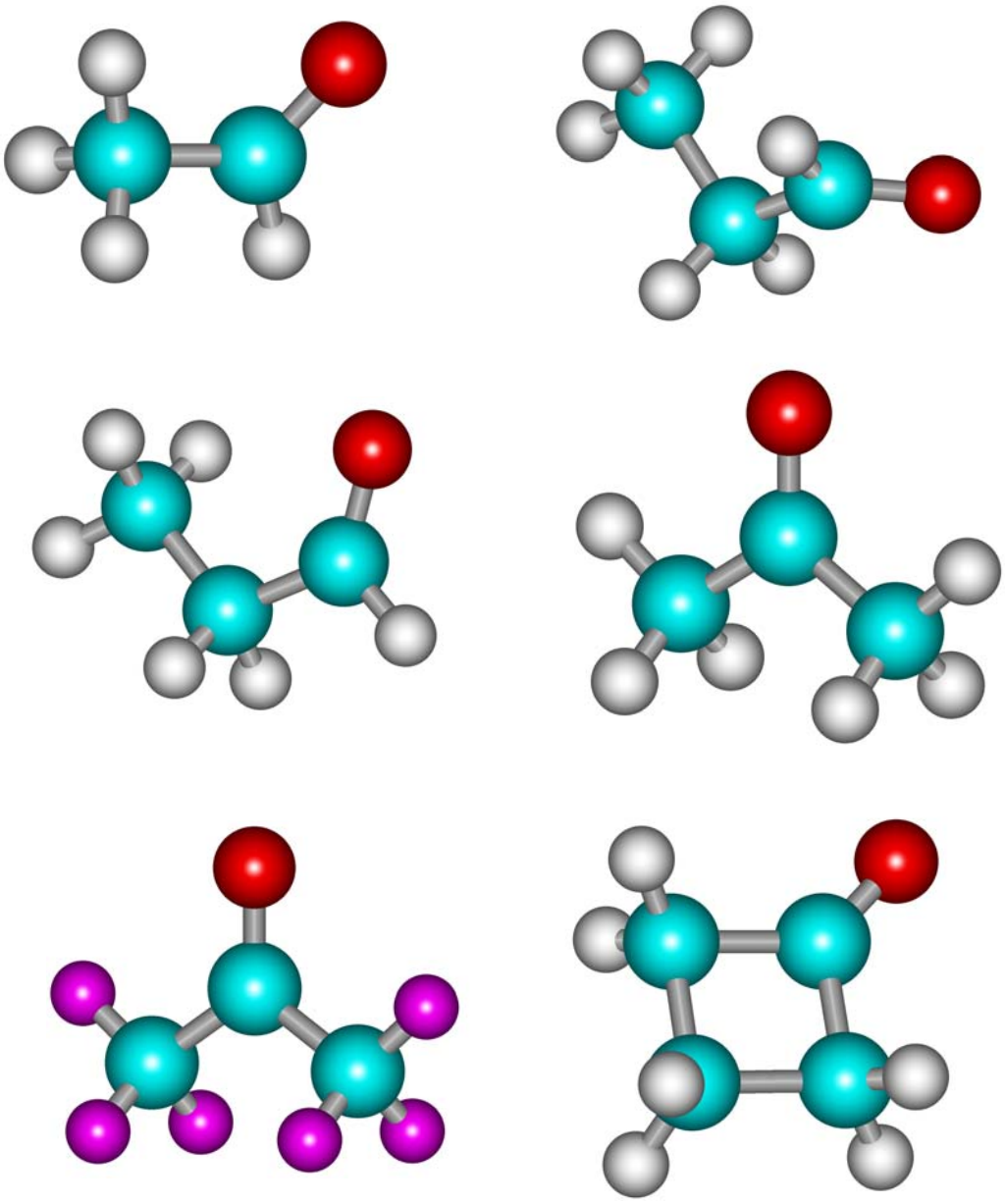

Figure 4.1 Optimized molecular geometries (from top left to bottom right) of acetaldehyde, propanal (*gauche*), propanal (*cis*), acetone, deuterated acetone (d_6), and cyclobutanone.

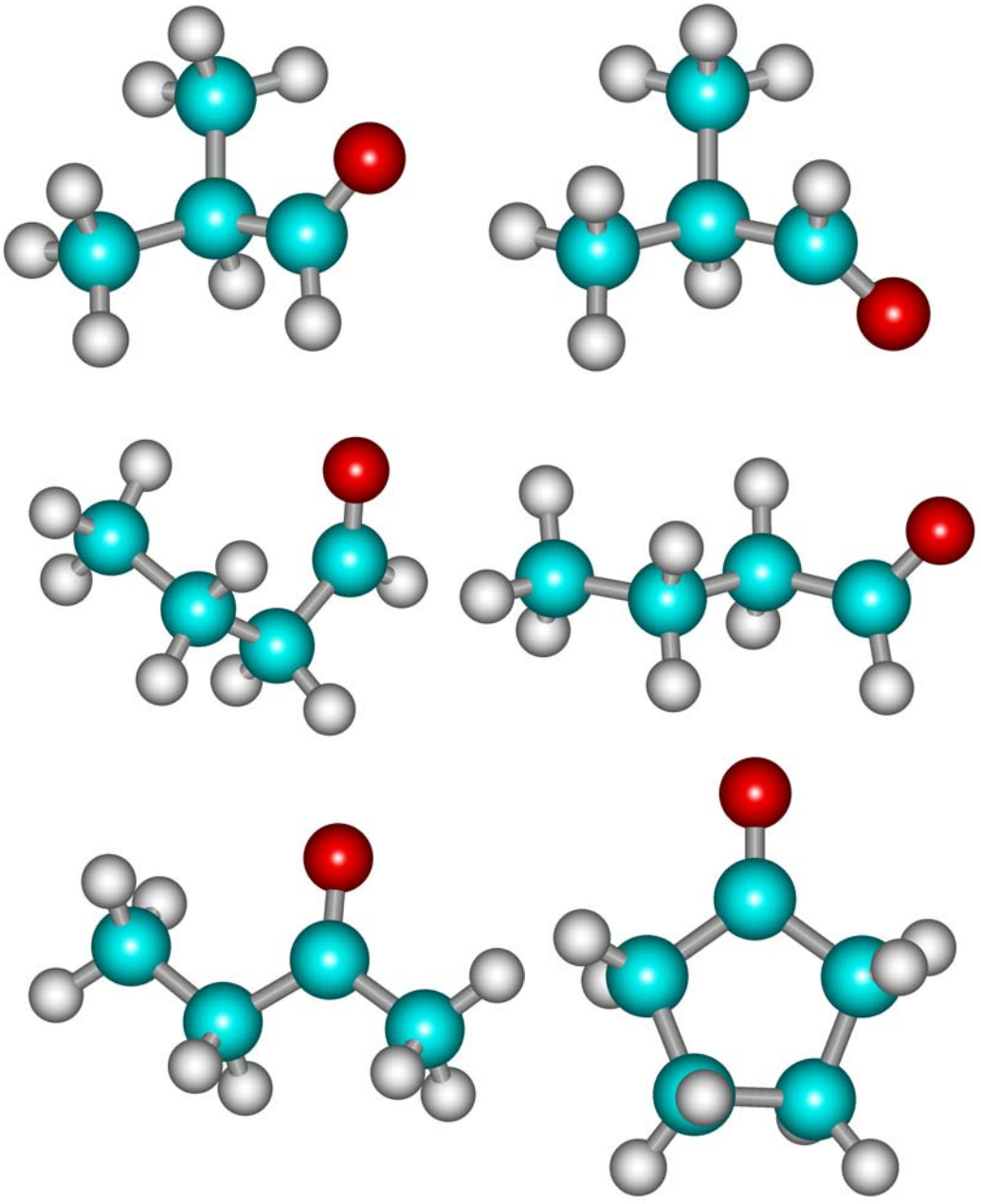

Figure 4.2 Optimized molecular geometries (from top left to bottom right) of 2-methylpropanal (*gauche*), 2-methylpropanal (*trans*), butanal (*cis/gauche*), butanal (*cis/trans*), butanone, and cyclopentanone.

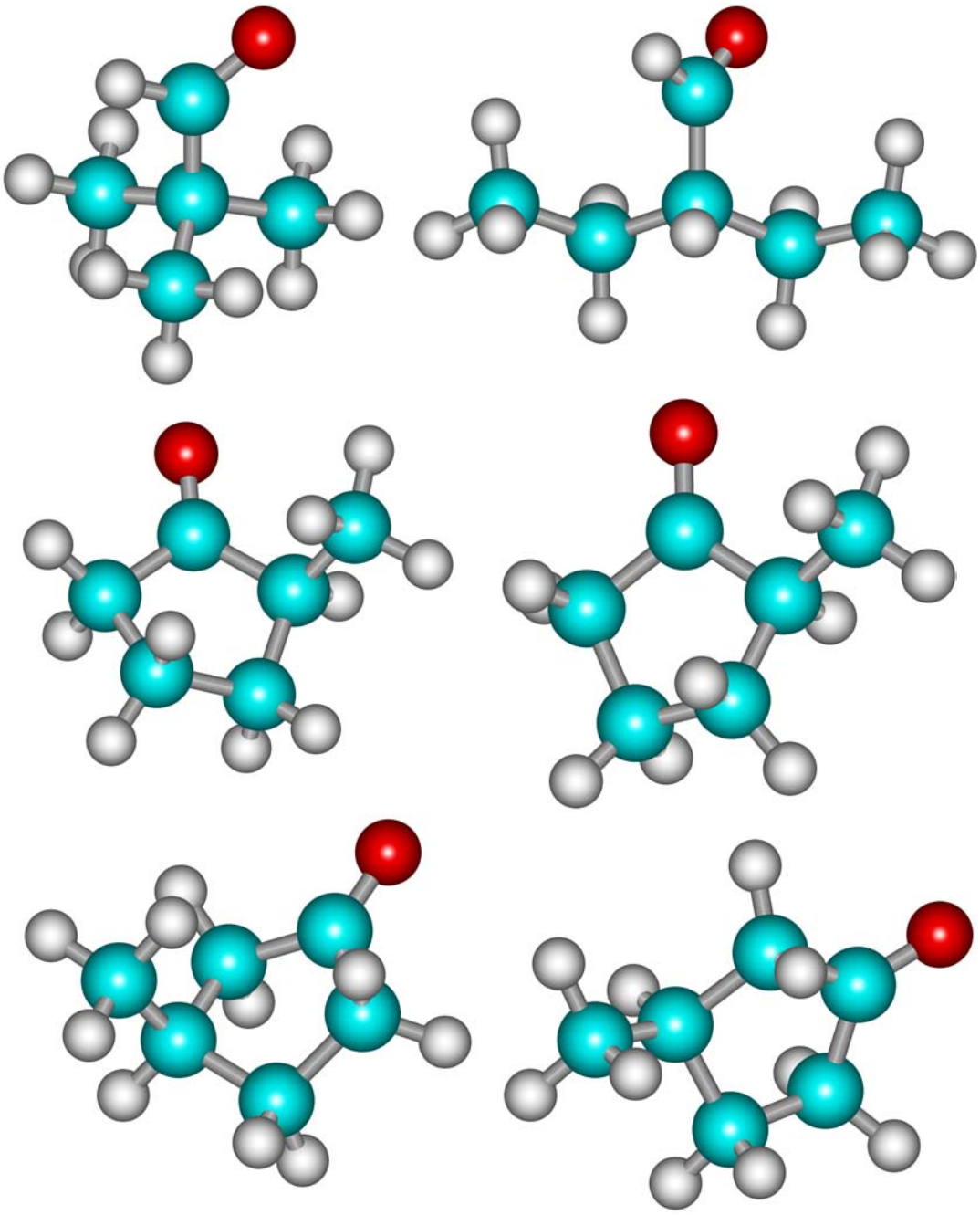

Figure 4.3 Optimized molecular geometry (from top left to bottom right) of pivalaldehyde, energy minimized structure of 2-ethylbutanal, and optimized molecular geometries of 2-methylcyclopentanone (axial), 2-methylcyclopentanone (equatorial), 3-methycyclopentanone (axial), and 3-methylcyclopentanone (equatorial).

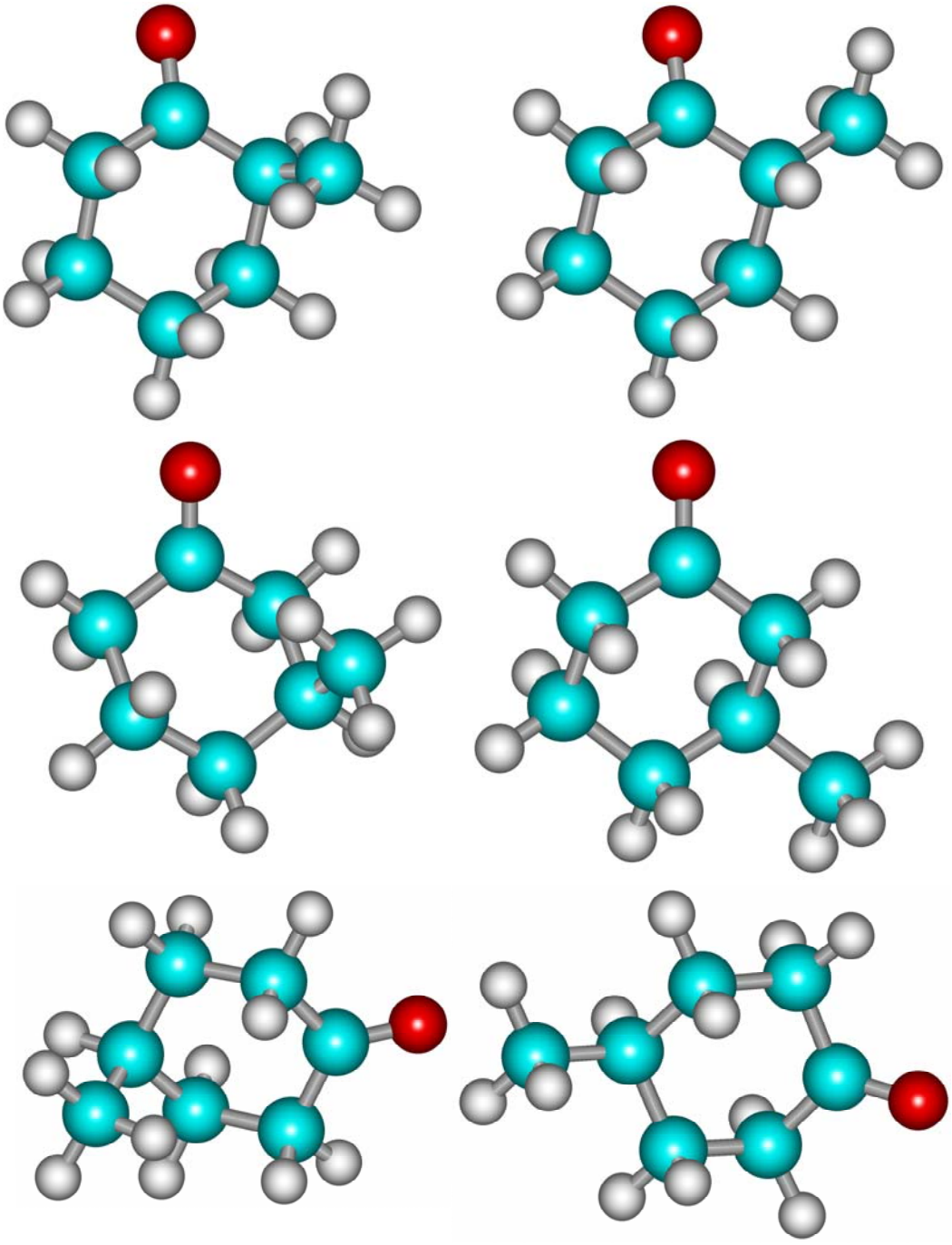

Figure 4.4 Energy minimized molecular geometries (from top left to bottom right) of 2-methylcyclohexanone (axial), 2-methylcyclohexanone (equatorial), 3-methylcyclohexanone (axial), 3-methylcyclohexanone (equatorial), 4-methyl-cyclohexanone (axial), 4-methylcyclohexanone (equatorial).

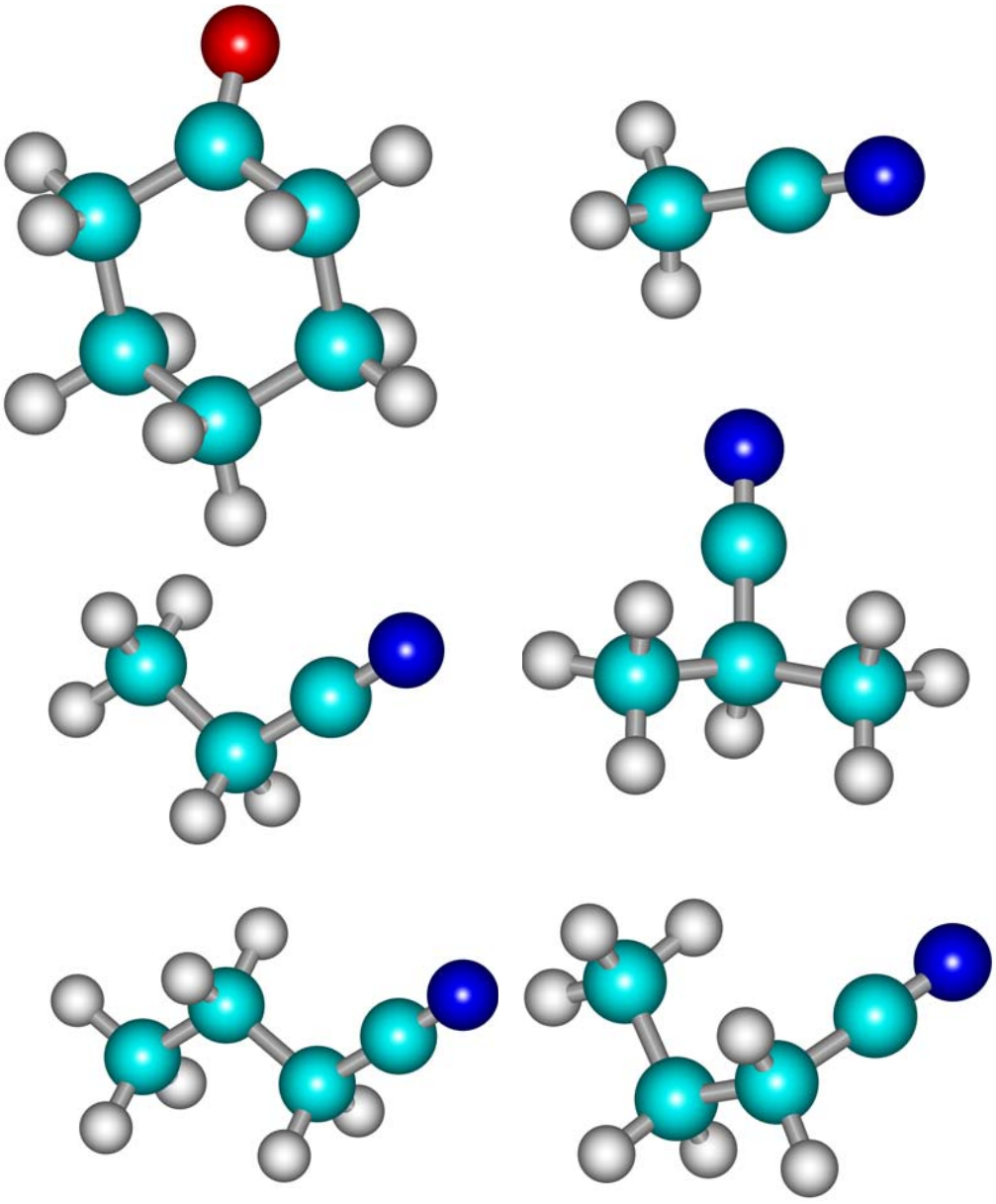

Figure 4.5 Optimized molecular geometries (from top right to bottom right) of cyclohexanone, acetonitrile, propanenitrile, 2-methylpropanenitrile, butanenitrile, and butanenitrile (*cis*).

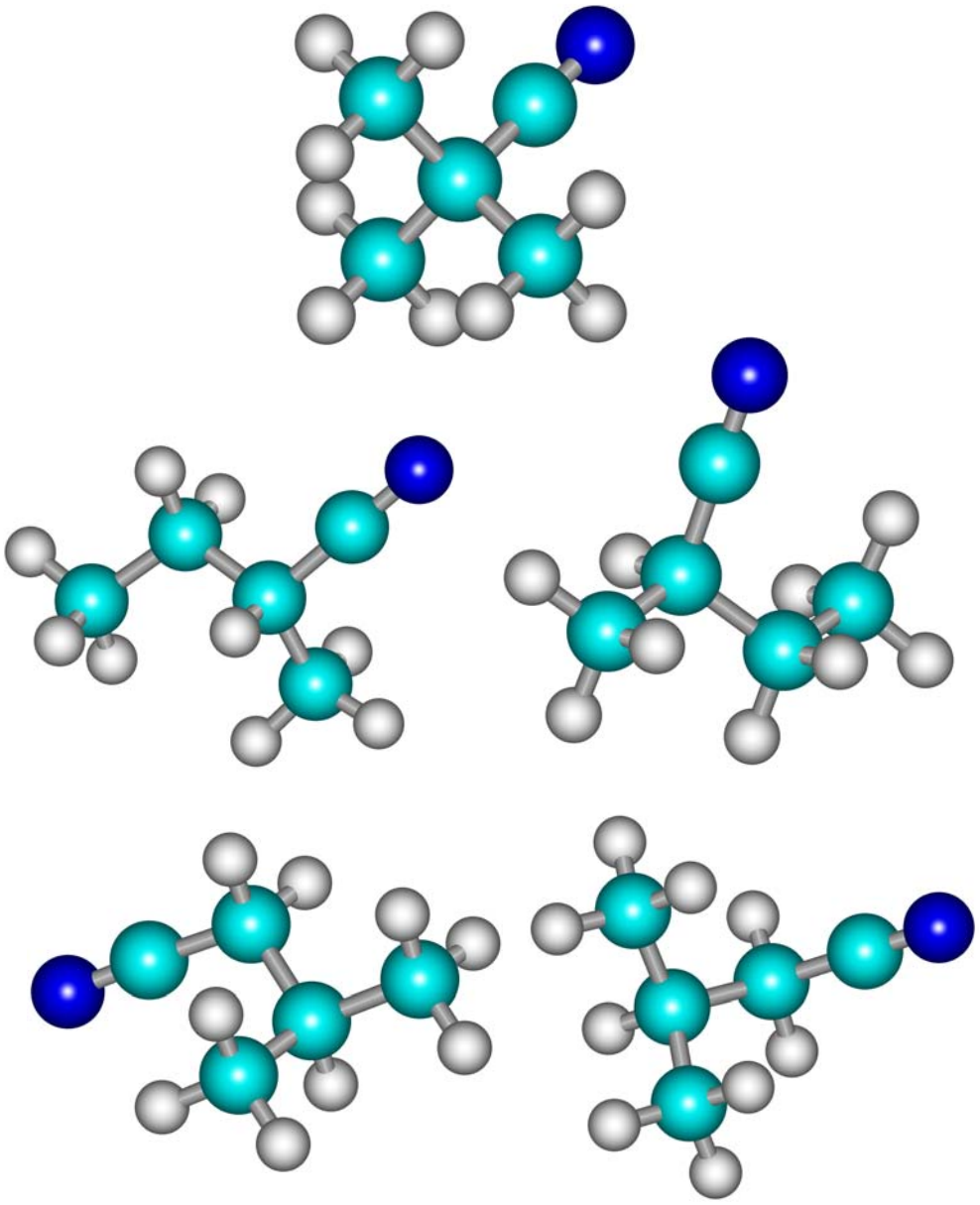

Figure 4.6 Optimized molecular geometries (from top left to bottom right) of 2,2-dimethylpropanenitrile, 2-methylpropanenitrile (*cis*), 2-methylpropanenitrile, 3-methylpropanenitrile (*cis*), and 3-methylpropanenitrile.

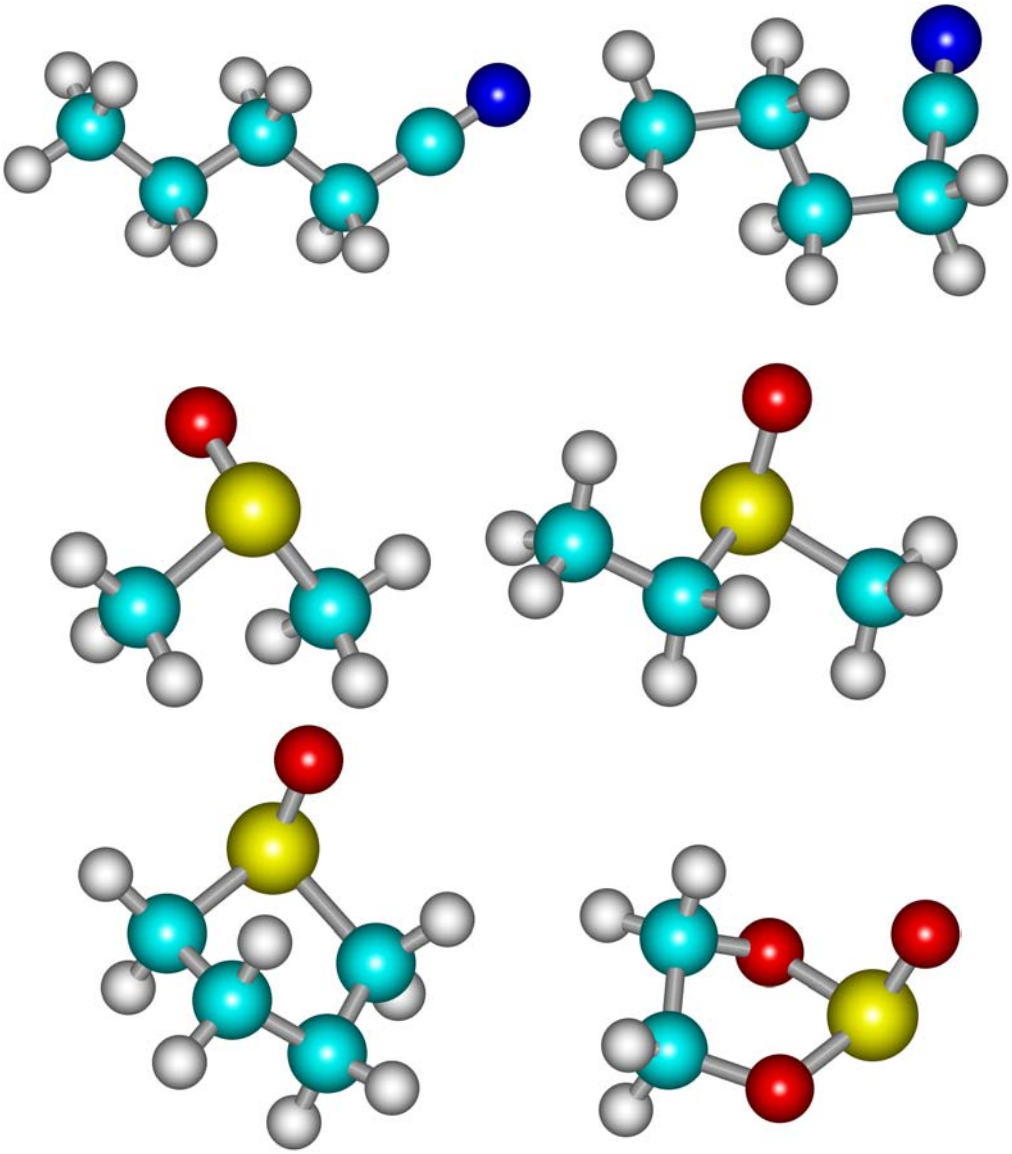

Figure 4.7 Optimized molecular geometries (from top left to bottom right) of pentanenitrile and pentanenitrile (*cis*) and energy minimized molecular geometries of dimethylsulfoxide, methylethylsulfoxide, tetramethylenesulfoxide, and glycol sulfite.

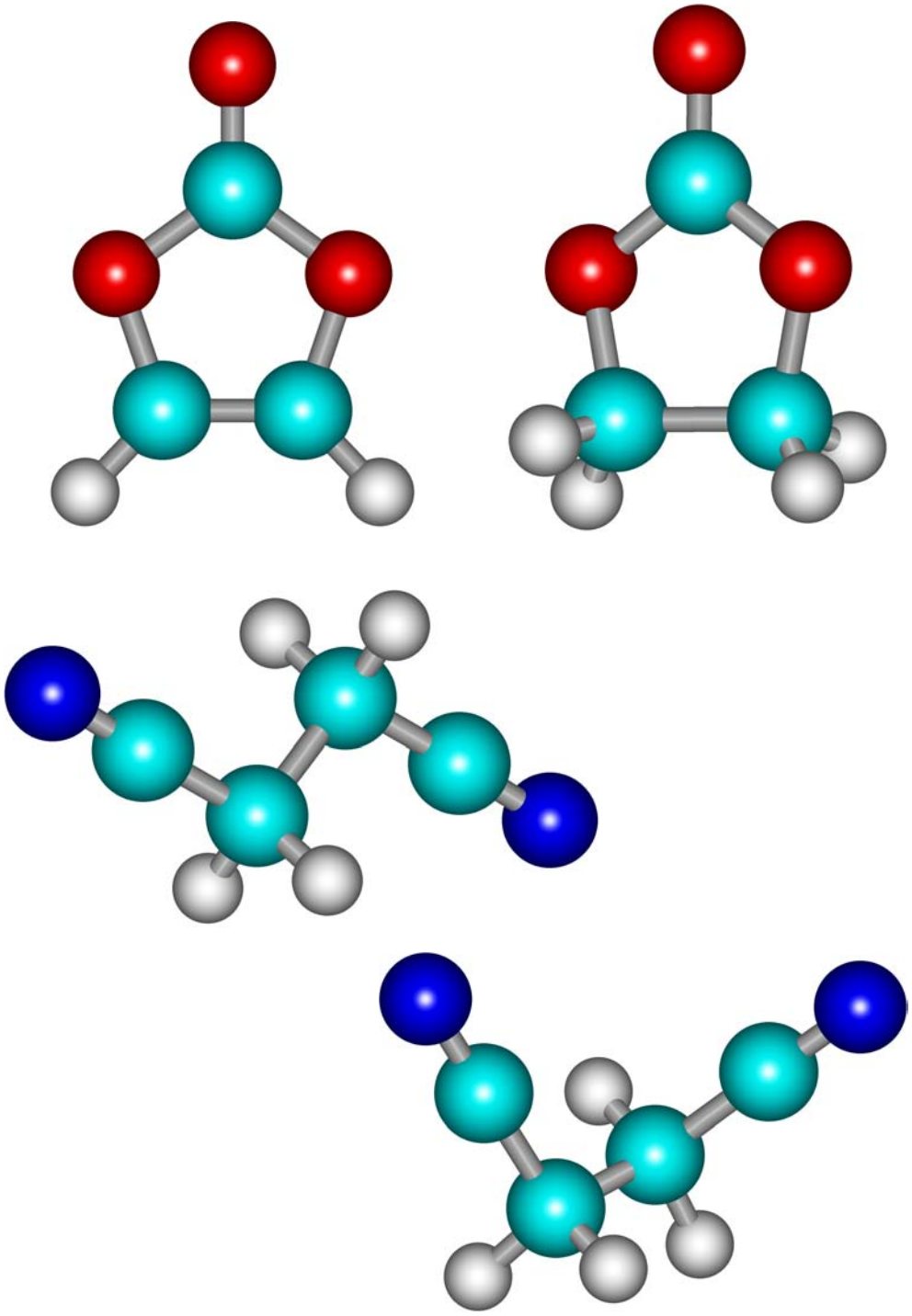

Figure 4.8 Optimized molecular geometries (from top left to bottom right) of vinylene carbonate, ethylene carbonate, succinonitrile (*anti*), and succinonitrile (*gauche*).

moment, frequencies, etc.) In order to expedite the calculation it is useful to have an initial molecular geometry to input into *Gaussian 98*. To this end the molecular structures were first calculated using *PC Model*.[139] *PC Model* optimizes molecular geometries but at a lower level of theory than *Gaussian 98*, however, these optimizations take just seconds to run and provide adequate starting geometries for *Gaussian 98* calculations. *PC Model* has a user-friendly graphical interface that allows for easy input of atoms and chemical bonds and angles. Geometry files can be saved in *PC Model* in a number of file formats (such as .pdb – protein database format) and then opened in *Gaussian 98*. A third software package, *Hyperchem*,[139] was used to generate the graphical renderings shown in Figures 4.1 - 4.8 using the geometries calculated from *Gaussian 98*.

Calculation of Optimized Geometries

Approximate molecular structures were entered into *PC Model* and then optimized using the MMX force field.[141] *PC Model* employs molecular mechanics, which is a theoretical method that uses classical mechanics to calculate the structure and energy of molecules based on nuclear motions. In this method electrons are not considered explicitly, but rather it is assumed that they follow the nuclei as they are moved to "optimum" positions. This is based on the Born-Oppenheimer approximation which says that for the most part the motions of the electrons and nuclei in atoms are separable. The optimum positions are determined by minimizing the potential energy of the molecule. The potential energy of a molecule can be written as a sum of simple functions:

$$V = \sum_{r} V_r(r) + \sum_{\vartheta} V_{\vartheta}(\vartheta) + \sum_{\beta} V_{\beta}(\beta) + \sum_{\gamma} V_{\gamma}(\gamma) + \sum_{\tau} V_{\tau}(\tau) + \sum_{r'} V_{ED}(r') + \sum_{r'} V_C(r') + \sum_{i,j,\ldots} V_{ij\ldots}(R_i, R_j, \ldots) \quad . \tag{4.1}$$

where r is the bond length, θ is the bond angle, β is the linear bond angle, γ is the out-of-plane angle, τ is the torsion angle, r' is some nonbonded internuclear distance, V_{ED} is exchange repulsion-dispersion interaction, V_c is the Coulomb interaction, and V_{ij} is a multivariable function that represents other interactions.[142] Different molecular mechanics software packages use different numbers of variables and different mathematical forms to describe the various potential functions. The force field being generated by such a potential function and acting on the nuclei is called the molecular force field. Early force fields were constructed based solely on experimental data but later ones incorporate results from quantum mechanical calculations.

The MMX force field was developed by J.J. Gajewski and K. E. Gilbert as an enhanced version of MM2,[143] an earlier force field written by N. L. Allinger that proved very useful in predicting structures and heats of formation of stable conformations of organic compounds. The parameters in the MM2 and MMX force fields are based upon the specific atom types in a molecule. For example, a carbonyl carbon is treated differently that an SP3 hybridized carbon and therefore interacts differently with other types of atoms. Most of the potential functions used by MM2 were incorporated into MMX. An example is the exchange repulsion-dispersion potential used by MM2, which is:

$$V_{\exp-6}(r'_{ij}) = \varepsilon_{ij}\left\{ b_{ij} \exp\left(-c_{ij} \frac{r'_{ij}}{r'^{e}_{ij}} \right) - a_{ij}\left(\frac{r'^{e}_{ij}}{r'_{ij}} \right)^6 \right\} \tag{4.2}$$

where a_{ij} and c_{ij} are parameters that are fixed at 2.25 and 12.5, respectively, and $r_{ij}'^{e}$ is the radius at the potential's minimum. The MMX force field has 60 different atom types, which includes radicals, cations, anions, and transition metals. This was a big improvement over MM2.

To optimize the geometry the overall potential energy of the molecule is minimized. This can be accomplished by changing the relative atomic positions in steps and calculating the potential energy at each step. Alternately, the slope of the potential energy can be calculated at each step and the next step chosen depending upon the success of the previous step. At a stationary point the first derivative of the energy is zero. This occurs at a minimum, maximum, or saddle point (see Figure 4.9). Once a geometry was optimized using *PC Model*, an input file could be generated for *Gaussian 98*. A sample input file for acetone is shown in Figure 4.10. The geometry of the molecule is in a Z-Matrix format. In this format each atom's position is relative to the positions of the other atoms in the molecule. Found in Appendix A are energy minimized geometries for all of the molecules studied here. For some of the molecules a frequency calculation was performed to insure that the geometry was a true minimum (no negative frequencies). A number of computers were used to run *Gaussian 98*. The two computers used most often include a 1.9 GHz Pentium 4 Windows 2000 machine with 1 GB RAM and a dual processor 1.8 GHz AMD Athlon Linux machine with 4 GB RAM.

Calculation of Dipole Moments and Molecular Polarizabilities

The calculations performed using *Gaussian 98* were ab initio electronic structure calculations. This means that the laws of quantum mechanics rather than classical

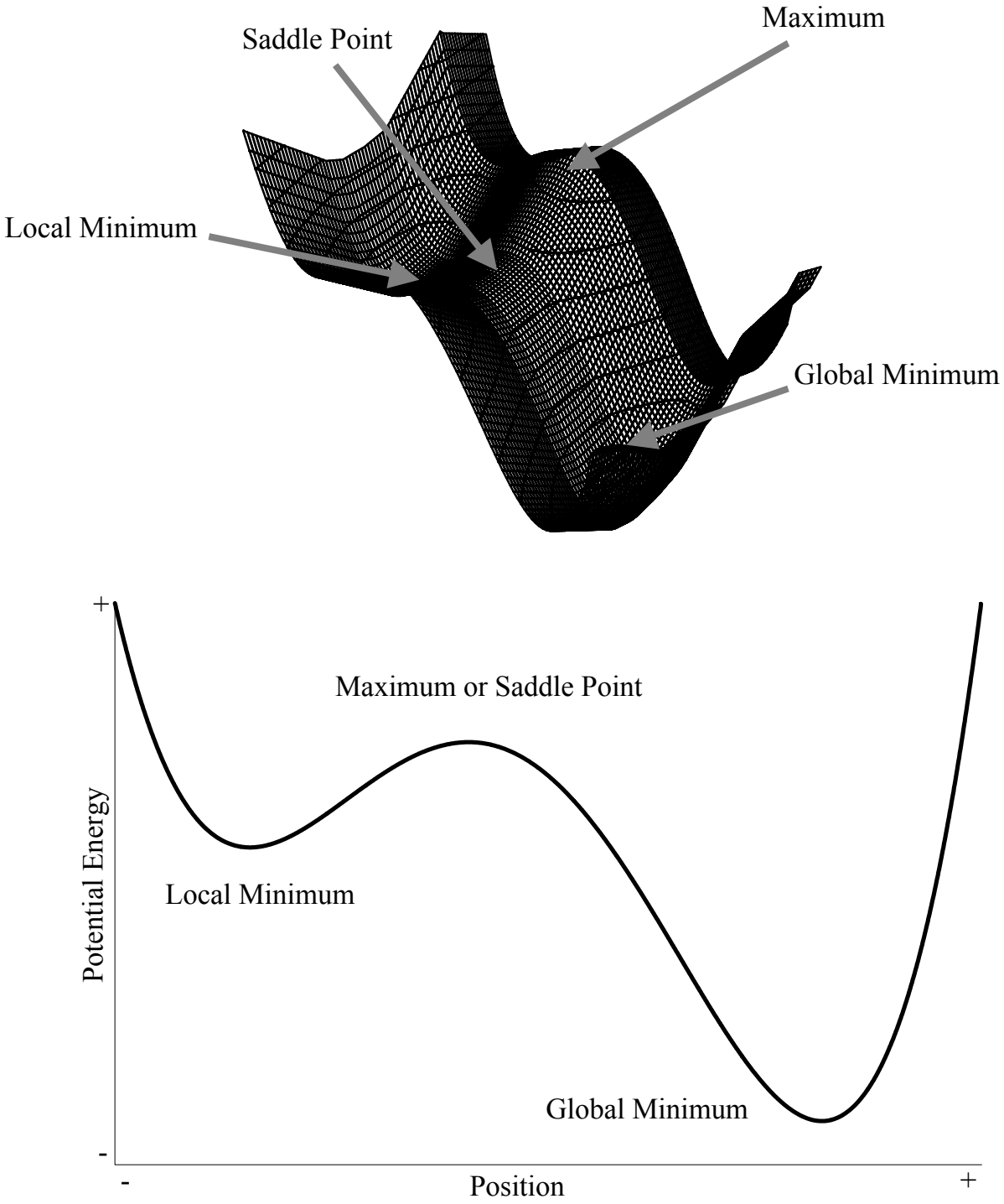

Figure 4.9 Idealized potential energy surface (top) and 2D slice (bottom).

```
%rwf=a.rwf,1900mb,b.rwf,1900mb,c.rwf,1900mb,d.rwf,1900mb,e.rwf,1900mb

%mem=1000mb
#MaxDisk=70000mb
#mp2/aug-cc-pvtz opt density=current pop=(chelpg, dipole)

Acetone Geometry Optimization and Dipole Moment Calculation

0 1
C
C,1,R2
H,1,R3,2,A3
H,1,R4,2,A4,3,D4,0
H,1,R5,2,A5,3,D5,0
C,2,R6,1,A6,3,D6,0
O,2,R7,1,A7,6,D7,0
H,6,R8,2,A8,1,D8,0
H,6,R9,2,A9,8,D9,0
H,6,R10,2,A10,8,D10,0
Variables:
R2=1.51951209
R3=1.11415798
R4=1.11250258
R5=1.11401122
R6=1.51878932
R7=1.21107968
R8=1.1139035
R9=1.11407181
R10=1.11337595
A3=111.17757178
A4=110.04347764
A5=109.99042612
A6=115.75471612
A7=122.12924749
A8=111.20160096
A9=110.05536369
A10=110.03691228
D4=-119.97870388
D5=119.80996099
D6=-179.9495621
D7=-179.96384026
D8=-179.96218855
D9=119.91733684
D10=-119.92847957
```

Figure 4.10 Sample *Gaussian 98* input file for acetone.

physics were used as a basis for calculations. First principles such as physical constants are also used in these calculations rather than experimental parameters. In ab initio calculations solutions to the Schrödinger equation:

$$\hat{H}\Psi = E\Psi \tag{4.3}$$

are computed using mathematical approximations. The Hartree-Fock approximation assumes that electrons occupy molecular orbitals[144] and uses an exact Hamiltonian and approximate many-electron wave functions, the simplest of which is a single Slater determinant. According to the variational principle the optimum spin orbitals are those which minimize the electronic energy:

$$E_0 = \left\langle \Psi_0^* \middle| \hat{\mathrm{H}} \middle| \Psi_0 \right\rangle \tag{4.4}$$

where:

$$\left| \Psi_0 \right\rangle = \left| \chi_1 \chi_2 \cdots \chi_a \chi_b \cdots \chi_N \right\rangle . \tag{4.5}$$

The goal of the Hartree-Fock method is to determine the best spin orbitals $\{\chi_a\}$ that minimize this energy. The spin orbitals must remain orthonormal such that:

$$\left\langle \chi_a \mid \chi_b \right\rangle = \delta_{ab} . \tag{4.6}$$

The equation for the best Hartree-Fock spin orbitals is given by the Hartree-Fock Equation (in atomic units):

$$h(1)\chi_a(1) + \sum_{b \neq a} \left[\int dx_2 \left| \chi_b(2) \right|^2 r_{12}^{-1} \right] \chi_a(1) - \sum_{b \neq a} \left[\int dx_2 \chi_b^*(2) \chi_a(2) r_{12}^{-1} \right] \chi_b(1) = \varepsilon_a \chi_a(1) \tag{4.7}$$

where

$$h(1) = -\frac{1}{2}\nabla_1^2 - \sum_A \frac{Z_A}{r_{1A}} \tag{4.8}$$

is the kinetic and potential energy for attraction to the nuclei of one electron. The second term in Equation 4.7 can be separated out as the Coulomb operator:

$$J_b(1) = \int dx_2 |\chi_b(2)|^2 r_{12}^{-1} \tag{4.9}$$

and the third term can be separated out as the exchange operator:

$$K_b(1) = \int dx_2 \chi_b^*(2) \chi_a(2)\, r_{12}^{-1} \tag{4.10}$$

so that the Hartree-Fock Equation can be written as:

$$\left[h(1) + \sum_b J_b(1) - \sum_b K_b(1) \right] \chi_a(1) = \varepsilon_a \chi_a(1) \tag{4.11}$$

since:

$$[J_a(1) - K_a(1)] \chi_a(1) = 0. \tag{4.12}$$

Equation 4.11 is usually written as:

$$f |\chi_a\rangle = \varepsilon_a |\chi_a\rangle \tag{4.13}$$

and the Fock Operator *f* is usually written as:

$$f(i) = -\frac{1}{2}\nabla_i^2 - \sum_{A=1}^{M} \frac{Z_A}{r_{iA}} + v^{HF}(i) \tag{4.14}$$

where $v^{HF}(i)$ is the average potential experienced by the ith electron due to the presence of other electrons.

The procedure for solving the Hartree-Fock Equation is the self-consistent-field (SCF) method. In SCF, an initial guess is made of the spin orbitals and $v^{HF}(i)$ is calculated. A new set of spin orbitals is obtained by solving Equation 4.13. This procedure is repeated until self-consistency is achieved, which means that $v^{HF}(i)$ no longer changes. A finite set of spatial basis functions *K* is used to solve the Hartree-Fock

Equation. The larger and more complete the set of basis functions the lower the Hartree-Fock energy E_0 becomes. The unknown molecular orbitals are given by:

$$\Psi_i = \sum_{\mu=1}^{K} C_{\mu i}\phi_\mu \tag{4.15}$$

so that:

$$f(1)\sum_v C_{vi}\phi_v(1) = \varepsilon_i \sum_v C_{vi}\phi_v(1). \tag{4.16}$$

Equation 4.16 becomes a matrix equation:

$$\sum_v C_{vi}\int dr_1 \phi_\mu^*(1) f(1)\phi_v(1) = \varepsilon_i \sum_v C_{vi}\int dr_1 \phi_\mu^*(1)\phi_v(1) \tag{4.17}$$

that can be simplified to:

$$\sum_v F_{\mu v}C_{vi} = \varepsilon_i \sum_v S_{\mu v}C_{vi} \tag{4.18}$$

where $F_{\mu v}$ is called the Fock matrix:

$$F_{\mu v} = \int dr_1 \phi_\mu^*(1) f(1)\phi_v(1) \tag{4.19}$$

and $S_{\mu v}$ is called the overlap matrix:

$$S_{\mu v} = \int dr_1 \phi_\mu^*(1)\phi_v(1). \tag{4.20}$$

The core-Hamiltonian matrix can be separated from the Fock matrix as:

$$H_{\mu v}^{core} = \int dr_1 \phi_\mu^*(1) h(1)\phi_v(1) \tag{4.21}$$

so that the Fock matrix can be written as:

$$\begin{aligned} F_{\mu v} &= H_{\mu v}^{core} + \sum_a^{N/2} 2(\mu v \mid aa)(\mu a \mid av) = H_{\mu v}^{core} + \sum_{\lambda\sigma} P_{\lambda\sigma}\left[(\mu v \mid \sigma\lambda) - \frac{1}{2}(\mu\lambda \mid \sigma v)\right] \\ &= H_{\mu v}^{core} + G_{\mu v} \end{aligned}. \tag{4.22}$$

The core-Hamiltonian matrix is the one electron part of the Fock matrix and is fixed depending upon the basis set employed. The two electron part of the Fock matrix is $G_{\mu\nu}$. This part depends on the density matrix P and a set of two electron integrals:

$$(\mu\nu \mid \sigma\lambda) = \int dr_1 dr_2 \phi_\mu^*(1)\phi_\nu(1) r_{12}^{-1} \phi_\lambda^*(2)\phi_\sigma(2). \tag{4.23}$$

There are two common types of basis sets that are widely used, Slater-type and Gaussian-type. The basis sets *Gaussian 98* uses are Gaussian-type atomic functions. The 1s Gaussian-type function (centered at R_A) has the form:

$$\phi_{1s}^{GF}(\alpha, r - R_A) = (2\alpha/\pi)^{3/4} e^{-\alpha|r-R_A|^2} \tag{4.24}$$

where α is called the orbital exponent. Slater-type functions are actually better at describing molecular orbitals but Gaussian-type functions allow for much faster calculations. Therefore, it is useful to create linear combinations of primitive Gaussian functions to construct new functions that better model molecular orbitals. These new functions are called contracted Gaussian functions. The basis set selected for most of the calculations performed here was one of Dunning's correlation consistent basis sets, aug-cc-pVDZ.[145] Dunning established that compact sets of primitive Gaussian functions effectively and efficiently describe correlation effects if the exponents of the functions are optimized in atomic correlated calculations. The aug-cc-pVDZ is the augmented correlation consistent double-zeta basis set, being augmented with diffuse functions to better describe electron affinities and other molecular properties. This is important for the calculations performed here since the excess electron in dipole bound anions exists in very diffuse states.

The method used to optimize the geometry and calculate molecular properties was the 2nd order Møller-Plesset pertubabation theory (MP2).[146,147] MP2 takes into account some degree of electron correlation which makes its results closer to reality than those obtained from Hartree-Fock. This is because Hartree-Fock only evaluates the repulsion energy as an average over the whole molecular orbital. When *Gaussian 98* calculates the MP2 energy it first calculates the Hartree-Fock energy and then a Møller-Plesset correlation energy correction is made that is truncated at the second-order. It is an exact solution to an approximate Hamiltonian operator which is the sum of Fock operators for each electron. Perturbation theory in general divides the Hamiltonian into two parts, one that can be solved exactly (H_0) and then a part that is a perturbation, or small correction, to H_0. The perturbation here is the difference between the exact Hamiltonian operator and this sum of Fock operators. The Hartree-Fock result is the zero order term. The zero-order energy is the sum of orbital energies. The Hamiltonian is thus given by:

$$H = H_0 + \lambda V \tag{4.25}$$

where V is the perturbation. The exact energy and wavefunction can be expanded in λ as:

$$E_i = E_i^{(0)} + \lambda E_i^{(1)} + \lambda^2 E_i^{(2)} + \ldots \tag{4.26}$$

$$\Psi_i = \Psi_i^{(0)} + \lambda \Psi_i^{(1)} + \lambda^2 \Psi_i^{(2)} + \ldots . \tag{4.27}$$

Substituting these into the Schrödinger equation (Equation 4.3) yields:

$$H_0 \Psi_i^{(0)} = E_i^{(0)} \Psi_i^{(0)} \tag{4.28}$$

$$H_0 \Psi_i^{(1)} + V \Psi_i^{(0)} = E_i^{(0)} \Psi_i^{(1)} + E_i^{(1)} \Psi_i^{(0)} \tag{4.29}$$

$$H_0 \Psi_i^{(2)} + V \Psi_i^{(1)} = E_i^{(0)} \Psi_i^{(2)} + E_i^{(1)} \Psi_i^{(1)} + E_i^{(2)} \Psi_i^{(0)} . \tag{4.30}$$

Multiplying each of these equations on the left by $\Psi_i^{(0)}$ and integrating over all space yields expressions for $E^{(n)}$ in terms of V and $\Psi_i^{(n-1)}$:

$$E_i^{(0)} = \left\langle \Psi_i^{(0)} \middle| H_0 \middle| \Psi_i^{(0)} \right\rangle \tag{4.31}$$

$$E_i^{(1)} = \left\langle \Psi_i^{(0)} \middle| V \middle| \Psi_i^{(0)} \right\rangle \tag{4.32}$$

$$E_i^{(2)} = \left\langle \Psi_i^{(0)} \middle| V \middle| \Psi_i^{(1)} \right\rangle \tag{4.33}$$

$$E_i^{(3)} = \left\langle \Psi_i^{(0)} \middle| V \middle| \Psi_i^{(2)} \right\rangle \tag{4.34}$$

and so on. The Hartree-Fock energy is the sum of $E^{(0)}$ and $E^{(1)}$. By using the expansion:

$$\Psi_i^{(1)} = \sum_n c_n^{(1)} \Psi_n^{(0)} \tag{4.35}$$

an expression for the coefficients can be found:

$$c_n^{(1)} = \frac{\left\langle \Psi_n^{(0)} \middle| V \middle| \Psi_0^{(0)} \right\rangle}{E_n^{(0)} - E_0^{(0)}} . \tag{4.36}$$

The second-order Møller-Plesset (MP2) energy is therefore:

$$E_i^{(2)} = \frac{\left| \left\langle \Psi_i^{(0)} \middle| V \middle| \Psi_n^{(0)} \right\rangle \right|^2}{E_i^{(0)} - E_n^{(0)}} . \tag{4.37}$$

Higher order corrections can be calculated (MP3 and MP4) but these are much more demanding computationally and give similar results to the quantities studied here.

The MP2 energies obtained for all of the molecules and conformations of molecules studied here are shown in Table 4.1. For some of the molecules a frequency calculation was performed to verify that the geometry was a true minimum and not a maximum or a saddle point (see Figure 4.9). Since the frequencies vary as the square root of the second derivative of the potential energy, imaginary frequencies result from

Table 4.1 MP2 energies for a number of polar molecules. * denotes that a frequency calculation was performed to verify that the molecule was indeed at a true minimum.

Compound	MP2/aug-cc-pVDZ Energy
Acetaldehyde	-153.4183187*
Propanal (*cis*)	-192.6063829*
Propanal (*trans*)	-192.6048469*
Acetone	-192.6160805*
Cyclobutanone	-230.5804871*
2-Methylpropanal (*gauche*)	-231.7962581*
2-Methylpropanal (*trans*)	-231.7954926*
Butanal (*cis/gauche*)	-231.7937457*
Butanal (*cis/trans*)	-231.7927098*
2-Butanone	-231.8043765*
Cyclopentanone	-269.8029800*
Pivalaldehyde	-270.9898597*
2-Ethylbutanal	-310.1708588
2-Methylcyclopentanone (*axial* -CH_3)	-308.9937635
2-Methylcyclopentanone (*equatorial*)	-308.9950234
3-Methylcyclopentanone (*axial*)	-308.9939879
3-Methylcyclopentanone (*equatorial*)	-308.9948183
Cyclohexanone	-308.9977931*
2-Methylcyclohexanone (*axial*)	-348.1874630
2-Methylcyclohexanone (*equatorial*)	-348.1901761
3-Methylcyclohexanone (*axial*)	-348.1889361
3-Methylcyclohexanone (*equatorial*)	-348.1902527
4-Methylcyclohexanone (*axial*)	-348.1875864
4-Methylcyclohexanone (*equatorial*)	-348.1898447
Acetonitrile	-132.3835491*
Propanenitrile	-171.5705984*
2-Methylpropanenitrile	-210.7610087*
Butanenitrile	-210.7587459*
Butanenitrile (*gauche*)	-210.7593278*
2,2-Dimethylpropanenitrile	-249.9544282*
2-Methylbutanenitrile	-249.9486492*
2-Methylbutanenitrile (*gauche)*	-249.9501225*
3-Methylbutanenitrile	-249.9511940*
3-Methylbutanenitrile (*gauche*)	-249.9509027*
Pentanenitrile	-249.9466576*
Pentanenitrile (*gauche*)	-249.9472780*
Dimethyl Sulfoxide	-552.2405912
Methyl Ethyl Sulfoxide	-591.4310354
Tetramethylene Sulfoxide	-629.4357334
Glycol Sulfite	-701.1793866
Vinylene Carbonate	-340.3532507*
Ethylene Carbonate	-341.5684670*
Succinonitrile (*anti*)	-263.5849809*
Succinonitrile (*gauche*)	-263.5837450*

the geometry being at a saddle point or a maximum. *Gaussian 98* displays imaginary frequencies as negative numbers. For some of the larger molecules a frequency calculation was impractical due to required computing resources. Important is the fact that since many of the conformational energies are similar more than one exist at room temperature. *Gaussian 98* calculates the dipole moment automatically when the geometry is optimized and the MP2 energy is calculated. When frequencies are calculated the polarizability is also obtained. However, the larger molecules require extreme amounts of time and resources for frequency calculations. For this reason the MP2 energies of the larger molecules were calculated in various electric fields. The total Hamiltonian in the presence of an electric field is:

$$H(\vec{F}) = H_0 + \vec{F}\sum_i r(i) \tag{4.38}$$

where *r(i)* is the coordinate of electron *i*. The total energy of a molecule in the presence of the electric field can be expanded as a Taylor Series:

$$E(\vec{F}) = E_0 + \sum_i \left(\frac{\partial E(\vec{F})}{\partial F_i}\right)_0 F_i + \frac{1}{2}\sum_{ij}\left(\frac{\partial^2 E(\vec{F})}{\partial F_i \partial F_j}\right)_0 F_i F_j . \tag{4.39}$$

The sum is over the Cartesian components of the field (x, y, z). The dipole moment vector in the i^{th} direction is given by:

$$\mu_i = \left(\frac{\partial E(\vec{F})}{\partial F_i}\right)_0 \tag{4.40}$$

and the polarizability is given by

$$\alpha_{ij} = \left(\frac{\partial^2 E(\vec{F})}{\partial F_i \partial F_j}\right)_0 . \tag{4.41}$$

A plot of energy as a function of electric field can be estimated as a quadratic relationship. The linear coefficients yield the dipole moment and the quadratic coefficients yield the polarizability for a particular molecule. A portion of a *Gaussian 98* input file for such a calculation is shown in Figure 4.11 and the resulting plot is shown in Figure 4.12 for 4-methycyclohexanone (equatorial methyl group conformation).

Shown in Table 4.2 is a summary of the experimental (EXP) and calculated (MP2) dipole moments and polarizabilities for the molecules studied here. For some of the smaller molecules the aug-cc-pVTZ[145] basis set, which is larger (triple-zeta), was also used for comparison. For the carbonyl and nitrile containing molecules there is little change upon employing the larger basis set. However, there is a sizeable variation in the dipole moment for the sulfoxide containing molecules. One sees that the calculated dipole moment becomes closer to the experimental value when the larger basis set is employed. This is most likely due to the influence of the low-lying *d* atomic orbitals in sulfur.

The method of Miller and Savchik[148] (EMP) was also used to empirically estimate the molecular polarizabilities. This method calculates molecular polarizabilties (in $Å^3$) from individual atomic components:

$$\alpha = \frac{4}{N}\left[\sum_A \tau_A\right]^2 \tag{4.42}$$

where N is the number of electrons in the molecule and τ_A are atomic hybrid components. The atomic hybrid components for –H, –C–, –C≡, ≡N, and =O are 0.314, 1.294, 1.393, 1.304, and 1.216 $Å^{3/2}$, respectively. Thus, for acetone:

```
%rwf=a.rwf,1900mb,b.rwf,1900mb,c.rwf,1900mb,d.rwf,1900mb
%nosave
%chk=4mcyclo.chk
%mem=1500mb

#mp2/aug-cc-pvdz

4-methylcyclohexanone in various electric fields

0 1
O
C,1,1.23184971
C,2,1.52001399,1,122.59679043
C,2,1.52001547,1,122.59667172,3,-177.36210913,0
C,3,1.54383556,2,109.88449919,1,-124.09302556,0
C,4,1.54383381,2,109.88440738,1, 124.0928244,0
H,3,1.09997799,2,108.84906425,5, 123.13948424,0
H,3,1.10600739,2,108.22574756,5,-118.88222833,0
H,4,1.09997815,2,108.84869426,6,-123.13955102,0
H,4,1.10600840,2,108.22570044,6,118.88251466,0
C,5,1.53662431,3,111.86292268,2,-54.61703556,0
H,5,1.10365885,3,109.75484961,11,-122.67203396,0
H,5,1.10659274,3,109.22951663,11,120.4000964,0
H,6,1.10365930,4,109.75498937,2,177.28929325,0
H,6,1.10659180,4,109.22944157,14,116.92804872,0
C,11,1.53242384,5,111.15356488,3,-179.42523205,0
H,11,1.10859379,5,108.02060205,16,119.12466003,0
H,16,1.10214093,11,111.21179805,5,58.49909959,0
H,16,1.10345885,11,110.31691504,18,-119.76051289,0
H,16,1.10214214,11,111.21153686,18,120.47931434,0

--link1--
%rwf=a.rwf,1900mb,b.rwf,1900mb,c.rwf,1900mb,d.rwf,1900mb
%nosave
%chk=4mcyclo.chk
%mem=1500mb

#mp2/chkbasis geom=allcheck field=z+10
--link1--
%rwf=a.rwf,1900mb,b.rwf,1900mb,c.rwf,1900mb,d.rwf,1900mb
```
etc.

Figure 4.11 Sample *Gaussian 98* input file for a molecule in various electric fields. The first calculation is in zero field. The second calculation is performed in a field of magnitude 10 a.u. in the z direction. The third calculation is performed in a field of magnitude 8 a.u. This is repeated until calculations have been performed for fields -10 to 10 a.u. in the x, y, and z directions. The geometry only needs to be entered once.

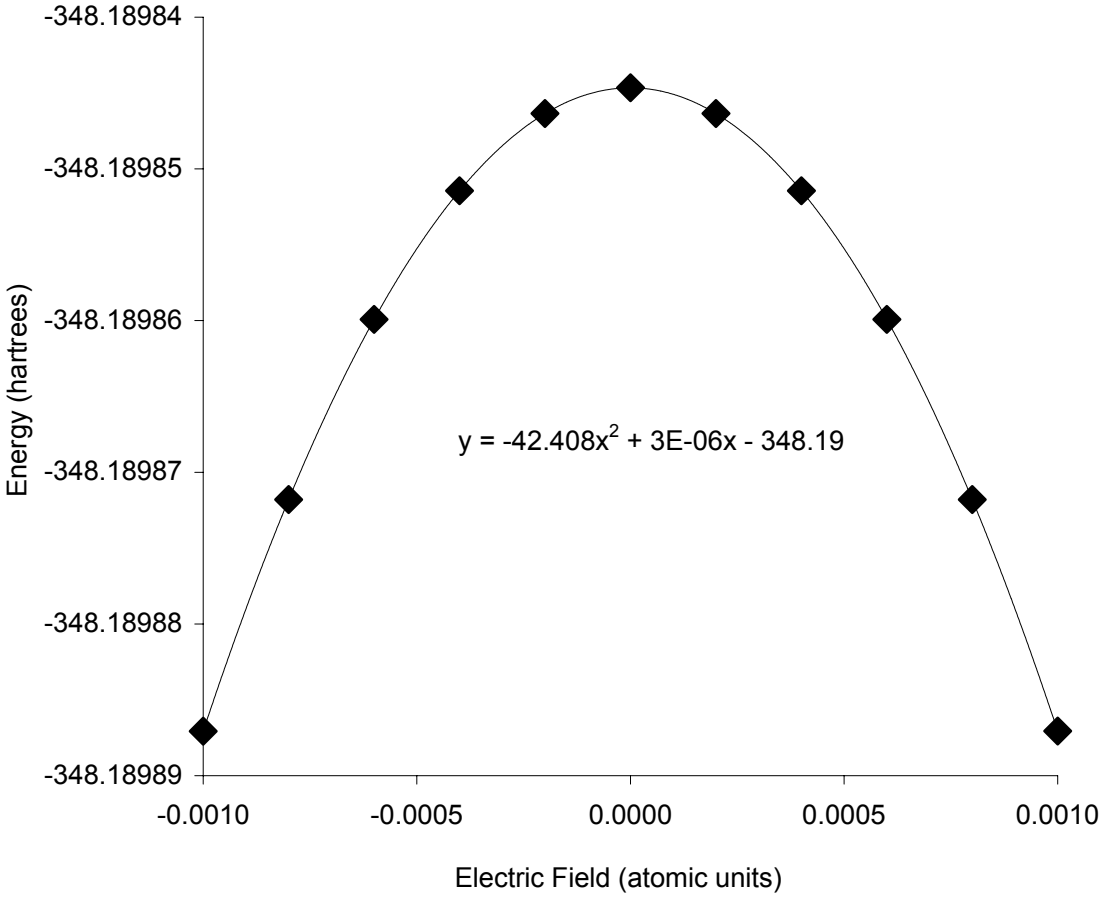

Figure 4.12 MP2 Energies of 4-methylcyclohexanone (equatorial methyl group) as a function of electric field. The fit of the curve to a quadratic relation is also given.

Table 4.2 Experimental and theoretical properties of polar molecules.

Molecule	Formula	Dipole Moment (D)			Polarizability (10^{-24} cm^3)		
		EXP	MP2 PVDZ	MP2 PVTZ	EXP	EMP	MP2 PVDZ
Acetaldehyde	CH_3CHO	2.75	2.81	2.80	4.6	4.5	4.50
Propanal (*cis*)	CH_3CH_2CHO	2.52	2.68	2.68	6.5	6.33	6.24
Propanal		2.86	2.91	2.91			6.29
Acetone	CH_3COCH_3	2.88	2.99	2.98	6.4	6.33	6.28
d-Acetone	CD_3COCD_3	2.89					
Cyclobutanone	C_4H_6O	2.89	2.93	2.92	7.7	7.45	7.51
2-Methylpropanal (*gauche*)	$(CH_3)_2CHCHO$	2.69	2.76			8.17	8.04
2-Methylpropanal (*trans*)		2.86	2.91	2.92			8.09
Butanal (*cis/gauche*)	$CH_3CH_2CH_2CHO$	2.72	2.57		8.2	8.17	8.15
Butanal (*cis/trans*)			2.97				8.15
2-Butanone	$CH_3CH_2COCH_3$	2.78	2.83		8.1	8.17	8.03
Cyclopentanone	C_5H_8O	2.88	3.13		9.3	9.28	9.08
Pivalaldehyde	$(CH_3)_3CCHO$	2.66	2.74		10	10.01	9.84
2-Ethylbutanal	$(CH_3CH_2)_2CHCHO$		2.62			11.83	11.56
2-Methylcyclopentanone (*axial)*	$C_6H_{10}O$		2.99			11.12	10.81
2-Methylcyclopentanone(*equatorial*)			2.97				10.87
3-Methylcyclopentanone (*axial*)	$C_6H_{10}O$	3.14	3.17			11.12	10.82
3-Methylcyclopentanone(*equatorial*)			3.17				10.96
Cyclohexanone	$C_6H_{10}O$	2.87	3.29		11.5	11.12	10.83
2-Methylcyclohexanone (*axial*)	$C_7H_{12}O$		3.21			12.97	12.56
2-Methylcyclohexanone (*equatorial*)			3.09				12.51
3-Methylcyclohexanone (*axial*)	$C_7H_{12}O$		3.24			12.97	12.53
3-Methylcyclohexanone (*equatorial*)			3.26				12.13
4-Methylcyclohexanone (*axial*)	$C_7H_{12}O$	3.26	3.35			12.97	12.57
4-Methylcyclohexanone (*equatorial*)			3.31				12.71
Acetonitrile	CH_3CN	3.92	3.92	3.94	4.44	4.42	4.36
Propanenitrile	CH_3CH_2CN	4.05	4.03	4.03	6.47	6.27	6.19
2-Methylpropanenitrile	$(CH_3)_2CHCN$	4.29	4.04		8.05	8.11	8.01
Butanenitrile	$CH_3(CH_2)_2CN$	4.07	4.15		8.4	8.11	8.06
Butanenitrile (*gauche*)			3.99				7.94
2,2-Dimethylpropanenitrile	$(CH_3)_3CCN$	3.95	4.02		9.59	9.95	9.80
2-Methylbutanenitrile	$CH_3CH_2CHCH_3CN$		4.15			9.95	9.81
2-Methylbutanenitrile (*gauche*)			3.99			9.95	9.88
3-Methylbutanenitrile	$(CH_3)_2CHCH_2CN$		4.04			9.95	9.82
3-Methylbutanenitrile (*gauche*)			3.98			9.95	9.71
Pentanenitrile	$CH_3(CH_2)_3CN$	4.12	4.26		10.4	9.95	9.92
Pentanenitrile (*gauche*)			3.95				9.80
Dimethyl Sulfoxide	CH_3SOCH_3	3.96	4.38	4.14			8.10
Methyl Ethyl Sulfoxide	$CH_3SOCH_2CH_3$		4.24	4.01			9.93
Tetramethylene Sulfoxide	C_4H_8OS		4.52				10.77
Glycol Sulfite	$C_2H_4O_3S$		3.39				8.33
Vinylene Carbonate	$C_3O_3H_2$	4.51	4.59				6.55
Ethylene Carbonate	$C_3O_3H_4$	5.35	5.39				6.80
Succinonitrile (*anti*)	$C_2H_4(CN)_2$		0.00			10.56	8.24
Succinonitrile (*gauche*)			5.70				8.09

$$\alpha = \frac{4}{32}\left[6(0.314) + 2(1.294) + 1(1.428) + 1(1.216)\right]^2 = 6.33 \text{ Å}^3 \qquad (4.43)$$

which agrees well with the accepted experimental value of 6.40 Å ^{3}. For the most part there is excellent agreement between the experimental, theoretical, and empirical polarizabilities. Parameters for the sulfoxide and sulfite groups were not available and thus empirical polarizabilities could not be calculated.

Dipole-Bound Electron Affinities and Molecular Orbitals

In order to explain experimental trends, theoretical electron affinities have been calculated using Equation 1.1. When performing these calculations a diffuse set of functions are added to the positive side of the dipole moment. This supplemental set of functions usually consists of s, p, and d Gaussian functions. Typical exponents used for the functions include 0.256, 0.064, 0.016, 0.004, 0.001, 0.00025, and 0.0000625. A good basis set will make use of all the functions when constructing the molecular orbitals. The location of the center of these diffuse functions is determined variationally by maximizing the electron affinity. In *Gaussian 98* a ghost atom represented by the atomic symbol Bq is used to specify the center of the diffuse functions. The molecular energies can then be calculated at various levels of theory and the electron affinity is simply the energy difference between the anion and neutral.

Dipole-bound molecular orbitals for molecules can also be calculated. A good approximation is at the Koopmans' Theorem level of theory.[100] The lowest unoccupied molecular orbital (LUMO) generated by a Hartree-Fock calculation corresponds to the dipole-bound anion orbital. The input file for such a calculation is shown in Figure 4.13. The *extrabasis massage* command in *Gaussian 98* allows one to add the extra orbitals.

```
%mem=800mb
%chk=pentg1.chk

#hf/aug-cc-pvdz
#extrabasis massage
#cube=(cards,orbitals)

Pentannitrile (gauche)

0 1
H
C,1,R2
H,2,R3,1,A3
C,2,R4,1,A4,3,D4,0
H,2,R5,1,A5,3,D5,0
H,4,R6,2,A6,1,D6,0
H,4,R7,2,A7,6,D7,0
C,4,R8,2,A8,6,D8,0
Bq,4,R9,2,A9,6,D9,0
H,8,R10,4,A10,2,D10,0
C,8,R11,4,A11,10,D11,0
H,8,R12,4,A12,10,D12,0
H,11,R13,8,A13,4,D13,0
H,11,R14,8,A14,13,D14,0
C,11,R15,8,A15,13,D15,0
N,15,R16,11,A16,8,D16,0
Variables:
R2=1.10149807
R3=1.10163878
R4=1.53144572
R5=1.10326697
R6=1.10472893
R7=1.10461668
R8=1.53195104
R9=2.02124442
R10=1.10519862
R11=1.54168285
R12=1.10423639
R13=1.10217104
R14=1.10324748
R15=1.47408616
R16=1.18599536
A3=108.00041724
A4=111.26821869
A5=107.8188609
A6=109.92967527
A7=109.73893966
A8=112.0864078
A9=106.37725039
A10=109.74337577
A11=112.88195656
A12=109.87481149
A13=110.86248263
A14=110.2781574
A15=111.47220299
A16=178.35745723
D4=-122.02886313
D5=116.32440138
D6=58.51089127
D7=-116.97888376
D8=121.5068209
D9=105.59289945
D10=-59.15084598
D11=-20.43359748
D12=117.54511099
D13=177.67524693
D14=-18.96259414
D15=120.68806946
D16=-6.25536025

Bq 0
S 1
 0.0000625 1.0
S 1
 0.00025 1.0
S 1
 0.001 1.0
S 1
 0.004 1.0
S 1
 0.016 1.0
S 1
 0.064 1.0
S 1
 0.256 1.0
P 1
 0.0000625 1.0
P 1
 0.00025 1.0
P 1
 0.001 1.0
P 1
 0.004 1.0
P 1
 0.016 1.0
P 1
 0.064 1.0
P 1
 0.256 1.0
D 1
 0.001 1.0
D 1
 0.008 1.0
****

pentg1.cub
 79    -70.0    -50.0    -50.0
 100     1.00     0.00     0.00
 100     0.00     1.00     0.00
 100     0.00     0.00     1.00
lumo
```

Figure 4.13 Sample *Gaussian 98* input file for a molecule with additional diffuse basis sets. The *extrabasis massage* command in *Gaussian 98* allows the addition of extra orbitals. The *cube* command creates a three dimensional grid where the orbital of interest (in this case the LUMO) or the electron density can be saved.

The *cube* command creates a three dimensional grid in which the orbital of interest (in this case the LUMO) or the electron density can be saved and then visualized later. Figure 4.14 shows dipole-bound molecular orbials of vinylene carbonate corresponding to contours of 0.00017, 0.00050, 0.00115, and 0.0030, respectively. These contours correspond to density probabilities of 90%, 70%, 50%, and 20%, respectively. In other words, for the top left figure the probability of finding the electron inside the volume outlined is 90%. For the most part, the overall shapes of the orbitals do not change when changing the contour that is displayed. All dipole-bound molecular orbitals presented here were rendered using *gOpenMol*.[149] Figures showing dipole-bound molecular orbitals that follow are shown using a large contour interval so that the orbital is seen relative to the shape of the molecules.

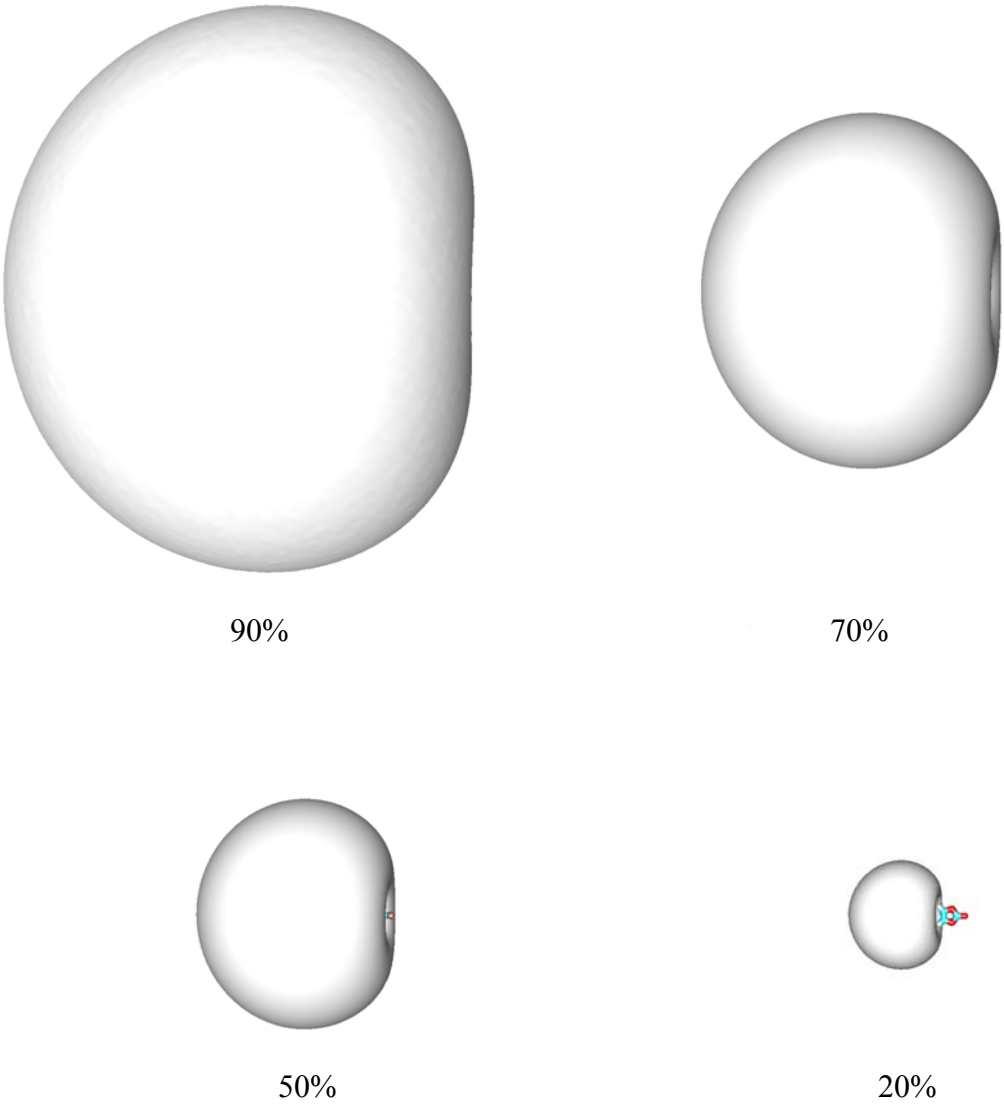

Figure 4.14 Dipole-bound molecular orbital of vinylene carbonate. These plots correspond to contours of 0.00017, 0.00050, 0.00115, and 0.0030 and density probabilities of 90%, 70%, 50%, and 20%, respectively. In other words, for the top left figure the probability of finding the electron within the shaded region is 90%. For the most part, the overall shape of the orbitals does not change when changing the contour that is displayed.

CHAPTER V

DIPOLE-BOUND ANIONS OF CARBONYL CONTAINING COMPOUNDS

Introduction

Dipole-bound anions of sixteen carbonyl containing compounds were studied.[75] Calculated geometries of these molecules can be found in Figures 4.1 - 4.5. The dipole moments of the carbonyl compounds are smaller than those of the nitrile, sulfoxide, sulfite, or carbonate containing compounds and are on the order of 2.5 – 3.3 Debye. Experimentally, dipole-bound anions were created by charge transfer from Rydberg atoms and detected in a time of flight mass spectrometer. Anions were created when the laser wavelength was tuned to excite the appropriate Rydberg levels of rubidium using two photons.

Figure 5.1 shows a representative dipole-bound anion formation spectrum for cyclohexanone using helium as the expansion gas. Appendix B contains anion formation spectra for all 32 molecules studied here. The maximum number of cyclohexanone anions are created from the unresolved nd = 21 ($^2D_{3/2,5/2}$) states. Since the quantum defect for rubidium (ℓ=2) is 1.3473 this corresponds to an n^* = 19.65. Similarly, the maximum is the ns series is the ns = 22, which corresponds to n^* = 18.87 (δ_0=3.1312). As can be seen, electron transfer to create dipole-bound states only occurs over a narrow range of n^*. Empirically, this range can be approximated by $\Delta n^*/n^* \sim 0.4$. Using Equation 1.11 electron affinities can be estimated from the nd and ns maximum n^* values. For cyclohexanone these yield 5.5 and 6.2 meV, respectively. However, since there is not an infinite number of obtainable Rydberg states there is inherent error in trying to use the

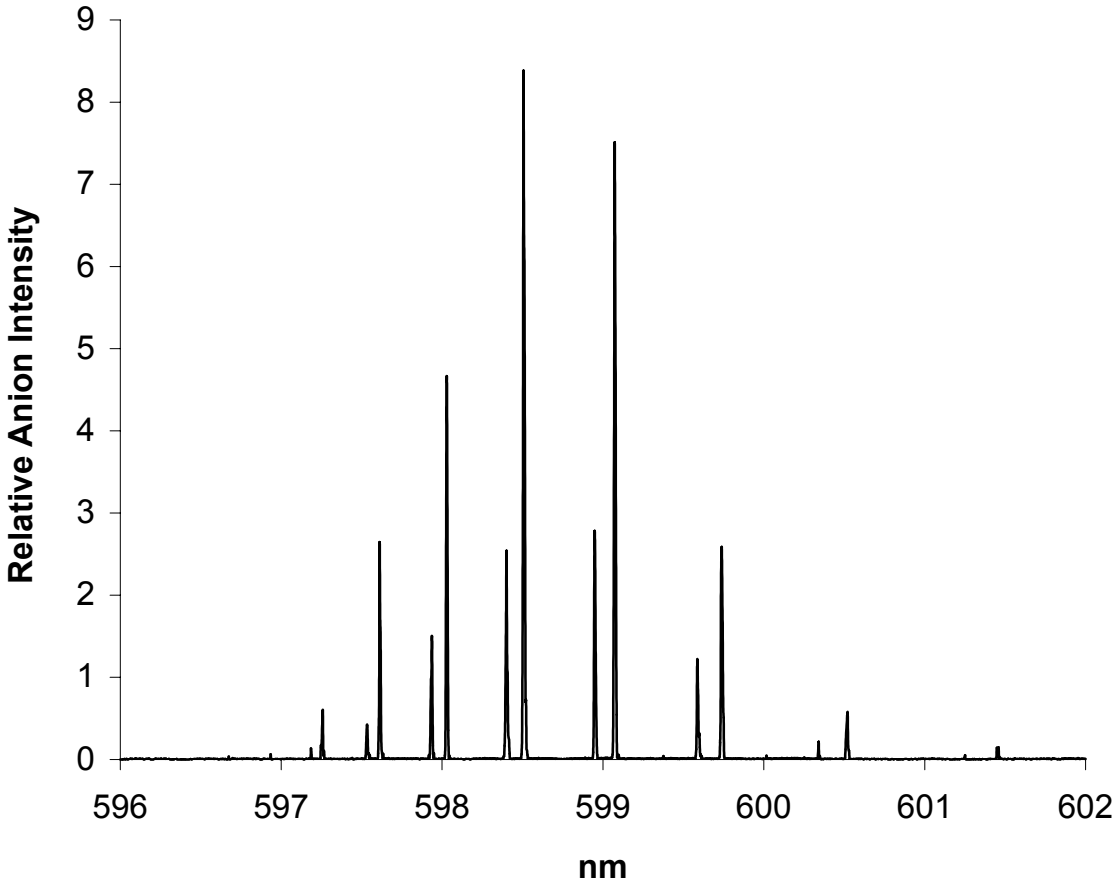

Figure 5.1 One-color dipole-bound anion formation spectrum for cyclohexanone.

experimentally observable maximum n^* in determining electron affinities. For this reason a fractional maximum n^* is estimated and compared to the curve-crossing model outlined in Chapter I and illustrated in Figure 1.4. A computer program that calculates absolute charge transfer cross-sections and compares them to experimental data has previously been written by our colleague Charles Desfrançois (Université Paris-Nord). The code has been updated for rubidium and data for all molecules studied have been analyzed. Theoretical charge transfer curves along with experimental data can be found along with the anion creation spectra in Appendix B. For the cyclohexanone data a fractional n^* of 19.4 is obtained which yields an electron affinity of 5.7 meV. A fit of the charge exchange data for cyclohexanone to the curve-crossing model is shown in Figure 5.2.

Field detachment studies were performed on all of the carbonyl containing compounds. As the electric field used to accelerate the anions down the flight tube is increased, electron detachment from the anion occurs as the electron begins to tunnel through the potential barrier. Eventually a critical field is reached in which the electron is no longer bound and all of the negative ion signal disappears. This is described theoretically in Chapter I and illustrated in Figure 1.6. Figure 5.3 shows the field detachment data and fitting to the theoretical model for cyclohexanone. The theoretical fit of the data yields an electron affinity of 5.9 meV, which agrees well with that obtained from Equation 1.11 (5.7 meV). Field detachment data fitted to theoretical curves for all of the carbonyl compounds can be found in Appendix C. Table 5.1 summarizes the experimental electron affinities for the carbonyls studied here.

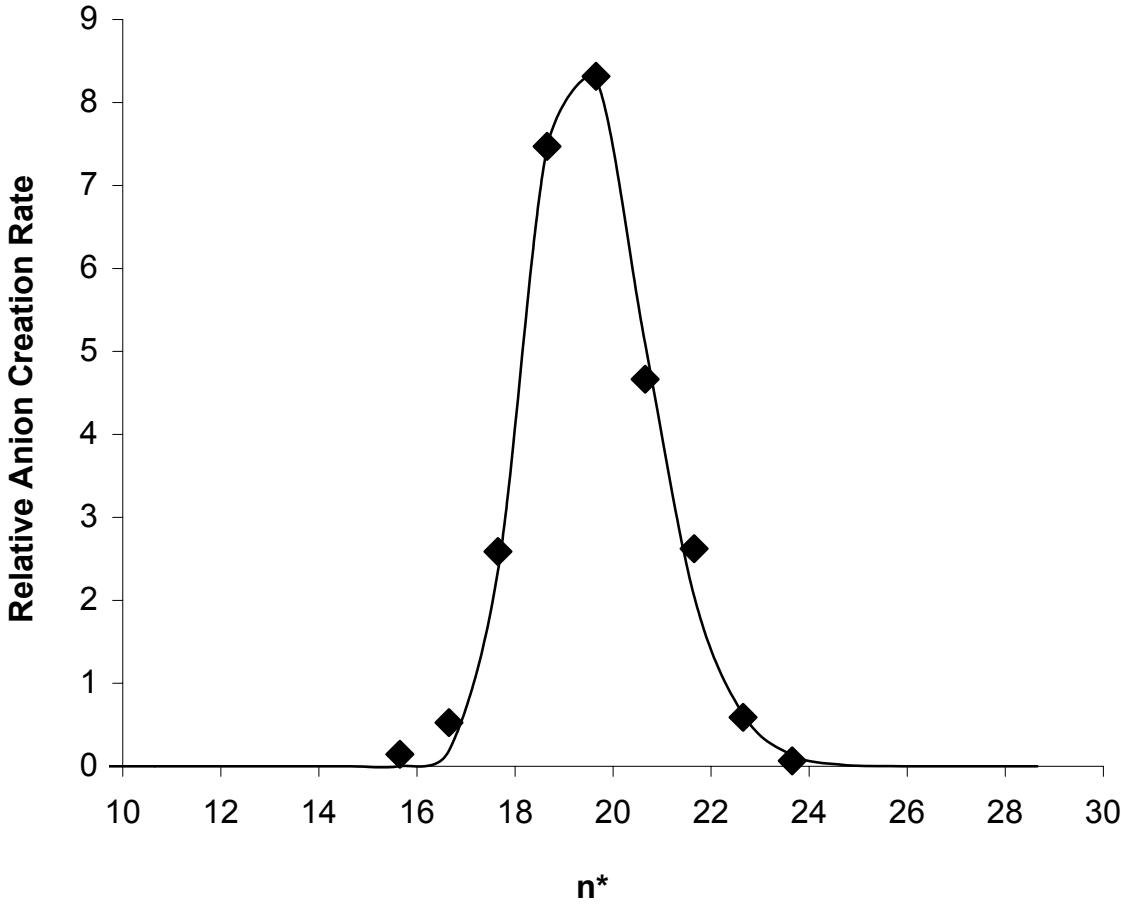

Figure 5.2 Fit of the experimental anion formation to the curve-crossing model for cyclohexanone. Only the $nd\ ^2D_{5/2,3/2}$ states are plotted.

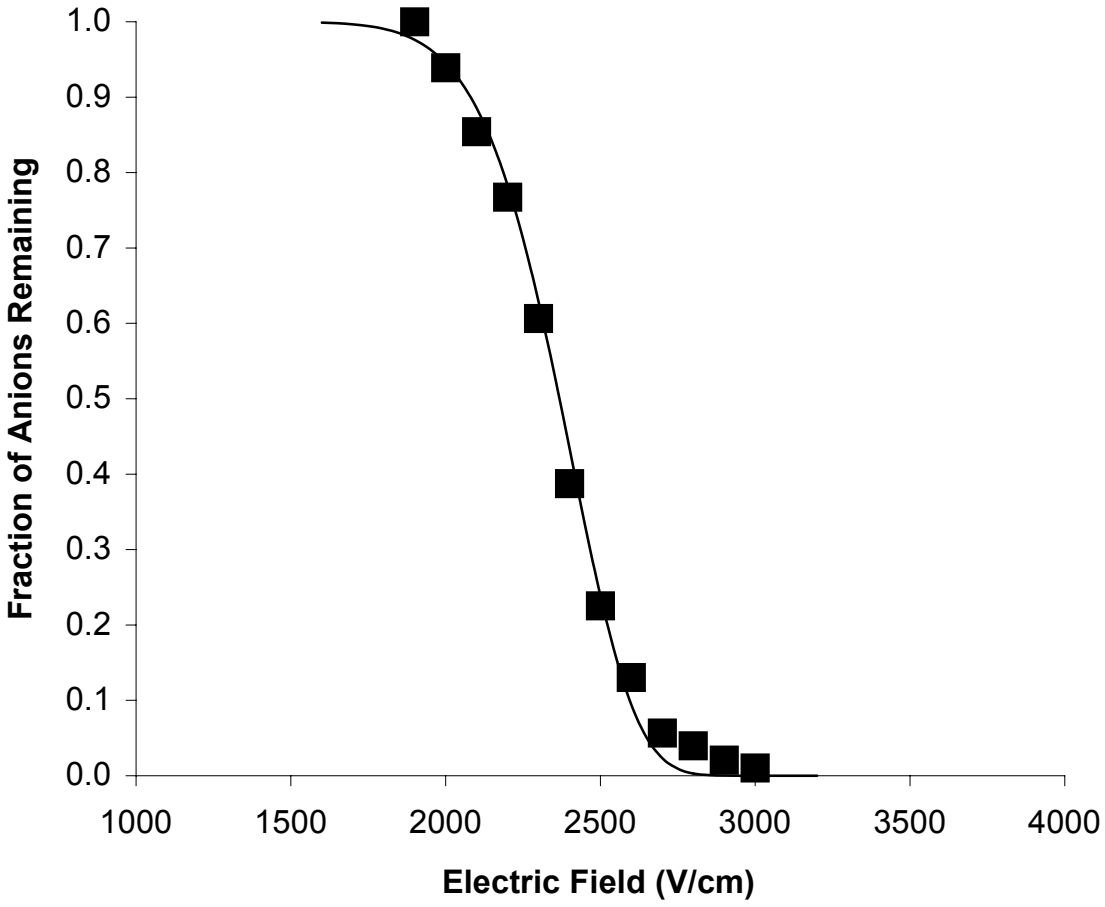

Figure 5.3 Experimental (squares) field detachment data and theoretical curve for cyclohexanone. The curve is a fit of the data that yields an electron affinity of 5.9 meV.

Table 5.1. Experimental electron affinities of carbonyls as calculated from Equation 1.11 (EMP), directly from the curve-crossing model (CALC), and from electric field detachment (FD).

	Molecule	Formula	n^*_{max}	Electron Affinity (meV)		
				RET EMP	RET CALC	FD
1	Acetaldehyde	CH_3CHO	42.8	0.6	0.6	0.6
2	Propanal (*cis*) Propanal (*gauche*)	CH_3CH_2CHO	35.8	1.0	1.0	1.0
3	Acetone	CH_3COCH_3	25.7	2.6	2.6	2.5
4	*d*-Acetone	CD_3COCD_3	25.9	2.5	2.5	2.4
5	Cyclobutanone	C_4H_6O	30.2	1.7	1.7	1.6
6	2-Methylpropanal (*gauche*) 2-Methylpropanal (*trans*)	$(CH_3)_2CHCHO$	31.5	1.5	1.6	1.1
7	Butanal (*cis/gauche*) Butanal (*cis/trans*)	$CH_3CH_2CH_2CHO$	29.1	1.8	1.8	1.3
8	2-Butanone	$CH_3CH_2COCH_3$	29.0	1.8	1.8	1.8
9	Cyclopentanone	C_5H_8O	24.9	2.8	2.8	2.8
10	Pivalaldehyde	$(CH_3)_3CCHO$	33.7	1.2	1.2	1.0
11	2-Ethylbutanal	$(CH_3CH_2)_2CHCHO$	31.2	1.5	1.5	1.2
12	2-Methylcyclopentanone (*axial*) 2-Methylcyclopentanone (*equatorial*)	$C_6H_{10}O$	26.7	2.3	2.4	2.2
13	3-Methylcyclopentanone (*axial*) 3-Methylcyclopentanone (*equatorial*)	$C_6H_{10}O$	24.5	3.0	3.0	3.0
14	Cyclohexanone	$C_6H_{10}O$	19.4	5.7	5.7	5.9
15	2-Methylcyclohexanone (*axial*) 2-Methylcyclohexanone (*equatorial*)	$C_7H_{12}O$	21.7	4.2	4.2	4.7
16a	3-Methylcyclohexanone (*axial*)	$C_7H_{12}O$	16.7	8.7	10.2	8.8
16e	3-Methylcyclohexanone (*equatorial*)		21.3	4.4	4.4	4.1
17	4-Methylcyclohexanone (*axial*) 4-Methylcyclohexanone (*equatorial*)	$C_7H_{12}O$	18.9	6.1	6.0	6.7

Trends in Electron Affinity and Effect of Conformations

A plot of electron affinity as a function of dipole moment for all of the carbonyl containing molecules studied is shown in Figure 5.4. The electron affinity value plotted is the mean of values determined from Equation 1.1, from the curve crossing model, and those determined from field detachment studies. The dipole moment plotted is the experimental value when available and the theoretical for all others. There is a steady trend of increasing electron affinity with dipole moment among the carbonyls with some notable exceptions as discussed below.

Propanal, whose dipole-bound anion has eluded detection until now, has the lowest experimental dipole moment (2.52 D) of any observed dipole-bound anion. This claim assumes that the experimentally measured dipole moment is accurate and that the *cis* form of propanal is present under the experimental conditions. The calculated dipole moments for the two lowest lying of propanal's four conformers support the experimental values. At 300K 19% of propanal is in the gauche form which has a much higher dipole moment (2.86 D).[150] Kim, Potts, and Baer have recently shown that the 3-methylcyclopentanone[151] and 3-methylcyclohexanone[152] conformers are rapidly "frozen out" in a molecular beam expansion. This would lead one to believe that the dipole-bound anions of both the cis and gauche conformers of propanal could be present. Propanal's experimentally determined electron affinity (1.0 meV), however, is higher than that of acetaldehyde (μ = 2.75, α=4.6, EA=0.6 meV) and approximately equal to that of pivalaldehyde (μ = 2.66, α=10.0, EA=1.2 meV). Thus the electron affinity of propanal seems too large for the cis conformer and too small for the gauche conformer. However, it has been previously noted that for molecules having similar values of μ,

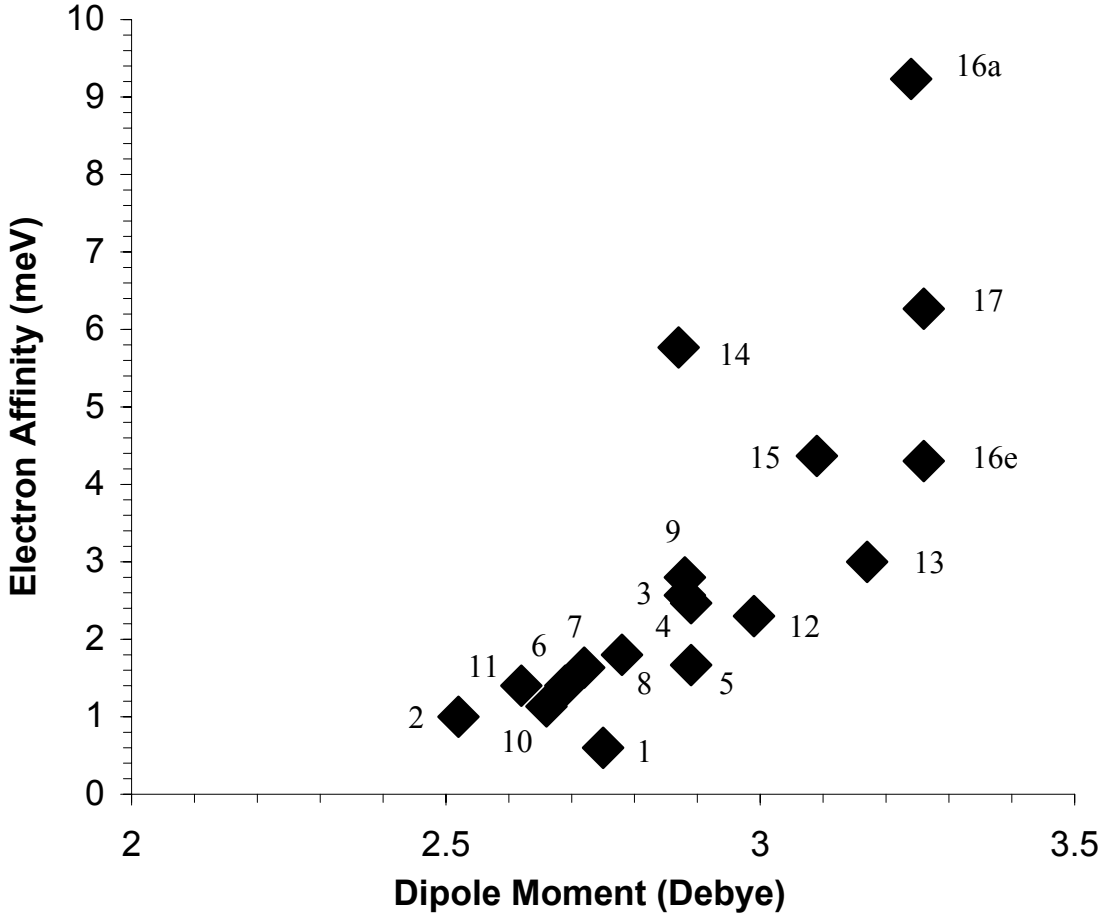

Figure 5.4 Experimental electron affinities of carbonyl containing compounds as a function of dipole moment. The numbers next to the data points correspond to Table 5.1.

larger values of α and smaller molecular sizes can result in higher electron affinities.[65] Assuming that the dipole-bound anion signal is due to the *cis* form it is possible that propanal's larger polarizability is responsible for its larger electron affinity as compared with acetaldehyde. The low polarizability of acetaldehyde might also explain why it has the lowest electron affinity of all of the molecules studied, even though its dipole moment is not the smallest.

Both 2-methylpropanal and butanal also have multiple conformations at room temperature. For 2-methylpropanal 90% of the molecules at room temperature are in the gauche conformation and 10% are in the trans conformation.[153] The energy difference between the two forms has been recently estimated to be about 0.7 kcal/mol[154] with a barrier of 1.5 kcal/mol.[155] Experimentally we observed one dipole-bound anion charge exchange maximum with an electron affinity of about 1.5 meV. Similarly, butanal has a number of possible conformations, at least two of which are populated at room temperature. The planar *cis/trans* conformer is predicted to be the lowest energy state with the *cis/gauche* only about 0.3 kcal/mol higher in energy with a barrier of rotation of about 3 kcal/mol.[155] The individual dipole moments for these two species have not been experimentally measured but have been calculated here to be 2.97 Debye for the *cis/trans* and 2.57 Debye for the *cis/gauche*. Experimentally, the dipole-bound anion of butanal is observed over a wide range of n^* and has a rather large shoulder at higher n^* when compared to the curve crossing model. This, along with butanal's field detachment profile is shown in Figure 5.5. Butanal's field detachment profile also exhibits a shoulder. This is rather unusual since the curve-crossing model and field detachment curves have excellent agreement for the other molecules studied. Both of the

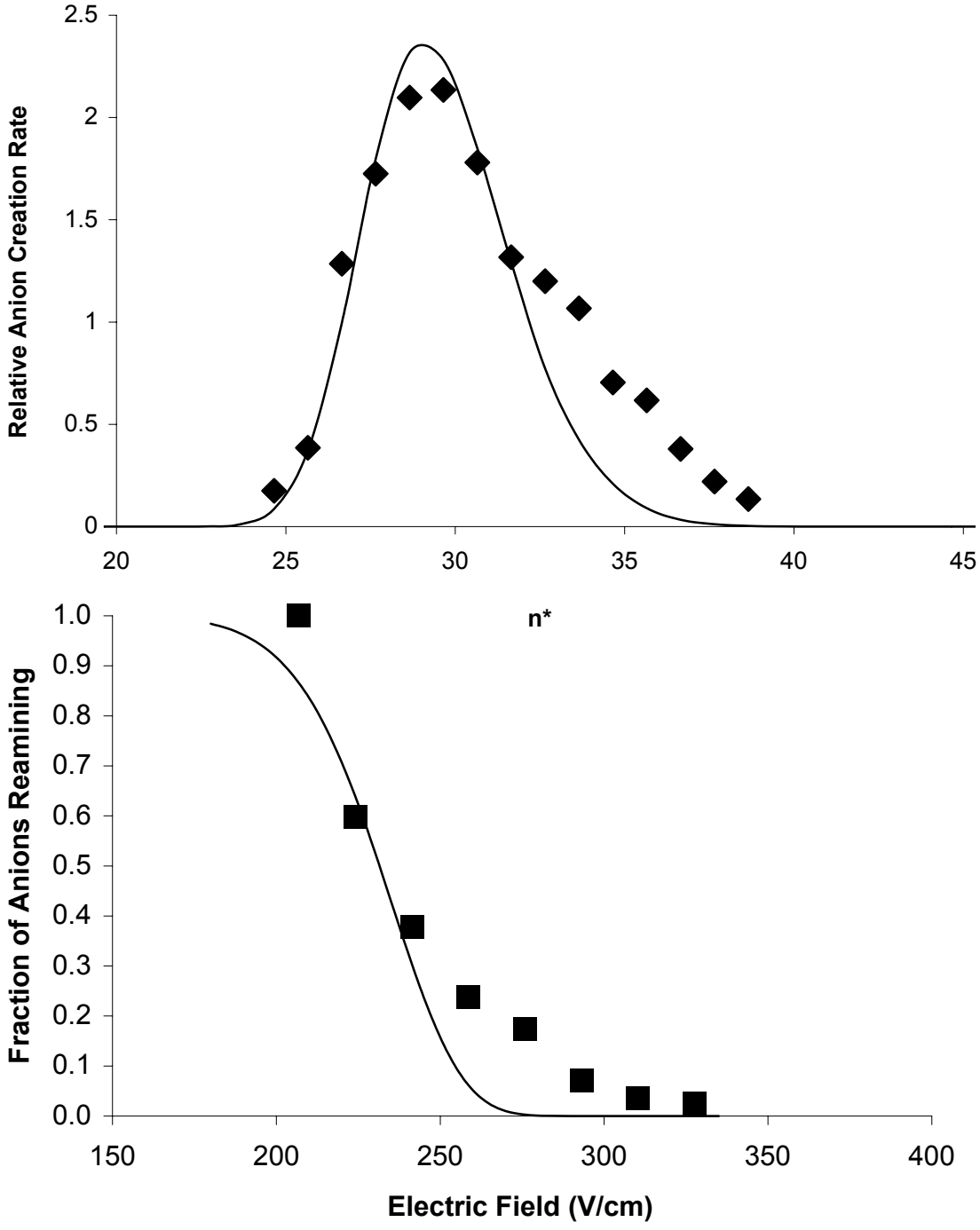

Figure 5.5 Dipole-bound anion intensity as a function of n^* (top) and field detachment curve (bottom) for butanal.

measurements indicate two charge exchange profiles that are overlapping. If one assumes that the two profiles are due to the two major species present (*cis/trans* and *cis/gauche*) then the major profile would correspond to the *cis/trans* species (μ_{mp2}=2.97 D) and the minor profile would correspond to the *cis/gauche* (μ_{mp2}=2.57 D). This is an unexpected result, however, due to the large difference in the dipole moments of the two conformers.

As can be seen in Table 5.1, cyclohexanone and its three possible methyl derivatives exhibit different n^*_{max}. Each methyl derivative consists of isomer pairs in which the methyl group can be in the axial or equatorial position. Although the dipole moments and polarizabilities of these molecules are similar, their charge exchange profiles are markedly different (see Appendix B). Cyclohexanone and 4-methylcyclohexanone have similar binding energies, whereas 2- and 3-methylcyclohexanone have lower binding energies. All five of the observed dipole-bound states in this series presented here (including the second bound state of 3-methylcyclohexanone) exhibit distinct field detachment thresholds (see Appendix C). There is no obvious explanation for the trend in electron affinity in the series of cyclohexanone derivatives. This is especially so with comparisons of electron affinity to dipole moment. The dipole moment of the axial form of 3-methylcyclohexanone is calculated to be slightly less (<1%) than the equatorial but the polarizability of the axial is calculated to be larger (3%). It seems reasonable to assume that the "shapes" of these molecules somehow contribute strongly to the properties of their dipole-bound states. Specifically, "shape" refers to the extent to which atoms extend out into the region of excess electron density.

3-methylcyclohexanone's additional maximum in the charge exchange spectra corresponds to a binding energy of about 9 meV and could possibly be due to an additional conformation present in the supersonic expansion. It has been shown recently[152] using multi-photon ionization spectroscopy that two conformations (axial and equatorial $-CH_3$) exist in the gas phase for 3-methylcyclohexanone following nozzle jet expansion. Different samples of racemic and resolved *(R)*-3-methylcyclohexanone were tested for purity via GC/MS to ensure that the anion signal was not due to an impurity of the same mass (resolution +/- 1 amu) contaminating the sample. Shown in Figure 5.6 are field detachment curves for 3-methylcyclohexanone at different values of *nd* that range from one maxima to the other. It can be seen that one can selectively field detach the lower electron affinity state and still detect the higher. This can be used to deconvolute the two overlapping charge exchange spectra. Estimates for the composition of 3-methylcyclohexanone at 300K include 94% equatorial, 5% axial, and 1% twist[156] and 83% equatorial, 9% axial, 7% twist, and 1% twist chair.[157] Baer has calculated the enthalpy of interconversion between the two conformers to be 1.55+/- 0.12 kcal/mol.[152] The ratio of dipole-bound anion signal of the higher electron affinity state to the lower is approximately 0.15, depending upon which carrier gas is employed. Assuming that both dipole-bound anions are created with the same rate constant this composition matches that which is predicted, especially when one takes into account the fact that the cross-section for photoexcitation decreases markedly with n^*. One would expect that the other molecules in this series of cyclohexanones (as well as 3-methylcyclopentanone) would also have multiple dipole-bound anion states corresponding to their various

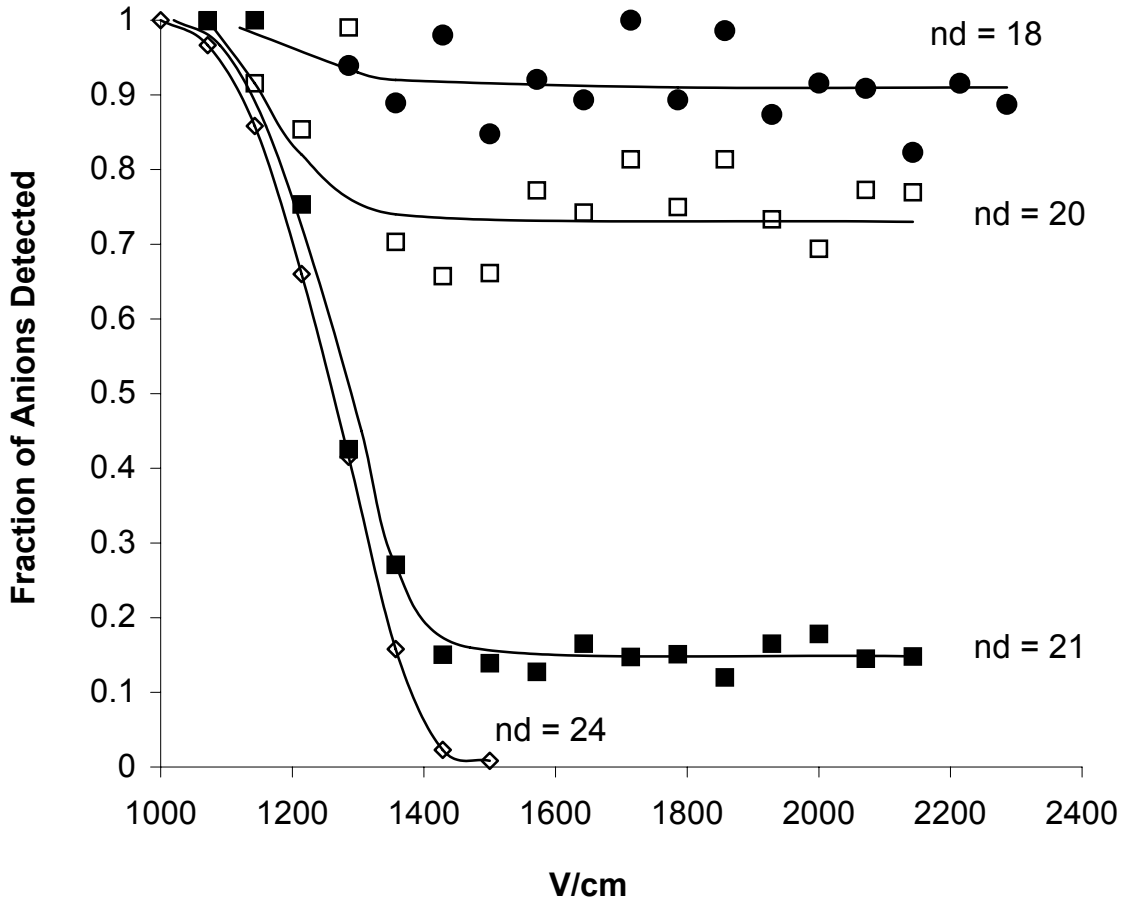

Figure 5.6 Electric field detachment curves of 3-methylcyclohexanone for anions formed using Rb Rydberg atoms in various values of *nd*. The anion signals are normalized to unity for E<~900 V/cm.

conformations. It appears that this is the case with 3-methylcyclopentanone and 2-methylcyclohexanone. Both of these molecules exhibit a shoulder in their charge exchange spectra. However, the effect is not as large as in the case of 3-methylcyclohexanone. A reason for this might lie in the energy differences between conformations. It can be seen from the values in Table 4.1 that the difference in energy between the axial and equatorial conformations in 3-methycyclohexanone at the MP2 level of theory is 0.83 kcal/mol whereas the difference in 2-ethylcyclohexanone and 4-methylcyclohexanone are higher at 1.7 and 1.4 kcal/mol, respectively. Calculations of the dipole-bound electron affinities of the two conformations by Jordan's group[75] indicate that there is little difference between the two. At the MP2 level they calculate electron affinities of 0.926 meV for the axial form and 0.635 meV for the equatorial. Both of these values agree poorly with experimental results, although the variation is in the correct direction.

Acetone (C_3H_6O) and deuterated acetone (C_3D_6O) have different dipole-bound electron affinities.[158] Shown in Figure 5.7 are the charge exchange spectra and the field detachment curves for the two species. Isotopic substitution lowers acetone's electron affinity by about 0.1 meV. Electron affinities obtained from n^*_{max}, the curve crossing model, and field detachment are consistent for the two species. The difference is consistently 0.1 meV. Our colleague Mark Pederson[158] (Naval Research Lab) calculated the dipole moments of acetone and deuterated acetone to be 2.98 D, differing from each other by only 0.3% with the deuterated species being slightly higher in magnitude. The explanation must lie elsewhere, possibly in the zero-point energy difference between the two molecules.

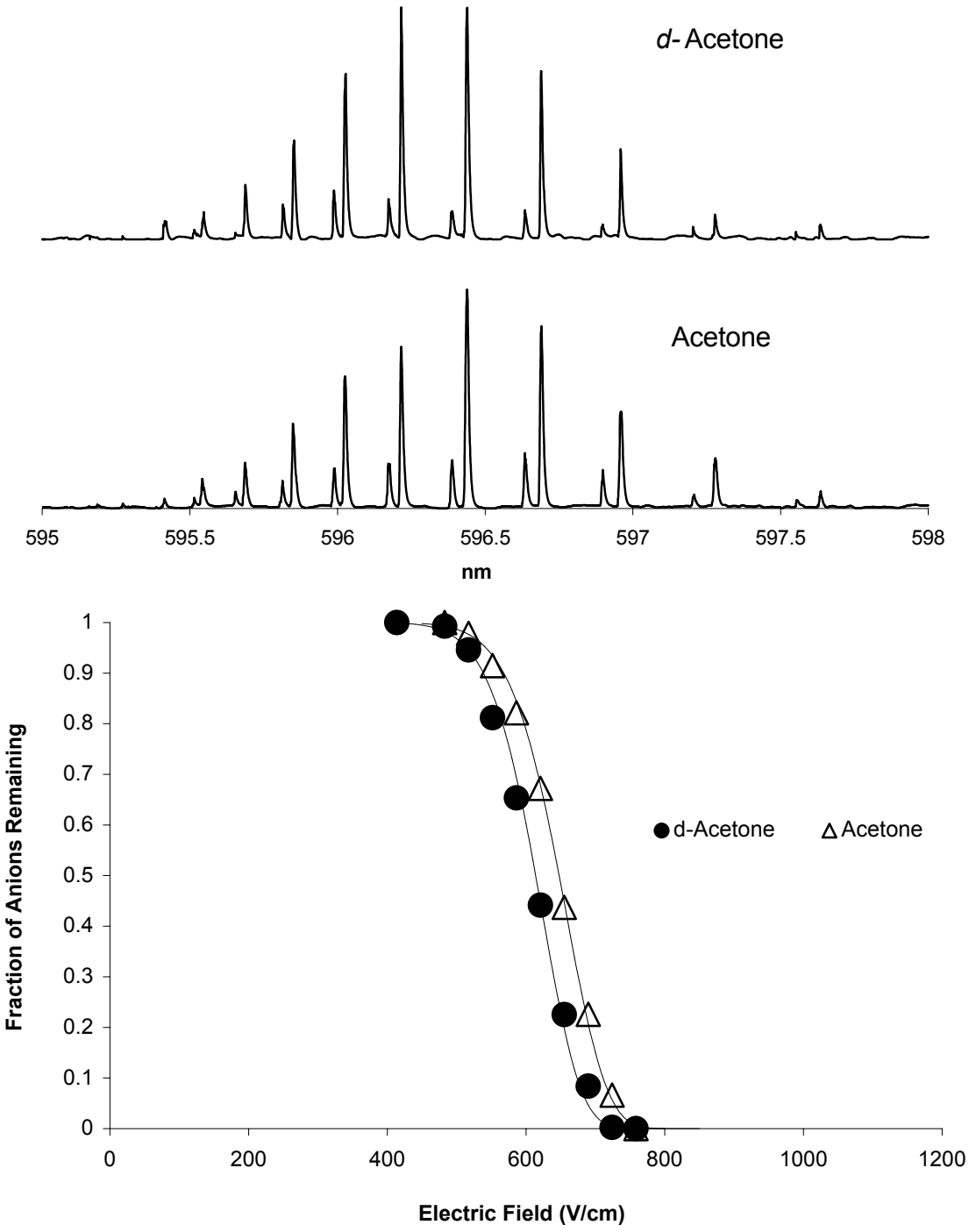

Figure 5.7 One-color charge exchange spectra and field detachment curves for acetone and perdeuterated acetone. The difference in electron affinity is 0.1 meV.

CHAPTER VI

DIPOLE-BOUND ANIONS OF NITRILE, SULFOXIDE, AND SULFITE CONTAINING COMPOUNDS

Introduction

Dipole-bound anions of eight nitrile, one sulfite and three sulfoxide containing compounds were studied.[75] Geometries of these molecules can be found in Figures 4.5 - 4.7. The dipole moments of these compounds are larger (3.9 – 4.5 Debye) than those of the carbonyl containing compounds but less than the carbonate containing compounds. As before, dipole-bound anions were created by charge transfer from Rydberg atoms and detected in a time of flight mass spectrometer. Anions were created when the laser wavelength was tuned to excite the appropriate Rydberg levels of rubidium using two photons.

Figure 6.1 shows a dipole-bound anion formation (RET) spectrum for pentanenitrile (see Appendix B for all other molecules). For the nitrile containing compounds a carrier gas was not required. In some instances, such as in the case of acetonitrile, employing a carrier gas actually reduced anion signal intensity. Although this is not totally understood, it is most likely due to a dilution of the overall number of CH_3CN molecules in the creation chamber when a carrier gas is used. This is to be contrasted to the case of the carbonyl molecules where a carrier gas was necessary to see negative ions. When compared to the carbonyl containing compounds the charge exchange profiles of the nitriles, sulfoxides, and sulfites contain fewer Rydberg states per wavelength range. This is because the energies of these lower Rydberg states are more spread out and fewer states can create dipole-bound anions. Table 6.1 summarizes the

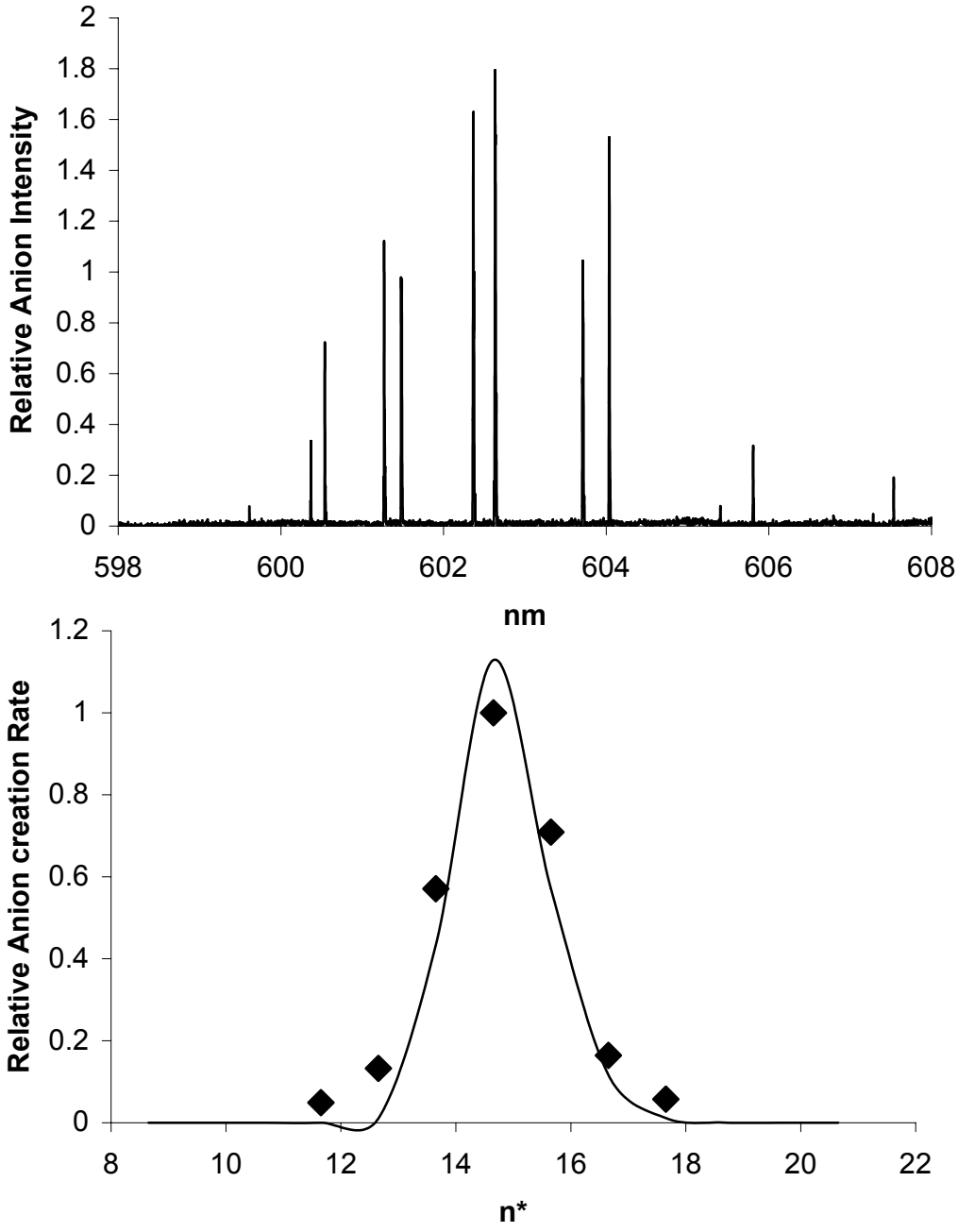

Figure 6.1 One-color dipole-bound anion formation spectrum for pentanenitrile (top) and fitting to curve-crossing model (bottom).

Table 6.1 Experimental electron affinities of nitriles as calculated from Equation 1.11 (EMP) and directly from the curve-crossing model (CALC).

	Molecule	Formula	n^*_{max}	Electron Affinity (meV)	
				RET EMP	RET CALC
1	Acetonitrile	CH_3CN	12.7	18.7	19.3
2	Propanenitrile	CH_3CH_2CN	13.7	15.1	15.8
3	2-Methylpropanenitrile	$(CH_3)_2CHCN$	15.0	11.7	11.6
4	Butanenitrile Butanenitrile (*gauche*)	$CH_3(CH_2)_2CN$	13.4	16.1	17.0
5	2,2-Dimethylpropanenitrile	$(CH_3)_3CCN$	14.6	12.6	13.2
6	2-Methylbutanenitrile 2-Methylbutanenitrile (*gauche*)	$CH_3CH_2CHCH_3CN$	14.5	12.9	13.5
7	3-Methylbutanenitrile 3-Methylbutanenitrile (*gauche*)	$(CH_3)_2CHCH_2CN$	15.0	11.7	11.7
8	Pentanenitrile Pentanenitrile (*gauche*)	$CH_3(CH_2)_3CN$	14.6	12.6	12.6
9	Dimethyl Sulfoxide	CH_3SOCH_3	14.1	13.9	13.9
10	Methyl Ethyl Sulfoxide	$CH_3SOCH_2CH_3$	14.7	12.4	12.5
11	Tetramethylene Sulfoxide	C_4H_8OS	13.0	17.5	17.5
12a	Glycol Sulfite	$C_2H_4O_3S$	13.5	15.7	13.5
12b			16.8	8.5	8.5

experimental electron affinities for the nitriles, sulfoxides, and sulfite containing molecules studied here. Field detachment of the compounds was not possible due to the large electric fields required.

A plot of the electron affinities of the nitrile, sulfoxide, and sulfite containing molecules is shown in Figure 6.2. Unlike the case of the carbonyl containing compounds, the electron affinities obtained from the empirical relation (RET EMP) do not agree well with the results of the curve-crossing model computer simulation (RET CALC). This is probably due to the fact that Equation 1.11 was calibrated with few dipole-bound anions of large electron affinity.

It is important to point out that two charge exchange maxima were observed in the case of glycol sulfite. This is shown in Figure 6.3 and is similar to the case of 3-methylcyclohexanone. However, glycol sulfite has no other conformation that could account for the extra dipole-bound state. It is interesting to point out that it is the minor charge exchange profile (at higher n^*=17) that correlates well with glycol sulfite's dipole moment. The dominant charge exchange profile matches a dipole moment on the order of 4 Debye (such as in the case of the nitriles). One possible explanation for this is the presence of a valence-bound state in glycol sulfite. A mass spectrum was run using a ZAB-EQ double focusing hybrid mass spectrometer but no parent ion peak was evident. A large SO_2^- peak, a weaker SO_3^- peak, and even weaker peaks at $O_2^-$and SO^- were evident in the mass spectrum.

Trends in Electron Affinity and Effect of Conformations

With few exceptions, a larger dipole moment generally results in a higher electron affinity for the carbonyl containing molecules. Although only four molecules were

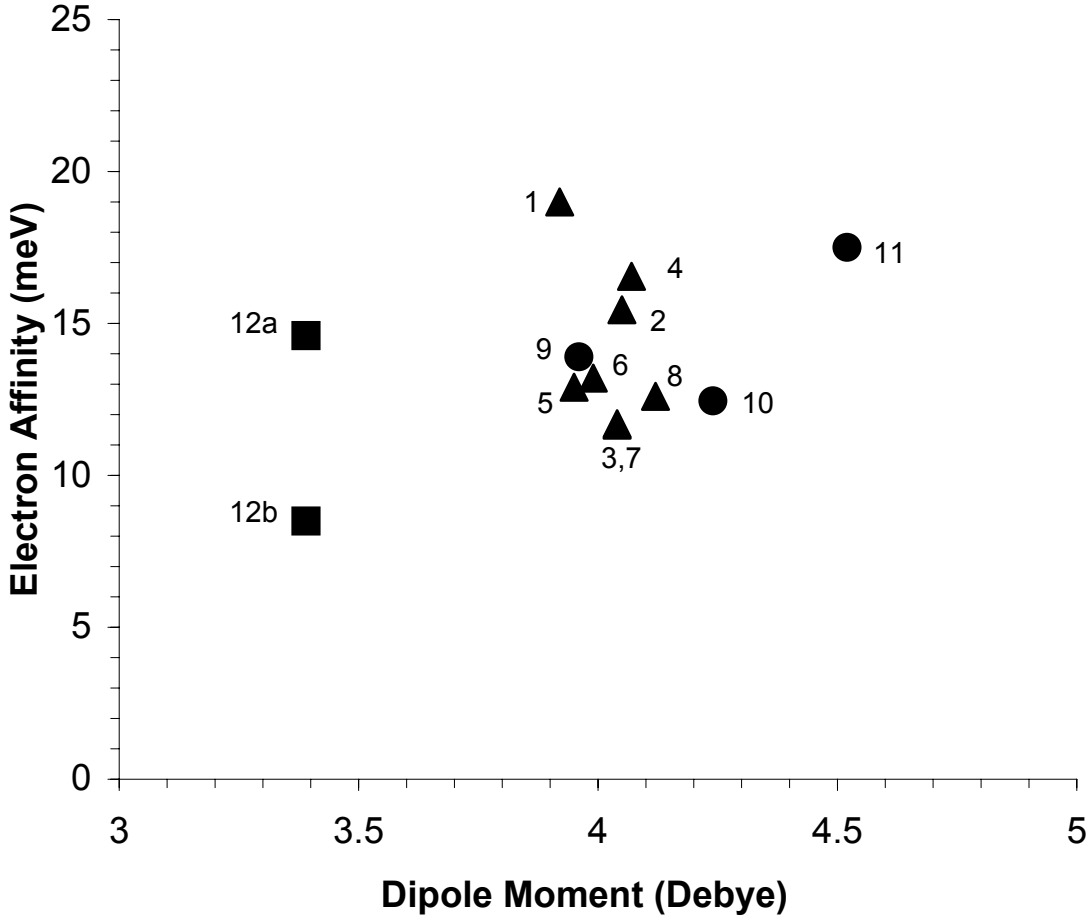

Figure 6.2 Experimental electron affinities of nitrile (triangles), sulfoxide (circles), and sulfite (squares) containing compounds as a function of dipole moment. The numbers next to the data points correspond to Table 6.1.

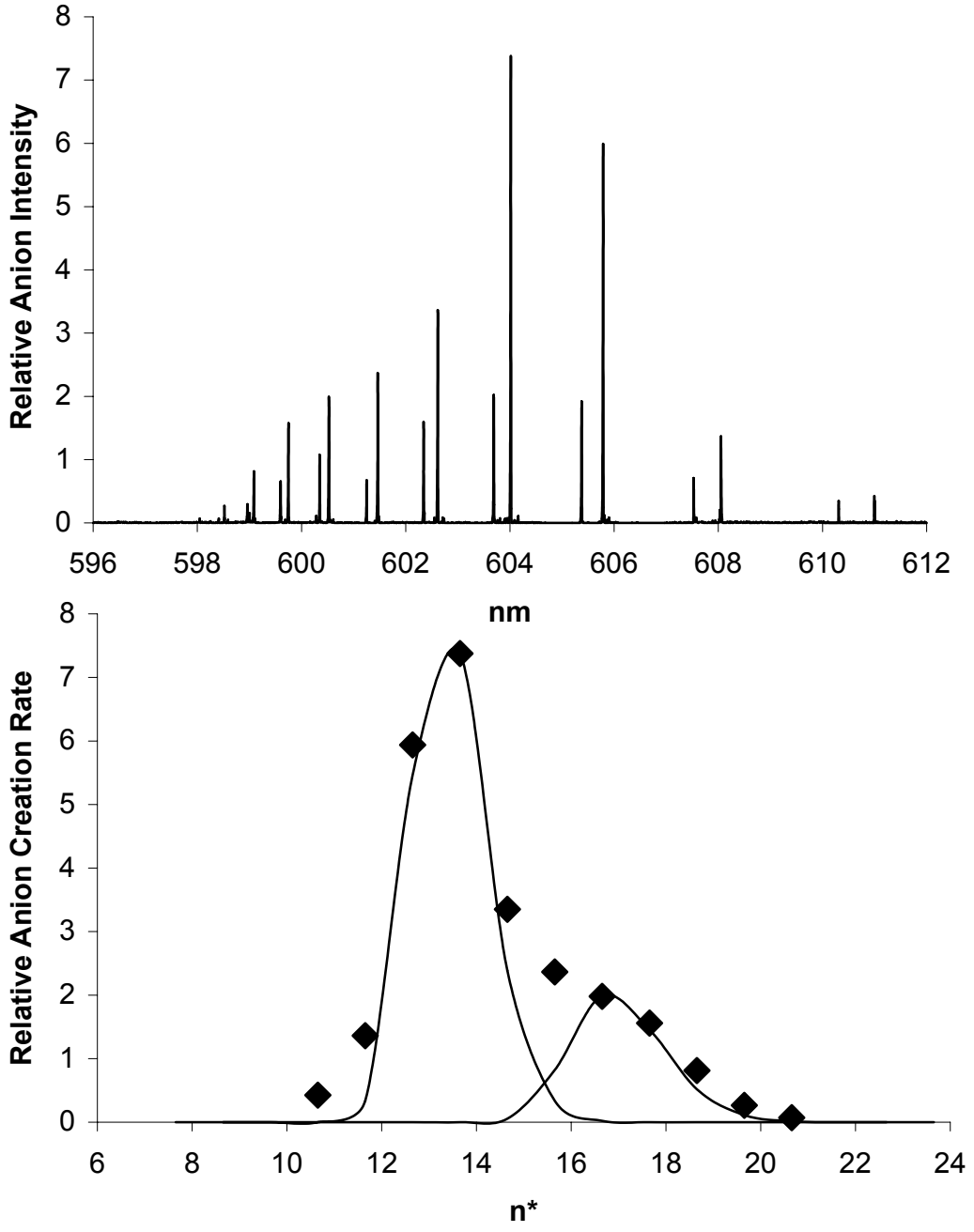

Figure 6.3 One-color dipole-bound anion formation spectrum for glycol sulfite (top) and fitting to curve-crossing model (bottom).

studied, the sulfoxide containing molecules also exhibit an increasing electron affinity with dipole moment. However this is not the case for the eight nitrile containing molecules, whose dipole moments vary only from 3.9 D to about 4.3 D. Within the estimated accuracy of the measured and calculated dipole moments (~0.1D) there are no obvious trends in the variation of μ with electron affinity. In fact, CH_3CN has the lowest dipole moment of this group but exhibits the largest electron affinity. With dipole moments being so similar, other factors must be responsible for this behavior. Since the polarizability grows with increasing molecular size, this too cannot be responsible for the observed trends. One notes that as the physical size of the molecule increases the electron affinity is noted to decrease. In addition, some of the molecules exhibit a broader charge exchange profile than others. For example, the charge exchange profile for 3-methylbutanenitrile spans a broader range of n^* than that of pentanenitrile by $\Delta n^* \approx 1$.

Pentanenitrile is best described as linear and there is little doubt where the positive charge density resides. However, the geometry of 3-methylbutanenitrile is more branched and allows for conformations that differ more than in the case of pentanenitrile. The theoretical dipole moment of the most stable conformation (see Table 4.1) of pentanenitrile is 3.95 D whereas that of 3-methylbutanenitrile is 4.04 D. Pentanenitrile, however, has a slightly larger binding energy (12.6 compared to 11.7 meV). The answer may well lie in the dispersion interaction between the dipole-bound electron and the valence electrons in the neutral molecule. Dipole-bound orbitals for 3-methylbutanenitrile (*gauche* conformer) and pentanenitrile (*gauche* conformer) are shown in Figure 6.4 using the same contour (0.002). It can be seen that there is more interaction of the dipole-bound electron with the backbone of pentanenitrile than there is

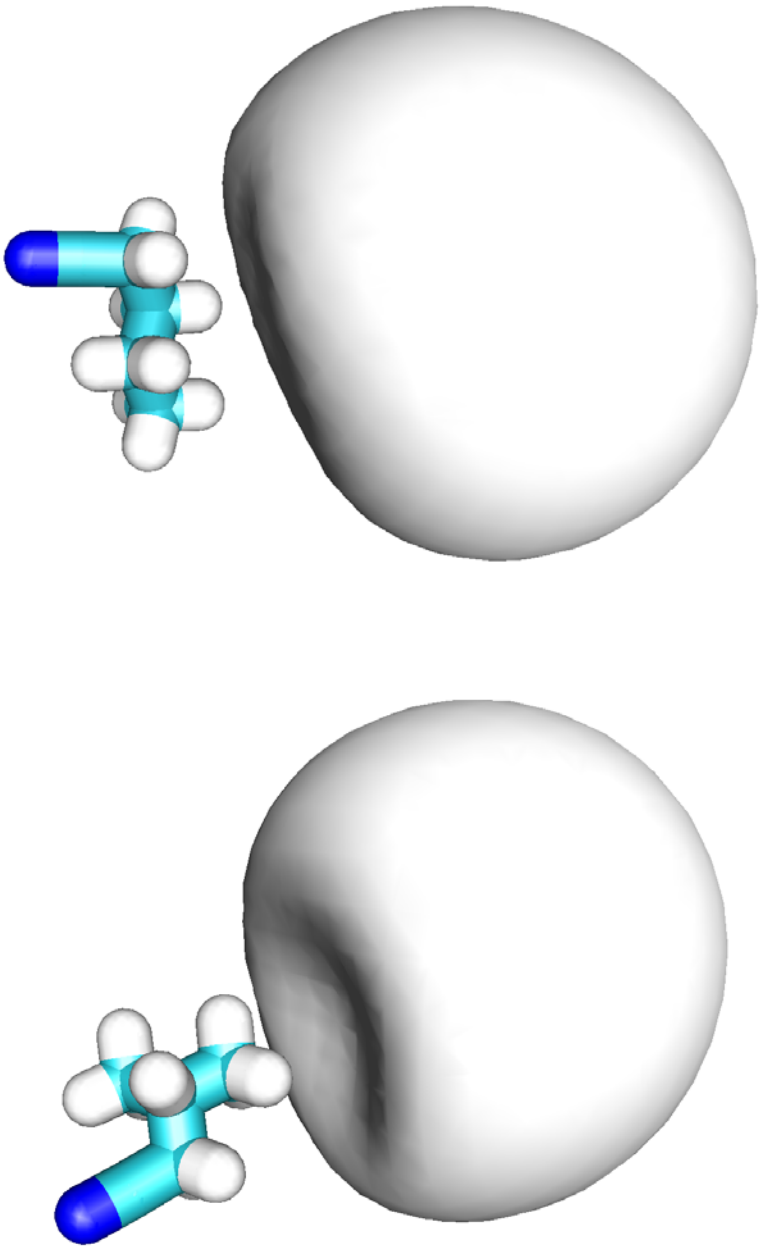

Figure 6.4 Dipole-bound anion molecular orbitals for *gauche*-pentanenitrile (top) and *gauche*-3-methylbutanenitrile (bottom). The electron in the dipole-bound molecular orbital can interact more with the electrons in *gauche*-pentanenitrile than in the case of *gauche*-3-methylbutanenitrile.

in the case of 3-methylbutanenitrile. In the case of 3-methylbutanenitrile the excess electron can only interact to any extent with the methyl group. This phenomenon may explain the trend in electron affinities for this series of nitriles. The more the excess electron interacts with the molecule the higher the electron affinity becomes.

Ab initio calculations at various levels of theory (using the aug-cc-pVDZ basis set) were performed by Ken Jordan's group[75] to model this effect in some of the nitrile containing molecules. As in previous calculations of electron affinities of dipole-bound anions they added a diffuse set of functions to the positive side of the dipole moment. Due to the Jordan group's substantial computing resources, CCSD(T) calculations were carried out for some of the molecules. The results (shown in Table 6.2) agree with experiment in that acetonitrile is predicted to have the largest electron binding energy. However, the calculated electron affinities are about 25% smaller than the measured (RET values). It is possible that the RET approach used to extract electron binding energies from the RET curves overestimates the electron binding energies of the nitriles. One reason for suspecting that this could be the case is that the RET model ignores the role of dispersion interactions on the electron binding. Although the MP2 procedure considerably underestimates the electron binding energies it is seen to qualitatively reproduce the trends from the RET experiments for all the nitriles from acetonitrile to pentanenitrile.

Table 6.2 Ab initio calculated electron affinities for some of the nitrile containing compounds. Electron affinities for two different conformations were calculated for butanenitrile, pentanenitrile, and 3-methylbutanenitrile.

Molecule	Formula	KT	HF	MP2	CCSD	CCSD(T)	EXP
Acetonitrile	CH_3CN	6.53	6.87	9.24	14.10	13.35	18.7
Propanenitrile	CH_3CH_2CN	4.63	4.97	6.72	11.76	11.09	15.1
Butanenitrile	$CH_3(CH_2)_2CN$	3.54	3.60	4.93	9.68	9.27	16.1
Butanenitrile (*g*)		3.54	3.84	5.43	10.70	-	
2-Methylpropanenitrile	$(CH_3)_2CHCN$	3.81	3.93	5.32	10.33	9.85	11.7
Pentanenitrile	$CH_3(CH_2)_3CN$	2.99	3.24	4.52	9.34	9.02	12.6
Pentanenitrile (*g*)		2.72	2.89	4.12	8.95	-	
3-Methylbutanenitrile	$(CH_3)_2CHCH_2CN$	2.72	2.81	3.98	9.01	-	11.7
3-Methylbutanenitrile (*g*)		3.27	3.29	5.22	12.56	-	

CHAPTER VII

DIPOLE-BOUND ANIONS OF LARGE DIPOLE MOMENT MOLECULES: VINYLENE AND ETHYLENE CARBONATE

Introduction

Dipole-bound anions of the large dipole moment molecules vinylene carbonate and ethylene carbonate were studied.[76] Geometries of these molecules can be found in Figure 4.8. The dipole moments of these compounds are larger than those of the carbonyl, nitrile, sulfoxide, or sulfite containing compounds and are 4.6 and 5.4 Debye, respectively. As before, dipole-bound anions were created by charge transfer from Rydberg atoms and detected in a time-of-flight mass spectrometer. Anions were created when the laser wavelength was tuned to excite the appropriate Rydberg levels of rubidium using two photons. The electron affinities of these two molecules are large, resulting in RET at low values of n^*. Since the Rydberg levels used to create these anions were very far apart in wavelength the laser was not scanned continuously as in the case of the lower electron affinity molecules.

Low-energy electron beam studies show that these molecules apparently do not form long-lived (t >1 μsec) valence-bound parent anions, but rather undergo dissociative electron attachment at energies above ~0.5 eV.[159,160] In addition, studies of fast alkali atom transfer in vinylene carbonate do not show evidence of a stable parent anion.[159] Electron attachment studies for vinylene carbonate show primarily $C_2H_2O^-$ and $C_2H_2O_2^-$ near electron impact energies of 1.5±0.1 and 3.0±0.2 eV, respectively. Both of these dissociative resonances are broad (FWHM ~ 1 eV). This interpretation was supported by calculations by Younkin et al.[161,162] who used a semiempirical method to show that the

$^2A_2$ and $^2B_1$ π^* anion states of vinylene carbonate are unbound by –2.0 and –2.1 eV, respectively. These calculations do not predict bound valence anions for ethylene carbonate or vinylene carbonate. Thus, it can be stated with some confidence that these molecules do not possess bound valence anion states.

Experimental Results

Figure 7.1 shows the relative dipole-bound anion intensity for ethylene carbonate (left) and vinylene carbonate (right) as a function of the effective quantum number, n^* for the unresolved nd $^2D_{5/2,\ 3/2}$ levels. The signal intensity for the ns levels is much weaker but shows similar behavior. The electron affinities for these molecules are estimated to be 49 meV and 24 meV, respectively, using fractional n^*_{max} values of 9.0 and 11.6. For dipole-bound anions with low electron affinities (<10 meV) such as the carbonyl containing molecules studied here, the parent Rydberg states (n^* ranges typically from 15-50) are closely spaced and smooth RET profiles are obtained. For such anions it is easy to obtain n^*_{max} with little uncertainty. This is not the case, however, with vinylene carbonate and ethylene carbonate, for which the larger electron binding energies necessarily imply that electron capture occurs from relatively low-lying, much more widely spaced Rydberg levels. It is unlikely that the true maximum in the RET profile for either molecule coincides closely to a specific rubidium nd state. This leads to sizable uncertainties in the electron affinities estimated using Equation 1.11 for high dipole moment molecules. For example, an uncertainty in the determination of n^*_{max} of ± 0.5 corresponds to an uncertainty of 3 and 8 meV, for vinylene carbonate and ethylene carbonate, respectively. In order to obtain a smoother RET profile other alkali Rydberg sources such as cesium could be employed as well as other angular momentum states of

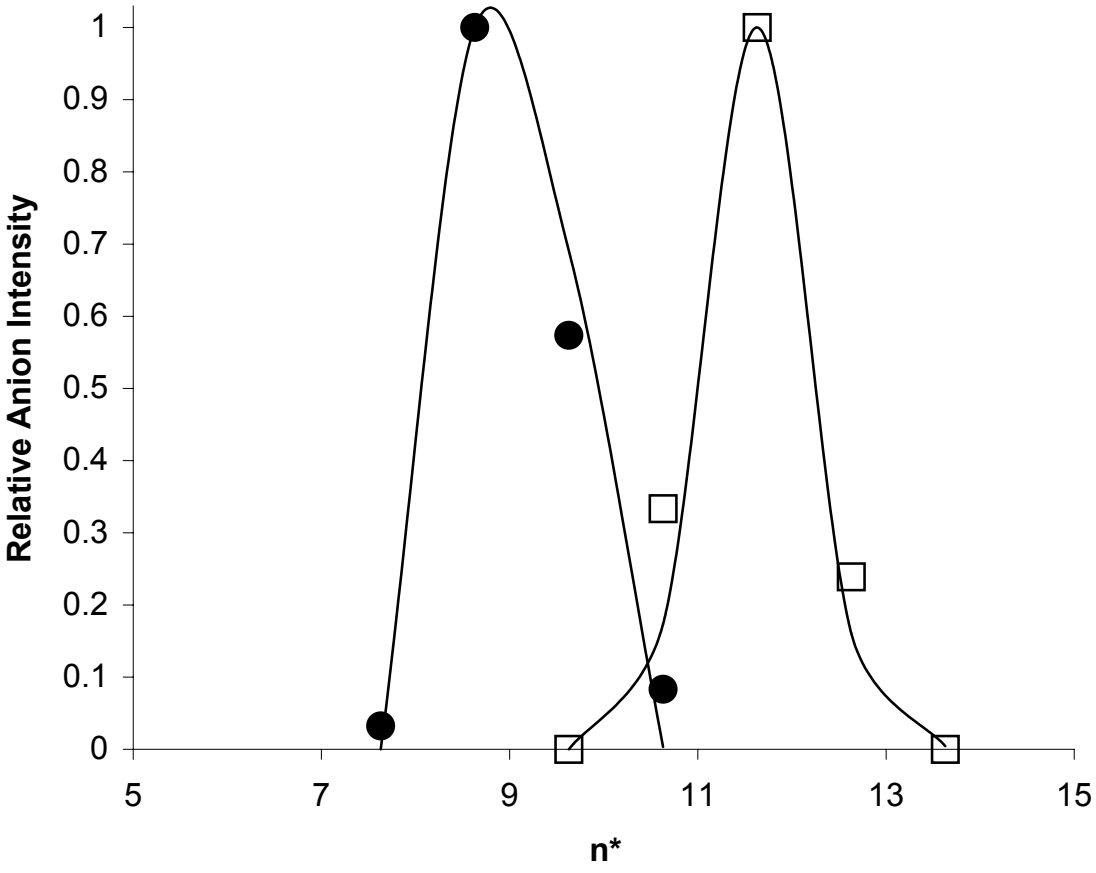

Figure 7.1 Dipole-bound anion formation rates for vinylene carbonate (squares) and ethylene carbonate (circles) from *nd* rubidium Rydberg states. The lines through the data are calculated using the curve-crossing model discussed in Chapter 1.

rubidium. However, this was not possible as a result of the large dipole moment and correspondingly small negative ion signal from rubidium *ns* states in this study. In some cases, there is sufficient data to fit a curve through all of the points and arrive at a "fractional" value of n^*_{max} which is expected to provide a more accurate electron affinity value. The curve shown in Figure 7.1 is an attempt at this procedure which yields n^*_{max} =9.0 and EA = 49 meV for ethylene carbonate and n^*_{max} = 11.6 and EA = 24 meV for vinylene carbonate. The smooth curve for each molecule is the result of the curve-crossing model, which gives calculated electron affinities of 24 meV for vinylene carbonate and 53 meV for ethylene carbonate. The slight disagreement between Equation 1.11 and the curve-crossing model for ethylene carbonate is also seen for some of the nitrile and sulfoxide containing molecules. Kit Bowen's group[76] has recently measured photoelectron spectra of ethylene carbonate and reports a binding energy of 49 meV. This spectrum is shown in Figure 7.2. Negative ions of vinylene carbonate were not observed in the photoelectron spectra, which is not surprising due to its relatively low binding energy. The negative ions formed in this apparatus occur in a discharge which is not conducive to the production of weakly-bound anions.

Comparsion with Theory

The dipole-bound anion states of vinylene carbonate and ethylene carbonate were calculated at the Koopmans' theorem (KT), Hartree-Fock (HF), MP2, CCSD, and CCSD(T) levels of theory, using the MP2/aug-cc-pVDZ optimized geometries of the neutral molecules and employing the aug-cc-pVDZ basis set augmented with a set of diffuse *s* and *p* primitive Gaussian functions located at a single center on the symmetry axis. Ken Jordan's group[76] at the University of Pittsburgh provided the CCSD and

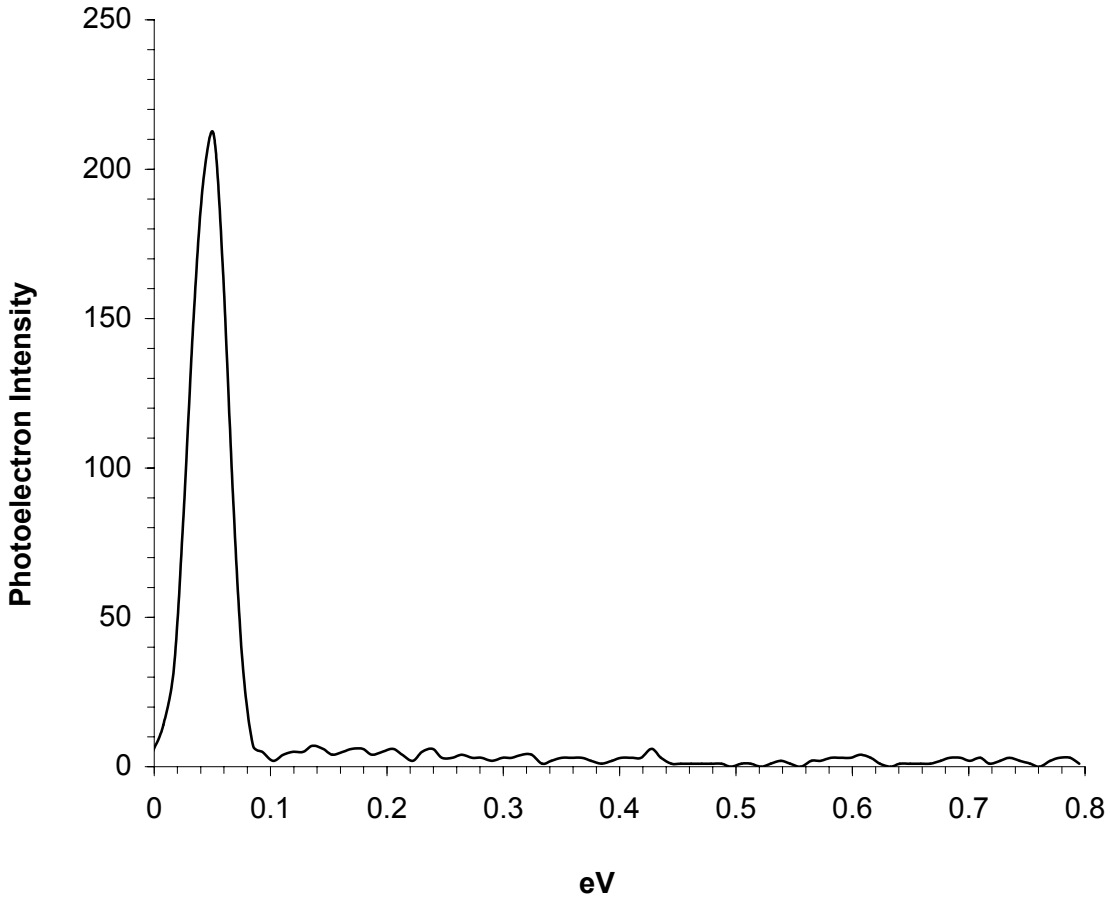

Figure 7.2 Photoelectron spectrum of ethylene carbonate. The peak corresponds to a binding energy of 49 meV. No valence-bound peak is evident.

CCSD(T) results. Shown in Figure 7.3 are the calculated dipole-bound orbitals for these molecules using the same contour interval (0.003). Whereas the orbital for vinylene carbonate is of almost spherical shape, that of ethylene carbonate is more "pear" shaped. This might be due to the influence of the two additional hydrogens and lack of a double bond in ethylene carbonate. Vinylene carbonate is found to be planar (see Figure 4.8) whereas ethylene carbonate is twisted. Shown in Table 7.1 is a summary of the calculations performed on vinylene carbonate and ethylene carbonate along with a comparison to the experimental values. The effect of enlarging the set of diffuse functions was investigated, however no significant change in the binding energy was observed. At the highest level of theory, the calculated electron binding energies are in excellent agreement with experiment. In addition, the electron binding energies increase by about 90% in going from the Koopmans' Theorem to the CCSD(T) levels of theory, with a significant portion of the increase coming from high-order electron correlation effects, *i.e.*, in going from the MP2 to the CCSD(T) method. Similar trends have been found for numerous other dipole-bound anions,[164-171] and primarily reflect the consequence of dispersion-type interaction between the excess electron and the outer valence electrons of the polar molecule.

It should be noted that since calculations are carried out using the geometries of the neutral molecules, vertical electron affinities are obtained, whereas the RET and photodetachment experiments give adiabatic electron affinities. The close agreement among the three different electron binding energies implies that the geometries of the neutral molecules and dipole-bound anions are very similar. Nevertheless, the small difference between theory and experiment (approximately 20%) may be attributable to

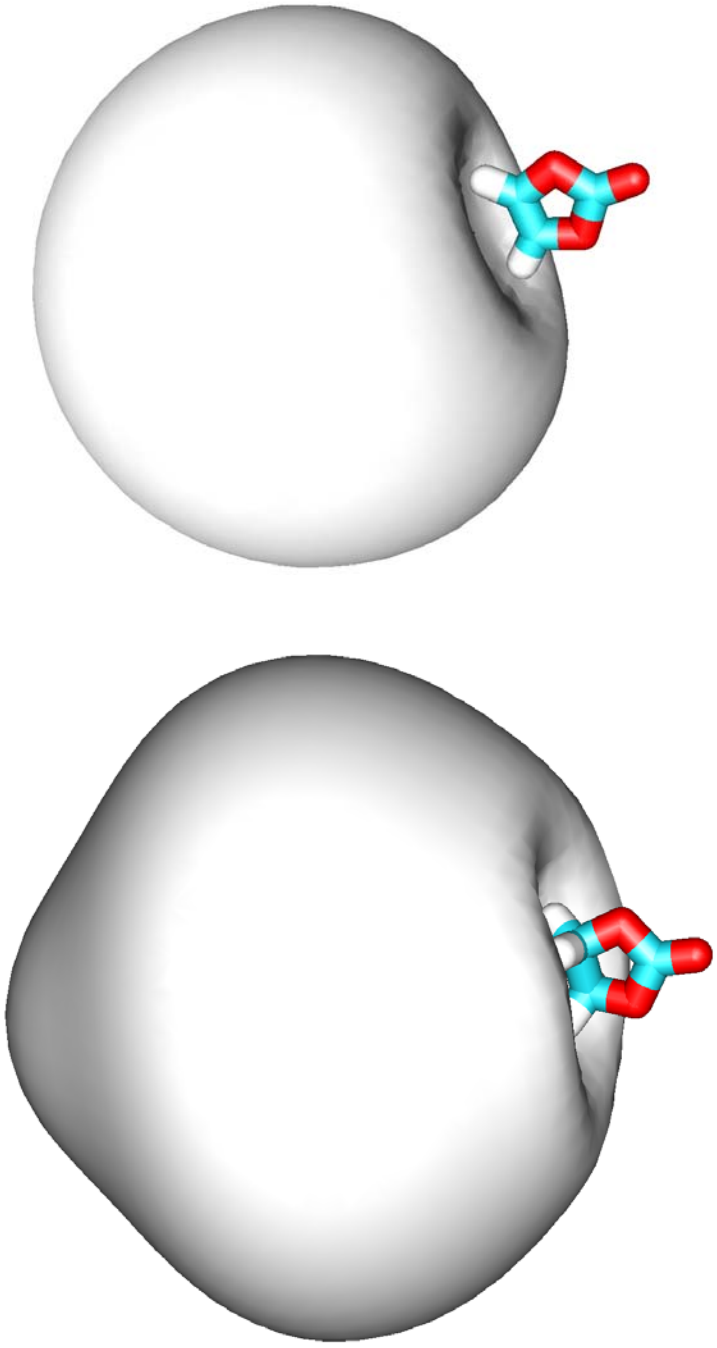

Figure 7.3 Dipole-bound anion molecular orbitals for vinylene carbonate (top) and ethylene carbonate (bottom). Whereas the orbital for vinylene carbonate is almost spherically symmetric due to the neutral's C_{2v} symmetry, the orbital for ethylene carbonate is irregularly shaped due to the additional hydrogen atoms and twisting of the C-C bond.

Table 7.1 Calculated vertical electron affinities (meV) of vinylene carbonate and ethylene carbonate.

	Vinylene Carbonate	Ethylene Carbonate
KT	11.97	23.95
HF	12.94	26.36
MP2	15.58	31.70
CCSD	20.43	40.43
CCSD(T)	20.11	40.88
Expt.[a]	24	49
Expt.[b]		49

[a] Using RET method.
[b] Photodetachment method (Kit Bowen).

relaxation of the dipole-bound anion. The assumption of identical geometries for dipole-bound anions and the neutral parent may be a good approximation for weakly bound anions but less so for strongly polar molecules.

CHAPTER VIII

DIPOLE-BOUND ANION AND POSSIBLE QUADRUPOLE-BOUND ANION OF SUCCINONITRILE

Introduction

In order to examine the question of electron binding to a quadrupole molecule, the succinonitrile molecule (see Figure 4.8) was studied.[77] Succinonitrile can loosely be considered as two acetonitrile molecules (see Figure 4.5) connected by a C-C bond. Rotation about this C-C bond produces two distinct conformations. The possibility that electrons might be also bound to a molecule as a result of a large quadrupole moment was first considered theoretically by Jordan and Liebman.[50] These authors predicted a rather large binding energy for the $(BeO)_2$ dimer of 0.65 eV. Gutowski and Skurski[172] have also performed calculations for the $(BeO)_2$ dimer and suggest that the D_{2h} ground state would support a quadrupole-bound anion. On the other hand, Gutsev et al.,[87] using the criterion that quadrupole-binding should be approximately as diffuse as that for the dipole-bound anion, could find no evidence of a diffuse bound state in $(BeO)_2^-$. They find an even more tightly bound valence type anion with a binding energy of 0.9 eV. In a related study, Gutowski et al.[172] presented experimental and theoretical studies of $(MgO)_n$ (n=1-5) clusters and found electron affinities on the order of one eV which they attribute to quadrupole-bound anions. However, using the argument of Gutsev et al.[87] these species might be better described as valence bound anions.

In 1990, Prasad, Wallis and Herman[173,174] calculated the binding energy of an electron to a finite linear electric quadrupole (Q) in two configurations: (A) one which has two positive charges each of charge +q, symmetrically placed about a negative charge

of –2q and (B) has the charges reversed. Their calculations predict that the minimum quadrupole moment Q_{min} required to bind an electron is $Q_{min}(A)$ =21 a.u. and $Q_{min}(B)$ = 2.66 a.u. Other experimental and theoretical studies have considered the possibility of quadrupole-bound anions. Compton, Dunning and Nordlander[175] reported pseudopotential calculations which suggest that an electron could be bound to the quadrupole field of carbon disulfide (Q = +3.3 a.u.) and might explain some anomalies in experiments of Rydberg charge exchange involving CS_2. Unfortunately, Gutsev, Bartlett, and Compton[176] reported more elaborate calculations that did not support a bound quadrupole anion for CS_2. Finally, Defranscois et al.[69] have observed Rydberg charge transfer from highly excited atoms to para-dinitrobenzene (pDNB) which they attribute to a quadrupole-bound anion state. Para-dinitrobenzene has a zero dipole moment and quadrupole moment tensor elements of Q_{xx} = +45 a.u., Q_{yy} = -59 a.u. and Q_{zz} = + 14 a.u. These results were complicated by the fact that pDNB also has a valence anion state. Thus upon consideration of these contributions, there is no firm experimental evidence for the existence of quadrupole bound anions at this point. In addition, as a result of the shorter range of the quadrupole potential as compared to the dipole potential, there is no convenient prediction as to the minimum quadrupole moment required to bind an excess electron.

Succinonitrile exists in two forms, an *anti* form which has a zero dipole moment and a *gauche* form, which has a large dipole moment of about 6 Debye (see Figure 4.8 for conformational geometries). However, the *anti* form (sometimes incorrectly called *trans* in the literature), has a rather large quadrupole moment and there is little doubt that a dipole-bound anion should exist for the *gauche* form. Desfrançois[77] has calculated the

quadrupole moment of *anti*-succinonitrile at the MP2/6-31++G** and Density Functional Theory (DFT) levels of theory to be -47 and –45 a.u.

Results and Discussion

The RET spectrum for succinonitrile seeded in a helium nozzle jet expansion is shown in Figure 8.1. When compared to the dipole-bound spectra for the other molecules studied it is very unusual for a number of reasons. The first unusual aspect is that although a sharp peak is observed at $n^* \approx 12$ there is negative ion formation over a wide range of n^*. RET leading up to very high n^* generally is observed for molecules which have a valence negative ion state. The maximum at $n^* \approx 12$ correlates to an electron affinity of approximately 22 meV using Equation 1.11. This in turn correlates to a dipole moment in the range of 4.5 – 5 Debye and does not correspond to the dipole moment of the *gauche* form (calculated to be 5.7 Debye). For a dipole moment of 5.7 D an electron affinity of approximately 100 meV is expected. Thus it is tempting to assume that this peak corresponds to the quadrupole-bound state of the *anti* form. However, if this represents the quadrupole-bound state, one could ask, "Where is the dipole-bound state for the *gauche* form?" since we expect both forms to be present in the nozzle jet expansion. To answer this question careful experiments were performed at low n^*. A constant concentration of SF_6 and succonitrile was used to generate data points of n values down to *6d*. The succinonitrile negative ion yield was compared to the SF_6^- yield and a small enhancement in succinonitrile negative ion signal was observed at $nd = 8$ ($n^* \approx 6.7$), which corresponds to an electron affinity of approximately 114 meV. Although this "peak" is not obvious, many runs over this region consistently provided evidence for a rise in the signal compared to SF_6^-. However, with Rydberg states

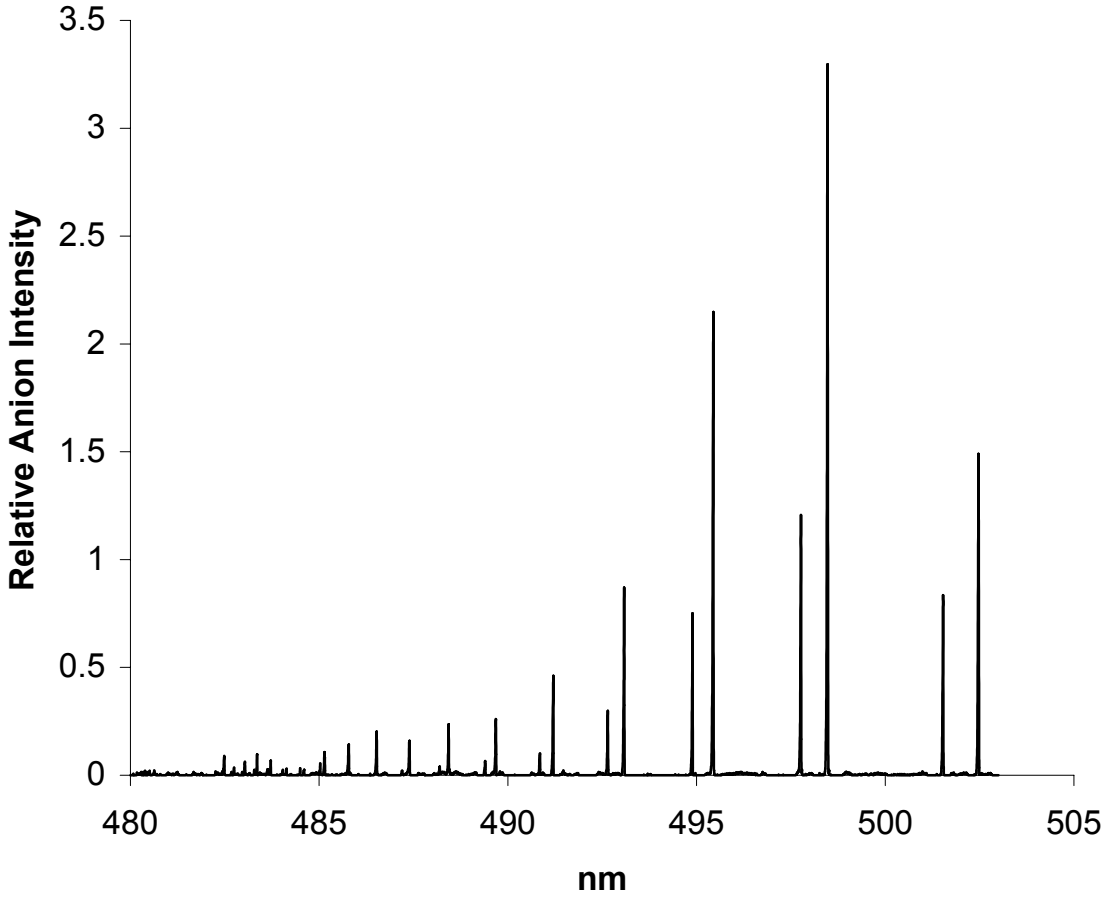

Figure 8.1 Two-color negative ion formation spectrum for succinonitrile.

so far apart at these low values of *n*, the true maximum almost certainly lies at some fractional value of *n**. As in the case of ethylene carbonate, using other Rydberg atoms, such as cesium, might enhance the data. The negative ion signal was too small to be observed from *ns* Rydberg levels. The resulting plot of relative negative ion signal of succinonitrile as a function of *n** is shown in Figure 8.2. Kit Bowen's group[77] at Johns Hopkins University has recently provided evidence for this interpretation using photoelectron spectrometry of the succinonitrile anion formed in a discharge. They obtain an electron affinity of 108 meV. Many studies of the Bowen group have found that their experiment does not allow for the detection of low electron affinity negative ions (EA<50 meV) and therefore they do not see the lower electron affinity state of succinonitrile. It is also important to point out that their observation also confirms the lack of a valence-bound state for succinonitrile. Desfrançois[77] has also looked at succinonitrile negative ions created with Xe *nf* Rydberg atoms. He obtains an identical electron affinity as observed here from both RET and field ionization (22 meV from both).

A potential energy curve corresponding to the rotation of the C_2-C_3 bond (the central bond) in neutral succinonitrile is shown in Figure 8.3. Energies were calculated at the MP2/aug-cc-pVDZ level of theory using *Gaussian 98* and the *opt=modredundant* command. The input file for this calculation is shown in Figure 8.4. The energy difference between the two conformations is rather small with the *anti* form lying lower than the *gauche*. At this level of theory this energy difference is 0.036 eV or about 0.8 kcal per mole. This corresponds to an equilibrium mixture of approximately 80% *anti* and 20% *gauche* at 300 K. Assuming that the molecules are locked into these

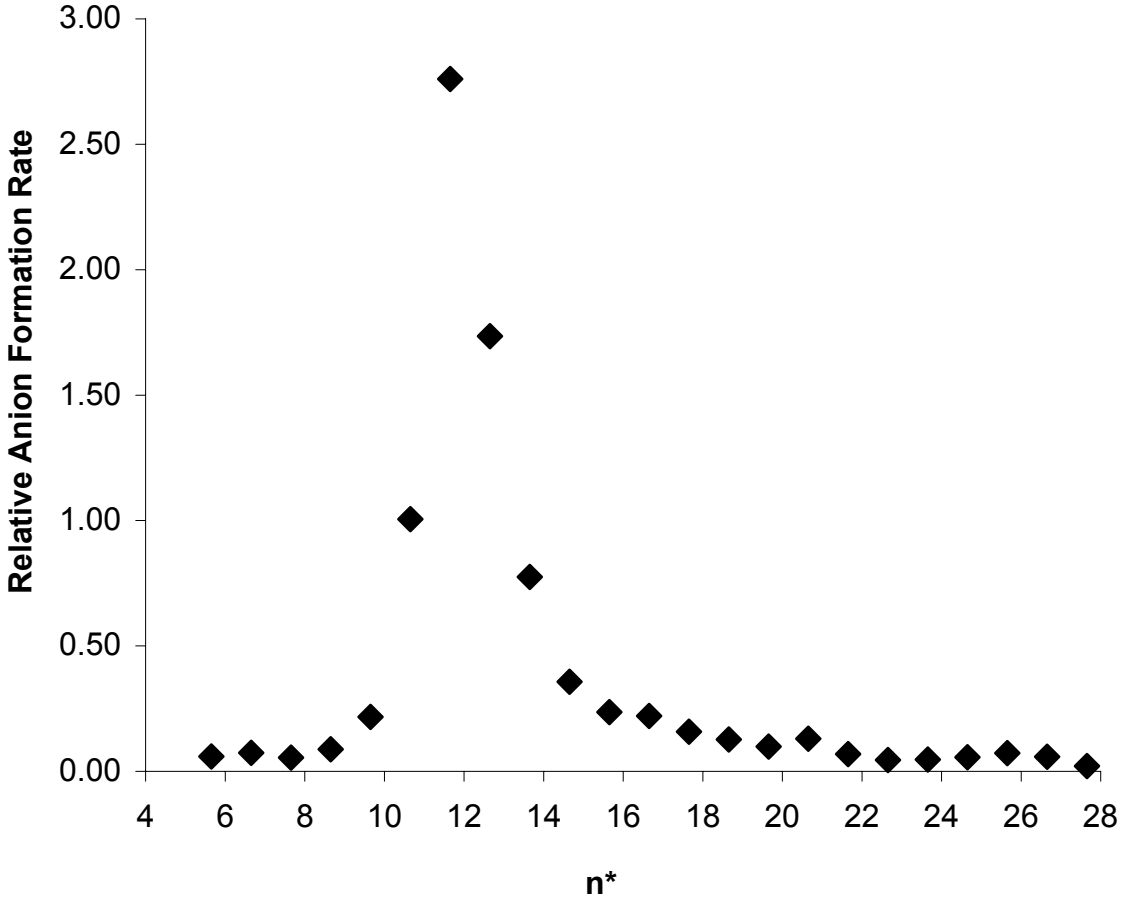

Figure 8.2 Relative anion formation rates for succinonitrile over a wide range of n^*.

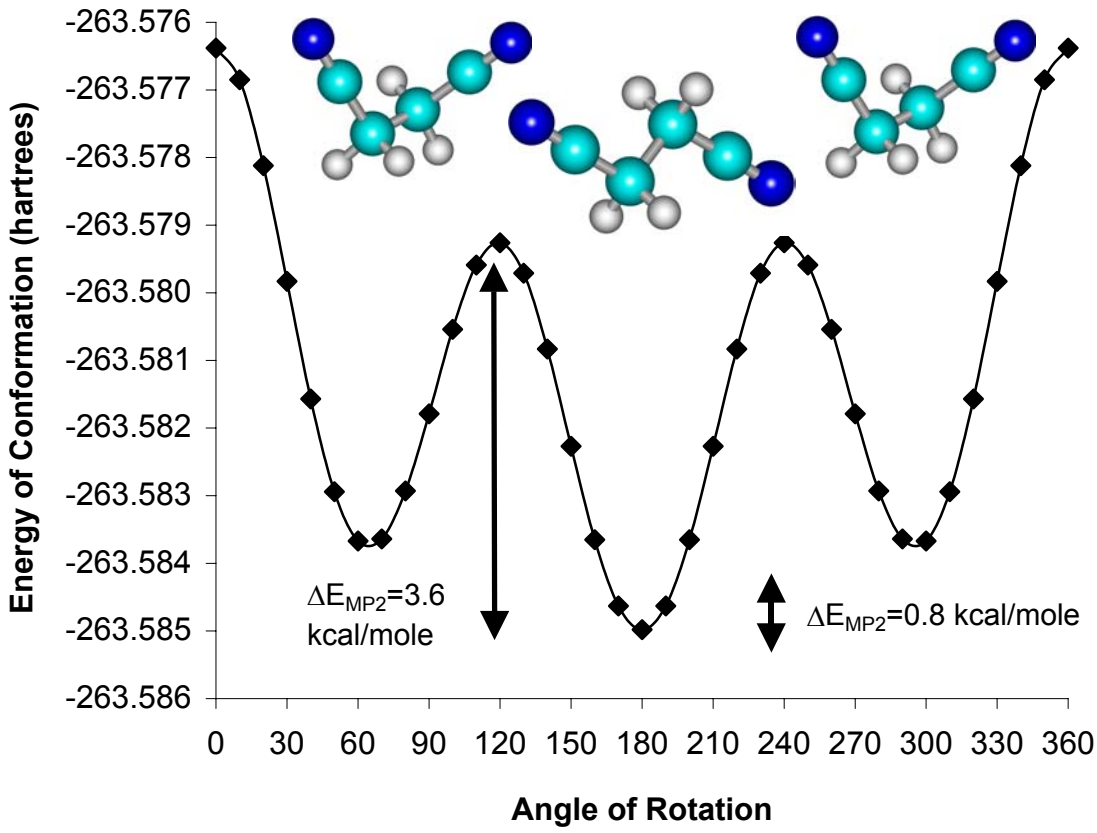

Figure 8.3 Potential energy curve for the rotation of the C_2-C_3 bond in succinonitrile. 180^o corresponds to the *anti* form.

```
%mem=800mb

#mp2/aug-cc-pvdz opt=modredundant scf=tight

succinonitrile opt=modredundant relaxed potential surface scan

0 1
C
C,1,R2
C,1,R3,2,A3
H,1,R4,2,A4,3,D4,0
H,1,R5,2,A5,3,D5,0
C,2,R6,1,A6,3,D6,0
N,3,R7,1,A7,2,D7,0
H,2,R8,1,A8,6,D8,0
H,2,R9,1,A9,6,D9,0
N,6,R10,2,A10,1,D10,0
Variables:
R2=1.5469926
R3=1.47270326
R4=1.10070614
R5=1.10070747
R6=1.47270143
R7=1.18645576
R8=1.10070881
R9=1.10070231
R10=1.18645579
A3=110.38822553
A4=110.17239081
A5=110.17152323
A6=110.38910486
A7=178.17619506
A8=110.17086287
A9=110.17229969
A10=178.1764146
D4=-120.56581968
D5=120.5645879
D6=-179.99969128
D7=0.04564224
D8=-120.56656103
D9=120.56518989
D10=0.58173307

6 2 1 3 = -180.0 S 18 -10.0
```

Figure 8.4 *Gaussian 98* input file for the calculation of a number of conformational energies of succinonitrile. The *opt=modredundant* command allows for one variable to be adjusted while keeping all others constant. In this case the angle formed by the two acetonitrile groups is adjusted so that the molecule gradually moves from the *anti* to the *gauche* form.

conformations at the time of the nozzle jet supersonic expansion,[151,152] anions from both conformations are expected. At the present time it is suggested that both conformers are observed in the RET experiment with the quadrupole-bound anion in greater abundance as a result of the greater abundance of the *anti* conformer. The dipole-bound anion is seen exclusively in the discharge experiments. This is consistent with many other studies of the discharge technique: only large binding energy anhions are observed (EA > 40 meV).

Shown in Figure 8.5 is the same potential energy curve as in Figure 8.3 with the experimental electron affinities sketched in as a dotted line. The potential energy of the anion in the region between the two minima is unknown and has simply been estimated from the neutral. From this it can be seen that the dipole-bound anion of the *gauche* conformer is now the global minimum. The possibility of tunneling from one potential minimum to the other (*anti/gauche* transformation) was investigated but determined to be unlikely. The large barrier estimated between the two (3.6 kcal/mole) also makes conversion from one anion to the other unlikely. The possibility that the quadrupole-bound state acts as a doorway to the dipole-bound state does not seem likely since field detachment data corresponds to the low electron affinity. Collisions or photoexcitation might, however, interconnect the two states. Shown in Figure 8.6 is the dipole-bound molecular orbital for the *gauche* form and what is taken to be the quadrupole-bound molecular orbital for the *anti* form. Although the dipole-bound state is shown to be bound by Koopmans' Theorem, the quadrupole bound state is not. The "doughnut" shape of this molecular orbital (the lowest unoccupied molecular orbital for the *anti* form) is what is expected for a quadrupole-bound state for this molecular geometry.

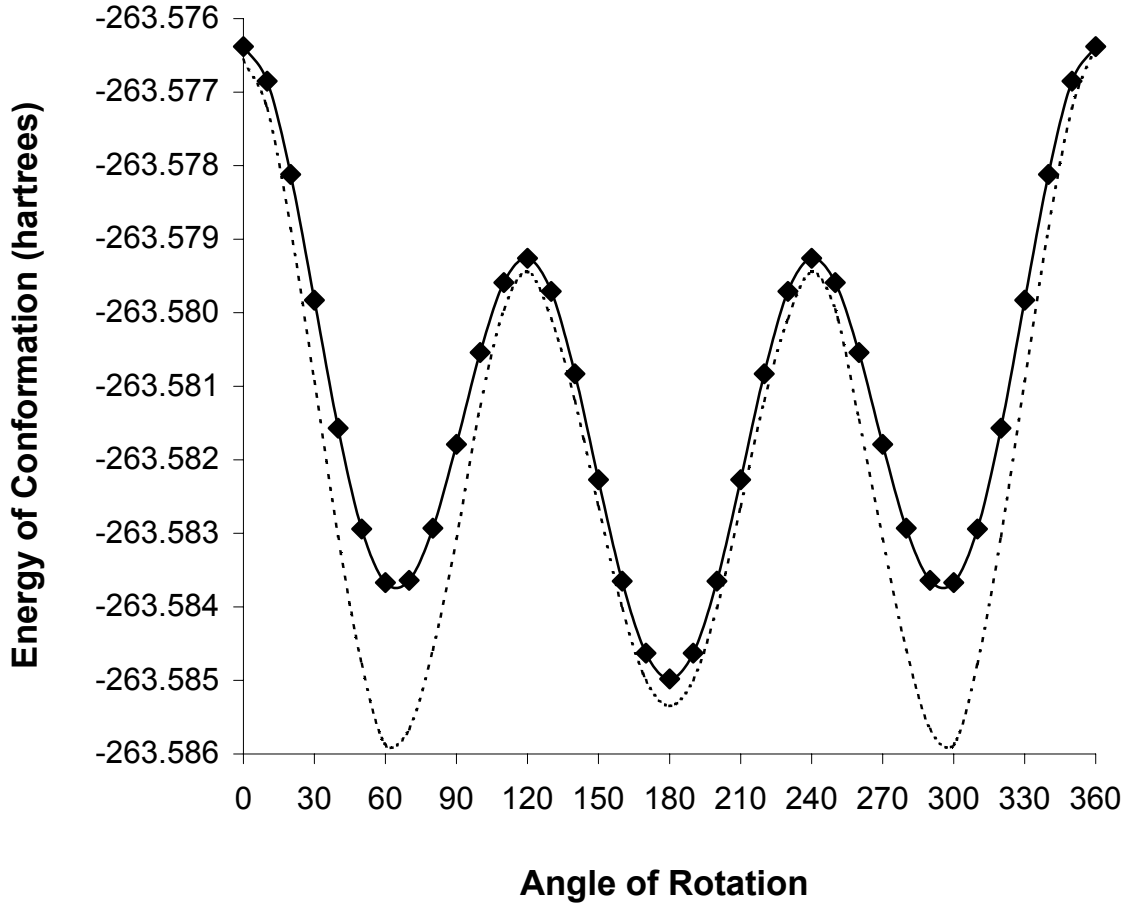

Figure 8.5 Potential energy curve for the rotation of the C_2-C_3 bond in succinonitrile (solid line) and possible negative ion potential energy curve (dashed).

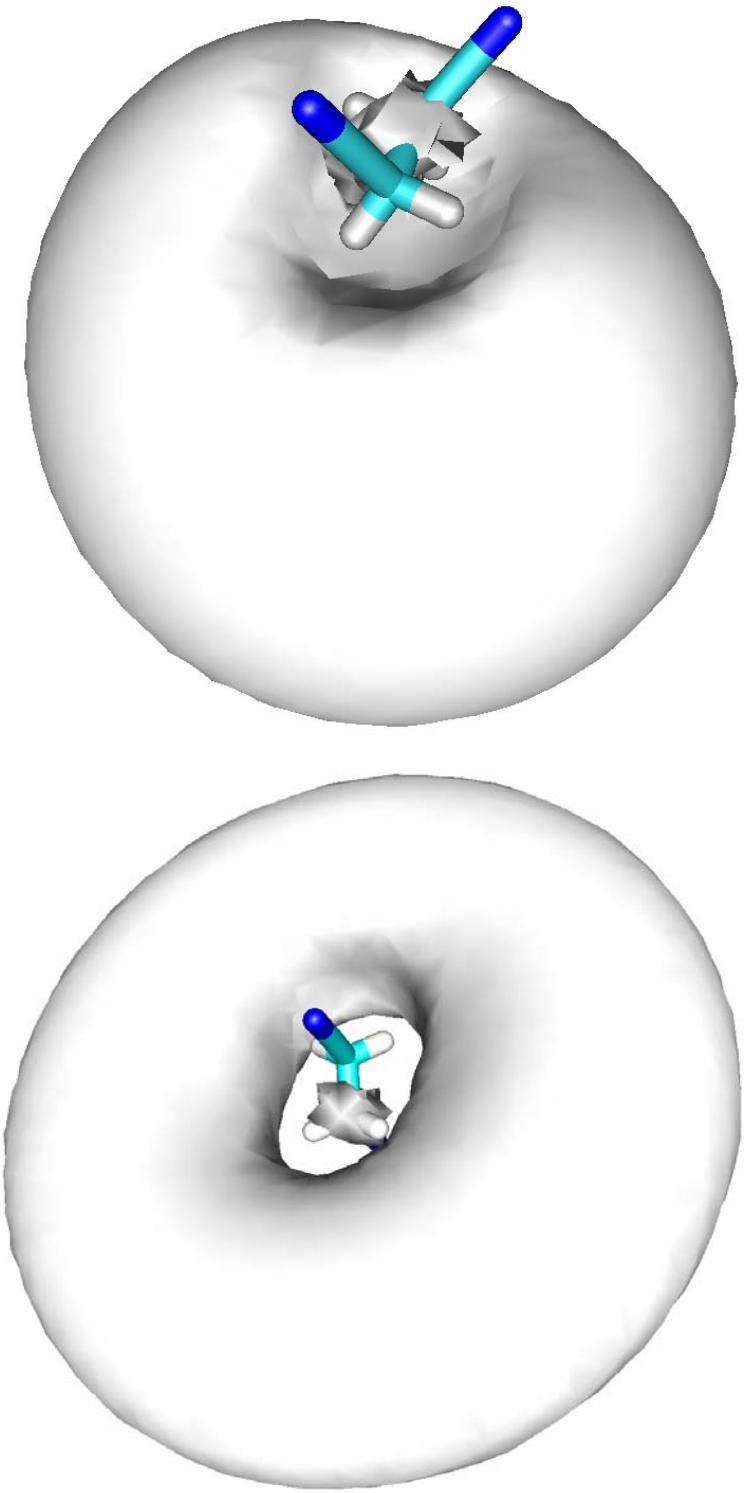

Figure 8.6 Dipole-bound molecular orbital for *anti*-succinonitrile (top) and possible quadrupole-bound molecular orbital for *gauche*-succinonitrile (bottom).

CHAPTER IX

CONCLUSIONS

This dissertation presents studies of a large number of dipole-bound anions of compounds with different physical properties. Theoretical calculations are provided along with the measurements in order to examine the molecular properties affecting electron binding energies. Shown in Figure 9.1 is a plot of the electron affinities of all of the molecules studied as a function of their dipole moments. A line is provided as a guide to the eye when observing the trend and has no physical interpretation. From the plot it is apparent that electron affinity increases rapidly with dipole moment following an initial critical value of ~2.5 D. Fermi and Teller[9] first derived 1.625 Debye as the minimum dipole moment for the ficticious "point dipole" to bind an electron. Wallis[16] later showed that the binding energy to a point dipole was very small (<1 meV) below ~2.5 Debye but rapidly increased above this value. The dependence of electron binding energy versus the point dipole predicted by Wallis is also shown in Figure 9.1. Later, Garrett and Crawford[18-27] showed that for any real, rotating polar molecule, this minimum dipole moment had to be much higher, on the order of 2.5 Debye. The experimental plot in Figure 9.1 agrees with this prediction. Indeed, creating anions of the molecules with the lowest dipole moments (especially acetaldehyde and propanal) was experimentally challenging. Small electric fields, on the order of 100 V/cm, efficiently field detach the excess electron. For lower electron affinities than this minimum value experimentally observed here (0.6 meV) even smaller electric fields would be required. This makes the experimental observation of such anions very challenging.

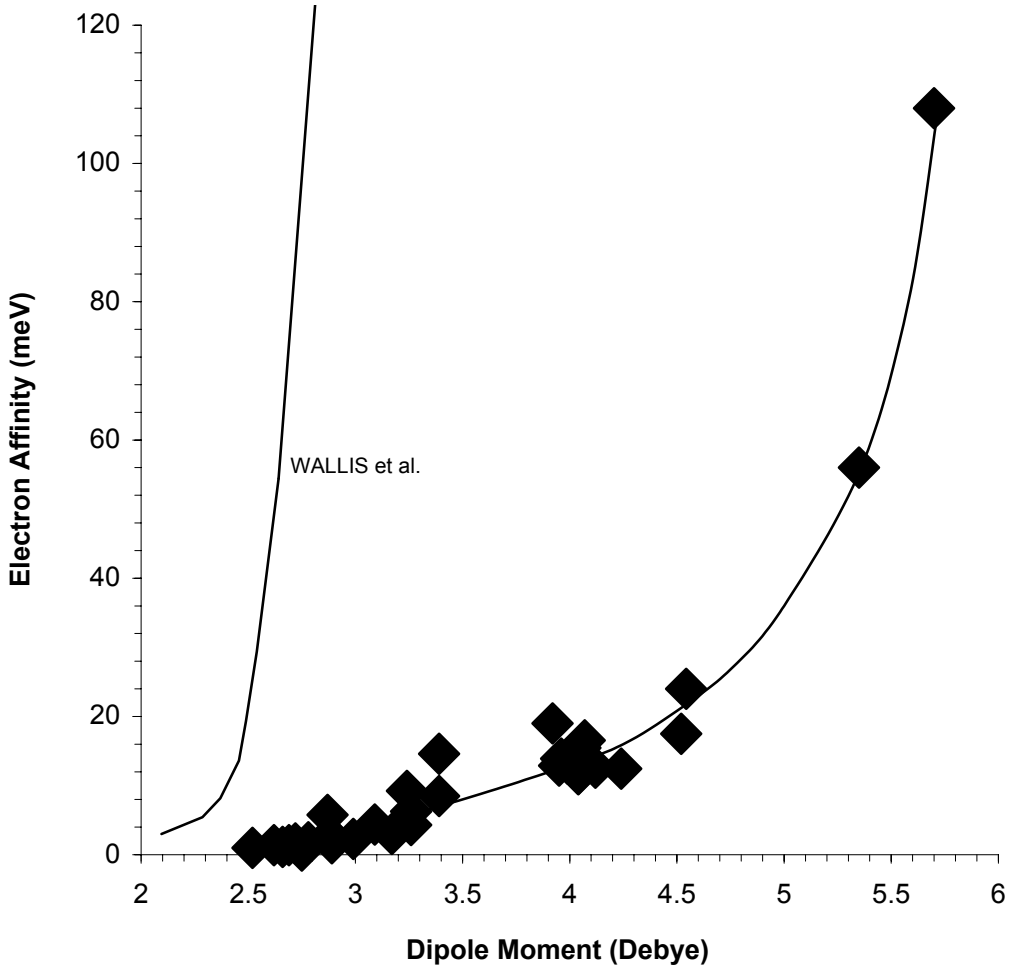

Figure 9.1 Electron affinity as a function of dipole moment for 32 dipole-bound anions. The smooth curve is drawn as an aid to the eye when viewing and has no scientific basis. The 1960 theoretical curve by Wallis[16] is shown for comparison.

For the most part, the electron affinity values for the compounds studied here lie along a central line in Figure 9.1. However, EA values for a number of molecules lie above or below this line. One possibility for this "scatter" is that the experimental dipole moments for some of these molecules are not correct. A good example of this is the case of cyclohexanone. If the theoretical dipole moment is used in place of the experimental value, the electron affinity for cyclohexanone is in agreement with the other molecules. Additionally, if all of the carbonyl compounds' electron affinities are plotted as a function of theoretical dipole moment there is a smooth and continuous trend of increasing electron affinity with dipole moment. Exceptions to this, however, are the two lowest dipole moment molecules, propanal and pivalaldehyde, and the smallest molecule, acetaldehyde. Reasons for their anomalous electron affinities might lie in the molecular polarizabilties for these molecules. Other deviations from the curve in Figure 9.1 include the second RET peaks for 3-methylcyclohexanone and glycol sulfite. The two EA values for these molecules are still not understood. The general scatter among the nitriles and sulfoxides also require further explanation. The calculated dipole moments of the sulfoxides almost certainly contain a large amount of error, based upon the calculations using dimethyl sulfoxide. In order to obtain more reliable theoretical values larger basis sets must be used. For the nitriles the scatter in data points about the line seems to be due to the "shapes" of the molecules in relation to the diffuse dipole-bound orbital. Increasing dispersion interactions of the dipole-bound electron with electrons in the molecule might be the explanation for this local disagreement. Over a wide range of dipole moments from 2.5 to 6 D, however, there is a steady trend of increasing dipole moment. The slope of this curve depends heavily on the values at large dipole moment.

Any experimental error in the electron affinity values for ethylene carbonate and succinonitrile would drastically affect the shape of the curve.

There is uncertainty in most of the experimental electron affinity values of dipole-bound anions. The empirical relation (Equation 1.11) that relates n^* to electron affinity is not derived from first principles but rather relies upon a theoretical curve-crossing model. The effect of reaction conditions (such as relative velocities of the reactants) also has been shown to affect application of this model to reproduce consistent electron affinities. Field detachment data is more trustworthy but again is based upon theoretical assumptions. Photoelectron values for some of the higher electron affinity molecules represent direct measurements and are perhaps the most reliable electron affinities available, but these can only be applied to electron affinities greater than ~50 meV. The best method for the determination of electron affinities of dipole-bound anions would be direct photodetachment of the excess electron and measurement of the electron energy either through an electrostatic energy analyzer or through time of flight analysis. This would be a direct measurement of the adiabatic electron affinity without the assumption inherent in field detachment or RET spectra. However, even for photodetachment spectroscopy the uncertainty lies in the range of 5 meV at best.

The study of dipole-bound anions promises to yield insight into the weak interactions of electrons with molecules, surfaces,[177,178] and perhaps even biological systems.[179,180] The notion has even been made recently that the diffuse interstellar bands are due to dipole-bound states.[181] The idea of electron transport along surfaces and in biological systems is not very well understood. If polar molecules are distributed along a surface one can imagine resonant electron transport from one molecule to another

through weak interactions, such as with the dipole- or quadrupole-bound anions. Although biological systems are far from the gas phase, the notion of solvated electrons and electrons being bound to multipole moments of molecules is a topic that has much promise. Future experiments studying resonance charge transfer from one polar molecule to another is an important next step in examining this special class of negative ions.

REFERENCES

1. H. Hotop and W. C. Lineberger, J. Phys. Chem. Ref. Data **14**, 735 (1985).
2. K. R. Lykke, K. K. Murray, and W. C. Lineberger, Phys. Rev. A **43**, 6104 (1991).
3. C. L. Pekeris, Phys. Rev. **126**, 1470 (1962).
4. C. E. Melton, *Principles of Mass Spectrometry and Negative Ions* (Marcel Dekker, New York, 1970).
5. H. S. W. Massey, *Negative Ions* (Cambridge University Press, London, 1976).
6. B. M. Smirnov, *Negative Ions* (McGraw-Hill, New York, 1982).
7. G. J. Schulz, Rev. Mod. Phys. **45**, 378 (1973).
8. G. J. Schulz, Rev. Mod. Phys. **45**, 423 (1973).
9. E. Fermi and E. Teller, Phys. Rev. **72**, 406 (1947).
10. A. S. Wightman, Phys. Rev. **77**, 521 (1949).
11. J. E. Turner and K. Fox, Phys. Rev. Lett. **23**, 547 (1966).
12. M. H. Mittleman and V. P. Meyerscough, Phys Lett. **23**, 545 (1966).
13. J. M. Levy-Leblond, Phys. Rev. **153**, 1 (1967).
14. W. B. Brown and R. E. Roberts, J. Chem. Phys. **46**, 2006 (1967).
15. J. E. Turner, Am. J. Phys. **45**, 758 (1977).
16. R. F. Wallis, R. Herman, and H. W. Milnes, J. Mol. Spectrosc. **4**, 51 (1960).
17. J. E. Turner, V.E. Anderson, and K. Fox, Phys. Rev. **174**, 81 (1968).
18. W. R. Garrett, Chem. Phys. Lett. **5**, 393 (1970).
19. W. R. Garrett, Phys. Rev. A **3**, 961 (1971).
20. O. H. Crawford, Mol. Phys. **20**, 585 (1971).
21. W. R. Garrett, Mol. Phys. **24**, 465 (1972).
22. O. H. Crawford and W. R. Garrett, J. Chem. Phys. **66**, 4968 (1977).
23. W. R. Garrett, J. Chem. Phys. **69**, 2621 (1978).
24. W. R. Garrett, Chem. Phys. Lett. **62**, 325 (1979).
25. W. R. Garrett, J. Chem. Phys. **71**, 651 (1979).
26. W. R. Garrett, J. Chem. Phys. **73**, 5721 (1980).
27. W. R. Garrett, J. Chem. Phys. **77**, 3666 (1982).
28. J. A. D. Stockdale, F. J. Davis, R. N. Compton, and C. E. Klots, J. Chem. Phys. **60**, 4279 (1974).
29. S. F. Wong and G. Schulz, Phys. Rev. Lett. **33**, 134 (1974).
30. K. Rohr and F. Linder, J. Phys. B **9**, 2521 (1976).
31. A. H. Zimmerman and J. I. Brauman, J. Chem. Phys. **66**, 5823 (1977).
32. R. L. Jackson, A. H. Zimmerman, and J. I. Brauman, J. Chem. Phys. **71**, 2088 (1979).
33. R. L. Jackson, P. C. Hiberty, and J. I. Brauman, J. Chem. Phys. **74**, 3705 (1981).
34. R. D. Mead, K. R. Lykke, W. C. Lineberger, J. Marks, and J. I. Brauman, J. Chem. Phys. **81**, 4883 (1984).
35. J. Marks, P. B. Comita, and J. I. Brauman, J. Am. Chem. Soc. **107**, 3718 (1985).
36. J. Marks, D. M. Wetzel, P. B. Comita, and J. I. Brauman, J. Chem. Phys. **84**, 5284 (1986).
37. E. A. Brinkman, S. Berger, J. Marks, and J. I. Brauman, J. Chem. Phys. **99**, 7586 (1993).
38. K. R. Lykke, R. D. Mead, and W. C. Lineberger, Phys. Rev. Lett. **52**, 2221

(1984).
39. K. R. Lykke, D. M. Neumark, T. Anderson, V. Trapa, and W. C. Lineberger, in *Laser Spectroscopy VII*, T. W. Hansch and Y. R. Shen, editors, (Springer, Berlin, 1985).
40. T. Anderson, K. R. Lykke, D. M. Neumark, and W. C. Lineberger, J. Chem. Phys. **87**, 1858 (1987).
41. K. R. Lykke, D. M. Neumark, T. Anderson, V. J. Trapa, and W. C. Lineberger, J. Chem. Phys. **87**, 6482 (1987).
42. J. Marks, J. I. Brauman, R. D. Mead, K. R. Lykke, and W. C. Lineberger, J. Chem. Phys. **88**, 6785 (1988).
43. A. S. Mullin, K. K. Murray, C. P. Schultz, D. M. Szaflarski, and W. C. Lineberger, Chem. Phys. **166**, 207 (1992).
44. A. S. Mullins, K. K. Murray, C. P. Schultz, and W. C. Lineberger, J. Phys. Chem. **97**, 10281 (1993).
45. K. D. Jordan and W. Luken, J. Chem. Phys. **64**, 2760 (1976).
46. K. D. Jordan, K. M. Griffing, J. Kenney, E. L. Anderson, and J. Simons, J. Chem. Phys. **64**, 4730 (1976).
47. K. D. Jordan, J. Chem. Phys. **66**, 3305 (1977).
48. K. D. Jordan and J. J. Wendoloski, Chem. Phys. **21**, 145 (1977).
49. K. D. Jordan, Acc. Chem. Res. **12**, 36 (1979).
50. K. D. Jordan and J. F. Liebman, Chem. Phys. Lett. **62**, 143 (1979).
51. R. W. Wetmore, H. F. Schaefer III, C. P. Hiberty, and J. I. Brauman, J. Am. Chem. Soc. **102**, 5470 (1980).
52. L. Adamowicz and E. A. McCullough, Chem. Phys. Lett. **107**, 72 (1984).
53. J. Simons and K. D. Jordan, Chem Rev. **87**, 535 (1987).
54. D. C. Clary, J. Phys. Chem. **92**, 3173 (1988).
55. J. V. Coe, G. H. Lee, J. G. Eaton, S. T. Arnold, H. W. Sarkas, K. H. Bowen, C. Ludewigt, H. Haberland, D. R. Worsnop, J. Chem. Phys. **92**, 3980 (1990).
56. C. Desfrançois, N. A. Khelifa, A. Lisfi, J. P. Schermann, J. G. Eaton, K. H. Bowen, J. Chem. Phys. **95**, 7760 (1991).
57. C. Desfrançois, B. Baillon, J. P. Schermann, S. T. Arnold, J. H. Hendricks, K. H. Bowen, Phys. Rev. Lett., **72**, 48 (1994).
58. J. H. Hendricks, S. A. Lyapustina, H. L. de Clercq, J. T. Snodgrass, and K. H. Bowen, J. Chem. Phys. **104**, 7788 (7788).
59. R. Hashemi, E. Illenberger, J. Phys. Chem. **95**, 6402 (1991).
60. C. Desfrançois, H. Abdoul-Carime, N. Khelifa, and J. P. Schermann, Phys. Rev. Lett. **73**, 2436 (1994).
61. C. E. H. Dessent, C. G. Bailey, and M. J. Johnson, Chem. Phys. **102**, 6335 (1995).
62. C. Desfrançois, H. Abdoul-Carime, N. Khelifa, J. P. Schermann, V. Brenner, and P. Millie, J. Chem. Phys. **102**, 4952 (1995).
63. C. Desfrançois, Phys. Rev. A **51**, 3667 (1995).
64. C. Desfrançois, H. Abdoul-Carime, and J. P. Schermann, J. Chem. Phys. **104**, 7792 (1996).
65. C. Desfrançois, H. Abdoul-Carime, and J. P. Schermann, Int. J., Mod. Phys. B

10, 1339 (1996).
66. R. N. Compton, H. S. Carman, Jr., C. Desfrançois, H. Abdoul-Carmine, J. P. Schermann, J. H. Hendricks, S. A. Lyapustina, and K. H. Bowen, J. Chem. Phys. **105**, 3472 (1996).
67. R. Abdoul-Carime, and C. Desfrançois, Eur. Phys. J. D **2**, 149 (1998).
68. C. Desfrançois, H. Abdoul-Carime, S. Carles, V. Périquet, J. P. Schermann, D. M. A. Smith, and L. Adamowicz, J. Chem. Phys. **110**, 11876 (1999).
69. C. Desfrançois, V. Périquet, S. A. Lyapustina, T. P. Lippa, D. W. Robinson, K. H. Bowen, H. Nonaka, and R. N. Compton, J. Chem. Phys. **111**, 4569 (1999).
70. G. H. Lee, S. T. Arnold, J. G. Eaton, and K. H. Bowen, Chem. Phys. Lett. **321**, 333 (2000).
71. S. Carles, C. Desfrançois, J. P. Schermann, J. Berges, and C. Houee-Levin, Int. J. Mass. Spec. **205**, 227 (2001).
72. S. Carles, C. Desfrançois, J. P. Schermann, A. F. Jalbout, and L. Adamowicz, Chem. Phys. Lett. **334**, 374 (2001).
73. R. N. Compton and N. I. Hammer, "Multipole-Bound Molecular Anions" in *Advances in Gas-Phase Ion Chemistry Volume 4*, edited by N. Adams and L. Babcock (Elsevier Science, 2001).
74. N. I. Hammer, F. Gao, R. M. Pagni, and R. N. Compton, "Charge Transfer Reactions between Chiral Rydberg Atoms and Chiral Molecules," J. Chem. Phys. **117**, 4299 (2002).
75. N. I. Hammer, K. Diri, K. D. Jordan, C. Desfrançois, and R. N. Compton, "Dipole-Bound Anions of Carbonyl, Nitrile, and Sulfoxide Containing Molecules," to be published.
76. N. I. Hammer, K. Diri, K. D. Jordan, D. Radisic, K. H. Bowen, and R. N. Compton, "Dipole-Bound Anions of Highly Polar Molecules: Ethylene Carbonate and Vinylene Carbonate," to be published.
77. C. Desfrançois, V. Périquet, Y. Bouteiller, L. Adamowicz, K.H. Bowen, J.P. Schermann, N.I. Hammer, and R.N. Compton, "Electron Binding to Quadrupolar Molecules: Succinonitrile," to be published.
78. G. L. Gutsev, A. L. Sobolewski, and L. Adamowicz, Chem. Phys. **196**, 1 (1995).
79. G. L. Gutsev and L. Adamowicz, Chem. Phys. Lett. **235**, 377 (1995).
80. G. L. Gutsev and L. Adamowicz, J. Phys. Chem. **99**, 13412 (1995).
81. G. L. Gutsev and R. J. Bartlett, J. Chem. Phys. **105**, 8785 (1996).
82. T. Sommerfeld, Phys. Chem. Chem. Phys. **4**, 2511 (2002).
83. R. Ramaekers, D. M. A. Smith, J. Smets, and L. Adamowicz, J. Chem. Phys. **107**, 9475 (1997).
84. G. L. Gutsev, M. Nooijen, and R. J. Bartlett, Phys. Rev. A. **57**, 1646 (1998).
85. D. M. A. Smith, J. Smets, Y. Elkadi, and L. Adamowicz, Chem. Phys. Lett. **305**, 169 (1999).
86. H. Chen and W. Sheua, J. Chem. Phys. **110**, 9032 (1999)
87. G. L. Gutsev, P. Jena, and R. J. Bartlett, J. Chem. Phys. **111**, 504 (1999).
88. P. Skurski, M. Gutowski, and J. Simons, J. Chem. Phys. **111**, 9469 (1999).
89. P. Skurski and J. Simons, J. Chem. Phys. **112**, 6563 (2000).

90. M. Gutowski, P. Skurski, and J. Simons, J. Am. Chem. Soc. **122**, 10159 (2000).
91. P. Skurski, M. Gutowski, and J. Simons, Chem. Phys. Lett. **322**, 175 (2000).
92. M. Gutowski, P. Skurski, and J. Simons, Int. J. Mass. Spec. **201**, 245 (2000).
93. P. Skurski, M. Gutowski, and J. Simons, Int. J. Quan. Chem. **76**, 197 (2000).
94. P. Skurski, M. Gutowski, and J. Simons, Int. J. Quan. Chem. **80**, 1024 (2000).
95. P. Skurski and J. Simons, J. Chem. Phys. **115**, 8373 (2001).
96. P. Skurski and J. Simons, J. Chem. Phys. **115**, 10731 (2001).
97. P. Skurski and J. Simons, J. Chem. Phys. **116**, 6118 (2002).
98. F. Wang and K. D. Jordan, J. Chem. Phys. **114**, 10717 (2001).
99. F. Wang and K. D. Jordan, J. Chem. Phys. **116**, 6973 (2002).
100. K. D. Jordan and F. Wang, Annu. Rev. Phys. Chem. **54**, 367 (2003).
101. Moore, C. E. Atomic *Energy Levels*, National Bureau of Standards, 1952.
102. W. L. Fite, "Expansion of Gases from Molecular Beam Sources," *Research Note #1*, (Extranuclear Laboratories, Inc., 1971).
103. J. E. Mathis, "High Resolution Multi- and Single-Photon Electron Spectroscopy Using a Hemispherical Electron Spectrometer with Position-Sensitive Detection," Ph. D. Dissertation, (University of Tennessee, 1995).
104. N. I. Hammer and R. N. Compton, "Effects of Electric Fields and Collisions on Highly Excited Rubidium Atoms," Eur. Phys. J. D, in press.
105. R. N. Compton, in *The Role of Rydberg States in Spectroscopy and Photochemistry*, edited by C. Sandorfy (Kluwer Academic Publishers, 1999).
106. S. H. Lin, Y. Fujimura, H. J. Neusser, and E. W. Schlag, *Multiphoton Spectroscopy of Molecules* (Academic Press, London, 1984).
107. F. H. M. Faisal, *Theory of Multiphoton Processes* (Plenum Press, New York, 1987).
108. *Multiphoton Ionization of Atoms*, edited by S. L. Chin and P. Lambropoulos (Academic Press, Toronto, 1984).
109. P. Lambropoulos, "Topics on Multiphoton Processes in Atoms" in *Advances in Atomic and Molecular Physics*, edited by D. R. Bates and B. Bederson (Academic Press, New York, 1976).
110. N. I. Hammer and R. N. Compton, "Effects of dc Electric Fields on Multiphoton Ionization of Rubidium Atoms at Low and High Densities" in *Tenth International Symposium on RIS Proceedings*, edited by J. Parks and J. Young, (American Institute of Physics, 2001).
111. K. P. Huber and G. Herzberg, *Molecular Spectra and Molecular Structure IV: Constants of Diatomic Molecules*, (Van Nostrand Reinhold Company, New York, 1979).
112. W. Christian, R. N. Compton, J. A. D. Stockdale, J. C. Miller, C. D. Cooper, X. Tang, and P. Lambropoulos, Phys. Rev. A, **30**, 1775 (1984).
113. R. F. Stebbings and F. B. Dunning, *Rydberg States of Atoms and Molecules*, (Cambridge Press, 1983).
114. I. L. Beigman and V. S. Lebedev¸ Phys. Rep. **250**, 95 (1995).
115. B. L. Feringa and R. A. van Delden, Angew. Chem. Int. Ed. **38**, 3418 (1977).
116. W.A. Bonner, Origin of Life **21**, 59 (1996).
117. H. Rau, Chem. Rev. **83**, 535 (1983).

118. G. Balavoine, A. Moradpour and H.B. Kagan, J. Am. Chem. Soc. **96**, 5152 (1974).
119. P. Frank, W. A. Bonner and R. N. Zare, *On One Hand But Not The Other: The Challenge of the Origin and Survival of Homochirality in Prebiotic Chemistry for the 21st Century*, edited by E. Keinan and I. Schechter (Wiley-VCH, Weinheim, Germany, 2000).
120. R.N. Compton and R.M. Pagni, in *Advances in Atomic, Molecular and Optical Physics*, B. Bederson, Ed. (Elsevier Science, New York, 2002).
121. *Asymmetric Synthesis* Edited by J.D. Morrison, (Academic, New York, 1985).
122. L. D. Barron, Mol. Phys. **43**, 1395 (1981).
123. L. D. Barron Chem. Phys. Lett. **123**, 423 (1986).
124. L. D. Barron J. Am. Chem.Soc. **108**, 5339 (1986).
125. L. E. Cuellar, C. S. Feigerle, H. S. Carman, R. N. Compton, Phys. Rev. A, **43**, 6432 (1991).
126. C. S. Feigerle, R. N. Compton, L. E. Cuellar, N. A. Cherepkov, L. V. Chernyshera, Phys. Rev. A, **53** 4183 (1996).
127. S. A. Harris and P. R. Brooks, J. Chem. Phys. **114**, 10569 (2001).
128. *Handbook of Chemistry and Physics*, 74th Edition, edited by D. R. Lide (CRC, Boca Raton, 1994).
129. J. Randall, J. A. Hardy, and A. P. Cox, J. Chem. Soc., Faraday Trans. 2, **84**, 1199, (1988).
130. O. L. Stiefvater, Z. Naturforsch, **41a**, 783, (1986).
131. P. Ausloos and S. G. Lias, J. Am. Chem. Soc. **103**, 3641 (1981).
132. Y.S. Li, J. Mol. Spec. **104**, 302 (1984).
133. J. E. Lee, M. K. Ahn, and J. J. Oh, Bull. Korean Chem. Soc. **20**,1506 (1999).
134. G. R. Slayton, J. W. Simmons, and J. H. Goldstein J. Chem. Phys. **22**, 1678 (1954).
135. A. H. Saadi and W. H. Lee J. Chem. Soc. *(B)* **1**, 5 (1966).
136. K. L. Dorris, C. O. Britt, and J. E. Boggs J. Chem. Phys. **44**, 1352 (1966).
137. J. L. Alonso, R. Cervellati, A. D. Esposti, D. G. Lister, and P. Palmieri, J. Chem. Soc., Faraday Trans. 2 **82**, 357 (1986).
138. M. J. Frisch, G. W. Trucks, H. B. Schlegel *et al.*, *Gaussian 98,* Gaussian, Inc., Pittsburgh PA, 1998.
139. *PC Model for Windows Version 7.00*, Serena Software, 1998.
140. *Hyperchem Pro,* Version 5.1.
141. J. J. Gajewski, K. E. Gilbert, and J. Mc Kelvey, "MMX: An Enhanced Version of MM2" in *Advances in Molecular Modeling,* edited by D. Liotta, (JAI Press, Greenwich, CT, 1990)
142. K. Machida, *Principles of Molecular Mechanics* (Kodansha, Tokyo and Wiley, New York, 1999).
143. N. L. Allinger, J. Am. Chem. Soc. **99**, 8127 (1977).
144. A. Szabo and N. S. Ostlund, *Modern Quantum Chemistry: Introduction to Advanced Electronic Structure Theory* (Dover, Mineola, New York, 1996).
145. T. H. Dunning, Jr., J. Chem. Phys. **90**, 1007 (1989).
146. C. Møller and M. S. Plesset, *Phys. Rev.* **46**, 618 (1934).

147. M. Head-Gordon, J. A. Pople and M. J. Frisch, *Chem. Phys. Lett.* **153**, 503 (1988).
148. K. J. Miller and J. Savchik, J. Am. Chem. Soc. **101**, 7206 (1979).
149. L. Laaksonen, *gOpenMol* version 2.20, 1997-2002.
150. P. Van Nuffel, L. Van Den Enden, and C. Van Alsenoy, J. Mol. Spec. **116**, 99 (1984).
151. D. Kim and T. Baer, Chem. Phys. **256**, 251 (2000).
152. A. R. Potts and T. Baer, J. Chem. Phys. **105**, 7605 (1996).
153. J. P. Guillory and L. S. Bartell, J. Chem. Phys. **43**, 654 (1965).
154. G. F. Metha, M. A. Buntine, A. J. Bradley, and R. J. S. Morrison, J. Mol. Spec. **206**, 73 (2001).
155. C. H. Langley, J Lii, and N. L. Allinger, J. Comp. Chem. **22**, 1396 (2001).
156. N. L. Allinger, H. M. Blattner, L. A. Frieberg, and F. J. Karkowski, J. Am. Chem. Soc. **88**, 2999 (1966).
157. T. Nakamura and S. J. l'Haya, Bull. Chem. Soc. Japan **49**, 3461 (1976).
158. N. Hammer, M. Pederson, and R. Compton, "Dipole-Bound Anions of Acetone and Perdeuterated Acetone," to be published.
159. R. N. Compton, P.W. Reinhardt, and H. C. Schweinler, Int. J. Mass Spec. Ion Phys. **49**, 113 (1983).
160. M. Stephanovic, Y. Pariat, and M. Allan, J. Chem. Phys. **110**, 11376 (1999).
161. J. M. Younkin, L. J. Smith, and R. N. Compton, Theor. Chim. Acta **41,** 157 (1976).
162. R. N. Compton, Y. Yoshiko, and K. D. Jordan, Theor. Chim. Acta **54**, 259 (1980).
163. M. Gutowski, P. Skurski, A. I. Boldyrev, J. Simons, and K. D. Jordan, Phys Rev. A **54**, 1906 (1996).
164. M. Gutowski, K. D. Jordan, P. Skurski, J. Phys. Chem. A. **102**, 2624 (1998).
165. K. Yokoyama, G. W. Leach, J. B. Kim, W. C. Lineberger, A. I. Boldyrev, M. Gutowski, J. Chem. Phys. **105**, 10706 (1996).
166. M. Gutowski and P. Skurski, Recent Res. Dev. Phys. Chem. **3**, 245 (1999).
167. M. Gutowski and P. Skurski, Chem. Phys. Lett. **300**, 331 (1999).
168. L. Adamowicz, J. Chem. Phys. **91**, 7787 (1989).
169. L. Adamowicz and E. A. McCullough, J. Phys. Chem. **88**, 2045 (1984).
170. C. Desfrançois, V. Périquet, S. Carles, J. P. Schermann, D. M. A. Smith, and L. Adamowicz, J. Chem. Phys. **110**, 4309 (1999).
171. M. Gutowski and P. Skurski, Chem. Phys. Lett. **65**, 303 (1999).
172. M. Gutowski, P. Skurski, Xi Li, and L. S. Wang, Phys. Rev. Lett. **85**, 3145 (2000).
173. M. V. N. Prasad, R. F. Wallis, and R. Herman, Phys. Rev. B, **40**, 5924 (1989).
174. M. V. N. Prasad, R. F. Wallis, and R. Herman, Sol. State Comm. **77**, 973 (1991).
175. R. N. Compton, F.B. Dunning, and P. Nordlander, Chem. Phys. Lett. **253**, 8 (1996).
176. G. Gutsev, R. J. Bartlett, and R. N. Compton, J. Chem. Phys. **108**, 6756 (1998).
177. Q. B. Lu and L. Sanche, Phys. Rev. B **63**, 63 (2001).
178. Q. B. Lu and L. Sanche, J. Chem. Phys. **115**, 5711 (2001).

179. H. Abdoul-Carime and L. Sanche, Int. J. Radiat. Biol. **78**, 89 (2001).
180. H. Abdoul-Carime, S. Cecchini, and L. Sanche, Rad. Res. **158**, 23 (2002).
181. F. Güthe, M. Tulej, M. V. Pachkov, and J. P. Maier, The Astrophys. J. **555**, 466 (2001).

APPENDICES

APPENDIX A: OPTIMIZED AND ENERGY MINIMIZED Z-MATRICES

acetaldehyde
MP2/aug-cc-pVDZ

C
C,1,R2
H,1,R3,2,A3
H,1,R4,2,A4,3,D4,0
H,1,R5,2,A5,3,D5,0
O,2,R6,1,A6,3,D6,0
H,2,R7,1,A7,6,D7,0
Variables:
R2=1.507886
R3=1.09802728
R4=1.10292738
R5=1.10292411
R6=1.22599656
R7=1.11663344
A3=110.62926769
A4=109.22058954
A5=109.22045947
A6=124.40601087
A7=115.70366519
D4=-121.63582927
D5=121.63512294
D6=-0.00670546
D7=-179.99103359

acetaldehyde
MP2/aug-cc-pVTZ

C
C,1,R2
H,1,R3,2,A3
H,1,R4,2,A4,3,D4,0
H,1,R5,2,A5,3,D5,0
O,2,R6,1,A6,3,D6,0
H,2,R7,1,A7,6,D7,0
Variables:
R2=1.49785937
R3=1.09109803
R4=1.09112428
R5=1.08603325
R6=1.21533679
R7=1.10538315
A3=109.2908759
A4=109.2711274
A5=110.65450644
A6=124.44265039
A7=115.56703753
D4=-116.76172084
D5=121.63524031
D6=-121.73873674
D7=-179.99044269

cis-propanal
MP2/aug-cc-pVDZ

C
C,1,R2
C,1,R3,2,A3
H,1,R4,2,A4,3,D4,0
H,1,R5,2,A5,3,D5,0
O,2,R6,1,A6,3,D6,0
H,2,R7,1,A7,6,D7,0
H,3,R8,1,A8,2,D8,0
H,3,R9,1,A9,8,D9,0
H,3,R10,1,A10,8,D10,0
Variables:
R2=1.51203938
R3=1.52789976
R4=1.10616238
R5=1.1061628
R6=1.22628353
R7=1.11721813
R8=1.10015599
R9=1.09992108
R10=1.09992273
A3=113.75361554
A4=106.80996733
A5=106.80774193
A6=124.4024488
A7=115.52949604
A8=110.57517735
A9=110.69987971
A10=110.69975829
D4=-123.89194049
D5=123.88947047
D6=0.
D7=-179.99219244
D8=179.99717472
D9=-120.42285223
D10=120.42324987

cis-propanal
MP2/aug-cc-pVTZ

C
C,1,R2
C,1,R3,2,A3
H,1,R4,2,A4,3,D4,0
H,1,R5,2,A5,3,D5,0
O,2,R6,1,A6,3,D6,0
H,2,R7,1,A7,6,D7,0
H,3,R8,1,A8,2,D8,0
H,3,R9,1,A9,8,D9,0
H,3,R10,1,A10,8,D10,0
Variables:
R2=1.50179412
R3=1.51790645
R4=1.09466451
R5=1.09466476
R6=1.2156481
R7=1.10593164
R8=1.08819883
R9=1.08818641
R10=1.08818659
A3=113.57834822
A4=106.87724871
A5=106.87614435
A6=124.42063292
A7=115.40039882
A8=110.66515922
A9=110.67079232
A10=110.67079596
D4=-123.88353653
D5=123.88237412
D6=-0.00013855
D7=-179.9916339
D8=179.99820999
D9=-120.50740573
D10=120.50792752

gauche-propanal
MP2/aug-cc-pVDZ

C
C,1,R2
C,1,R3,2,A3
H,1,R4,2,A4,3,D4,0
H,1,R5,2,A5,3,D5,0
O,2,R6,1,A6,3,D6,0
H,2,R7,1,A7,6,D7,0
H,3,R8,1,A8,2,D8,0
H,3,R9,1,A9,8,D9,0
H,3,R10,1,A10,8,D10,0
Variables:
R2=1.5105051
R3=1.54008815
R4=1.10477828
R5=1.10006455
R6=1.22645989
R7=1.11864264
R8=1.09993156
R9=1.10099123
R10=1.10196895
A3=110.14087069
A4=107.86426931
A5=108.75526075
A6=124.79125409
A7=115.2964043
A8=110.64360922
A9=110.71154482
A10=111.12168501
D4=-119.4198953
D5=122.5750229
D6=-117.07582533
D7=178.56640995
D8=-176.74059809
D9=-119.95881801
D10=119.79714184

gauche-propanal
MP2/aug-cc-pVTZ

C
C,1,R2
C,1,R3,2,A3
H,1,R4,2,A4,3,D4,0
H,1,R5,2,A5,3,D5,0
O,2,R6,1,A6,3,D6,0
H,2,R7,1,A7,6,D7,0
H,3,R8,1,A8,2,D8,0
H,3,R9,1,A9,8,D9,0
H,3,R10,1,A10,8,D10,0
Variables:
R2=1.5002831
R3=1.53003768
R4=1.09331557
R5=1.08839915
R6=1.21551713
R7=1.10787428
R8=1.08801433
R9=1.08906413
R10=1.09014476
A3=110.22638397
A4=107.68630179
A5=108.84080046
A6=124.97584347
A7=114.93971181
A8=110.68364479
A9=110.74688365
A10=111.0393679
D4=-119.32467778
D5=122.95745534
D6=-119.81509384
D7=178.72663147
D8=-176.07275749
D9=-120.03883096
D10=119.81037366

acetone
MP2/aug-cc-pVDZ

C
C,1,R2
H,1,R3,2,A3
H,1,R4,2,A4,3,D4,0
H,1,R5,2,A5,3,D5,0
C,2,R6,1,A6,3,D6,0
O,2,R7,1,A7,6,D7,0
H,6,R8,2,A8,1,D8,0
H,6,R9,2,A9,8,D9,0
H,6,R10,2,A10,8,D10,0
Variables:
R2=1.51823292
R3=1.09726016
R4=1.10266655
R5=1.10267066
R6=1.51823112
R7=1.23075908
R8=1.09726105
R9=1.10266618
R10=1.10267006
A3=110.01043877
A4=109.87075726
A5=109.86760196
A6=116.54574944
A7=121.72746001
A8=110.0107743
A9=109.87022769
A10=109.86851337
D4=-121.198534
D5=121.19559327
D6=179.98806072
D7=179.99634182
D8=-179.99275404
D9=121.19826284
D10=-121.19549595

acetone
MP2/aug-cc-pVTZ

C
C,1,R2
H,1,R3,2,A3
H,1,R4,2,A4,3,D4,0
H,1,R5,2,A5,3,D5,0
C,2,R6,1,A6,3,D6,0
O,2,R7,1,A7,6,D7,0
H,6,R8,2,A8,1,D8,0
H,6,R9,2,A9,8,D9,0
H,6,R10,2,A10,8,D10,0
Variables:
R2=1.50873795
R3=1.0855686
R4=1.09075549
R5=1.09075809
R6=1.50874081
R7=1.21971091
R8=1.08556833
R9=1.09075566
R10=1.09075823
A3=110.05868731
A4=109.83918833
A5=109.83552023
A6=116.2535531
A7=121.87298612
A8=110.05869577
A9=109.83806073
A10=109.83568566
D4=-121.24034459
D5=121.23732386
D6=179.9765292
D7=-179.98983612
D8=-179.99429914
D9=121.24030052
D10=-121.23668234

cyclobutanone
MP2/aug-cc-pVDZ

C
C,1,R2
C,1,R3,2,A3
O,1,R4,2,A4,3,D4,0
C,2,R5,1,A5,3,D5,0
H,2,R6,1,A6,5,D6,0
H,2,R7,1,A7,5,D7,0
H,3,R8,1,A8,2,D8,0
H,3,R9,1,A9,8,D9,0
H,5,R10,2,A10,1,D10,0
H,5,R11,2,A11,10,D11,0
Variables:
R2=1.5427322
R3=1.54273635
R4=1.21600884
R5=1.56557499
R6=1.10122213
R7=1.10122231
R8=1.10122151
R9=1.1012219
R10=1.09807615
R11=1.09807555
A3=92.77609814
A4=133.61194854
A5=88.09447023
A6=113.26537934
A7=113.2656065
A8=113.26583249
A9=113.26466733
A10=113.97150165
A11=113.97082951
D4=180.
D5=0.00173328
D6=-117.63541752
D7=117.63574965
D8=-117.63782668
D9=-124.72919877
D10=-116.92137675
D11=-126.16137918

cyclobutanone
MP2/aug-cc-pVTZ

C
C,1,R2
C,1,R3,2,A3
O,1,R4,2,A4,3,D4,0
C,2,R5,1,A5,3,D5,0
H,2,R6,1,A6,5,D6,0
H,2,R7,1,A7,5,D7,0
H,3,R8,1,A8,2,D8,0
H,3,R9,1,A9,8,D9,0
H,5,R10,2,A10,1,D10,0
H,5,R11,2,A11,10,D11,0
Variables:
R2=1.5316463
R3=1.53164676
R4=1.2055898
R5=1.55456021
R6=1.08935163
R7=1.08935119
R8=1.08935098
R9=1.08935169
R10=1.08617075
R11=1.08617099
A3=92.77247294
A4=133.61377033
A5=88.10689722
A6=113.28679032
A7=113.2868742
A8=113.28708055
A9=113.28652233
A10=113.98422216
A11=113.98390094
D4=179.99302316
D5=0.0047029
D6=-117.61432789
D7=117.61512727
D8=-117.62005357
D9=-124.77060662
D10=-116.93069821
D11=-126.14822341

gauche-2-methylpropanal
MP2/aug-cc-pVDZ

C
C,1,R2
H,1,R3,2,A3
H,1,R4,2,A4,3,D4,0
H,1,R5,2,A5,3,D5,0
C,2,R6,1,A6,3,D6,0
C,2,R7,1,A7,6,D7,0
H,2,R8,1,A8,6,D8,0
O,6,R9,2,A9,1,D9,0
H,6,R10,2,A10,9,D10,0
H,7,R11,2,A11,1,D11,0
H,7,R12,2,A12,11,D12,0
H,7,R13,2,A13,11,D13,0
Variables:
R2=1.54128618
R3=1.10214878
R4=1.10077548
R5=1.10242032
R6=1.51611989
R7=1.52820852
R8=1.10809947
R9=1.22610788
R10=1.11886924
R11=1.10117938
R12=1.10107993
R13=1.10000735
A3=111.6945478
A4=110.29796604
A5=110.25607842
A6=108.34968829
A7=112.43109464
A8=107.73781802
A9=124.93673428
A10=115.00956586
A11=110.26574837
A12=110.32559072
A13=111.26542582
D4=-120.07400694
D5=120.46297012
D6=-54.05586155
D7=-124.54034044
D8=113.8110825
D9=-121.11403851
D10=178.98641253
D11=-59.42404738
D12=119.9126349
D13=-120.71308012

trans-2-methylpropanal
MP2/aug-cc-pVDZ

C
C,1,R2
H,1,R3,2,A3
H,1,R4,2,A4,3,D4,0
H,1,R5,2,A5,3,D5,0
C,2,R6,1,A6,3,D6,0
C,2,R7,1,A7,6,D7,0
H,2,R8,1,A8,6,D8,0
O,6,R9,2,A9,1,D9,0
H,6,R10,2,A10,9,D10,0
H,7,R11,2,A11,1,D11,0
H,7,R12,2,A12,11,D12,0
H,7,R13,2,A13,11,D13,0
Variables:
R2=1.53826044
R3=1.10123968
R4=1.10331864
R5=1.10147167
R6=1.51363654
R7=1.53824725
R8=1.10198103
R9=1.22610842
R10=1.12088382
R11=1.10331953
R12=1.1014713
R13=1.10123905
A3=111.45599402
A4=110.66239974
A5=110.19455204
A6=108.89590366
A7=111.04618247
A8=110.27575509
A9=125.2723606
A10=114.67928681
A11=110.66328861
A12=110.19314374
A13=111.45588087
D4=120.5914102
D5=-120.24221461
D6=-61.67378677
D7=-119.90174446
D8=117.55208444
D9=119.39743505
D10=179.99572461
D11=60.98451214
D12=-119.16627538
D13=120.59196098

trans-2-methylpropanal
MP2/aug-cc-pVTZ

C
C,1,R2
H,1,R3,2,A3
H,1,R4,2,A4,3,D4,0
H,1,R5,2,A5,3,D5,0
C,2,R6,1,A6,3,D6,0
C,2,R7,1,A7,6,D7,0
H,2,R8,1,A8,6,D8,0
O,6,R9,2,A9,1,D9,0
H,6,R10,2,A10,9,D10,0
H,7,R11,2,A11,1,D11,0
H,7,R12,2,A12,11,D12,0
H,7,R13,2,A13,11,D13,0
Variables:
R2=1.52846158
R3=1.08953001
R4=1.09179571
R5=1.08972396
R6=1.50323823
R7=1.52846344
R8=1.09055527
R9=1.2151579
R10=1.11033341
R11=1.09179581
R12=1.08972404
R13=1.08952988
A3=111.49694974
A4=110.55571685
A5=110.12711742
A6=108.82576998
A7=110.81115365
A8=110.38757265
A9=125.50184085
A10=114.25613724
A11=110.55569401
A12=110.12715462
A13=111.49683602
D4=120.56713693
D5=-120.38390648
D6=-61.99001079
D7=-119.62355338
D8=117.77139504
D9=119.57938155
D10=179.99459625
D11=61.04685586
D12=-119.04896087
D13=120.56709613

cis/gauche-butanal
MP2/aug-cc-pVDZ

C
C,1,R2
O,1,R3,2,A3
H,1,R4,2,A4,3,D4,0
C,2,R5,1,A5,3,D5,0
H,2,R6,1,A6,5,D6,0
H,2,R7,1,A7,5,D7,0
C,5,R8,2,A8,1,D8,0
H,5,R9,2,A9,8,D9,0
H,5,R10,2,A10,8,D10,0
H,8,R11,5,A11,2,D11,0
H,8,R12,5,A12,11,D12,0
H,8,R13,5,A13,11,D13,0
Variables:
R2=1.51362825
R3=1.22650246
R4=1.11724285
R5=1.53087353
R6=1.1066322
R7=1.10745962
R8=1.53411543
R9=1.10196049
R10=1.1026271
R11=1.10107934
R12=1.10299229
R13=1.10021476
A3=124.57698262
A4=115.43839099
A5=114.28738285
A6=107.57960037
A7=105.77875652
A8=112.27713416
A9=108.87671041
A10=108.74925684
A11=111.05179823
A12=110.70282818
A13=110.88629975
D4=178.8084182
D5=8.10425203
D6=124.51161328
D7=-123.30753175
D8=71.27916518
D9=-121.82798161
D10=121.6283154
D11=179.38484617
D12=-119.64566518
D13=119.99950702

cis/trans-butanal
MP2/aug-cc-pVDZ

C
C,1,R2
H,1,R3,2,A3
H,1,R4,2,A4,3,D4,0
H,1,R5,2,A5,3,D5,0
C,2,R6,1,A6,3,D6,0
H,2,R7,1,A7,6,D7,0
H,2,R8,1,A8,6,D8,0
C,6,R9,2,A9,1,D9,0
H,6,R10,2,A10,9,D10,0
H,6,R11,2,A11,9,D11,0
O,9,R12,6,A12,2,D12,0
H,9,R13,6,A13,12,D13,0
Variables:
R2=1.53275359
R3=1.10097101
R4=1.10211925
R5=1.10183326
R6=1.54156305
R7=1.10333549
R8=1.10429401
R9=1.50936035
R10=1.10116138
R11=1.10566125
R12=1.22683127
R13=1.11819098
A3=111.18825889
A4=110.80836943
A5=110.78488381
A6=111.87123047
A7=109.99306954
A8=109.72668954
A9=110.18983703
A10=110.93268446
A11=109.09136917
A12=124.63124196
A13=115.44012347
D4=120.13893921
D5=-120.07757354
D6=179.34727099
D7=-121.09416071
D8=121.6698863
D9=176.99474504
D10=120.80000632
D11=-118.99324017
D12=111.41182978
D13=-178.00388985

2-butanone
MP2/aug-cc-pVDZ

C
C,1,R2
H,1,R3,2,A3
H,1,R4,2,A4,3,D4,0
H,1,R5,2,A5,3,D5,0
C,2,R6,1,A6,3,D6,0
H,2,R7,1,A7,6,D7,0
H,2,R8,1,A8,6,D8,0
C,6,R9,2,A9,1,D9,0
O,6,R10,2,A10,9,D10,0
H,9,R11,6,A11,2,D11,0
H,9,R12,6,A12,11,D12,0
H,9,R13,6,A13,11,D13,0
Variables:
R2=1.52783495
R3=1.10050513
R4=1.09976435
R5=1.09976571
R6=1.52287758
R7=1.1055117
R8=1.1055115
R9=1.51856732
R10=1.23104526
R11=1.10257364
R12=1.09739371
R13=1.10257567
A3=110.54944859
A4=110.68654427
A5=110.6859622
A6=113.43800575
A7=111.35083829
A8=111.35027326
A9=116.48051928
A10=121.78845368
A11=109.9089846
A12=109.93605915
A13=109.90729023
D4=120.45176487
D5=-120.4514927
D6=-179.99969708
D7=-121.33455027
D8=121.33160473
D9=-179.9965124
D10=179.99073756
D11=58.8581088
D12=121.12801468
D13=-117.74553042

cyclopentanone
MP2/aug-cc-pVDZ

O
C,1,R2
C,2,R3,1,A3
C,2,R4,1,A4,3,D4,0
C,3,R5,2,A5,1,D5,0
C,4,R6,2,A6,1,D6,0
H,3,R7,2,A7,5,D7,0
H,3,R8,2,A8,5,D8,0
H,4,R9,2,A9,6,D9,0
H,4,R10,2,A10,6,D10,0
H,5,R11,3,A11,2,D11,0
H,5,R12,3,A12,11,D12,0
H,6,R13,4,A13,2,D13,0
H,6,R14,4,A14,13,D14,0
Variables:
R2=1.22516881
R3=1.53359584
R4=1.53358688
R5=1.53889815
R6=1.53890689
R7=1.0995782
R8=1.1054097
R9=1.09957866
R10=1.10540911
R11=1.10010254
R12=1.10373849
R13=1.10010191
R14=1.10373602
A3=125.75082898
A4=125.75022293
A5=104.2276541
A6=104.22791417
A7=110.81412411
A8=106.98499678
A9=110.81349764
A10=106.98682901
A11=113.37858941
A12=109.86889771
A13=113.37807532
A14=109.86916277
D4=-179.98873143
D5=-167.33703202
D6=-167.35513609
D7=125.35450608
D8=-117.37165364
D9=125.35368602
D10=-117.37250248
D11=-155.37225421
D12=-120.78938538
D13=-155.37146961
D14=-120.79008339

pivalaldehyde
MP2/aug-cc-pVDZ

C
C,1,R2
H,1,R3,2,A3
H,1,R4,2,A4,3,D4,0
H,1,R5,2,A5,3,D5,0
C,2,R6,1,A6,3,D6,0
C,2,R7,1,A7,6,D7,0
C,2,R8,1,A8,6,D8,0
O,6,R9,2,A9,1,D9,0
H,6,R10,2,A10,9,D10,0
H,7,R11,2,A11,1,D11,0
H,7,R12,2,A12,11,D12,0
H,7,R13,2,A13,11,D13,0
H,8,R14,2,A14,1,D14,0
H,8,R15,2,A15,14,D15,0
H,8,R16,2,A16,14,D16,0
Variables:
R2=1.54122032
R3=1.10246099
R4=1.10307815
R5=1.10220515
R6=1.52078306
R7=1.52986496
R8=1.54118666
R9=1.22556616
R10=1.12074976
R11=1.10222971
R12=1.10077609
R13=1.10078125
R14=1.10245837
R15=1.10220885
R16=1.10307873
A3=109.72764669
A4=111.33967746
A5=111.09141169
A6=107.0906928
A7=111.08592402
A8=109.44387549
A9=125.48802787
A10=114.43740469
A11=109.85529608
A12=110.92848199
A13=110.92795456
A14=109.72929883
A15=111.09258218
A16=111.33817125
D4=119.40514305
D5=-119.71535132
D6=-175.64725114
D7=-121.20137445
D8=115.76870939
D9=-121.29609613
D10=179.9975844
D11=-61.03664371
D12=120.18829251
D13=-120.18599412
D14=59.88824683
D15=119.71590621
D16=-119.40520328

2-ethylbutanal
MP2/aug-cc-pVDZ

C
C,1,R2
H,1,R3,2,A3
H,1,R4,2,A4,3,D4,0
H,1,R5,2,A5,3,D5,0
C,2,R6,1,A6,3,D6,0
H,2,R7,1,A7,6,D7,0
H,2,R8,1,A8,6,D8,0
C,6,R9,2,A9,1,D9,0
C,6,R10,2,A10,9,D10,0
H,6,R11,2,A11,9,D11,0
C,9,R12,6,A12,2,D12,0
O,10,R13,6,A13,2,D13,0
H,9,R14,6,A14,12,D14,0
H,9,R15,6,A15,12,D15,0
H,10,R16,6,A16,13,D16,0
H,12,R17,9,A17,6,D17,0
H,12,R18,9,A18,17,D18,0
H,12,R19,9,A19,17,D19,0
Variables:
R2=1.53372377
R3=1.10110655
R4=1.10095565
R5=1.10280719
R6=1.53387823
R7=1.10396371
R8=1.10233385
R9=1.54827028
R10=1.5193855
R11=1.10777828
R12=1.53512
R13=1.22793089
R14=1.10359213
R15=1.10422033
R16=1.11596104
R17=1.10098211
R18=1.10248854
R19=1.10130718
A3=111.04754607
A4=111.02093897
A5=110.81634588
A6=112.90917762
A7=109.83032722
A8=109.97063205
A9=111.34987029
A10=111.77431726
A11=110.03699962
A12=114.31445465
A13=123.7382574
A14=107.61943848
A15=107.99979392
A16=116.55860952
A17=110.65618641
A18=110.90228591
A19=111.85649507
D4=119.78120427
D5=-119.76788323
D6=178.18558065
D7=-120.81829864
D8=121.37687214
D9=-173.392199
D10=-121.01302694
D11=119.73805578
D12=177.54633945
D13=30.27344228
D14=-121.91525984
D15=122.9318601
D16=177.80836231
D17=-174.91897865
D18=119.59940644
D19=-119.70346992

2-methylcyclopentanone
(axial methyl group)
MP2/aug-cc-pVDZ

O
C,1,R2
C,2,R3,1,A3
C,2,R4,1,A4,3,D4,0
C,3,R5,2,A5,1,D5,0
C,4,R6,2,A6,1,D6,0
C,4,R7,2,A7,6,D7,0
H,3,R8,2,A8,5,D8,0
H,3,R9,2,A9,5,D9,0
H,4,R10,2,A10,6,D10,0
H,5,R11,3,A11,2,D11,0
H,5,R12,3,A12,11,D12,0
H,6,R13,4,A13,2,D13,0
H,6,R14,4,A14,13,D14,0
H,7,R15,4,A15,2,D15,0
H,7,R16,4,A16,15,D16,0
H,7,R17,4,A17,15,D17,0
Variables:
R2=1.22614499
R3=1.53190052
R4=1.53629668
R5=1.53909963
R6=1.5424338
R7=1.54015107
R8=1.10577906
R9=1.09957325
R10=1.10199008
R11=1.10015878
R12=1.10258459
R13=1.10160151
R14=1.10381757
R15=1.10258443
R16=1.10054205
R17=1.10148411
A3=125.83993708
A4=125.00026771
A5=104.19061969
A6=103.77751142
A7=108.45780679
A8=106.83169907
A9=111.03691221
A10=108.93606938
A11=113.19269775
A12=110.08535786
A13=112.6590113
A14=110.01800984
A15=111.05711334
A16=110.33877014
A17=110.32119536
D4=-178.28696849
D5=-164.5746999
D6=-170.96431356
D7=-120.38211952
D8=-117.07872057
D9=125.58341353
D10=120.88885068
D11=-154.69302283
D12=-120.43257617
D13=-153.50968239
D14=-120.30873573
D15=61.28266278
D16=-119.86342429
D17=119.82017787

2-methylcyclopentanone
(equatorial methyl group)
MP2/aug-cc-pVDZ

O
C,1,R2
C,2,R3,1,A3
C,2,R4,1,A4,3,D4,0
C,3,R5,2,A5,1,D5,0
C,4,R6,2,A6,1,D6,0
C,4,R7,2,A7,6,D7,0
H,3,R8,2,A8,5,D8,0
H,3,R9,2,A9,5,D9,0
H,4,R10,2,A10,6,D10,0
H,5,R11,3,A11,2,D11,0
H,5,R12,3,A12,11,D12,0
H,6,R13,4,A13,2,D13,0
H,6,R14,4,A14,13,D14,0
H,7,R15,4,A15,2,D15,0
H,7,R16,4,A16,15,D16,0
H,7,R17,4,A17,15,D17,0
Variables:
R2=1.2257983
R3=1.53319652
R4=1.53529189
R5=1.54025724
R6=1.53903039
R7=1.52683005
R8=1.09985998
R9=1.10506214
R10=1.10928325
R11=1.10011377
R12=1.10332938
R13=1.10084521
R14=1.10571915
R15=1.10123633
R16=1.10233353
R17=1.10015907
A3=125.71931556
A4=125.28236855
A5=104.41068147
A6=103.04231484
A7=112.91469297
A8=110.85298191
A9=106.9024304
A10=105.15827733
A11=113.20454159
A12=110.06188494
A13=113.06582166
A14=109.1576367
A15=111.04513538
A16=110.15227008
A17=110.46684879
D4=178.42054409
D5=-172.8419042
D6=-162.00126651
D7=127.0723213
D8=125.35093414
D9=-117.66761874
D10=-113.3167776
D11=-152.70980208
D12=-120.75895157
D13=-158.34455491
D14=-120.06947304
D15=176.84910117
D16=120.00272543
D17=-120.76960198

3-methylcyclopentanone
(axial methyl group)
MP2/aug-cc-pVDZ

O
C,1,R2
C,2,R3,1,A3
C,2,R4,1,A4,3,D4,0
C,3,R5,2,A5,1,D5,0
C,4,R6,2,A6,1,D6,0
H,3,R7,2,A7,5,D7,0
H,3,R8,2,A8,5,D8,0
H,4,R9,2,A9,6,D9,0
H,4,R10,2,A10,6,D10,0
H,6,R11,4,A11,2,D11,0
C,5,R12,3,A12,2,D12,0
H,5,R13,3,A13,12,D13,0
H,6,R14,4,A14,11,D14,0
H,12,R15,5,A15,3,D15,0
H,12,R16,5,A16,15,D16,0
H,12,R17,5,A17,15,D17,0
Variables:
R2=1.22523656
R3=1.53211449
R4=1.53513112
R5=1.54064076
R6=1.54127425
R7=1.10046739
R8=1.10606514
R9=1.10022555
R10=1.10302747
R11=1.10130538
R12=1.53476145
R13=1.10226278
R14=1.10332034
R15=1.1018287
R16=1.10341016
R17=1.10198251
A3=125.93481515
A4=125.50871191
A5=104.15900012
A6=104.50415053
A7=111.17172822
A8=106.8719763
A9=110.09400674
A10=107.65748849
A11=113.29848582
A12=110.98567796
A13=111.57896261
A14=109.82071437
A15=110.86441567
A16=111.23452401
A17=111.04823009
D4=-179.60797078
D5=-161.05859163
D6=-174.3348271
D7=124.83596993
D8=-117.40162903
D9=123.88487406
D10=-119.55687497
D11=-150.4487225
D12=83.88396698
D13=122.05392225
D14=-120.5417818
D15=64.44728296
D16=-119.49415174
D17=120.29669734

3-methylcyclopentanone
(equatorial methyl group)
MP2/aug-cc-pVDZ

C
C,1,R2
C,1,R3,2,A3
O,1,R4,2,A4,3,D4,0
C,2,R5,1,A5,3,D5,0
C,3,R6,1,A6,2,D6,0
H,2,R7,1,A7,5,D7,0
H,2,R8,1,A8,5,D8,0
H,3,R9,1,A9,6,D9,0
H,3,R10,1,A10,6,D10,0
C,6,R11,3,A11,1,D11,0
H,5,R12,2,A12,1,D12,0
H,5,R13,2,A13,12,D13,0
H,6,R14,3,A14,11,D14,0
H,11,R15,6,A15,3,D15,0
H,11,R16,6,A16,15,D16,0
H,11,R17,6,A17,15,D17,0
Variables:
R2=1.534893
R3=1.53181402
R4=1.22507918
R5=1.53833023
R6=1.53913192
R7=1.09982209
R8=1.1051047
R9=1.1000946
R10=1.10756882
R11=1.52748705
R12=1.10111905
R13=1.10539422
R14=1.10690766

R15=1.10237546
R16=1.10188703
R17=1.10337965
A3=108.31419113
A4=125.67531011
A5=104.08644786
A6=104.61545302
A7=110.79112071
A8=107.03835747
A9=111.36680673
A10=107.14135275
A11=114.43678647
A12=113.67519686
A13=110.07360409
A14=108.32796599
A15=111.09478119
A16=111.4399402
A17=110.16354666
D4=-179.82498925
D5=-11.14479776
D6=-14.20111952
D7=-125.21039659
D8=117.57060778
D9=-125.76115148
D10=116.48106235
D11=157.57967893
D12=154.76995078
D13=121.05910388
D14=122.15077247
D15=-177.76023987
D16=-120.42384284
D17=119.69852439

2-methylcyclohexanone
(axial methyl group)
MP2/aug-cc-pVDZ

O
C,1,R2
C,2,R3,1,A3
C,2,R4,1,A4,3,D4,0
C,3,R5,2,A5,1,D5,0
C,4,R6,2,A6,1,D6,0
C,4,R7,2,A7,6,D7,0
H,3,R8,2,A8,5,D8,0
H,3,R9,2,A9,5,D9,0
H,4,R10,2,A10,6,D10,0
C,5,R11,3,A11,2,D11,0
H,5,R12,3,A12,11,D12,0
H,5,R13,3,A13,11,D13,0
H,6,R14,4,A14,2,D14,0
H,6,R15,4,A15,14,D15,0
H,7,R16,4,A16,2,D16,0
H,7,R17,4,A17,16,D17,0
H,7,R18,4,A18,16,D18,0
H,11,R19,5,A19,3,D19,0
H,11,R20,5,A20,19,D20,0
Variables:
R2=1.23278925
R3=1.52160279
R4=1.52531
R5=1.54383238
R6=1.5466423
R7=1.54177054
R8=1.10014474
R9=1.10550933
R10=1.10266429
R11=1.53539308
R12=1.10256181
R13=1.10532873
R14=1.10445273
R15=1.10543811
R16=1.10155558
R17=1.10056343
R18=1.10210111
R19=1.10307391
R20=1.10445534
A3=122.10203013
A4=121.83698982
A5=110.36095745
A6=110.07130713
A7=109.94654275
A8=108.2878084
A9=108.46308215
A10=106.23526163
A11=110.82719819
A12=109.72178163
A13=109.05018375
A14=109.07296975
A15=108.79141673
A16=110.72236719
A17=112.07996895
A18=109.74000957
A19=110.07561582
A20=109.60030963
D4=179.35048917
D5=127.32514902
D6=-129.553454
D7=-124.07247801
D8=-123.28641453
D9=119.44673263
D10=118.67505687
D11=54.81263361
D12=122.74419072
D13=-120.33482247
D14=-174.67054145
D15=-116.22273561
D16=-57.18898279
D17=120.82044905
D18=-119.33581064
D19=-179.35150837
D20=-116.96323581

2-methylcyclohexanone
(equatorial methyl group)
MP2/aug-cc-pVDZ

O
C,1,R2
C,2,R3,1,A3
C,2,R4,1,A4,3,D4,0
C,3,R5,2,A5,1,D5,0
C,4,R6,2,A6,1,D6,0
C,4,R7,2,A7,6,D7,0
H,3,R8,2,A8,5,D8,0
H,3,R9,2,A9,5,D9,0
H,4,R10,2,A10,6,D10,0
C,5,R11,3,A11,2,D11,0
H,5,R12,3,A12,11,D12,0
H,5,R13,3,A13,11,D13,0
H,6,R14,4,A14,2,D14,0
H,6,R15,4,A15,14,D15,0
H,7,R16,4,A16,2,D16,0
H,7,R17,4,A17,16,D17,0
H,7,R18,4,A18,16,D18,0
H,11,R19,5,A19,3,D19,0
H,11,R20,5,A20,19,D20,0
Variables:
R2=1.23218077
R3=1.5202222
R4=1.52585503
R5=1.54464277
R6=1.54812231
R7=1.52720327
R8=1.10565371
R9=1.10008271
R10=1.10845336
R11=1.53505802
R12=1.10516588
R13=1.10258595
R14=1.10661276
R15=1.10372712
R16=1.10171277
R17=1.1000099
R18=1.10100536
R19=1.10595366
R20=1.1031417
A3=122.34006393
A4=122.56399571
A5=109.50726678
A6=107.93793186
A7=112.37001704
A8=108.56153394
A9=108.74721395
A10=106.51724934
A11=110.71751683
A12=108.95887343
A13=109.77898999
A14=108.42711502
A15=108.93540613
A16=110.19180836
A17=111.23391759
A18=110.34553022
A19=109.42427468
A20=110.13817684
D4=176.66294609
D5=120.49063654
D6=-121.28865802
D7=124.51262499
D8=118.91145595
D9=-122.7781852
D10=-114.87888998
D11=55.00351533
D12=-120.31715108
D13=122.71902307
D14=66.08733194
D15=116.04662632
D16=178.93017722
D17=-120.68616729
D18=120.02908889
D19=63.83299003
D20=117.39023804

3-methylcyclohexanone
(axial methyl group)
MP2/aug-cc-pVDZ

C
C,1,R2
C,1,R3,2,A3
C,1,R4,2,A4,3,D4,0
H,1,R5,2,A5,3,D5,0
C,2,R6,1,A6,3,D6,0
C,3,R7,1,A7,2,D7,0
H,2,R8,1,A8,6,D8,0
H,2,R9,1,A9,6,D9,0
H,3,R10,1,A10,7,D10,0
H,3,R11,1,A11,7,D11,0
H,4,R12,1,A12,2,D12,0
H,4,R13,1,A13,12,D13,0
H,4,R14,1,A14,12,D14,0
C,6,R15,2,A15,1,D15,0
O,6,R16,2,A16,15,D16,0
H,7,R17,3,A17,1,D17,0
H,7,R18,3,A18,17,D18,0
H,15,R19,6,A19,2,D19,0
H,15,R20,6,A20,19,D20,0
Variables:
R2=1.54953148
R3=1.54161149
R4=1.53631102
R5=1.10497137
R6=1.52022955
R7=1.53675365
R8=1.10567012
R9=1.10106848
R10=1.10622468
R11=1.10412056
R12=1.101774
R13=1.10201921
R14=1.10237386
R15=1.52027138
R16=1.23206076
R17=1.10323834
R18=1.10261195
R19=1.1061102
R20=1.10002555
A3=109.71156647
A4=110.41943183
A5=107.94045307
A6=109.59789953
A7=112.19116984
A8=109.24448568
A9=111.61507733
A10=108.95196166
A11=109.58994005
A12=110.52367082
A13=111.76352022
A14=110.8763279
A15=114.59458871
A16=122.70466912
A17=110.20871925
A18=110.20100578
A19=108.02553982
A20=109.01832595
D4=124.2757252
D5=-117.71955763
D6=-55.54459905
D7=57.25935138
D8=118.62320598
D9=-120.86171275
D10=-120.72832475
D11=122.60790189
D12=62.61858808
D13=-119.24265028
D14=119.9702195
D15=56.54974318
D16=-177.33013403
D17=64.85207274
D18=117.39644025
D19=63.46281725
D20=118.07626657

3-methylcyclohexanone
(equatorial methyl group)
MP2/aug-cc-pVDZ

O
C,1,R2
C,2,R3,1,A3
C,2,R4,1,A4,3,D4,0
C,3,R5,2,A5,1,D5,0
C,4,R6,2,A6,1,D6,0
H,3,R7,2,A7,5,D7,0
H,3,R8,2,A8,5,D8,0
H,4,R9,2,A9,6,D9,0
H,4,R10,2,A10,6,D10,0
C,5,R11,3,A11,2,D11,0
C,6,R12,4,A12,2,D12,0
H,5,R13,3,A13,11,D13,0
H,5,R14,3,A14,11,D14,0
H,6,R15,4,A15,12,D15,0
H,11,R16,5,A16,3,D16,0
H,11,R17,5,A17,16,D17,0
H,12,R18,6,A18,4,D18,0
H,12,R19,6,A19,18,D19,0
H,12,R20,6,A20,18,D20,0
Variables:
R2=1.23223394
R3=1.51962952
R4=1.51899177
R5=1.54450202
R6=1.5458893
R7=1.10599521
R8=1.0999112
R9=1.10735382
R10=1.10102978
R11=1.53542438
R12=1.53173098
R13=1.1050521
R14=1.10258582
R15=1.10763658
R16=1.10762461
R17=1.10419138
R18=1.10225788
R19=1.10356773
R20=1.10205461
A3=122.62485496
A4=122.5291844
A5=109.53959307
A6=110.45905649
A7=108.33742695
A8=108.90794286
A9=108.65928971
A10=108.9824433
A11=110.99725323
A12=110.731644
A13=109.05135541
A14=109.71901535
A15=107.72919844
A16=109.59504511
A17=110.12152083
A18=111.05443058
A19=110.27100524
A20=111.18999821
D4=176.71358782
D5=122.75350829
D6=-122.04079963
D7=118.72706186
D8=-123.0266534
D9=-118.61956903
D10=122.99425234
D11=54.11804637
D12=-178.43148907
D13=-120.5087081
D14=122.58080358
D15=-118.67469104
D16=62.93746003
D17=117.39387047
D18=-178.00470466
D19=-119.76713276
D20=120.43511162

4-methylcyclohexanone
(axial methyl group)
MP2/aug-cc-pVDZ

O
C,1,R2
C,2,R3,1,A3
C,2,R4,1,A4,3,D4,0
C,3,R5,2,A5,1,D5,0
C,4,R6,2,A6,1,D6,0
H,3,R7,2,A7,5,D7,0
H,3,R8,2,A8,5,D8,0
H,4,R9,2,A9,6,D9,0
H,4,R10,2,A10,6,D10,0
C,5,R11,3,A11,2,D11,0
H,5,R12,3,A12,11,D12,0
H,5,R13,3,A13,11,D13,0
H,6,R14,4,A14,2,D14,0
H,6,R15,4,A15,14,D15,0
C,11,R16,5,A16,3,D16,0
H,11,R17,5,A17,16,D17,0
H,16,R18,11,A18,5,D18,0
H,16,R19,11,A19,18,D19,0
H,16,R20,11,A20,18,D20,0
Variables:
R2=1.23202802
R3=1.51992423
R4=1.51992484
R5=1.5462294
R6=1.54622901
R7=1.10008231
R8=1.1047921
R9=1.10008248
R10=1.10479173
R11=1.54101252
R12=1.10383271
R13=1.10509497
R14=1.10383292
R15=1.10509501
R16=1.53645011
R17=1.10573632
R18=1.10227942
R19=1.10128914
R20=1.10227954
A3=122.54267584
A4=122.54261455
A5=109.87122795
A6=109.87131469
A7=108.73242523
A8=108.39448875
A9=108.73233857
A10=108.39447113
A11=112.27753668
A12=109.70600569
A13=108.49805431
A14=109.70601114
A15=108.49805025
A16=112.22125798
A17=107.55588589
A18=110.61701767
A19=112.38276753
A20=110.61707503
D4=-177.20573265
D5=-123.78774364
D6=123.7879004
D7=122.40622416
D8=-120.03887139
D9=-122.40622223
D10=120.03899518
D11=-54.32681682
D12=-122.97873313
D13=120.55697841
D14=177.30524019
D15=116.46421306
D16=-69.12923584
D17=-117.92449398
D18=-177.77698195
D19=-120.2319398
D20=119.5361049

4-methylcyclohexanone
(equatorial methyl group)
MP2/aug-cc-pVDZ

O
C,1,R2
C,2,R3,1,A3
C,2,R4,1,A4,3,D4,0
C,3,R5,2,A5,1,D5,0
C,4,R6,2,A6,1,D6,0
H,3,R7,2,A7,5,D7,0
H,3,R8,2,A8,5,D8,0
H,4,R9,2,A9,6,D9,0
H,4,R10,2,A10,6,D10,0
C,5,R11,3,A11,2,D11,0
H,5,R12,3,A12,11,D12,0
H,5,R13,3,A13,11,D13,0
H,6,R14,4,A14,2,D14,0
H,6,R15,4,A15,14,D15,0
C,11,R16,5,A16,3,D16,0
H,11,R17,5,A17,16,D17,0
H,16,R18,11,A18,5,D18,0
H,16,R19,11,A19,18,D19,0
H,16,R20,11,A20,18,D20,0
Variables:
R2=1.23184971
R3=1.52001399
R4=1.52001547
R5=1.54383556
R6=1.54383381
R7=1.09997799
R8=1.10600739
R9=1.09997815
R10=1.1060084
R11=1.53662431
R12=1.10365885
R13=1.10659274
R14=1.1036593
R15=1.1065918
R16=1.53242384
R17=1.10859379
R18=1.10214093
R19=1.10345885
R20=1.10214214
A3=122.59679043
A4=122.59667172
A5=109.88449919
A6=109.88440738
A7=108.84906425
A8=108.22574756
A9=108.84869426
A10=108.22570044
A11=111.86292268
A12=109.75484961
A13=109.22951663
A14=109.75498937
A15=109.22944157
A16=111.15356488
A17=108.02060205
A18=111.21179805
A19=110.31691504
A20=111.21153686
D4=-177.36210913
D5=-124.09302556
D6=124.0928244
D7=123.13948424
D8=-118.88222833
D9=-123.13955102
D10=118.88251466
D11=-54.61703556
D12=-122.67203396
D13=120.4000964
D14=177.28929325
D15=116.92804872
D16=-179.42523205
D17=119.12466003
D18=58.49909959
D19=-119.76051289
D20=120.47931434

Cyclohexanone
MP2/aug-cc-pVDZ

C
C,1,R2
C,1,R3,2,A3
O,1,R4,2,A4,3,D4,0
C,2,R5,1,A5,3,D5,0
C,3,R6,1,A6,2,D6,0
H,2,R7,1,A7,5,D7,0
H,2,R8,1,A8,5,D8,0
H,3,R9,1,A9,6,D9,0
H,3,R10,1,A10,6,D10,0
C,5,R11,2,A11,1,D11,0
H,5,R12,2,A12,11,D12,0
H,5,R13,2,A13,11,D13,0
H,6,R14,3,A14,1,D14,0
H,6,R15,3,A15,14,D15,0
H,11,R16,5,A16,2,D16,0
H,11,R17,5,A17,16,D17,0
Variables:
R2=1.52014269
R3=1.52015136
R4=1.23210696
R5=1.54512428
R6=1.5451268
R7=1.09998421
R8=1.10607039
R9=1.09998415
R10=1.10606905
R11=1.53569678
R12=1.10258387
R13=1.10519733
R14=1.10258346
R15=1.10519714
R16=1.10308612
R17=1.1061908
A3=114.88842824
A4=122.52964564
A5=109.85198578
A6=109.85089693
A7=108.83177927
A8=108.24984556
A9=108.83130106
A10=108.25057608
A11=110.97876339
A12=109.67372349
A13=109.01831085
A14=109.6743073
A15=109.01825066
A16=110.07783694
A17=109.38348789
D4=177.41132859
D5=-54.03034406
D6=54.0305713
D7=-123.14205192
D8=118.80494338
D9=123.14098407
D10=-118.80477207
D11=54.48247399
D12=122.68618817
D13=-120.4474948
D14=-177.16960091
D15=-116.86647601
D16=-179.65106942
D17=-117.32562337

acetonitrile
MP2/aug-cc-pVDZ

C
C,1,R2
H,1,R3,2,A3
H,1,R4,2,A4,3,D4,0
H,1,R5,2,A5,3,D5,0
N,2,R6,1,A6,3,D6,0
Variables:
R2=1.47084904
R3=1.0989947
R4=1.09899356
R5=1.09899554
R6=1.18527372
A3=109.86769349
A4=109.86092328
A5=109.85923768
A6=179.96177928
D4=120.00106665
D5=-119.99971348
D6=166.14241695

acetonitrile
MP2/aug-cc-pVTZ

C
C,1,R2
H,1,R3,2,A3
H,1,R4,2,A4,3,D4,0
H,1,R5,2,A5,3,D5,0
N,2,R6,1,A6,3,D6,0
Variables:
R2=1.45714184
R3=1.08730623
R4=1.08730653
R5=1.08730655
R6=1.16959292
A3=109.92610691
A4=109.92102743
A5=109.91930262
A6=179.96517885
D4=120.00113066
D5=-120.00031085
D6=162.32256806

2-methylpropanenitrile
MP2/aug-cc-pVDZ

N
C,1,R2
C,2,R3,1,A3
C,3,R4,2,A4,1,D4,0
C,3,R5,2,A5,4,D5,0
H,3,R6,2,A6,4,D6,0
H,4,R7,3,A7,2,D7,0
H,4,R8,3,A8,7,D8,0
H,4,R9,3,A9,7,D9,0
H,5,R10,3,A10,2,D10,0
H,5,R11,3,A11,10,D11,0
H,5,R12,3,A12,10,D12,0
Variables:
R2=1.18746048
R3=1.47775129
R4=1.53937635
R5=1.53939273
R6=1.10367662
R7=1.09989346
R8=1.10106201
R9=1.10099582
R10=1.09989126
R11=1.10106451
R12=1.10099442
A3=178.59933154
A4=110.06559179
A5=110.05002712
A6=106.78844475
A7=111.32469391
A8=109.47367635
A9=110.27917457
A10=111.32317791
A11=109.47298706
A12=110.27798923
D4=-64.29749919
D5=123.61576964
D6=-118.19551745
D7=-57.91340079
D8=-120.1329616
D9=120.46628806
D10=57.90538357
D11=120.13406299
D12=-120.46475613

propanenitrile
MP2/aug-cc-pVDZ

C
C,1,R2
H,1,R3,2,A3
H,1,R4,2,A4,3,D4,0
H,1,R5,2,A5,3,D5,0
C,2,R6,1,A6,3,D6,0
H,2,R7,1,A7,6,D7,0
H,2,R8,1,A8,6,D8,0
N,6,R9,2,A9,1,D9,0
Variables:
R2=1.53889677
R3=1.10001689
R4=1.09960194
R5=1.09959971
R6=1.47464454
R7=1.10147568
R8=1.101476
R9=1.18658149
A3=109.7237792
A4=110.69235666
A5=110.69222562
A6=111.73624989
7=110.68909446
A8=110.68850903
A9=178.53383333
D4=119.87448619
D5=-119.87536545
D6=179.99803245
D7=-120.53979045
D8=120.54402189
D9=-0.71176454

propanenitrile
MP2/aug-cc-pVTZ

C
C,1,R2
H,1,R3,2,A3
H,1,R4,2,A4,3,D4,0
H,1,R5,2,A5,3,D5,0
C,2,R6,1,A6,3,D6,0
H,2,R7,1,A7,6,D7,0
H,2,R8,1,A8,6,D8,0
N,6,R9,2,A9,1,D9,0
Variables:
R2=1.52949675
R3=1.08800624
R4=1.08767449
R5=1.08767443
R6=1.46092597
R7=1.08986006
R8=1.0898597
R9=1.17063352
A3=109.89816967
A4=110.65756395
A5=110.65745702
A6=111.62980873
A7=110.74087472
A8=110.74036697
A9=178.55266182
D4=119.96457904
D5=-119.96471137
D6=179.99824454
D7=-120.56554658
D8=120.56907849
D9=-0.58312201

butanenitrile
MP2/aug-cc-pVDZ

N
C,1,R2
C,2,R3,1,A3
C,3,R4,2,A4,1,D4,0
H,3,R5,2,A5,4,D5,0
H,3,R6,2,A6,4,D6,0
C,4,R7,3,A7,2,D7,0
H,4,R8,3,A8,7,D8,0
H,4,R9,3,A9,7,D9,0
H,7,R10,4,A10,3,D10,0
H,7,R11,4,A11,10,D11,0
H,7,R12,4,A12,10,D12,0
Variables:
R2=1.18672047
R3=1.47331577
R4=1.54082701
R5=1.10276181
R6=1.10276236
R7=1.53172288
R8=1.10201949
R9=1.10202141
R10=1.10050934
R11=1.10223232
R12=1.10223371
A3=178.30099096
A4=112.04689386
A5=108.39497046
A6=108.39577277
A7=111.04502326
A8=108.95599846
A9=108.95601438
A10=110.97079853
A11=110.98105588
A12=110.98043555
D4=-0.14221014
D5=121.91183037
D6=-121.91238983
D7=179.99979072
D8=-121.79814905
D9=121.79864554
D10=-179.99866458
D11=-119.95265374
D12=119.95067585

gauche-butanenitrile
MP2/aug-cc-pVDZ

H
C,1,R2
H,2,R3,1,A3
C,2,R4,1,A4,3,D4,0
H,2,R5,1,A5,3,D5,0
C,4,R6,2,A6,1,D6,0
H,4,R7,2,A7,6,D7,0
H,4,R8,2,A8,6,D8,0
H,6,R9,4,A9,2,D9,0
H,6,R10,4,A10,9,D10,0
C,6,R11,4,A11,9,D11,0
N,11,R12,6,A12,4,D12,0
Variables:
R2=1.1014237
R3=1.10238107
R4=1.53168563
R5=1.10056193
R6=1.54214462
R7=1.10218523
R8=1.10255863
R9=1.10167261
R10=1.10280003
R11=1.47475141
R12=1.18685165
A3=108.08704475
A4=110.95635745
A5=108.02534842
A6=112.37438474
A7=110.27002977
A8=110.24421327
A9=110.89628539
A10=110.27457019
A11=111.56295437
A12=178.21380697
D4=-121.67900348
D5=116.58881475
D6=60.88762544
D7=-121.75134437
D8=120.06253892
D9=178.02213498
D10=-119.04397125
D11=120.70517464
D12=-2.27141536

2,2-dimethylpropanenitrile
MP2/aug-cc-pVDZ

C
C,1,R2
H,1,R3,2,A3
H,1,R4,2,A4,3,D4,0
H,1,R5,2,A5,3,D5,0
C,2,R6,1,A6,3,D6,0
C,2,R7,1,A7,6,D7,0
C,2,R8,1,A8,6,D8,0
N,6,R9,2,A9,1,D9,0
H,7,R10,2,A10,1,D10,0
H,7,R11,2,A11,10,D11,0
H,7,R12,2,A12,10,D12,0
H,8,R13,2,A13,1,D13,0
H,8,R14,2,A14,13,D14,0
H,8,R15,2,A15,13,D15,0
Variables:
R2=1.54126326
R3=1.10083738
R4=1.1021796
R5=1.1008557
R6=1.48056757
R7=1.54151899
R8=1.54135062
R9=1.18811284
R10=1.10084329
R11=1.10083164
R12=1.1022062
R13=1.1008474
R14=1.10220994
R15=1.10084972
A3=110.96784066
A4=109.08822889
A5=110.96025098
A6=108.7155773
A7=110.24261449
A8=110.27782027
A9=179.9719139
A10=110.95913459
A11=110.97276644
A12=109.08288575
A13=110.96317022
A14=109.0909101
A15=110.98454229
D4=119.63110911
D5=-120.73354455
D6=60.32815746
D7=-118.98309236
D8=119.05841316
D9=-176.51749474
D10=179.42651448
D11=-120.74532964
D12=119.62249266
D13=-179.36107905
D14=-119.61962515
D15=120.74413231

2-methylbutanenitrile
MP2/aug-cc-pVDZ

C
C,1,R2
H,1,R3,2,A3
H,1,R4,2,A4,3,D4,0
H,1,R5,2,A5,3,D5,0
C,2,R6,1,A6,3,D6,0
H,2,R7,1,A7,6,D7,0
H,2,R8,1,A8,6,D8,0
C,6,R9,2,A9,1,D9,0
C,6,R10,2,A10,9,D10,0
H,6,R11,2,A11,9,D11,0
N,9,R12,6,A12,2,D12,0
H,10,R13,6,A13,2,D13,0
H,10,R14,6,A14,13,D14,0
H,10,R15,6,A15,13,D15,0
Variables:
R2=1.53293279
R3=1.1006302
R4=1.1002378
R5=1.10275056
R6=1.54551874
R7=1.10240151
R8=1.10360479
R9=1.47694576
R10=1.54024116
R11=1.1051502
R12=1.1874836
R13=1.09945022
R14=1.10141398
R15=1.09994195
A3=110.38696259
A4=111.94549954
A5=110.85655437
A6=112.63785992
A7=109.68266155
A8=110.45317721
A9=109.38737667
A10=113.02554618
A11=108.52351802
A12=178.49097381
A13=110.24521025
A14=110.17723706
A15=110.89091572
D4=119.71428994
D5=-119.36535184
D6=174.20964519
D7=-120.92922436
D8=121.51950823
D9=-175.04032464
D10=-122.58695681
D11=116.32590716
D12=-56.41490877
D13=-63.69831867
D14=120.11620658
D15=-119.84259108

gauche-2-methylbutanenitrile
MP2/aug-cc-pVDZ

C
C,1,R2
H,1,R3,2,A3
H,1,R4,2,A4,3,D4,0
H,1,R5,2,A5,3,D5,0
C,2,R6,1,A6,3,D6,0
H,2,R7,1,A7,6,D7,0
H,2,R8,1,A8,6,D8,0
C,6,R9,2,A9,1,D9,0
C,6,R10,2,A10,9,D10,0
H,6,R11,2,A11,9,D11,0
N,9,R12,6,A12,2,D12,0
H,10,R13,6,A13,2,D13,0
H,10,R14,6,A14,13,D14,0
H,10,R15,6,A15,13,D15,0
Variables:
R2=1.53160128
R3=1.10068306
R4=1.10138269
R5=1.10234969
R6=1.54281734
R7=1.10370249
R8=1.1035892
R9=1.47740411
R10=1.53941937
R11=1.10502869
R12=1.18763122
R13=1.10102227
R14=1.10002364
R15=1.10094136
A3=110.82804691
A4=111.02129128
A5=110.78940737
A6=113.12957852
A7=110.2162135
A8=110.40252962
A9=109.93888107
A10=112.02790251
A11=108.53806916
A12=178.3421123
A13=109.48930259
A14=111.30004885
A15=110.26477057
D4=-120.05626993
D5=119.78217152
D6=-178.62060484
D7=120.04960685
D8=-121.77942634
D9=-59.71129403
D10=-122.74797021
D11=116.56887405
D12=-53.34143345
D13=-59.31267439
D14=-120.12563469
D15=119.47101825

3-methylbutanenitrile
MP2/aug-cc-pVDZ

C
C,1,R2
H,1,R3,2,A3
H,1,R4,2,A4,3,D4,0
H,1,R5,2,A5,3,D5,0
C,2,R6,1,A6,3,D6,0
C,2,R7,1,A7,6,D7,0
H,2,R8,1,A8,6,D8,0
C,7,R9,2,A9,1,D9,0
H,6,R10,2,A10,1,D10,0
H,6,R11,2,A11,10,D11,0
H,6,R12,2,A12,10,D12,0
H,7,R13,2,A13,9,D13,0
H,7,R14,2,A14,9,D14,0
N,9,R15,7,A15,2,D15,0
Variables:
R2=1.53310904
R3=1.10135528
R4=1.10218309
R5=1.10271324
R6=1.53309382
R7=1.5466743
R8=1.10505355
R9=1.4751033
R10=1.10135541
R11=1.10271203
R12=1.10218163
R13=1.10252284
R14=1.10252292
R15=1.18706789
A3=110.56393379
A4=111.39704629
A5=110.49615018
A6=111.39187168
A7=110.90897968
A8=108.80748547
A9=111.56681147
A10=110.56499525
A11=110.49698732
A12=111.3979433
A13=110.47936631
A14=110.47963958
A15=178.14134445
D4=-120.17014549
D5=119.51297904
D6=-59.08027426
D7=-124.05441485
D8=119.9463263
D9=62.15694222
D10=59.08661319
D11=-119.51255667
D12=120.17043499
D13=-120.46595302
D14=120.46632344
D15=0.12116301

gauche-3-methylbutanenitrile
MP2/aug-cc-pVDZ

C
C,1,R2
H,1,R3,2,A3
H,1,R4,2,A4,3,D4,0
H,1,R5,2,A5,3,D5,0
C,2,R6,1,A6,3,D6,0
C,2,R7,1,A7,6,D7,0
H,2,R8,1,A8,6,D8,0
C,7,R9,2,A9,1,D9,0
H,6,R10,2,A10,1,D10,0
H,6,R11,2,A11,10,D11,0
H,6,R12,2,A12,10,D12,0
H,7,R13,2,A13,9,D13,0
H,7,R14,2,A14,9,D14,0
N,9,R15,7,A15,2,D15,0
Variables:
R2=1.53268801
R3=1.10143389
R4=1.10123822
R5=1.10379833
R6=1.53324115
R7=1.54466641
R8=1.10460955
R9=1.47308371
R10=1.10134214
R11=1.10360564
R12=1.10212426
R13=1.10403236
R14=1.10251577
R15=1.18692113
A3=110.58286367
A4=111.56335625
A5=110.24401095
A6=111.27001818
A7=110.8890962
A8=108.85769099
A9=112.15490164
A10=110.67143954
A11=110.4500646
A12=111.56595979
A13=109.69085778
A14=110.48547041
A15=178.07218362
D4=-120.37969395
D5=119.31262055
D6=-58.90751353
D7=-121.73519995
D8=120.03225036
D9=-60.4127066
D10=58.68549466
D11=-119.36910019
D12=120.29070863
D13=120.64818496
D14=-121.00351114
D15=-2.88754198

pentanenitrile
MP2/aug-cc-pVDZ

C
C,1,R2
H,1,R3,2,A3
H,1,R4,2,A4,3,D4,0
H,1,R5,2,A5,3,D5,0
C,2,R6,1,A6,3,D6,0
H,2,R7,1,A7,6,D7,0
H,2,R8,1,A8,6,D8,0
C,6,R9,2,A9,1,D9,0
H,6,R10,2,A10,9,D10,0
H,6,R11,2,A11,9,D11,0
C,9,R12,6,A12,2,D12,0
H,9,R13,6,A13,12,D13,0
H,9,R14,6,A14,12,D14,0
N,12,R15,9,A15,6,D15,0
Variables:
R2=1.53312053
R3=1.10088438
R4=1.10206947
R5=1.10207015
R6=1.53211789
R7=1.104594
R8=1.10459203
R9=1.54032288
R10=1.10335378
R11=1.10335522
R12=1.47330911
R13=1.10261605
R14=1.10261547
R15=1.18672797
A3=111.30639233
A4=110.80622076
A5=110.80629885
A6=112.07938514
A7=109.73717908
A8=109.73700537
A9=111.55406394
A10=109.98131172
A11=109.98099107
A12=111.99609385
A13=110.27602411
A14=110.27601937
A15=178.27884829
D4=120.12558065
D5=-120.126207
D6=-179.99984562
D7=-121.56240234
D8=121.56263703
D9=-179.99934961
D10=121.24817285
D11=-121.24758214
D12=179.99993535
D13=-120.79864302
D14=120.79840229
D15=-0.00279342

gauche-pentanenitrile
MP2/aug-cc-pVDZ

H
C,1,R2
H,2,R3,1,A3
C,2,R4,1,A4,3,D4,0
H,2,R5,1,A5,3,D5,0
H,4,R6,2,A6,1,D6,0
H,4,R7,2,A7,6,D7,0
C,4,R8,2,A8,6,D8,0
H,8,R9,4,A9,2,D9,0
C,8,R10,4,A10,9,D10,0
H,8,R11,4,A11,9,D11,0
H,10,R12,8,A12,4,D12,0
H,10,R13,8,A13,12,D13,0
C,10,R14,8,A14,12,D14,0
N,14,R15,10,A15,8,D15,0
Variables:
R2=1.1010772
R3=1.10213702
R4=1.53194582
R5=1.10271937
R6=1.10492217
R7=1.10434822
R8=1.53275112
R9=1.10450804
R10=1.54134681
R11=1.10398188
R12=1.10161427
R13=1.10278783
R14=1.47490373
R15=1.18617494
A3=107.96377155
A4=111.26760117
A5=107.86350615
A6=109.93099922
A7=109.73592894
A8=112.0595522
A9=109.73495702
A10=112.85178401
A11=109.88090598
A12=110.84986284
A13=110.3080233
A14=111.45974639
A15=178.33928668
D4=-121.97034802
D5=116.31902114
D6=58.49185344
D7=-117.02915349
D8=121.48710234
D9=-59.18389718
D10=-120.38496628
D11=117.56080375
D12=177.71524431
D13=-119.05490347
D14=120.61140667
D15=-4.87143727

dimethyl sulfoxide
MP2/aug-cc-pVDZ

C
S,1,R2
H,1,R3,2,A3
H,1,R4,2,A4,3,D4,0
H,1,R5,2,A5,3,D5,0
C,2,R6,1,A6,3,D6,0
O,2,R7,1,A7,6,D7,0
H,6,R8,2,A8,1,D8,0
H,6,R9,2,A9,8,D9,0
H,6,R10,2,A10,8,D10,0
Variables:
R2=1.82428335
R3=1.10130531
R4=1.09893458
R5=1.10059453
R6=1.82428244
R7=1.54458745
R8=1.10130487
R9=1.10059496
R10=1.09893365
A3=109.56937441
A4=106.65707626
A5=108.06773519
A6=95.87255227
A7=105.94253774
A8=109.56916226
A9=108.06769895
A10=106.65715419
D4=-119.4369217
D5=122.03441116
D6=-64.01130414
D7=-108.45438475
D8=64.01247518
D9=-122.0347221
D10=119.43671369

dimethyl sulfoxide
MP2/aug-cc-pVTZ

C
S,1,R2
H,1,R3,2,A3
H,1,R4,2,A4,3,D4,0
H,1,R5,2,A5,3,D5,0
C,2,R6,1,A6,3,D6,0
O,2,R7,1,A7,6,D7,0
H,6,R8,2,A8,1,D8,0
H,6,R9,2,A9,8,D9,0
H,6,R10,2,A10,8,D10,0
Variables:
R2=1.80468927
R3=1.08918632
R4=1.08726816
R5=1.08911836
R6=1.80469004
R7=1.50505636
R8=1.08918619
R9=1.08911901
R10=1.08726768
A3=109.63884429
A4=106.771277
A5=108.12476937
A6=95.71127134
A7=106.32748392
A8=109.63899865
A9=108.12463939
A10=106.77149564
D4=-119.49223199
D5=121.89447762
D6=-63.40896137
D7=-108.88659754
D8=63.40299707
D9=-121.894277
D10=119.49253909

methyl ethyl sulfoxide
MP2/aug-cc-pVDZ

C
S,1,R2
C,1,R3,2,A3
H,1,R4,2,A4,3,D4,0
H,1,R5,2,A5,3,D5,0
C,2,R6,1,A6,3,D6,0
O,2,R7,1,A7,6,D7,0
H,3,R8,1,A8,2,D8,0
H,3,R9,1,A9,8,D9,0
H,3,R10,1,A10,8,D10,0
H,6,R11,2,A11,1,D11,0
H,6,R12,2,A12,11,D12,0
H,6,R13,2,A13,11,D13,0
Variables:
R2=1.83579187
R3=1.52778301
R4=1.1028053
R5=1.10353625
R6=1.82370596
R7=1.5465286
R8=1.1005062
R9=1.10000838
R10=1.10120355
R11=1.10139762
R12=1.10054699
R13=1.09901791
A3=109.21823214
A4=106.0658444
A5=107.00997164
A6=96.03950076
A7=105.76417172
A8=110.09907975
A9=109.89318033
A10=111.10225812
A11=109.43938646
A12=108.0157167
A13=106.78754587
D4=-120.59114445
D5=122.03578684
D6=173.39266112
D7=-108.6059411
D8=-176.49167241
D9=119.66831229
D10=-119.96610184
D11=63.31598031
D12=-121.94396854
D13=119.45497271

methyl ethyl sulfoxide
MP2/aug-cc-pVTZ

C
S,1,R2
C,1,R3,2,A3
H,1,R4,2,A4,3,D4,0
H,1,R5,2,A5,3,D5,0
C,2,R6,1,A6,3,D6,0
O,2,R7,1,A7,6,D7,0
H,3,R8,1,A8,2,D8,0
H,3,R9,1,A9,8,D9,0
H,3,R10,1,A10,8,D10,0
H,6,R11,2,A11,1,D11,0
H,6,R12,2,A12,11,D12,0
H,6,R13,2,A13,11,D13,0
Variables:
R2=1.81410744
R3=1.51907456
4=1.0918156
R5=1.09183719
R6=1.80398075
R7=1.50716046
R8=1.08877906
R9=1.08865658
R10=1.08956764
R11=1.08927824
R12=1.08908201
R13=1.08731652
A3=109.07349472
A4=106.18264227
A5=107.15382567
A6=95.96887061
A7=106.13479325
A8=110.31707512
A9=109.90568588
A10=111.01007135
A11=109.54440534
A12=108.10182075
A13=106.90931955
D4=-120.61865481
D5=122.05650288
D6=174.08767639
D7=-109.07713106
D8=-176.77092546
D9=119.78805517
D10=-120.132979
D11=62.55954079
D12=-121.80884347
D13=119.51416886

tetramethylene sulfoxide
MP2/aug-cc-pVDZ

O
S,1,R2
C,2,R3,1,A3
C,2,R4,1,A4,3,D4,0
C,3,R5,2,A5,1,D5,0
C,4,R6,2,A6,1,D6,0
H,3,R7,2,A7,5,D7,0
H,3,R8,2,A8,5,D8,0
H,4,R9,2,A9,6,D9,0
H,4,R10,2,A10,6,D10,0
H,5,R11,3,A11,2,D11,0
H,5,R12,3,A12,11,D12,0
H,6,R13,4,A13,2,D13,0
H,6,R14,4,A14,13,D14,0
Variables:
R2=1.54892297
R3=1.86624064
R4=1.84384421
R5=1.54368003
R6=1.52894121
R7=1.10098633
R8=1.10081195
R9=1.10479372
R10=1.1001375
R11=1.1027598
R12=1.10094246
R13=1.10181209
R14=1.10147798
A3=105.05692529
A4=105.46384941
A5=109.06744009
A6=104.63255243
A7=101.61659979
A8=108.72795514
A9=107.4336947
A10=106.05615747
A11=109.71203503
A12=110.811892
A13=108.98628581
A14=111.79568692
D4=94.5585427
D5=96.75814281
D6=-70.88031158
D7=-119.70931767
D8=124.65617163
D9=-119.42802742
D10=122.60498158
D11=99.76013794
D12=118.85531255
D13=66.97782131
D14=120.17560487

glycol sulfite
MP2/aug-cc-pVDZ

O
S,1,R2
O,2,R3,1,A3
O,2,R4,1,A4,3,D4,0
C,3,R5,2,A5,1,D5,0
C,4,R6,2,A6,1,D6,0
H,5,R7,3,A7,2,D7,0
H,5,R8,3,A8,7,D8,0
H,6,R9,4,A9,2,D9,0
H,6,R10,4,A10,9,D10,0
Variables:
R2=1.48923537
R3=1.72283312
R4=1.70892224
R5=1.45157877
R6=1.45283093
R7=1.10094086
R8=1.09951666
R9=1.10143763
R10=1.09750828
A3=106.39278605
A4=109.37081479
A5=111.53732196
A6=106.85950045
A7=108.5362635
A8=107.38234614
A9=109.84719483
A10=106.61993911
D4=97.62533317
D5=101.49215811
D6=-74.4038419
D7=103.3895369
D8=119.71749364
D9=72.91692371
D10=120.08377707

vinylene carbonate
MP2/aug-cc-pVDZ

C
O,1,R2
O,1,R3,2,A3
O,1,R4,2,A4,3,D4,0
C,2,R5,1,A5,3,D5,0
C,3,R6,1,A6,2,D6,0
H,5,R7,2,A7,1,D7,0
H,6,R8,3,A8,1,D8,0
Variables:
R2=1.38225094
R3=1.38220843
R4=1.2024356
R5=1.39058907
R6=1.39062465
R7=1.08409204
R8=1.08409004
A3=108.12548763
A4=125.935814
A5=107.27237767
A6=107.2732694
A7=117.83297499
A8=117.8308035
D4=179.99983385
D5=-0.00129789
D6=-0.00078698
D7=-179.99334672
D8=-179.99419723

ethylene carbonate
MP2/aug-cc-pVDZ

C
O,1,R2
O,1,R3,2,A3
O,1,R4,2,A4,3,D4,0
C,2,R5,1,A5,3,D5,0
C,3,R6,1,A6,2,D6,0
H,5,R7,2,A7,1,D7,0
H,5,R8,2,A8,7,D8,0
H,6,R9,3,A9,1,D9,0
H,6,R10,3,A10,9,D10,0
Variables:
R2=1.37290326
R3=1.37290143
R4=1.20324368
R5=1.44620603
R6=1.44619952
R7=1.10065733
R8=1.09668834
R9=1.10065758
R10=1.09668916
A3=110.36009117
A4=124.81992057
A5=108.45874865
A6=108.45941051
A7=108.56411242
A8=108.31711997
A9=108.5644691
A10=108.31727031
D4=179.99016785
D5=9.44611781
D6=9.43897492
D7=96.25269836
D8=120.03117732
D9=96.2565547
D10=120.03082694

anti-succinonitrile
MP2/aug-cc-pVDZ

C
C,1,R2
C,1,R3,2,A3
H,1,R4,2,A4,3,D4,0
H,1,R5,2,A5,3,D5,0
C,2,R6,1,A6,3,D6,0
N,3,R7,1,A7,2,D7,0
H,2,R8,1,A8,6,D8,0
H,2,R9,1,A9,6,D9,0
N,6,R10,2,A10,1,D10,0
Variables:
R2=1.5469926
R3=1.47270326
R4=1.10070614
R5=1.10070747
R6=1.47270143
R7=1.18645576
R8=1.10070881
R9=1.10070231
R10=1.18645579
A3=110.38822553
A4=110.17239081
A5=110.17152323
A6=110.38910486
A7=178.17619506
A8=110.17086287
A9=110.17229969
A10=178.1764146
D4=-120.56581968
D5=120.5645879
D6=-179.99969128
D7=0.04564224
D8=-120.56656103
D9=120.56518989
D10=0.58173307

anti-succinonitrile
MP2/aug-cc-pVTZ

C
C,1,R2
C,1,R3,2,A3
H,1,R4,2,A4,3,D4,0
H,1,R5,2,A5,3,D5,0
C,2,R6,1,A6,3,D6,0
N,3,R7,1,A7,2,D7,0
H,2,R8,1,A8,6,D8,0
H,2,R9,1,A9,6,D9,0
N,6,R10,2,A10,1,D10,0
Variables:
R2=1.53755209
R3=1.45916047
R4=1.0893504
R5=1.08935047
R6=1.45916021
R7=1.17043627
R8=1.08935027
R9=1.08935076
R10=1.17043628
A3=110.42623137
A4=110.15961736
A5=110.15950594
A6=110.42636987
A7=178.15723366
A8=110.15926123
A9=110.15977354
A10=178.15738695
D4=-120.65672365
D5=120.65645476
D6=-179.99868221
D7=0.03614905
D8=-120.65832288
D9=120.65497178
D10=0.46086583

gauche-succinonitrile
MP2/aug-cc-pVDZ

C
C,1,R2
C,1,R3,2,A3
H,1,R4,2,A4,3,D4,0
H,1,R5,2,A5,3,D5,0
C,2,R6,1,A6,3,D6,0
N,3,R7,1,A7,2,D7,0
H,2,R8,1,A8,6,D8,0
H,2,R9,1,A9,6,D9,0
N,6,R10,2,A10,1,D10,0
Variables:
R2=1.54581619
R3=1.47318776
R4=1.10077577
R5=1.10115452
R6=1.47318746
R7=1.1865551
R8=1.10115441
R9=1.10077599
R10=1.18655582
A3=111.66642071
A4=110.21957474
A5=109.12279074
A6=111.66659146
A7=178.55547366
A8=109.12286528
A9=110.21954922
A10=178.55746592
D4=-121.35324398
D5=120.11349628
D6=64.60155122
D7=40.38582804
D8=120.11375886
D9=-121.352969
D10=40.3826226

gauche-succinonitrile
MP2/aug-cc-pVTZ

C
C,1,R2
C,1,R3,2,A3
H,1,R4,2,A4,3,D4,0
H,1,R5,2,A5,3,D5,0
C,2,R6,1,A6,3,D6,0
N,3,R7,1,A7,2,D7,0
H,2,R8,1,A8,6,D8,0
H,2,R9,1,A9,6,D9,0
N,6,R10,2,A10,1,D10,0
Variables:
R2=1.53651677
R3=1.4596218
R4=1.08940816
R5=1.08958047
R6=1.45962175
R7=1.17052198
R8=1.08958048
R9=1.08940819
R10=1.17052195
A3=111.68566271
A4=110.17921046
A5=109.25672259
A6=111.68576956
A7=178.6100508
A8=109.2567032
A9=110.1792065
A10=178.6113554
D4=-121.29840583
D5=120.22982068
D6=64.99052112
D7=41.41628733
D8=120.22994281
D9=-121.29826042
D10=41.40361883

APPENDIX B: RYDBERG ELECTRON TRANSFER SPECTRA

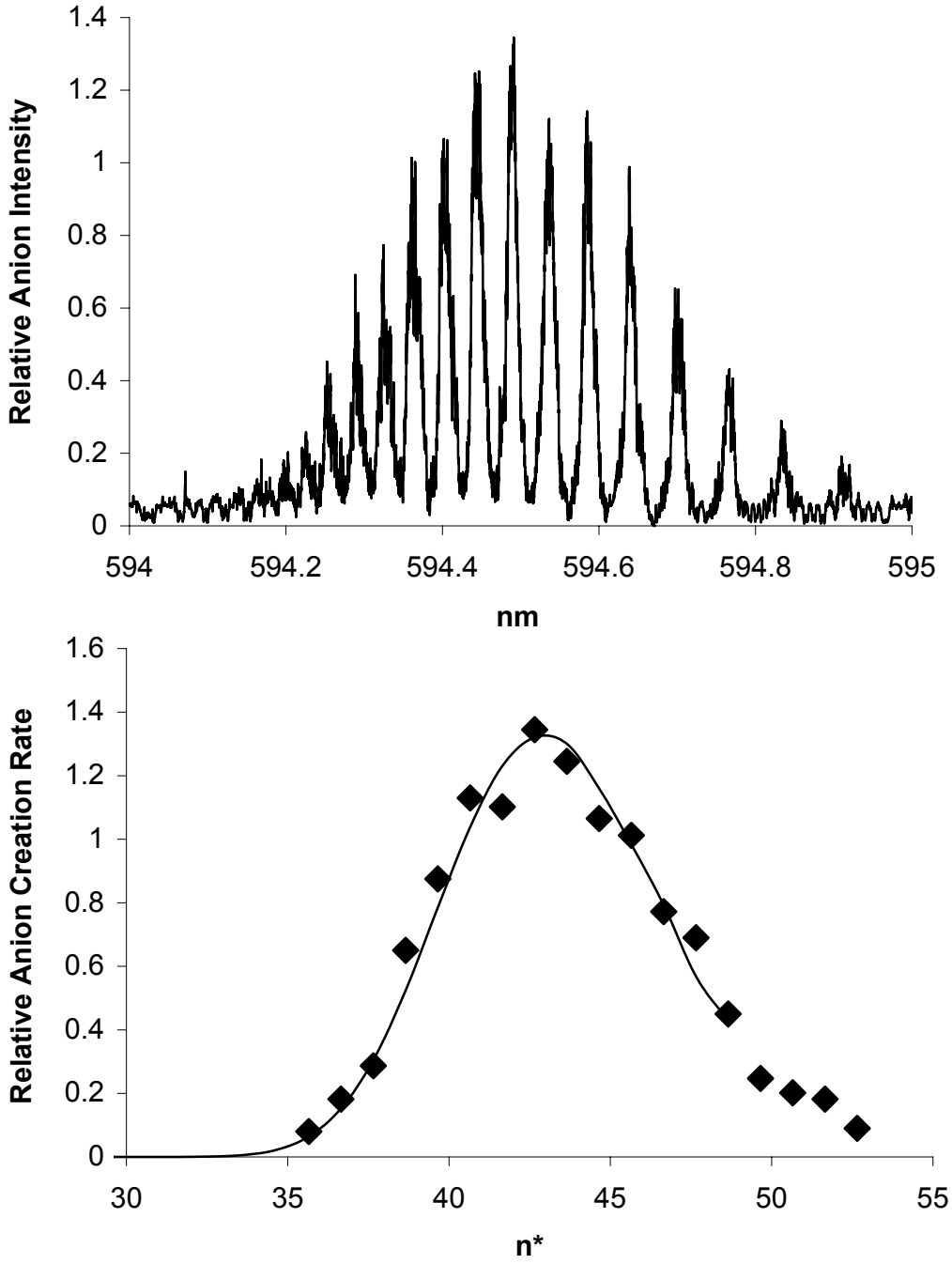

Figure B.1 One-color dipole-bound anion formation spectrum for acetaldehyde (top) and fitting to curve-crossing model (bottom).

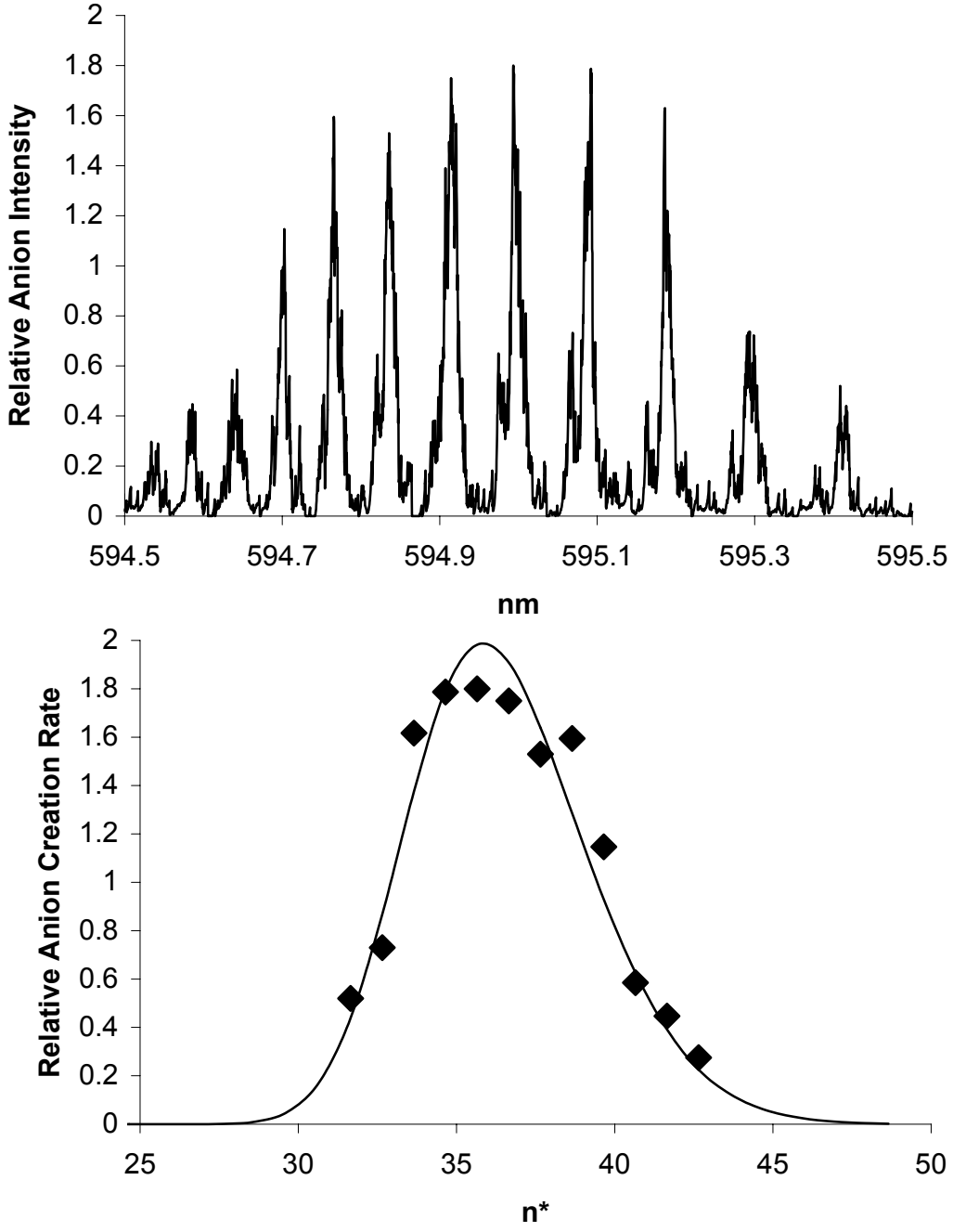

Figure B.2 One-color dipole-bound anion formation spectrum for propanal (top) and fitting to curve-crossing model (bottom).

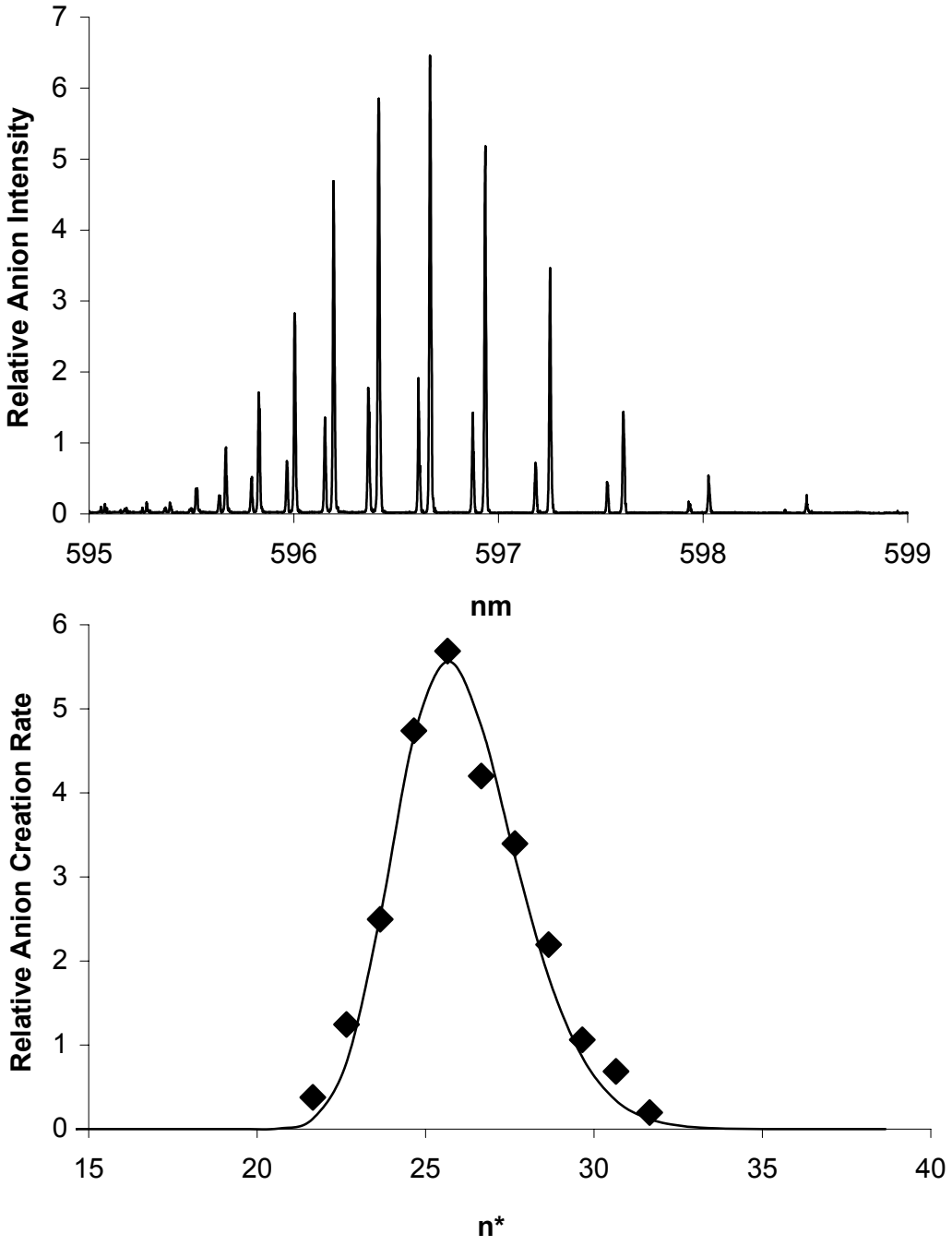

Figure B.3 One-color dipole-bound anion formation spectrum for acetone (top) and fitting to curve-crossing model (bottom).

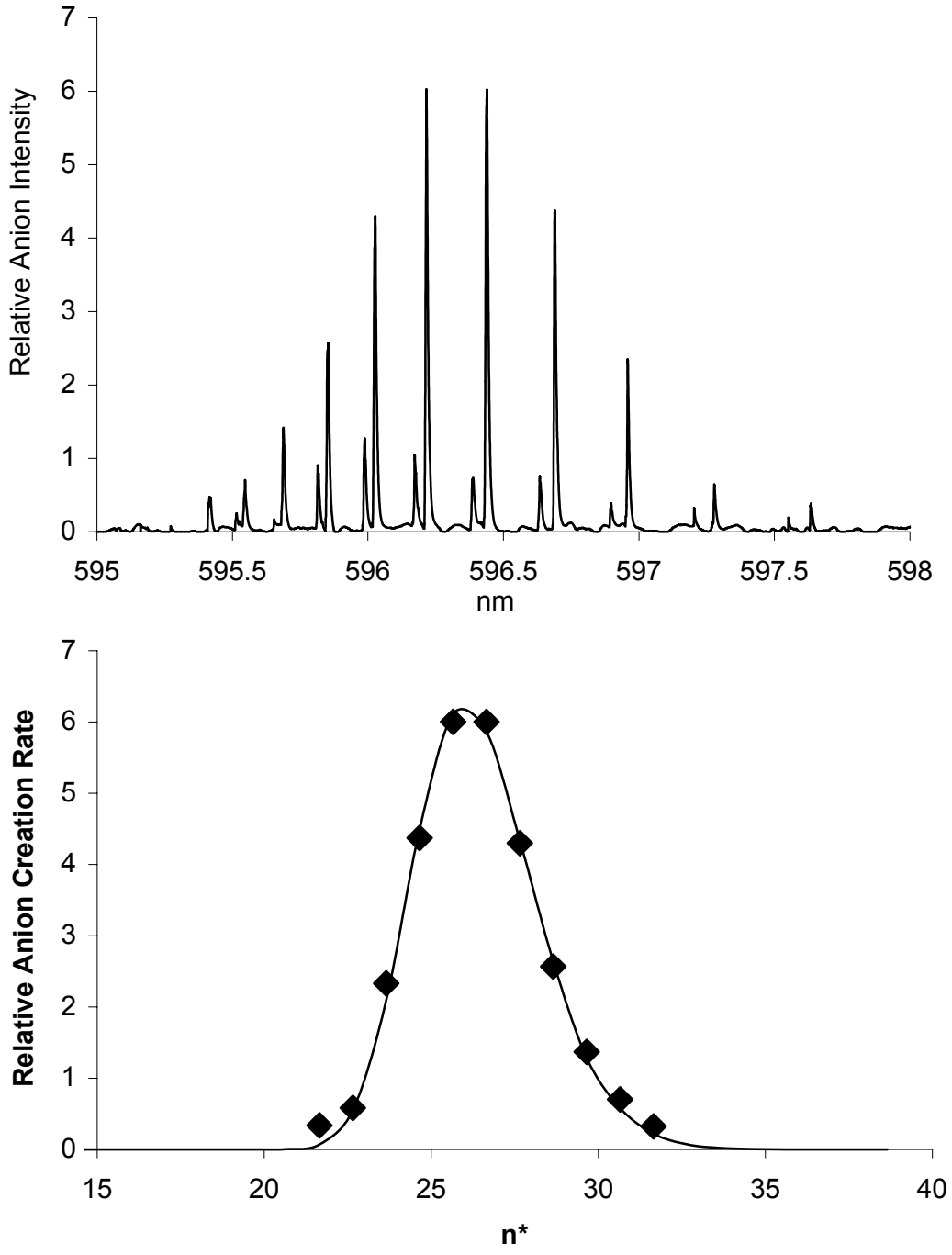

Figure B.4 One-color dipole-bound anion formation spectrum for perdeuterated acetone (top) and fitting to curve-crossing model (bottom).

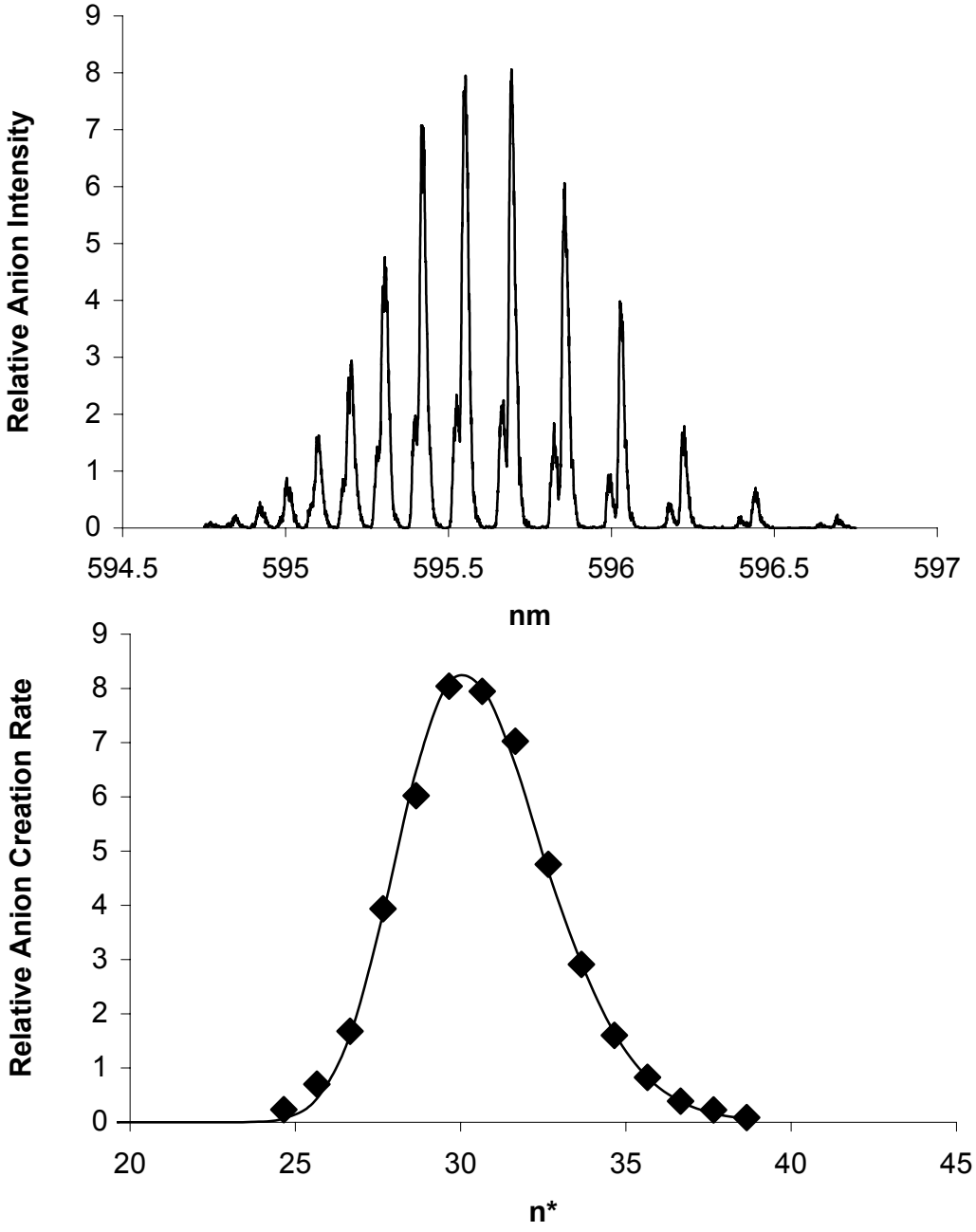

Figure B.5 One-color dipole-bound anion formation spectrum for cyclobutanone (top) and fitting to curve-crossing model (bottom).

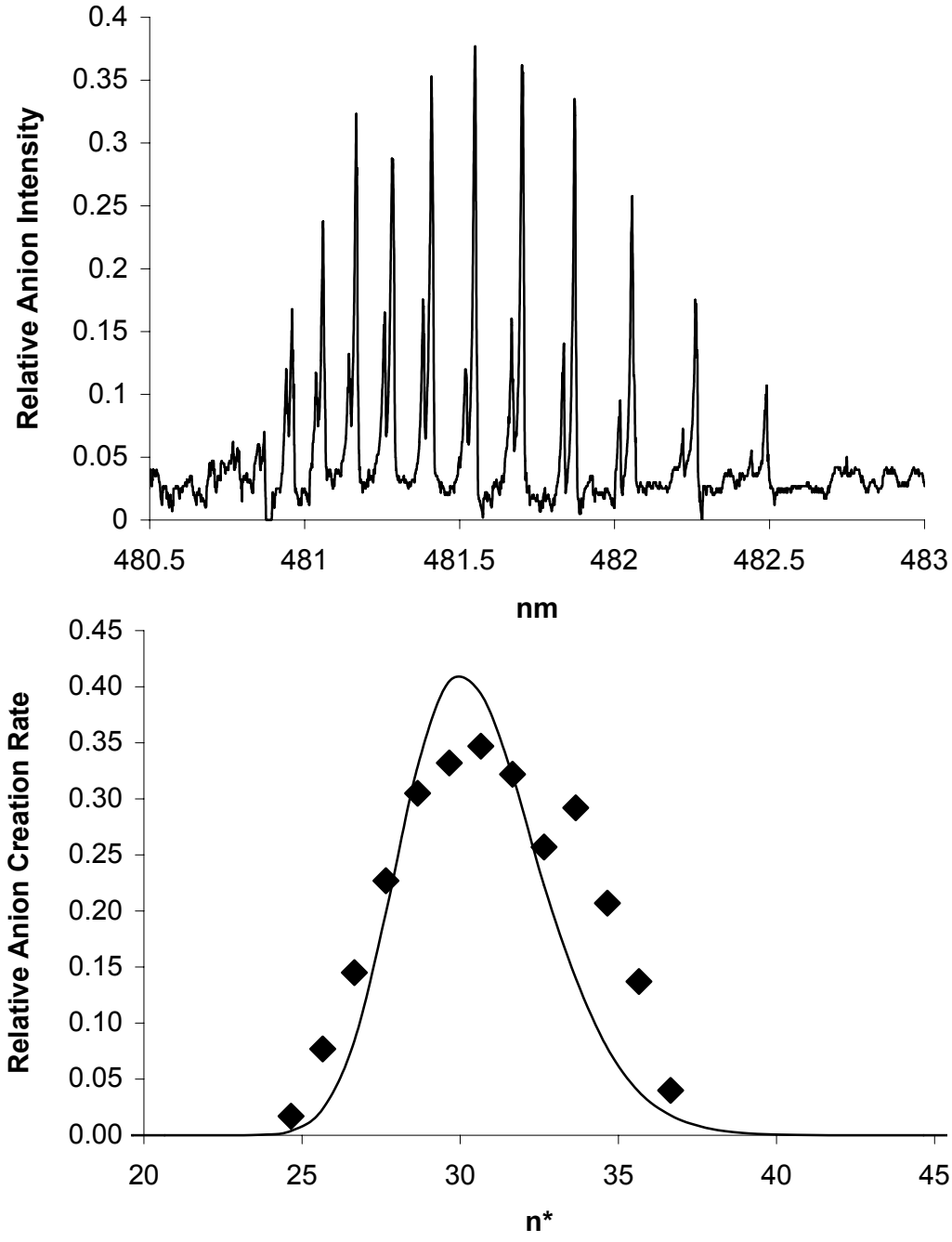

Figure B.6 Two-color dipole-bound anion formation spectrum for 2-methyl-propanal (top) and fitting to curve-crossing model (bottom).

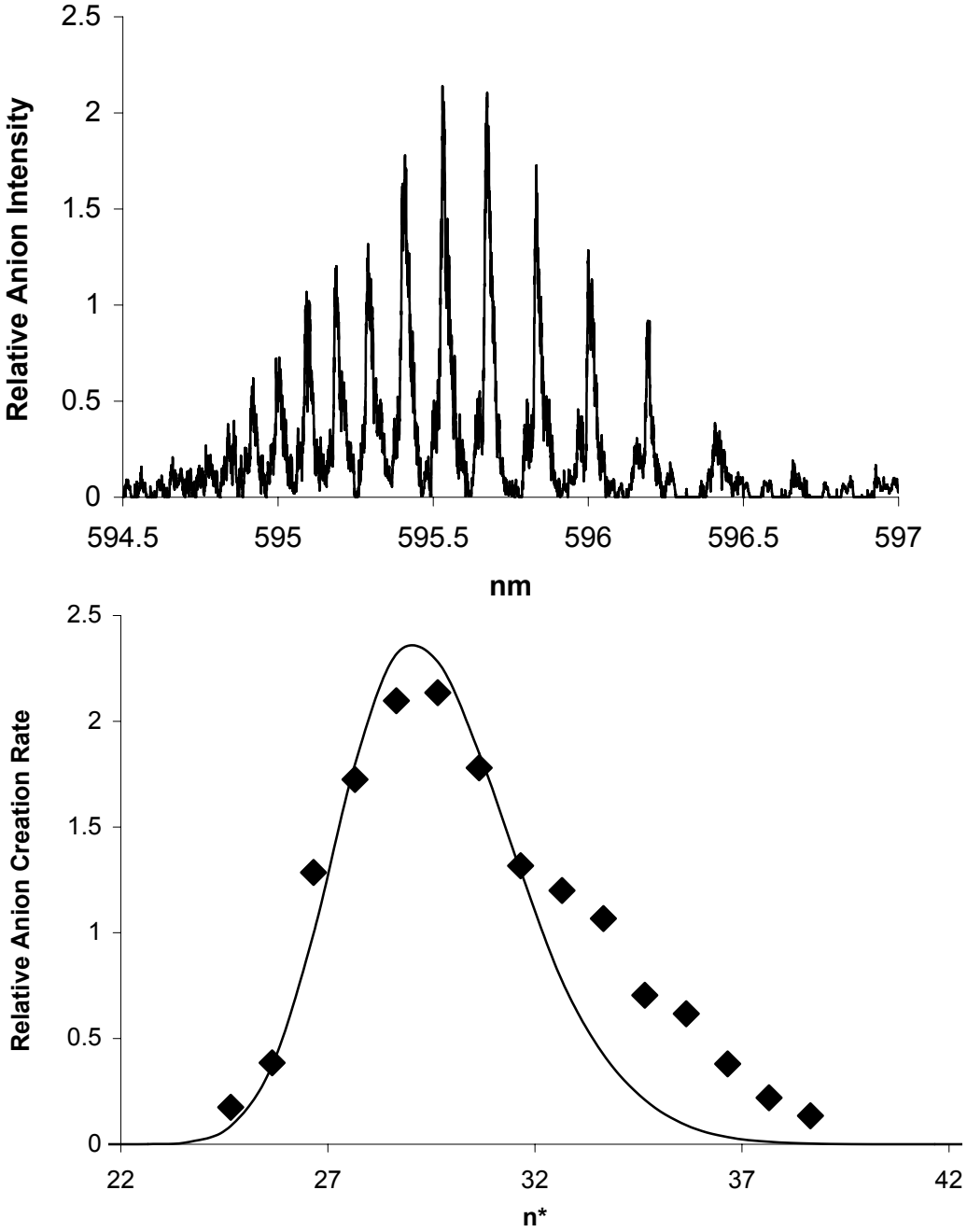

Figure B.7 One-color dipole-bound anion formation spectrum for butanal (top) and fitting to curve-crossing model (bottom).

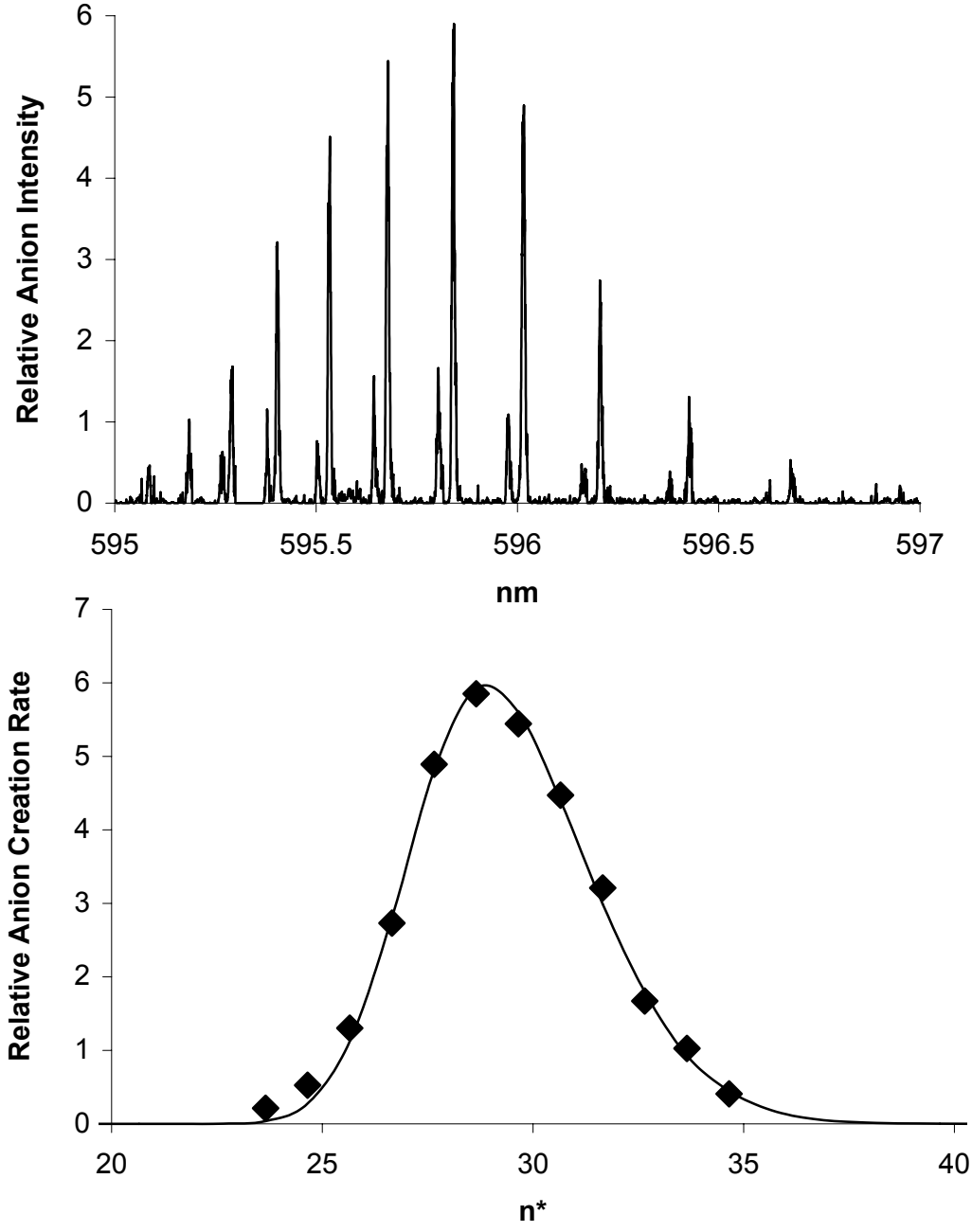

Figure B.8 One-color dipole-bound anion formation spectrum for 2-butanaone (top) and fitting to curve-crossing model (bottom).

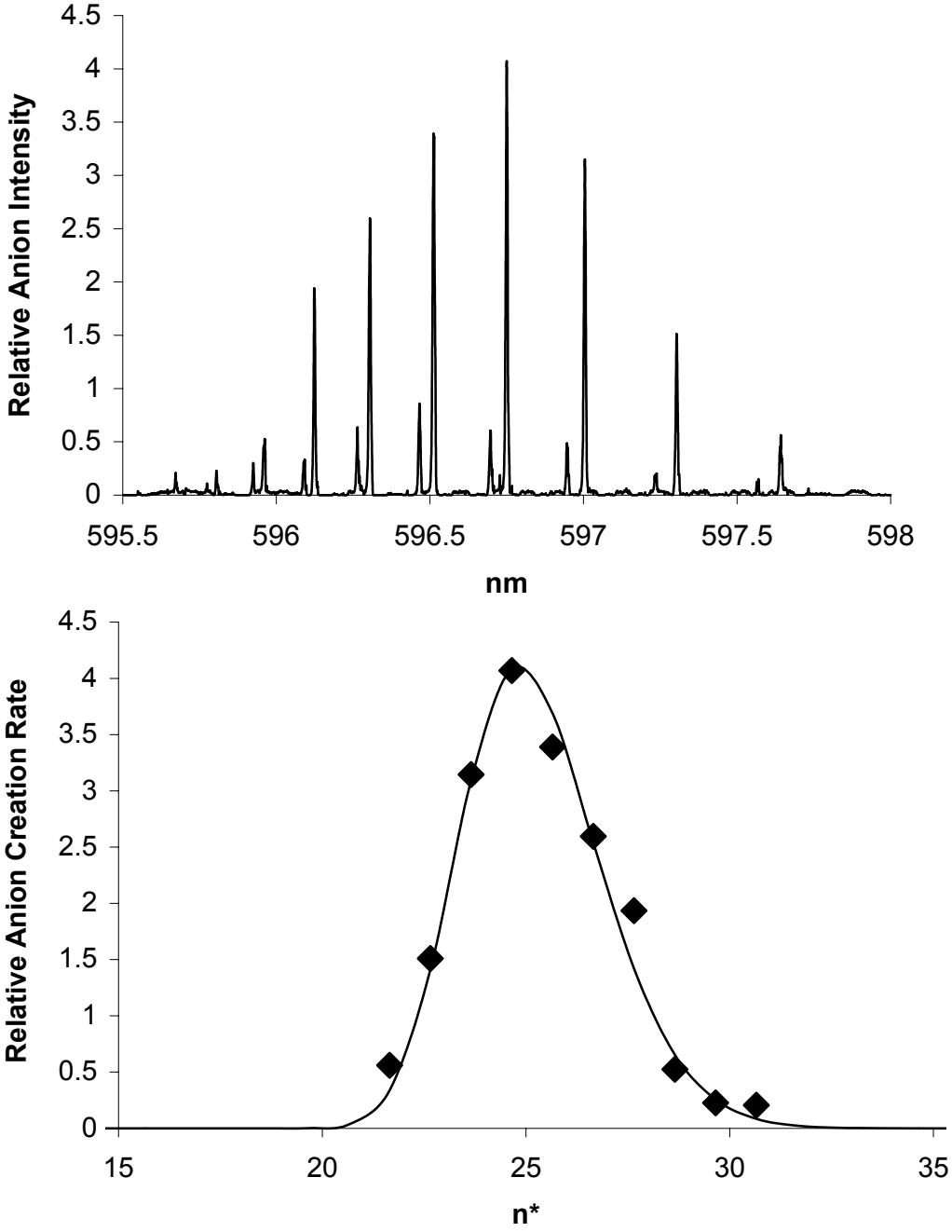

Figure B.9 One-color dipole-bound anion formation spectrum for cyclopentanone (top) and fitting to curve-crossing model (bottom).

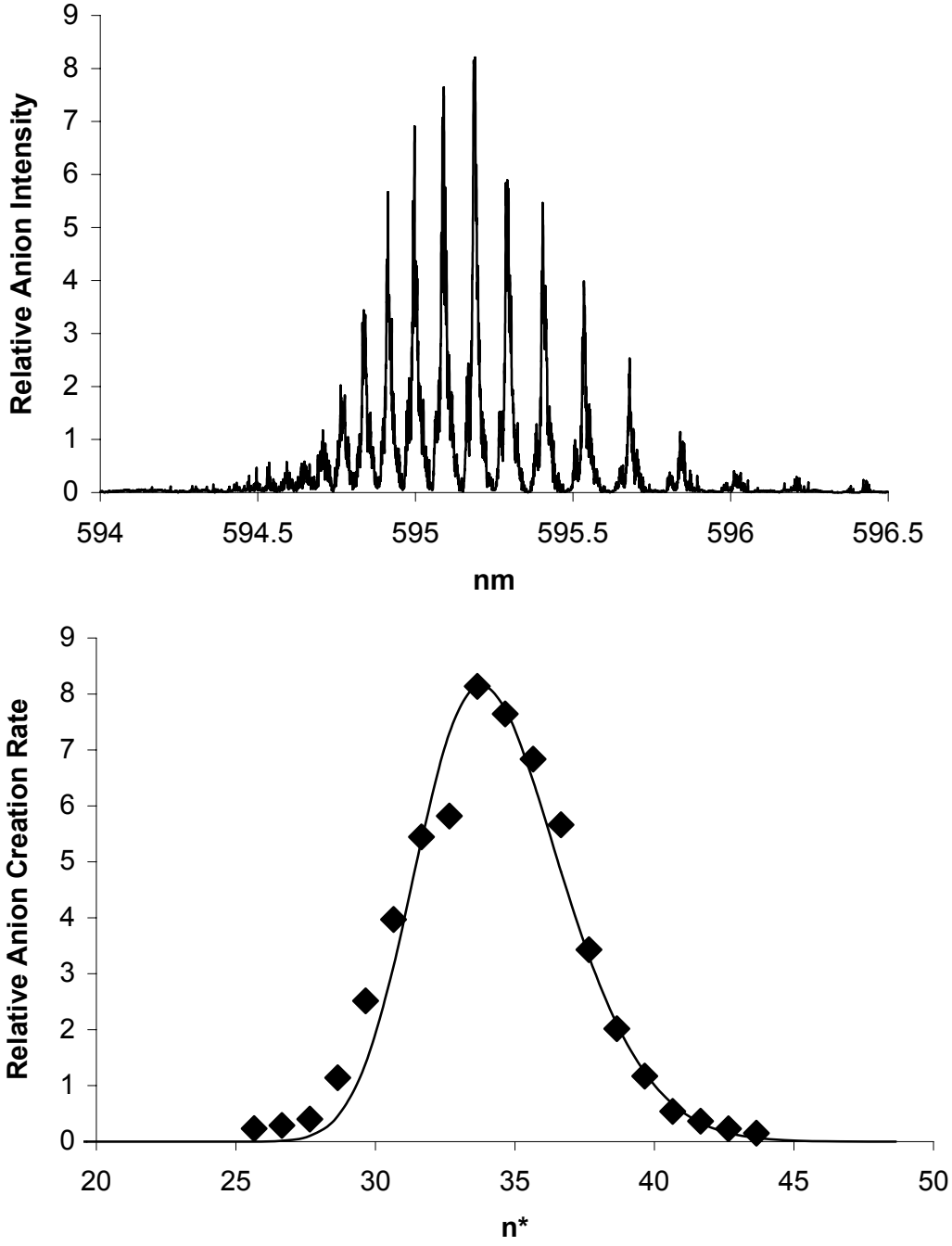

Figure B.10 One-color dipole-bound anion formation spectrum for pivaldehyde (top) and fitting to curve-crossing model (bottom).

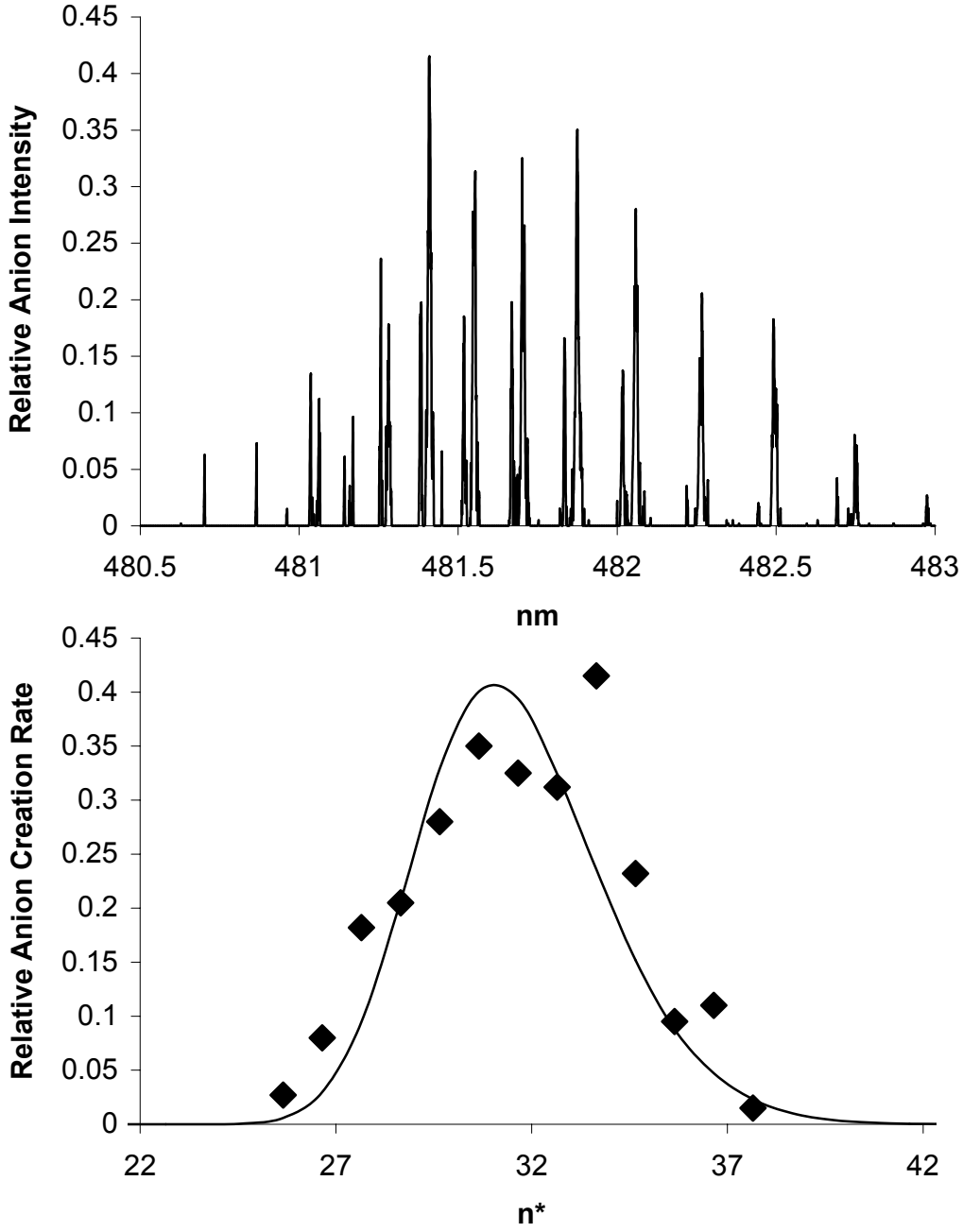

Figure B.11 Two-color dipole-bound anion formation spectrum for 2-ethylbutanal (top) and fitting to curve-crossing model (bottom).

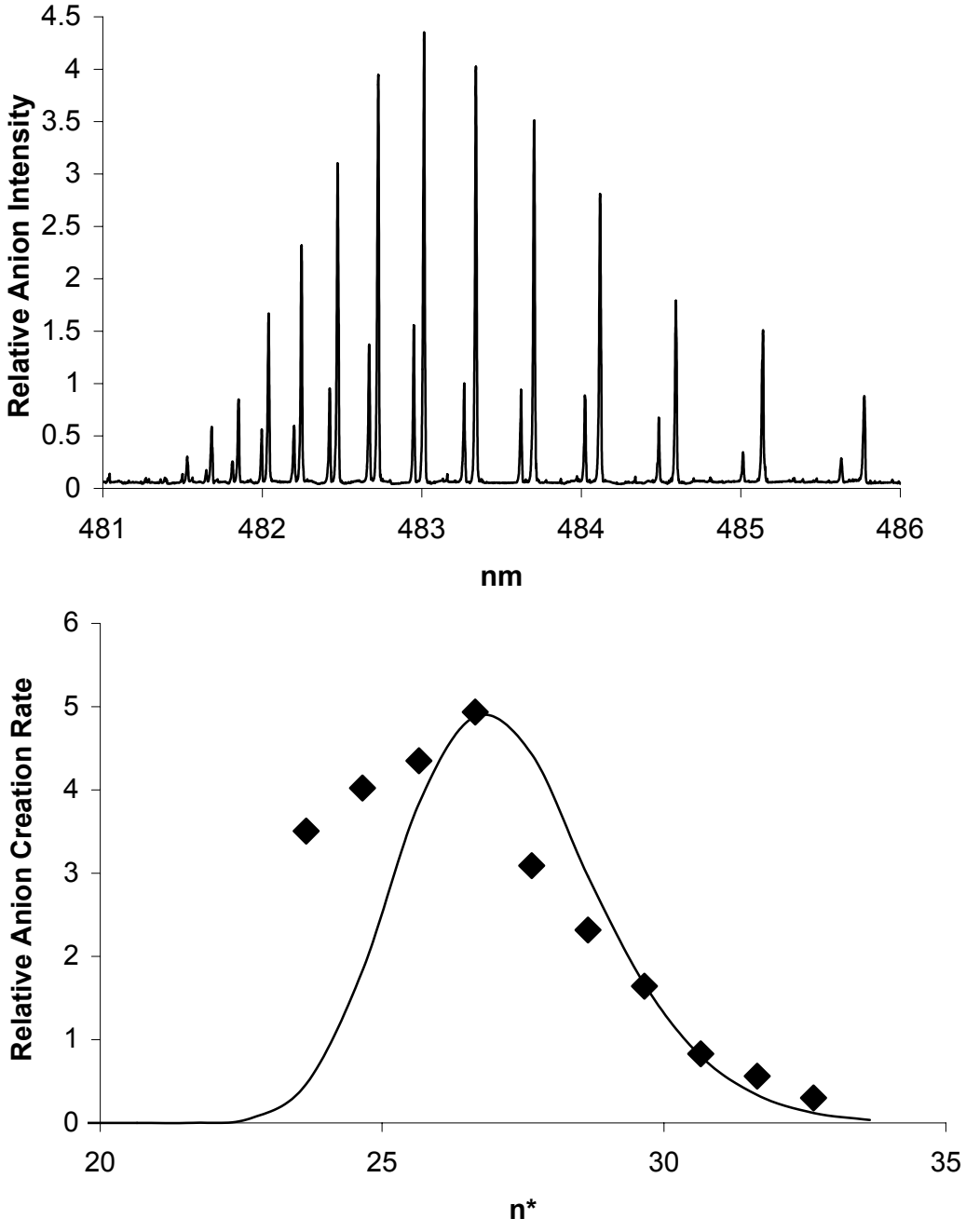

Figure B.12 Two-color dipole-bound anion formation spectrum for 2-methyl-cyclopentanone (top) and fitting to curve-crossing model (bottom). Contamination from 3-methylcyclopentanone is evident at n^* less than 24.

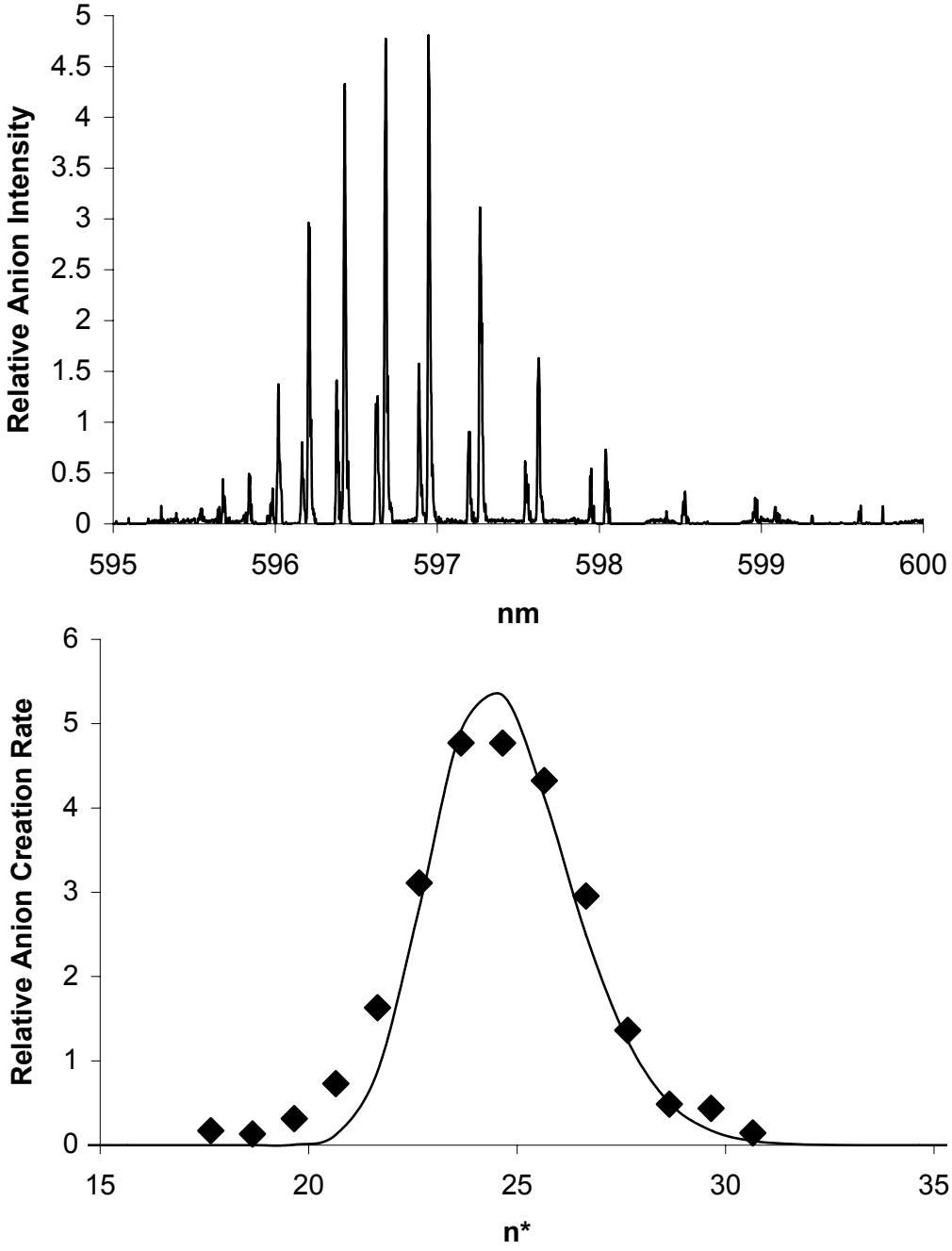

Figure B.13 One-color dipole-bound anion formation spectrum for 2-methyl-cyclopentanone (top) and fitting to curve-crossing model (bottom).

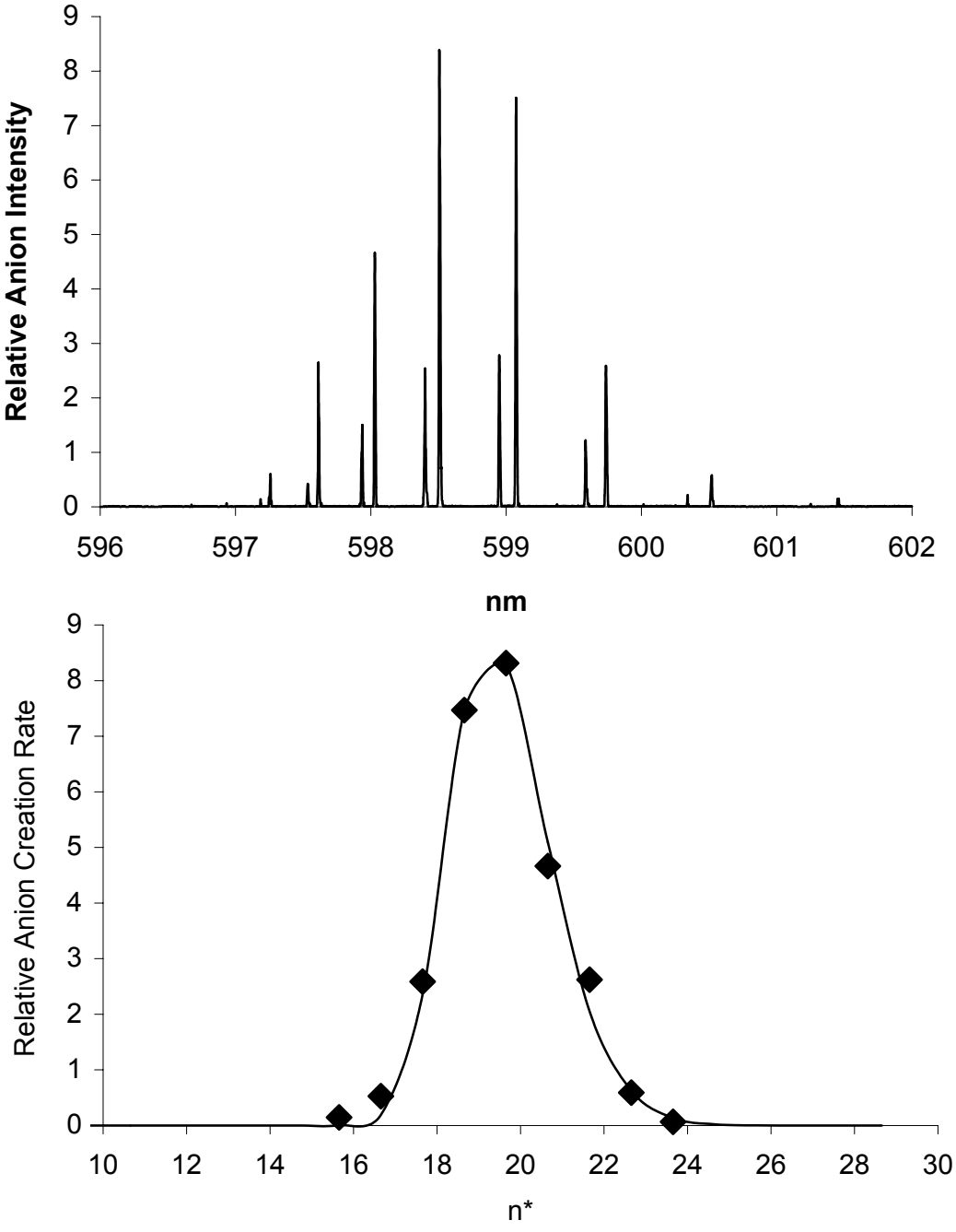

Figure B.14 One-color dipole-bound anion formation spectrum for cyclohexanone (top) and fitting to curve-crossing model (bottom).

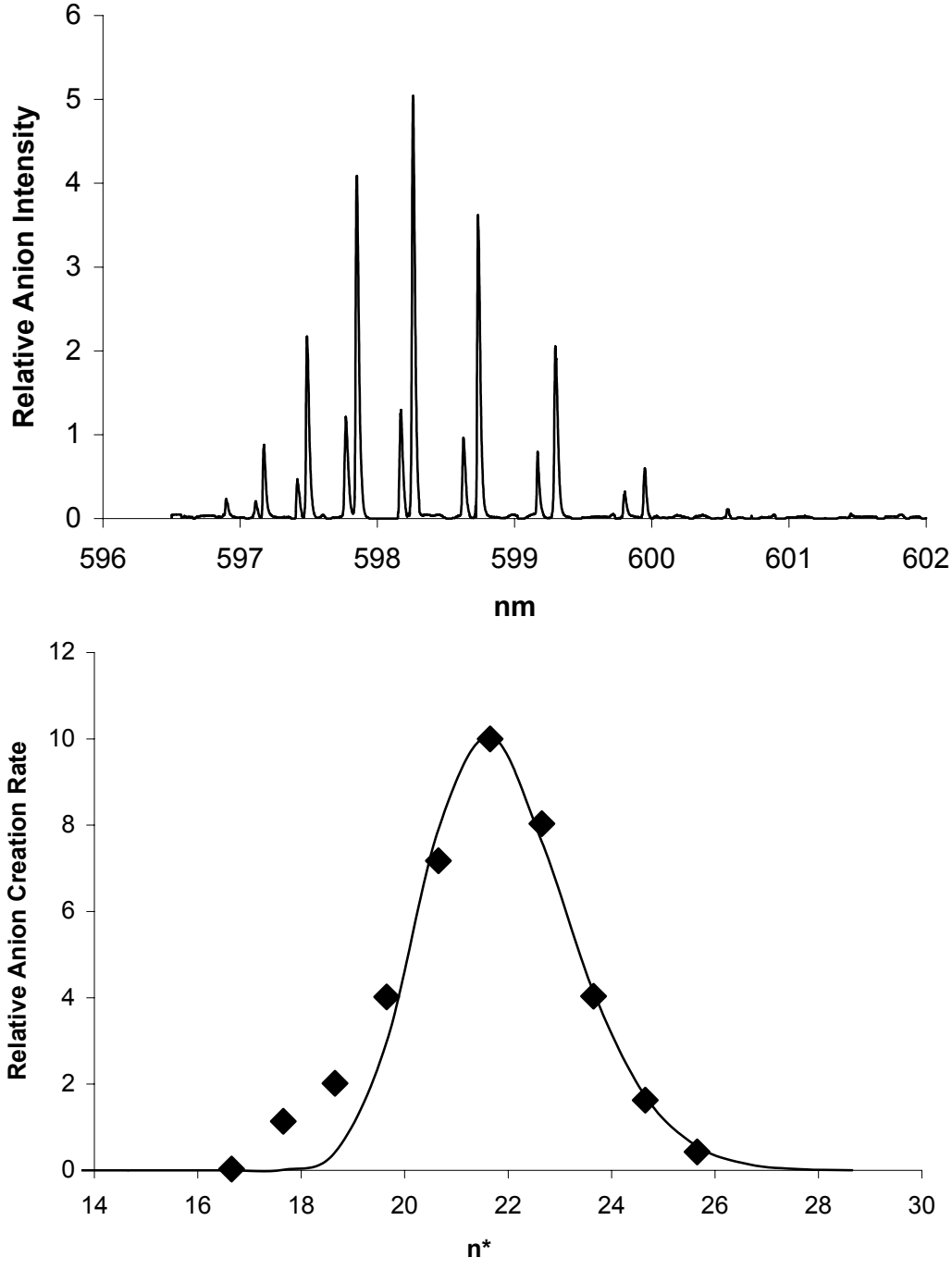

Figure B.15 One-color dipole-bound anion formation spectrum for 2-methyl-cyclohexanone (top) and fitting to curve-crossing model (bottom).

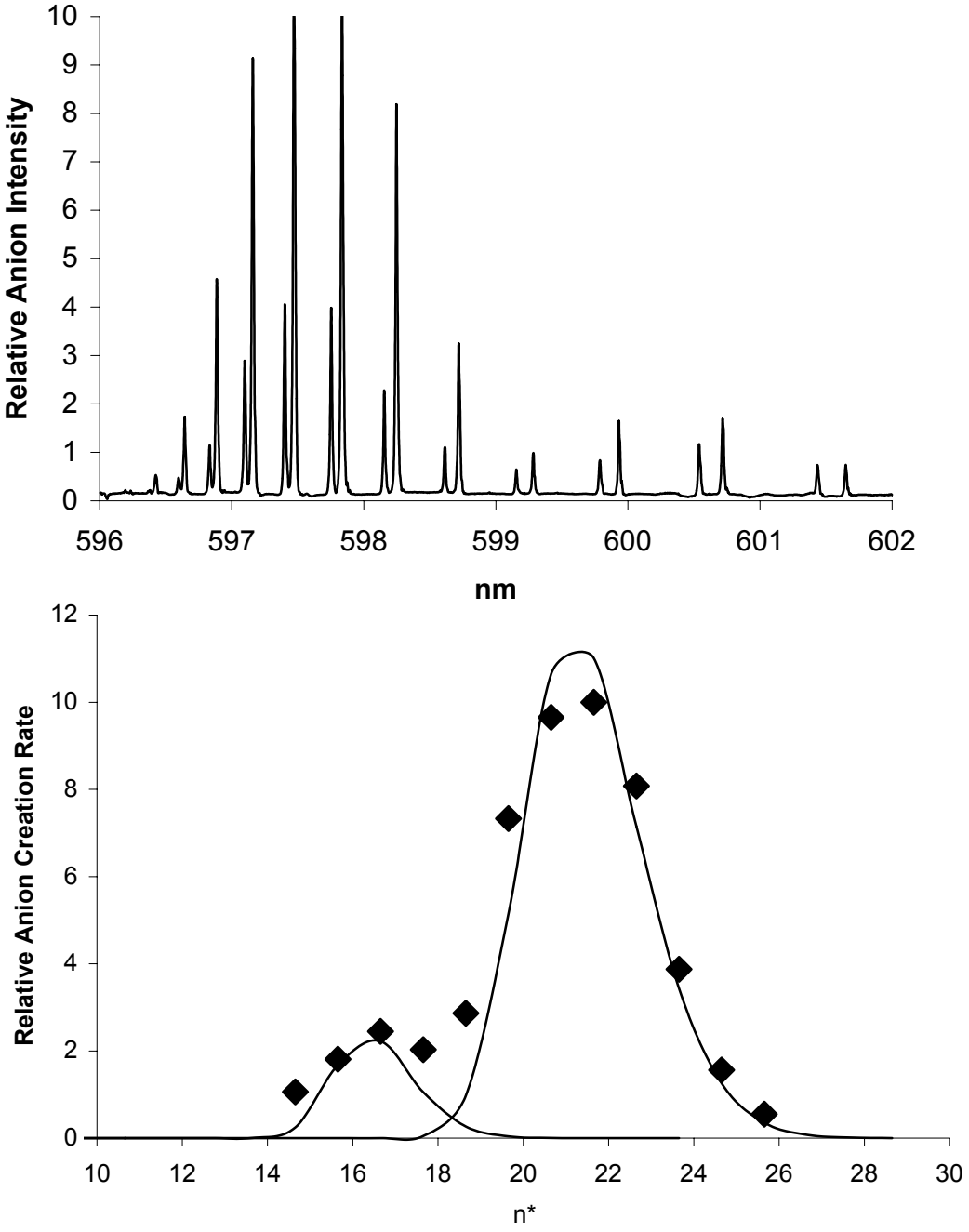

Figure B.16 One-color dipole-bound anion formation spectrum for 3-methyl-cyclohexanone (top) and fitting to curve-crossing model (bottom).

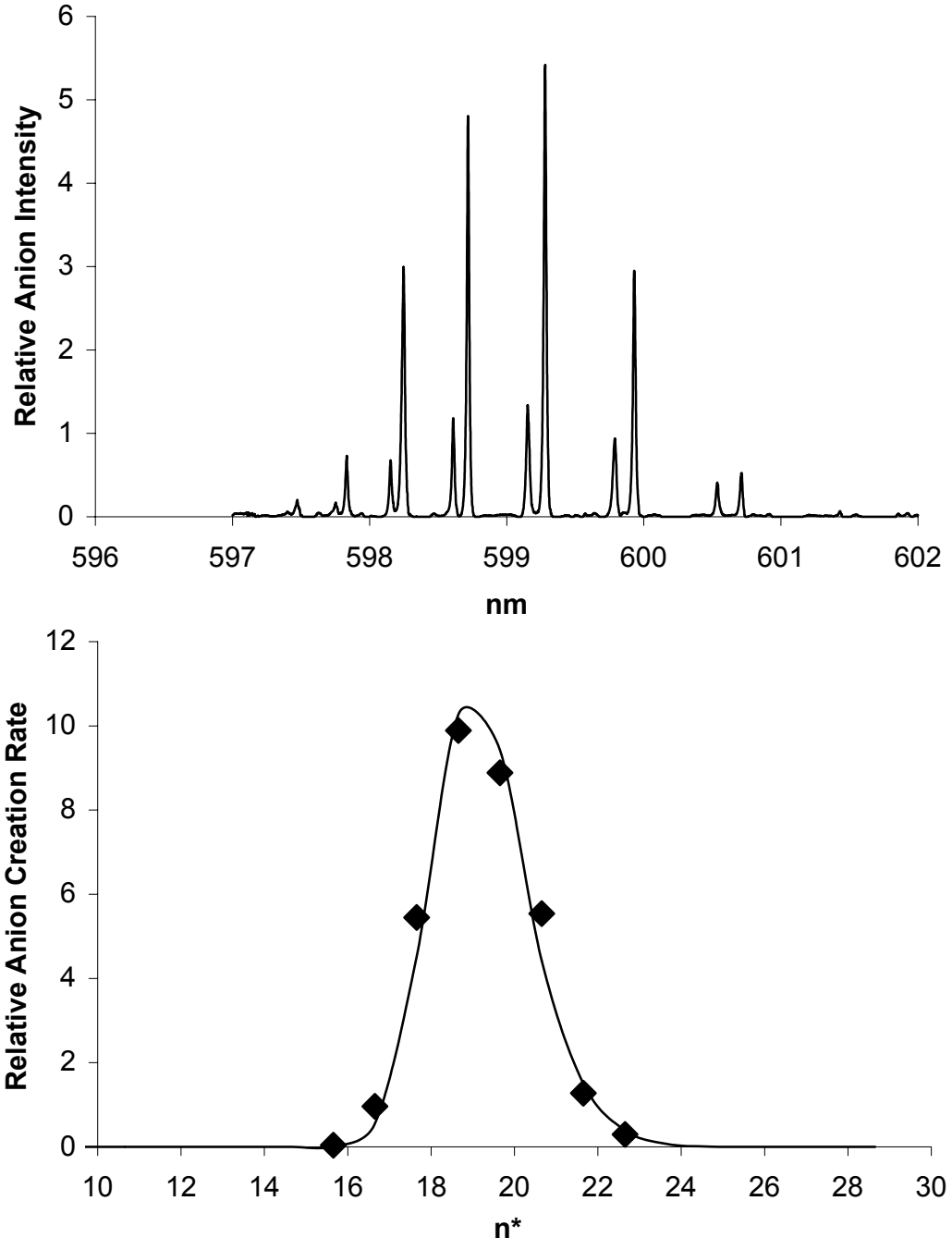

Figure B.17 One-color dipole-bound anion formation spectrum for 4-methyl-cyclohexanone (top) and fitting to curve-crossing model (bottom).

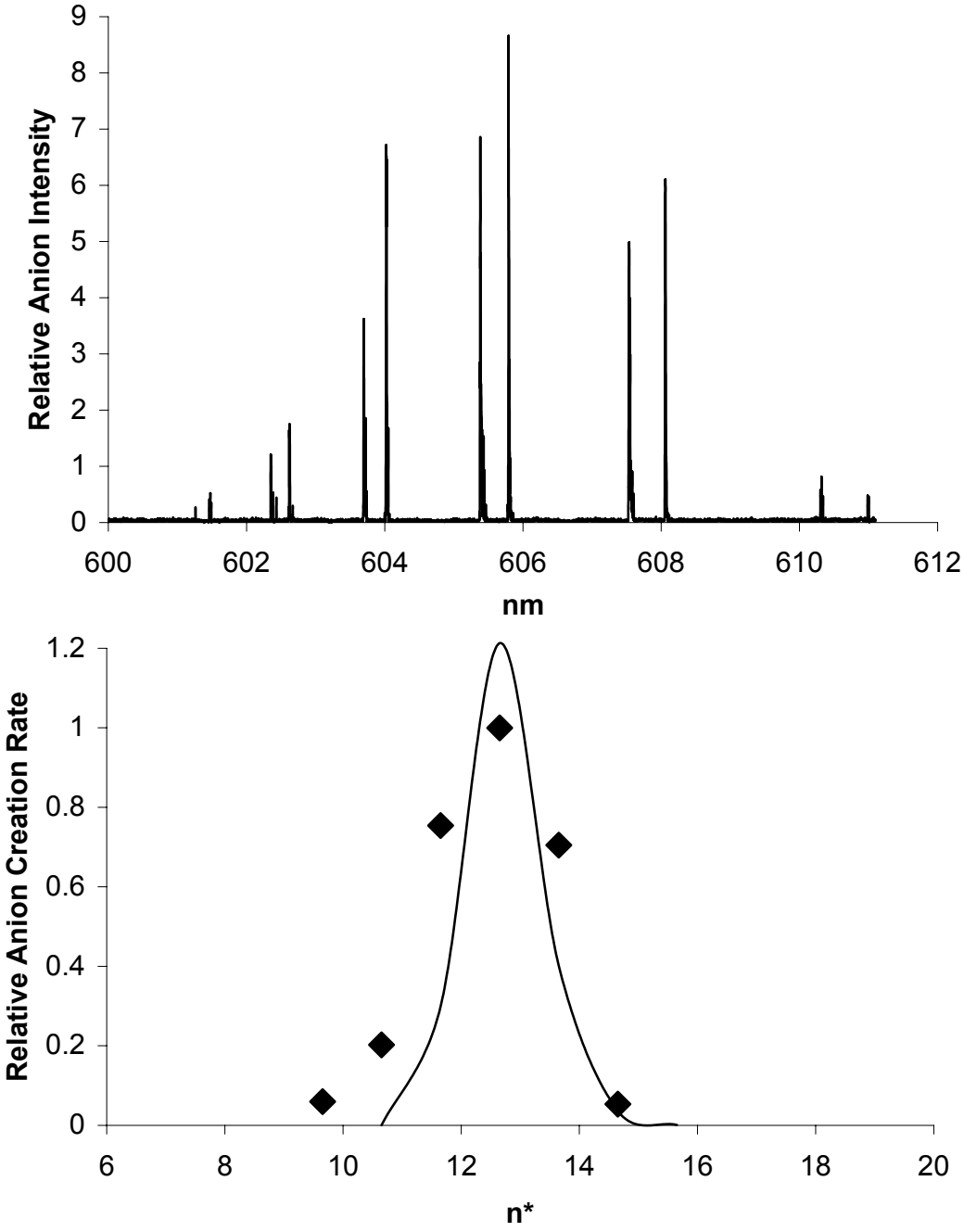

Figure B.18 One-color dipole-bound anion formation spectrum for acetonitrile (top) and fitting to curve-crossing model (bottom).

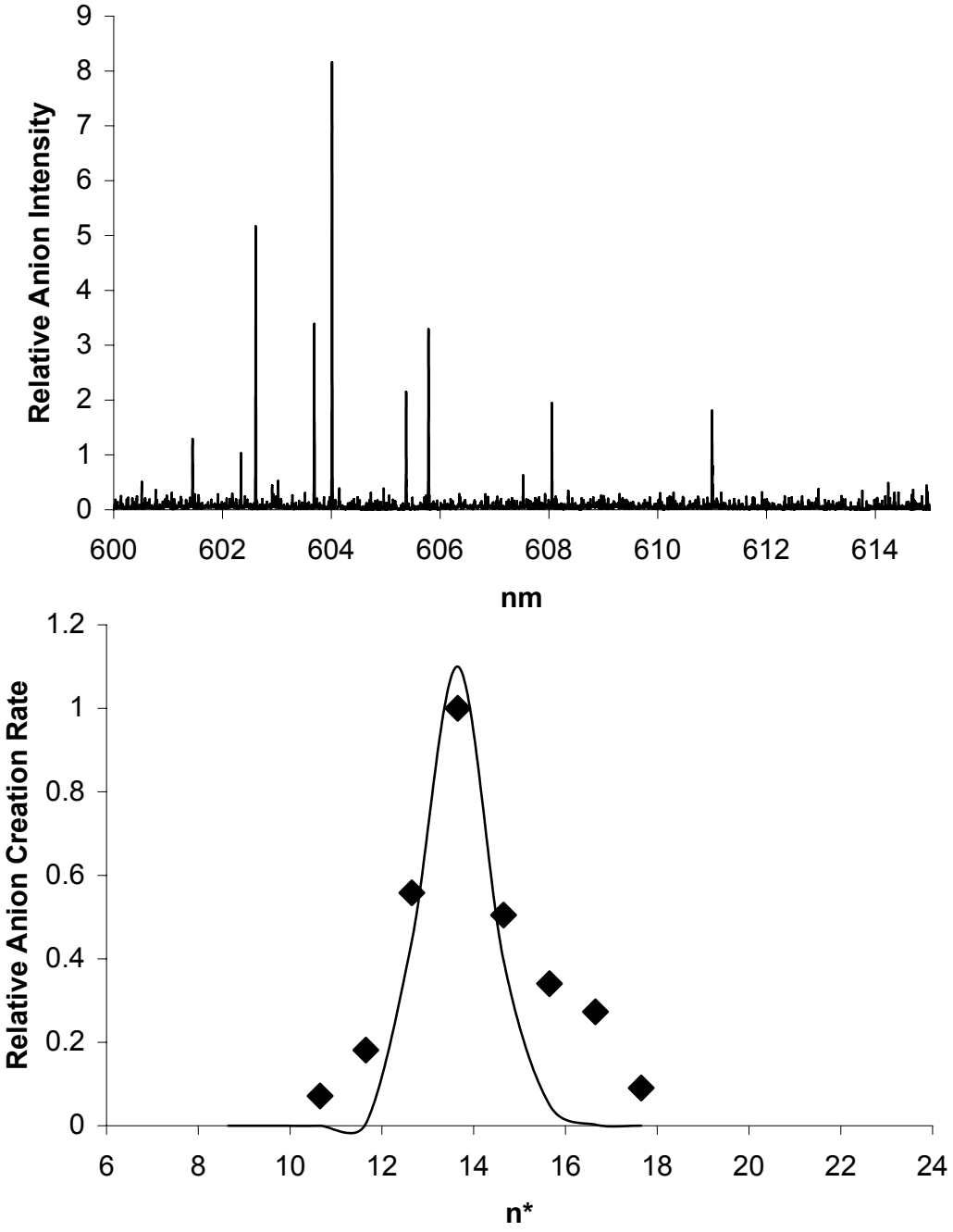

Figure B.19 One-color dipole-bound anion formation spectrum for propanenitrile (top) and fitting to curve-crossing model (bottom).

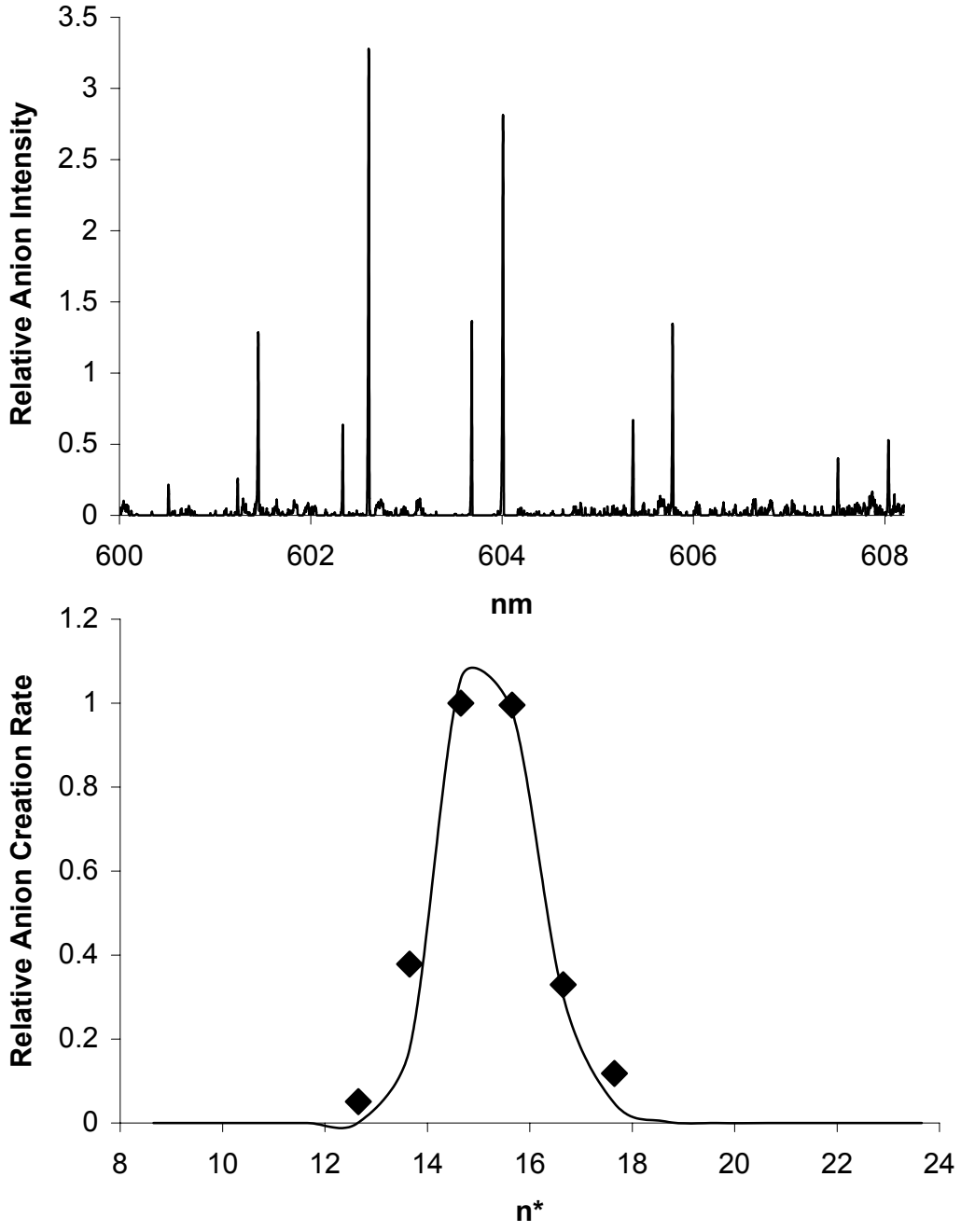

Figure B.20 One-color dipole-bound anion formation spectrum for 2-methyl-propanenitrile (top) and fitting to curve-crossing model (bottom).

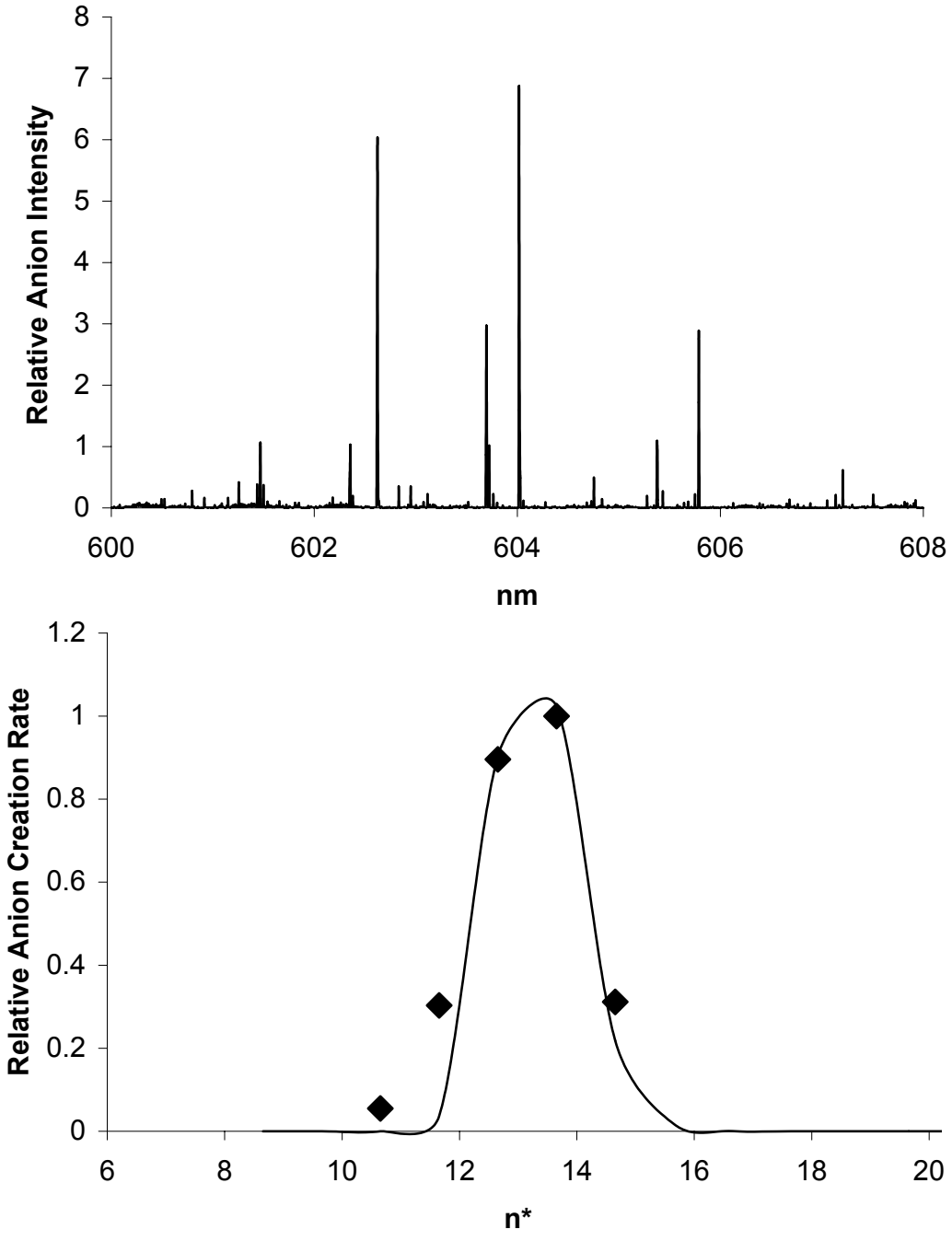

Figure B.21 One-color dipole-bound anion formation spectrum for butanenitrile (top) and fitting to curve-crossing model (bottom).

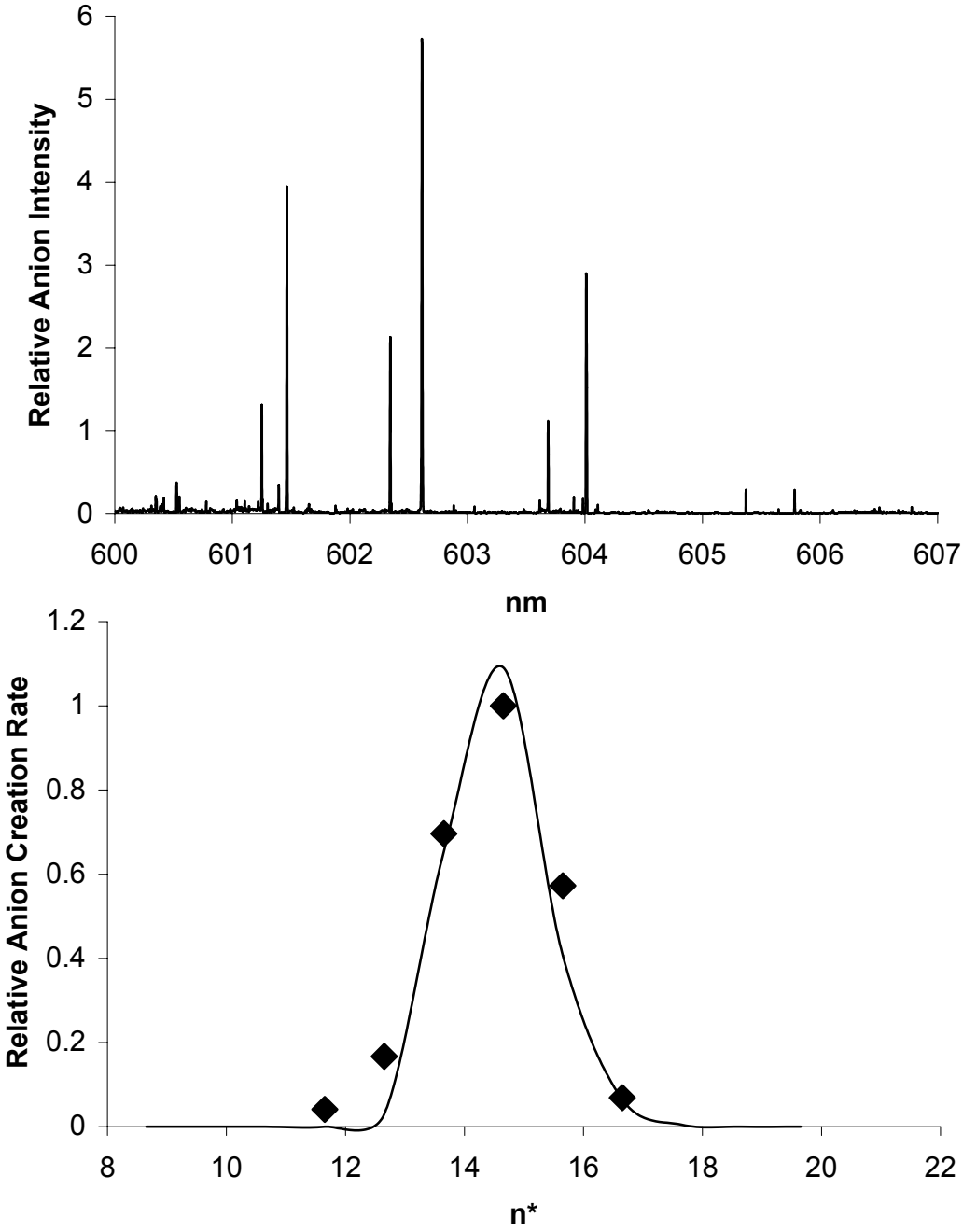

Figure B.22 One-color dipole-bound anion formation spectrum for 2,2-dimethyl-propnaenitrile (top) and fitting to curve-crossing model (bottom).

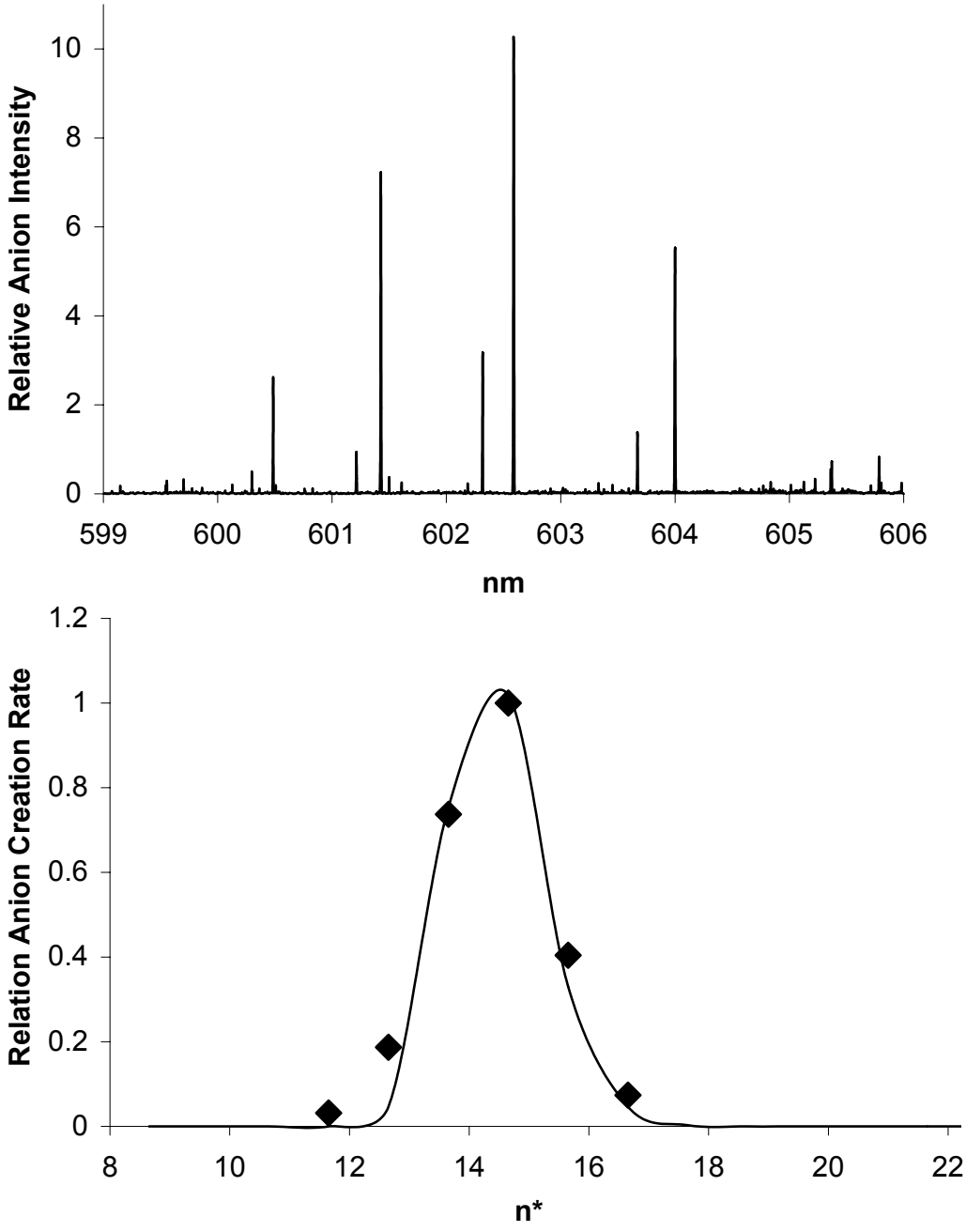

Figure B.23 One-color dipole-bound anion formation spectrum for 2-methyl-butanenitrile (top) and fitting to curve-crossing model (bottom).

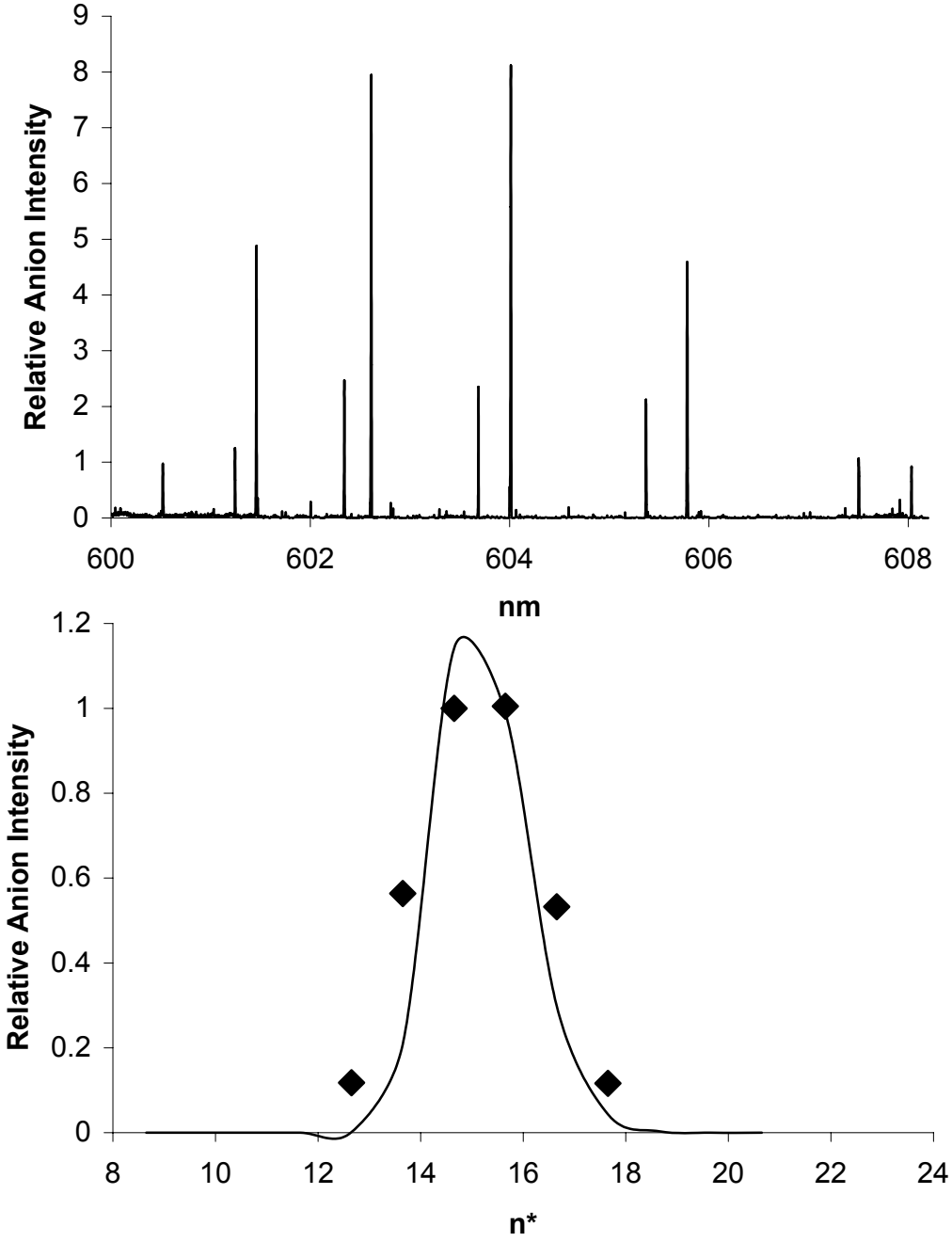

Figure B.24 One-color dipole-bound anion formation spectrum for 3-methyl-butanenitrile (top) and fitting to curve-crossing model (bottom).

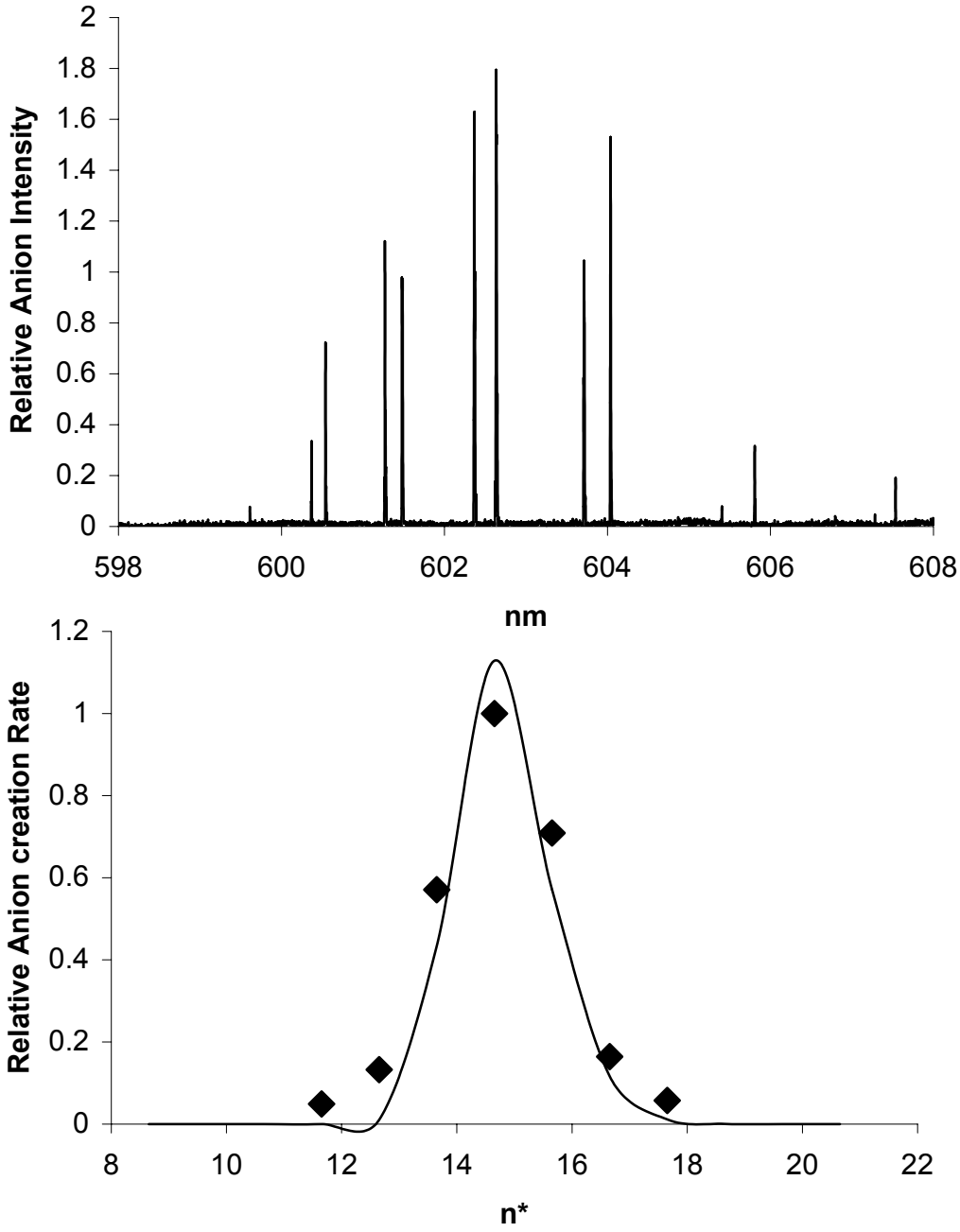

Figure B.25 One-color dipole-bound anion formation spectrum for pentanenitrile (top) and fitting to curve-crossing model (bottom).

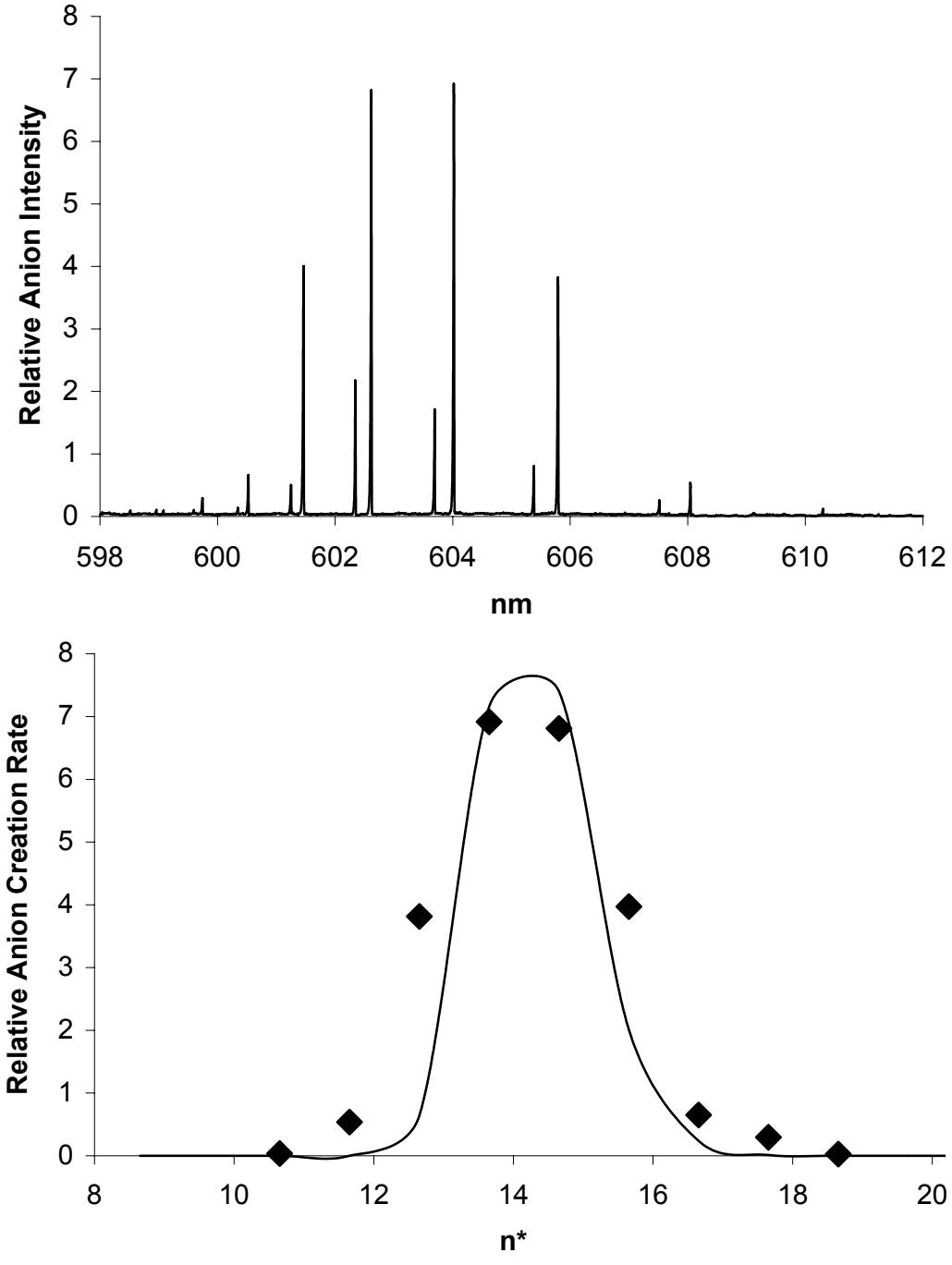

Figure B.26 One-color dipole-bound anion formation spectrum for dimethyl-sulfoxide (top) and fitting to curve-crossing model (bottom).

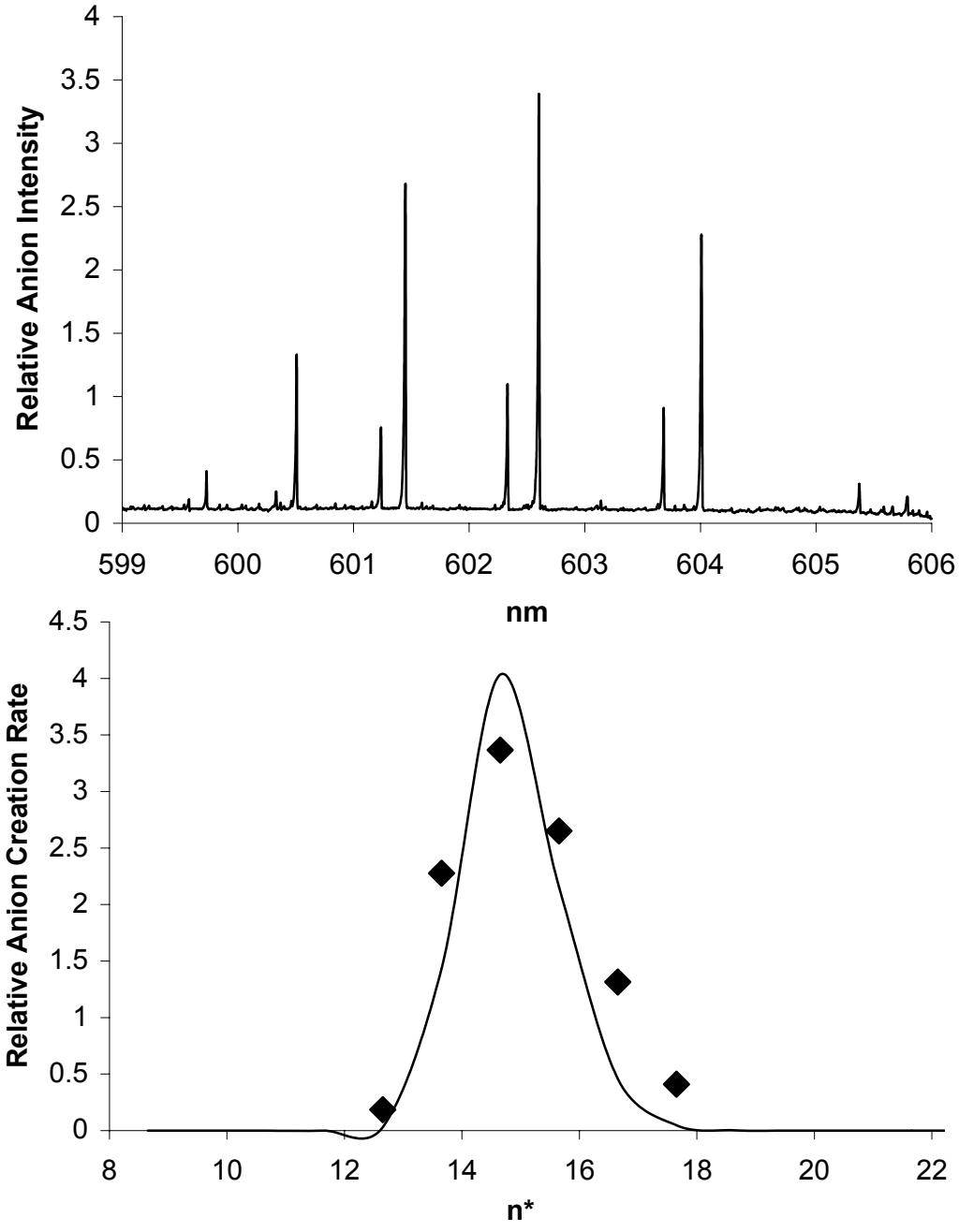

Figure B.27 One-color dipole-bound anion formation spectrum for methylethyl-sulfoxide (top) and fitting to curve-crossing model (bottom).

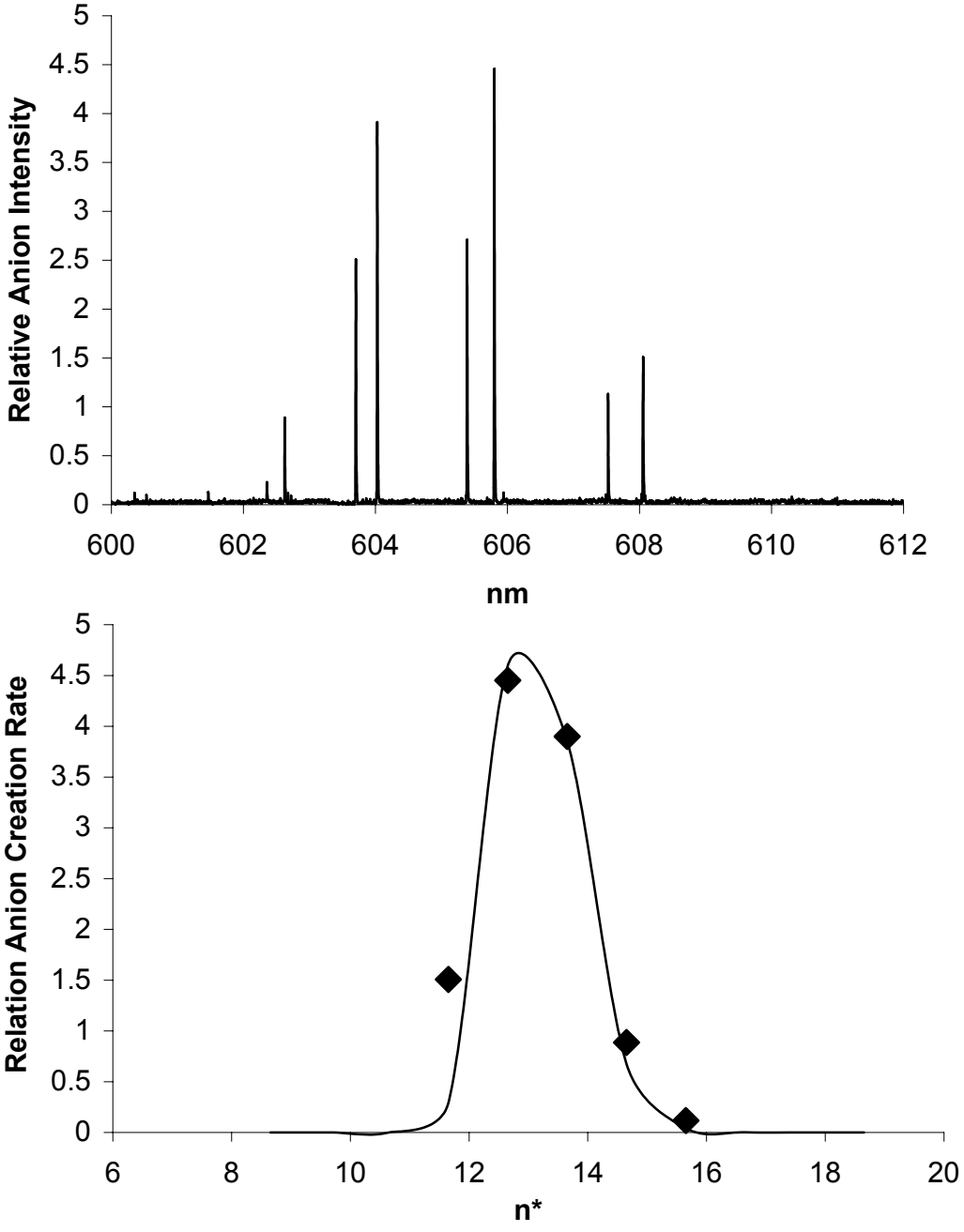

Figure B.28 One-color dipole-bound anion formation spectrum for tetra-methylene-sulfoxide (top) and fitting to curve-crossing model (bottom).

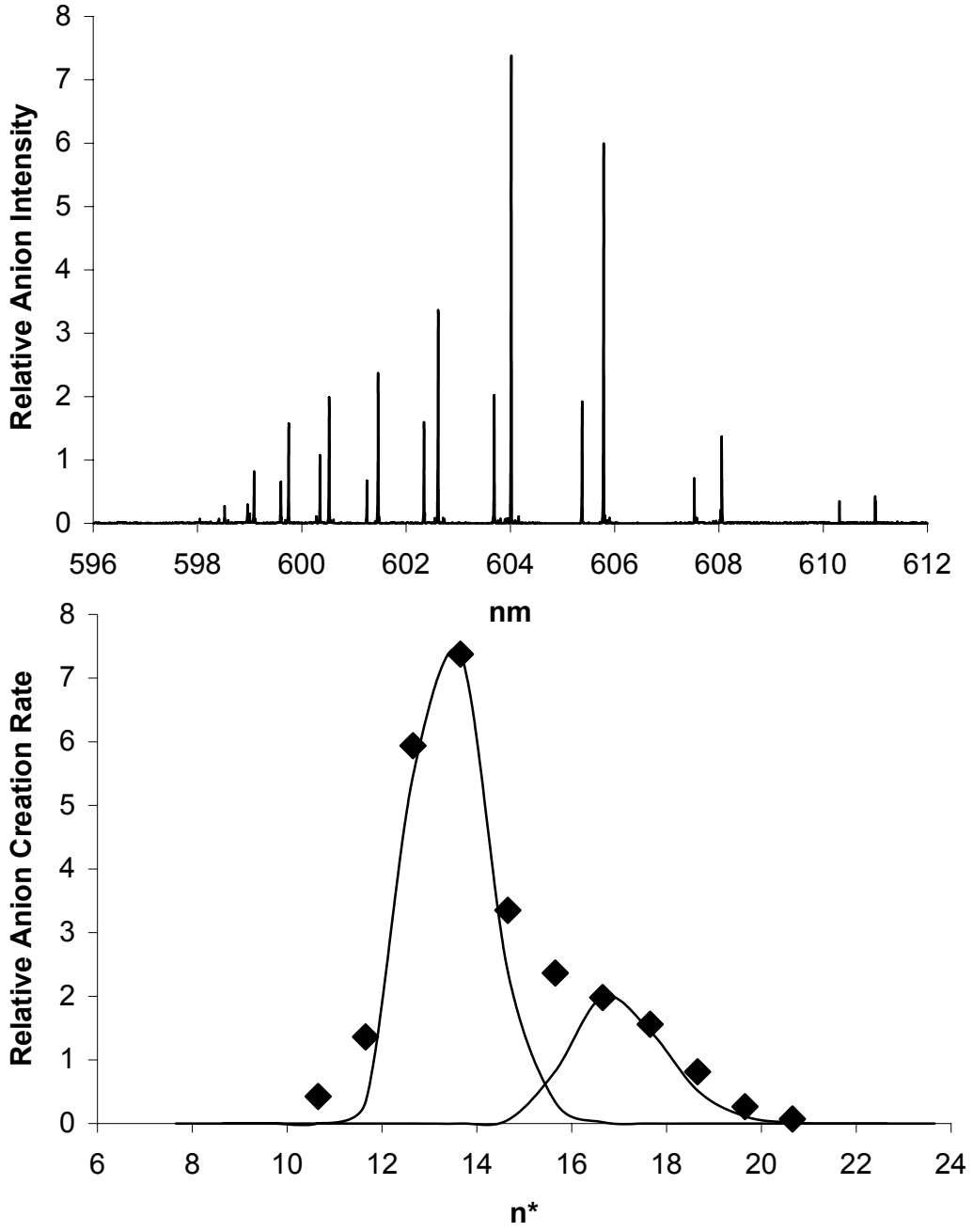

Figure B.29 One-color dipole-bound anion formation spectrum for glycol sulfite (top) and fitting to curve-crossing model (bottom).

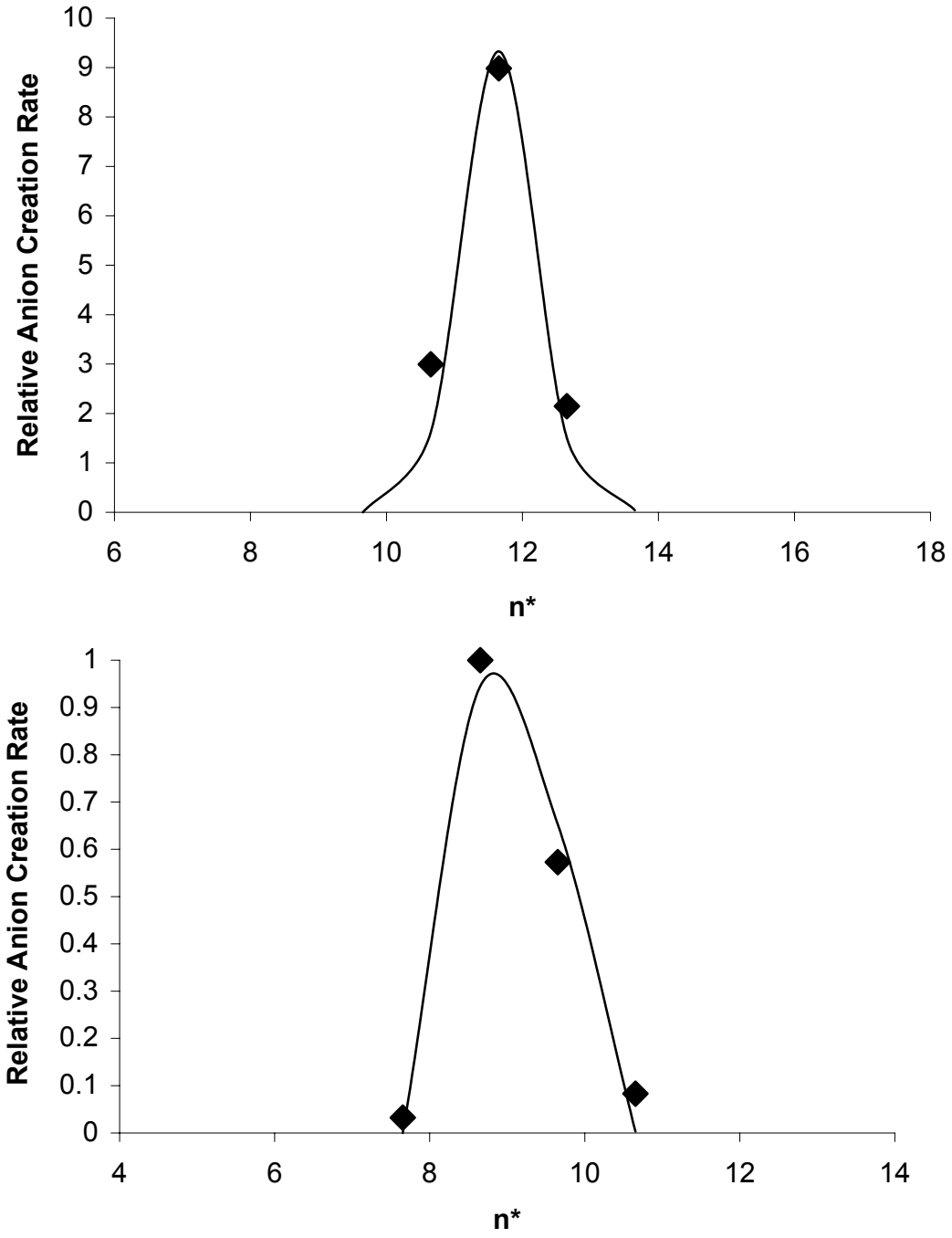

Figure B.30 Dipole-bound anion RET profile fittings to curve-crossing model for vinylene carbonate (top) and ethylene carbonate (bottom).

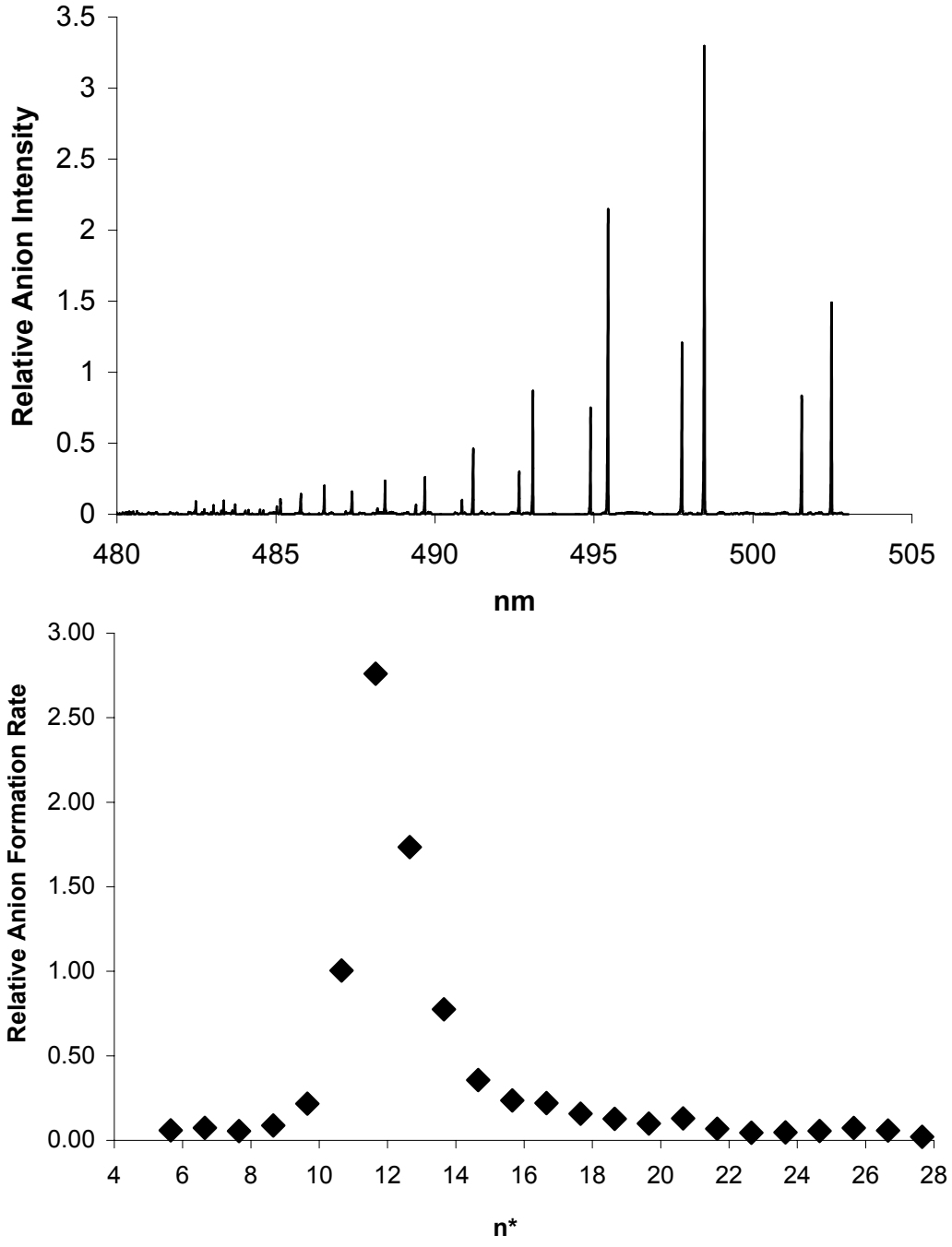

Figure B.31 Two-color negative ion formation spectrum for succinonitrile (top) and data over a wider range of n^* (bottom).

APPENDIX C: FIELD DETACHMENT CURVES

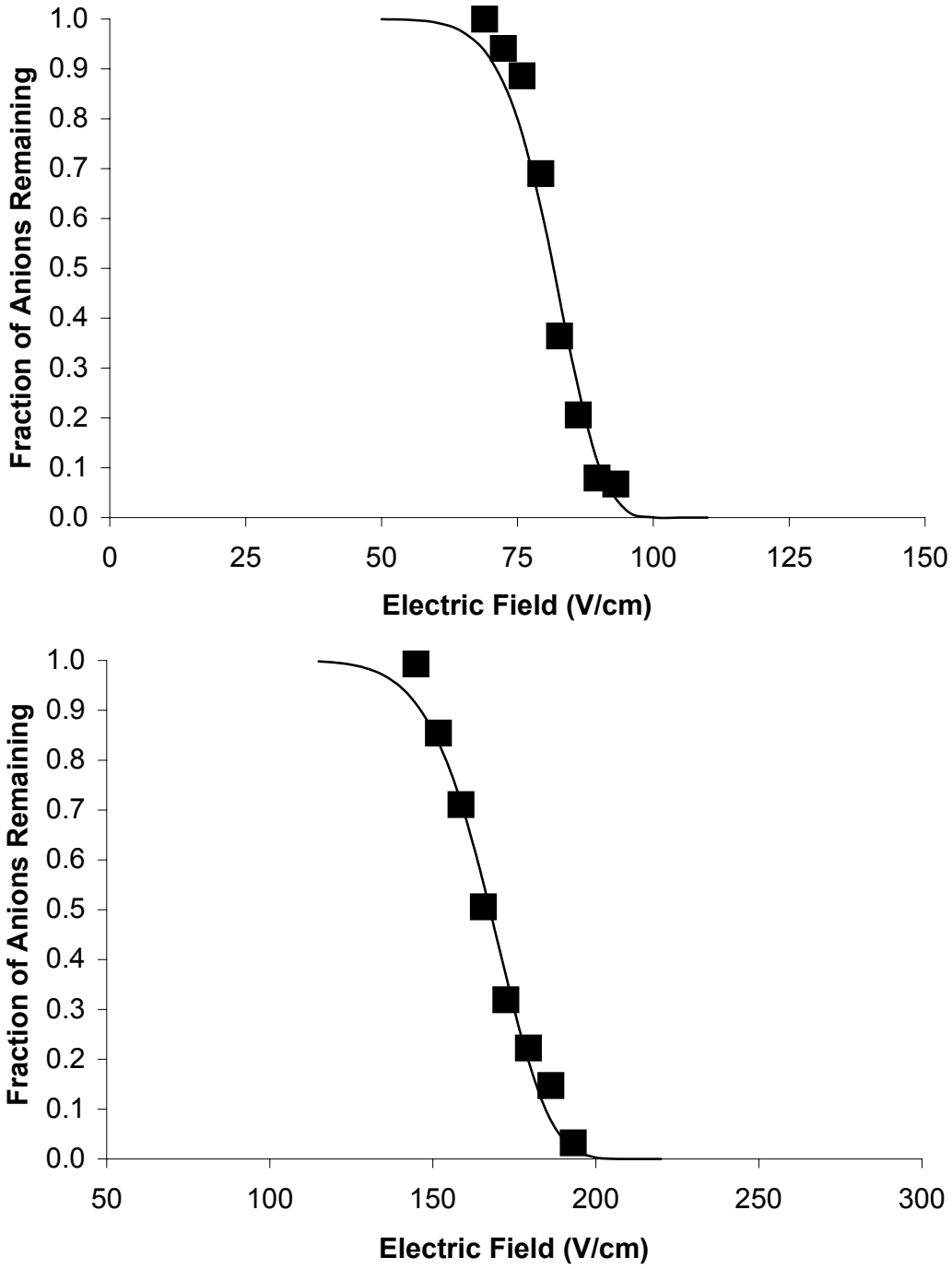

Figure C.1 Experimental electric field detachment curves and theoretical fits for acetaldehye and propanal.

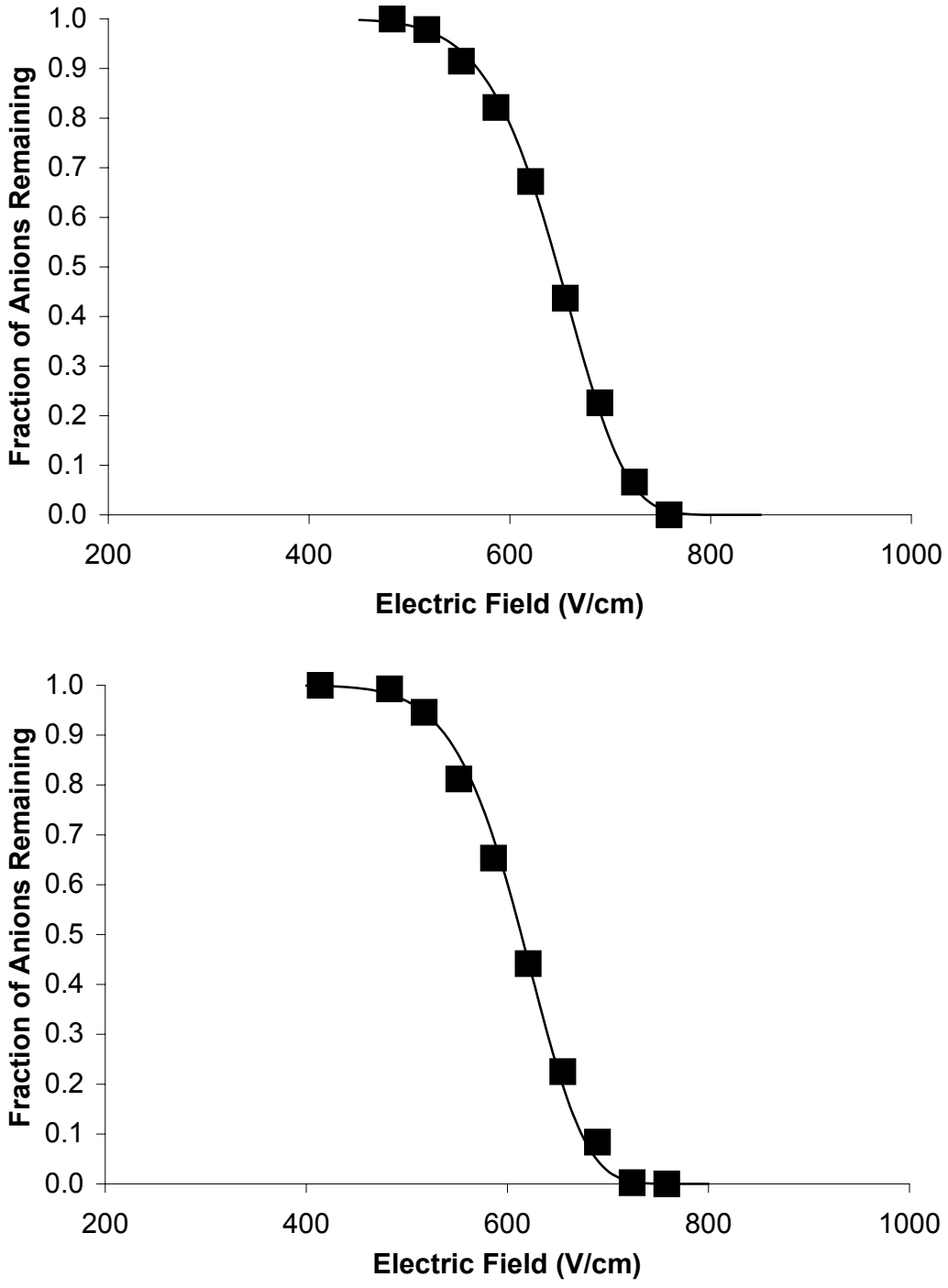

Figure C.2 Experimental electric field detachment curves and theoretical fits for acetone and perdeuterated acetone.

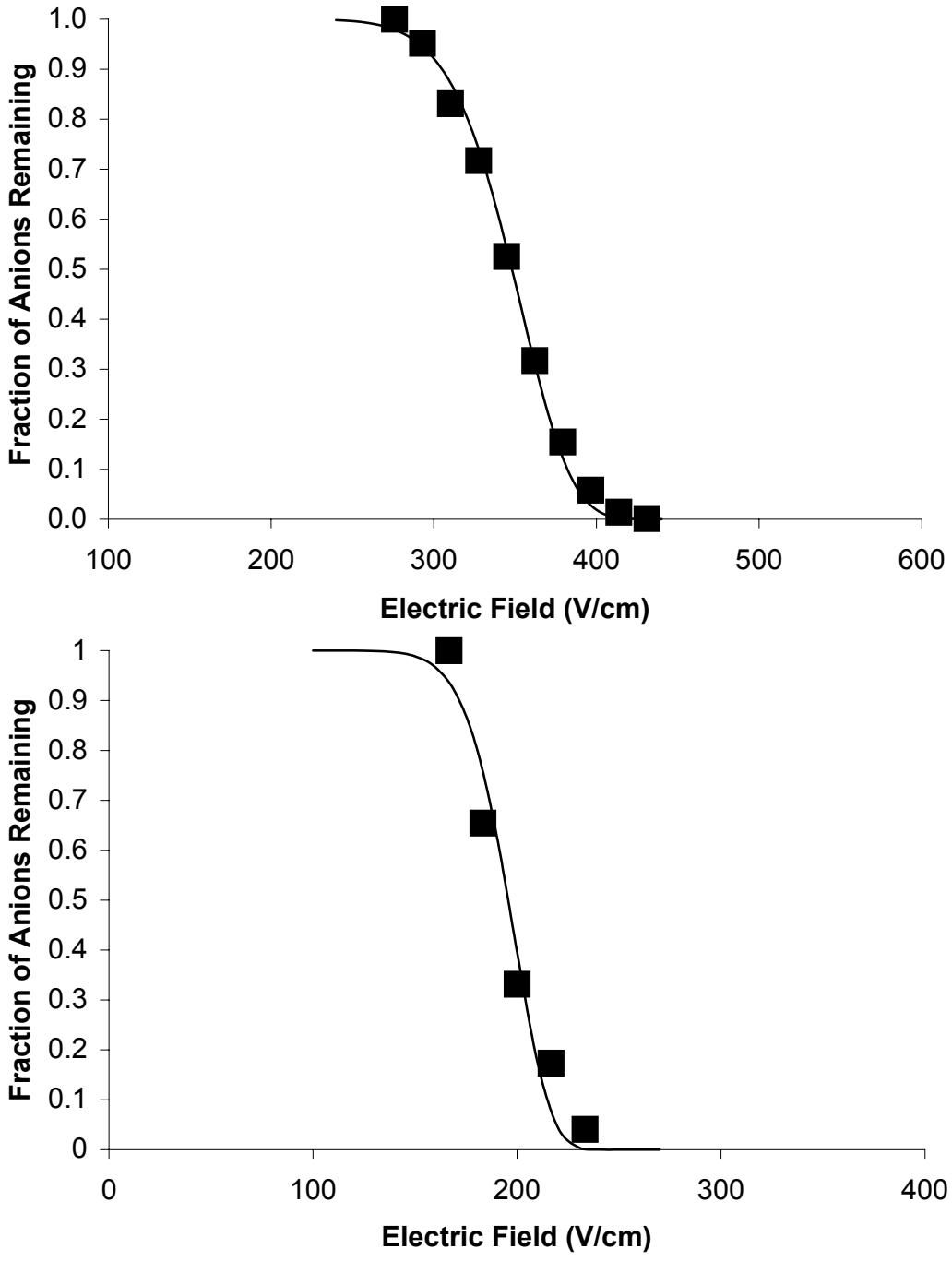

Figure C.3 Experimental electric field detachment curves and theoretical fits for cyclobutanone and 2-methylpropanal.

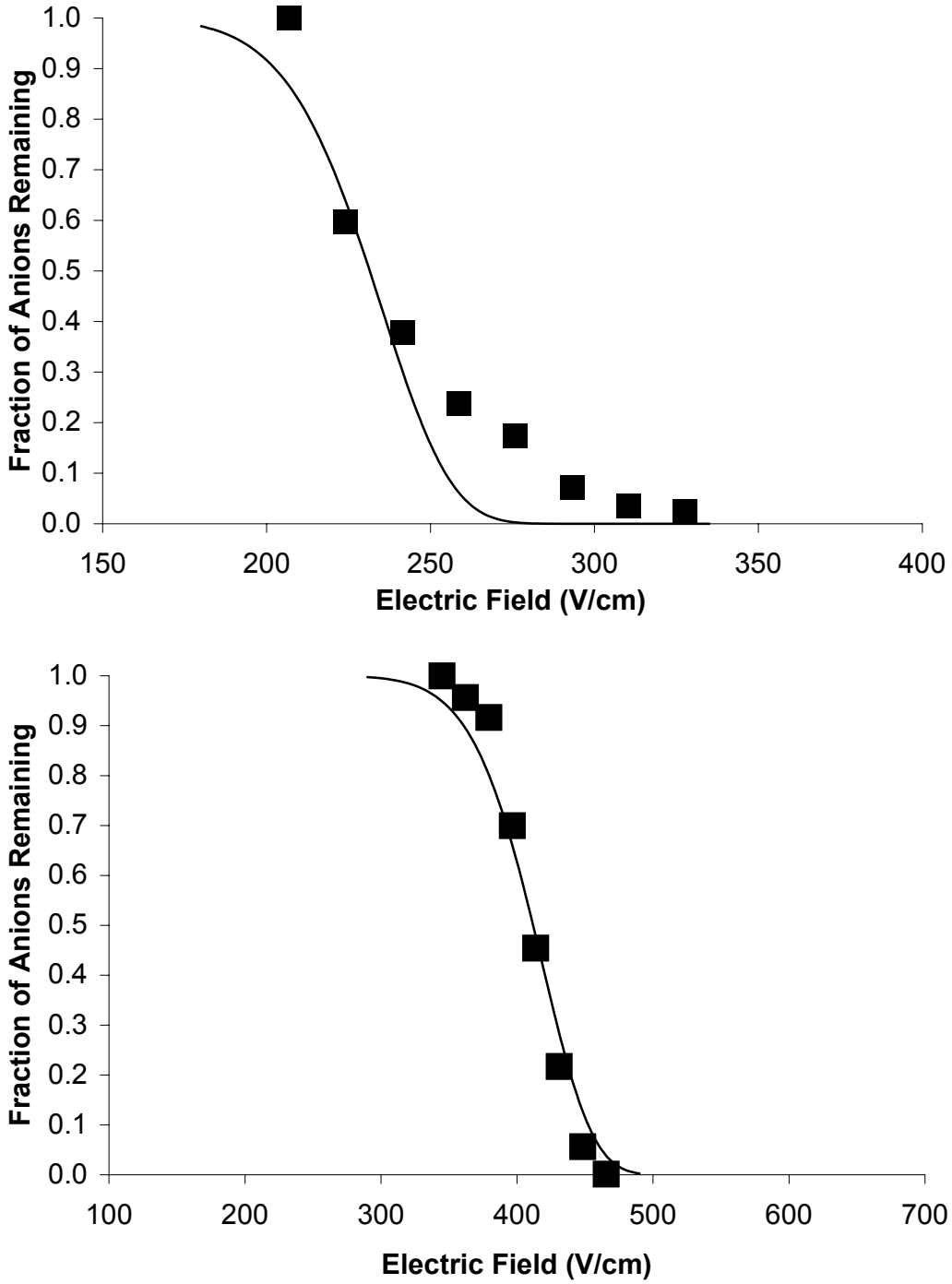

Figure C.4 Experimental electric field detachment curves and theoretical fits for butanal and 2-butanone.

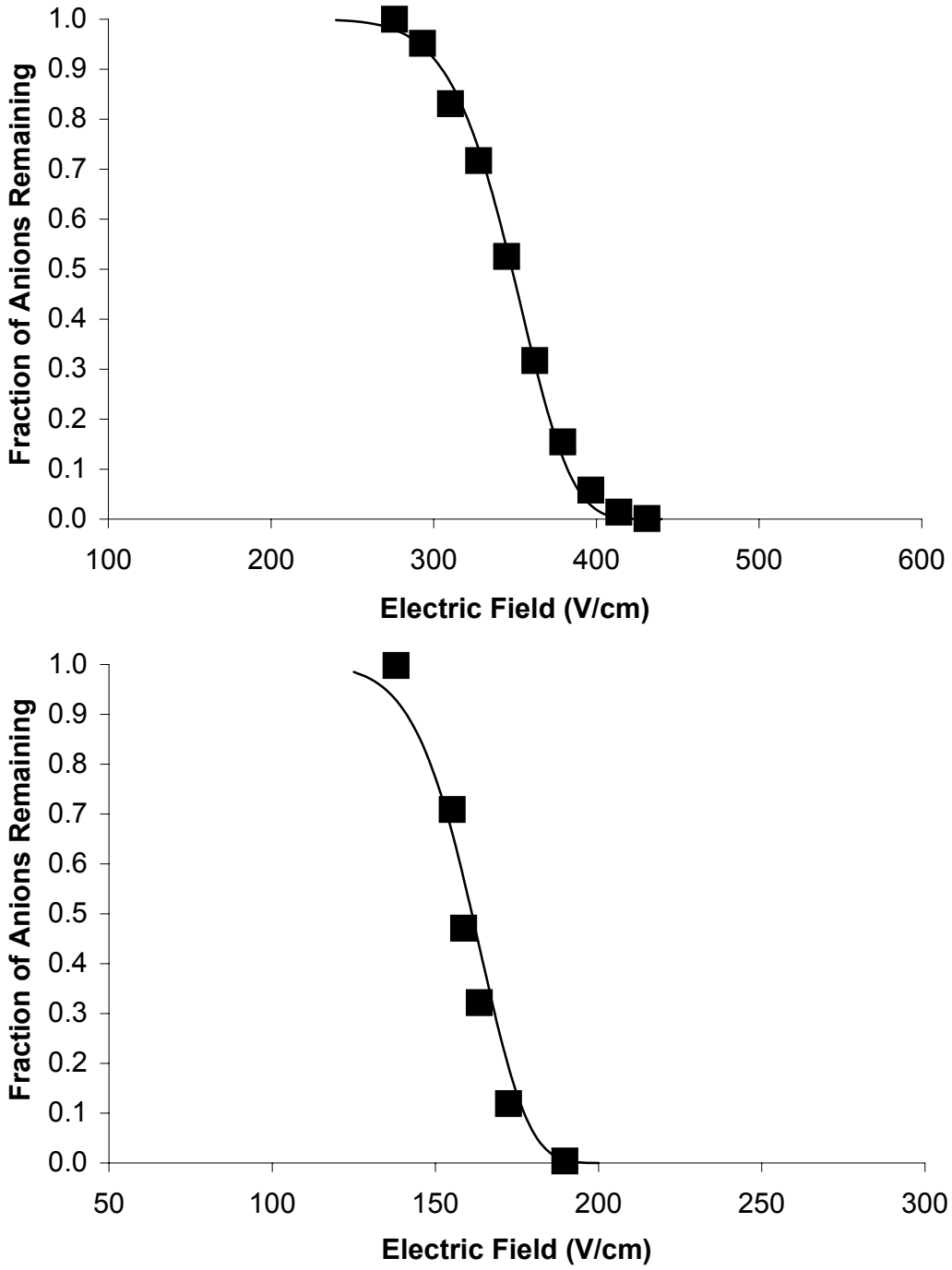

Figure C.5 Experimental electric field detachment curves and theoretical fits for cyclopentanone and pivalaldehyde.

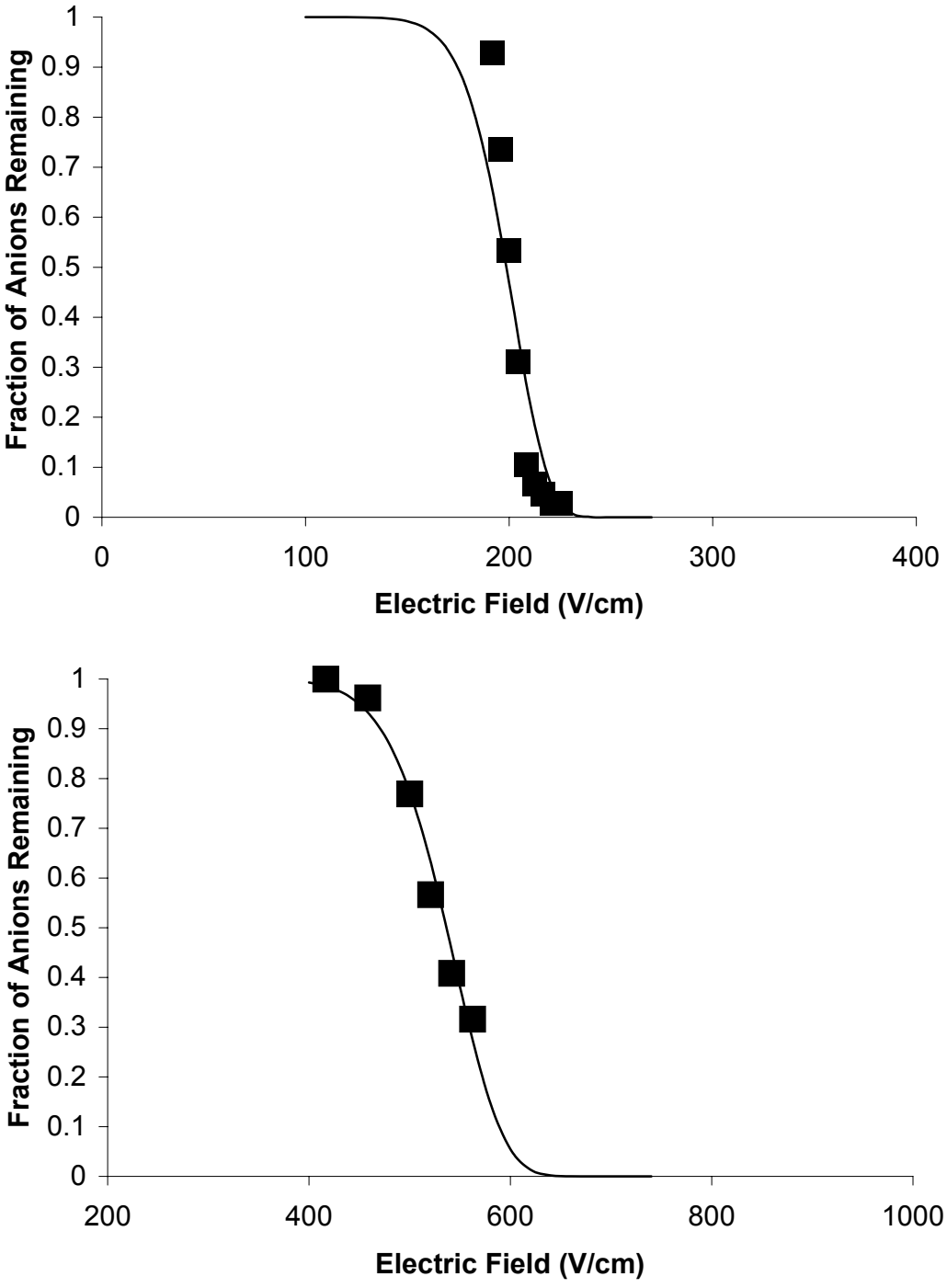

Figure C.6 Experimental electric field detachment curves and theoretical fits for 2-ethylbutanal and 2-methylcyclopentanone.

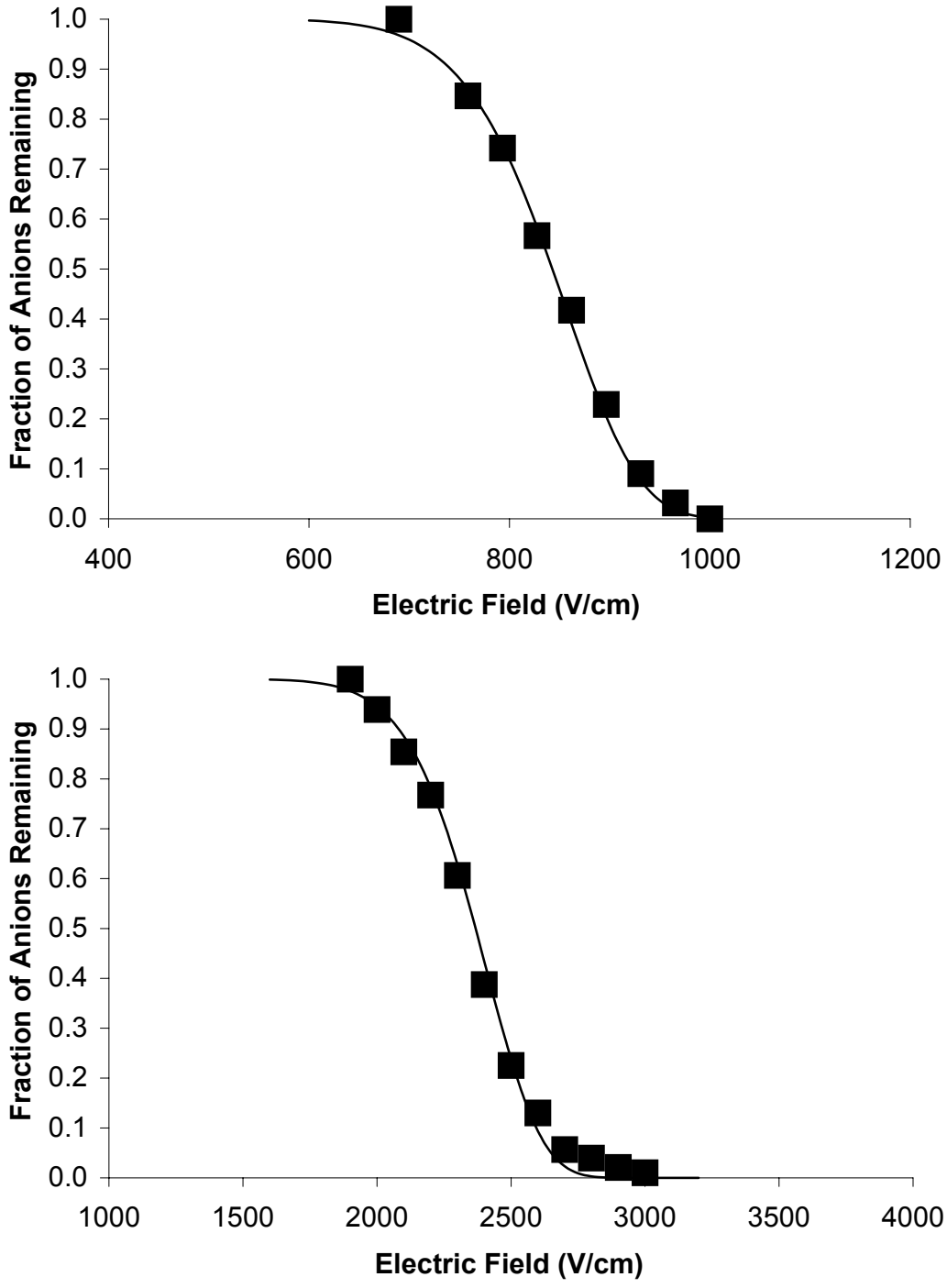

Figure C.7 Experimental electric field detachment curves and theoretical fits for 3-methylcyclopentanone and cyclohexanone.

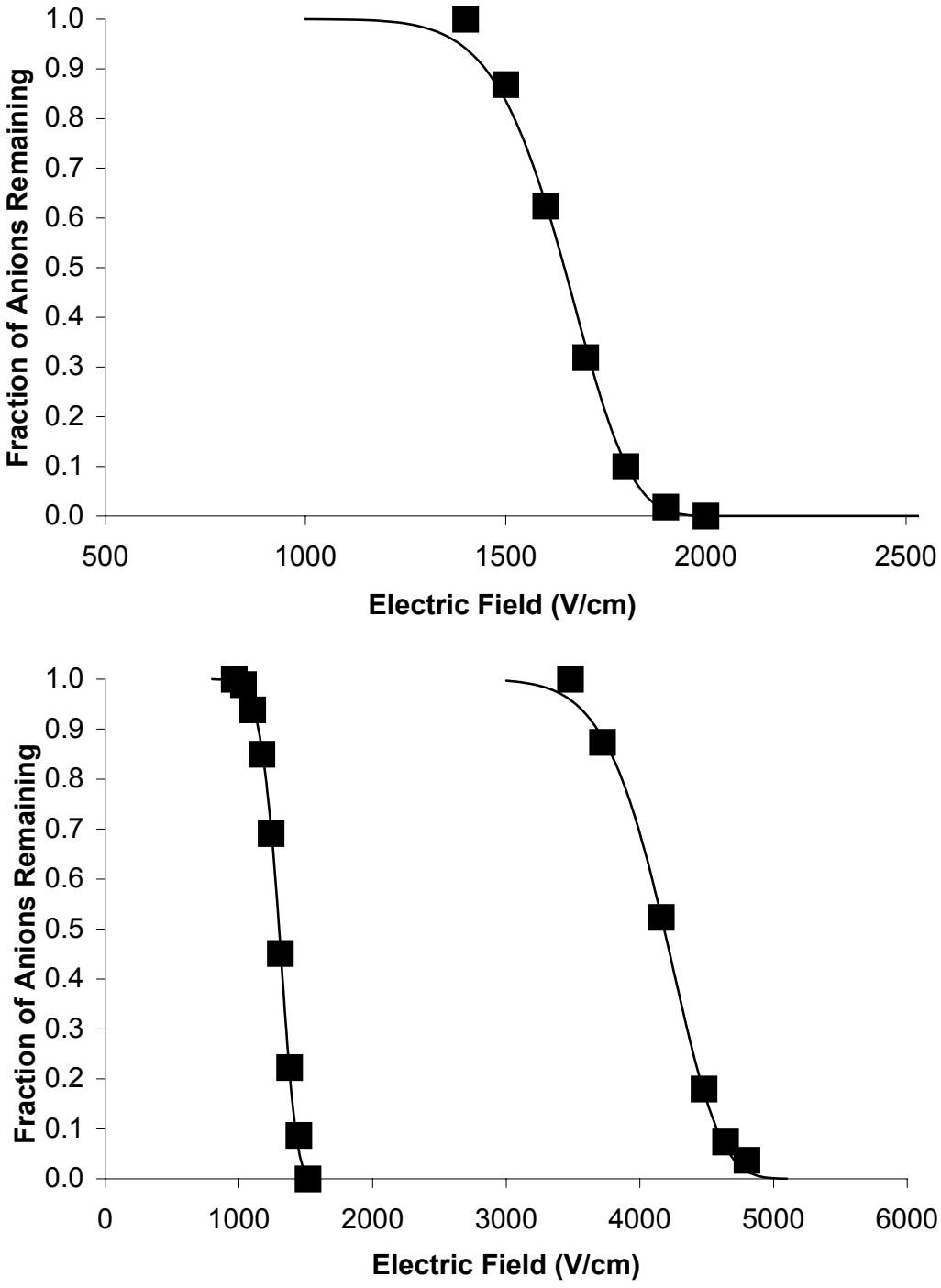

Figure C.8 Experimental electric field detachment curves and theoretical fits for 2-methylcyclohexanone and 3-methylcyclohexanone.

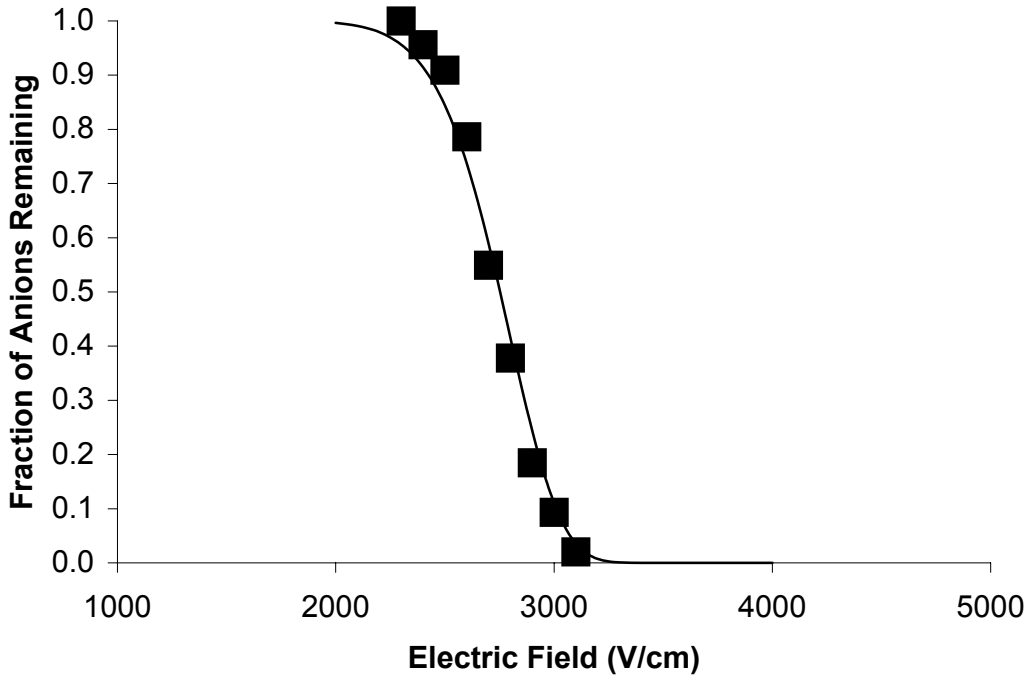

Figure C.9 Experimental electric field detachment curve and theoretical fit for 4-methylcyclohexanone.

VITA

Nathanael (Nathan) Hammer was born in Johnson City, Tennessee on March 18, 1976. He attended public schools in Denton, Texas, and in Shelby, Greene, and Williamson counties in Tennessee. He graduated valedictorian of Franklin High School in Franklin, Tennessee in May 1994 and received an Honors Bachelor of Science in Chemistry Degree from the University of Tennessee in May 1998 (summa cum laude). Nathan attended graduate school at the University of Tennessee where he worked under the direction of Dr. Robert Compton in the area of chemical physics. The doctoral degree was received May 2003.